DOCTOR OF PHILOSOPHY

Mathematical modelling of drug metabolism

using in silico techniques to investigate the cytochrome P450 enzyme system in hepatic reductase null mice

Hill, Lydia

Award date:
2011

DOCTOR OF PHILOSOPHY

Mathematical modelling of drug metabolism

using in silico techniques to investigate the cytochrome P450 enzyme system in hepatic reductase null mice

Lydia Hill

2011

University of Dundee

Mathematical Modelling of Drug Metabolism: Using *in silico* Techniques to Investigate the Cytochrome P450 Enzyme System in Hepatic Reductase Null Mice

Lydia Hill

Doctor of Philosophy

Division of Mathematics

University of Dundee

Dundee

2011

Contents

List of Figures

Declaration

I, Lydia A Hill, hereby certify that this thesis has been written by me, that it is the record of work carried out by me and that it has not been submitted in any previous application for a higher degree.

Signature of candidate..... **Date** .....

This is to certify that the Lydia Hill has complied with all the requirements for the submission of this Doctor of Philosophy thesis to the University of Dundee.

Signature of supervisor ..... **Date** .....

Acknowledgements

I would like to thank Prof Mark A J Chaplain for the opportunity to work on this project and for the support throughout. I would like to thank CXR Biosciences for funding and to Prof Roland Wolf and Dr Yury Kapelioukh for their support of the project.

I would like to thank Dr Kirsty Gordon for help and advice with the Java program that was developed further through my thesis. I would also like to thank all the members of the Mathematical Biology Group past and present for advice, help and support, with special reference to: Dr Hitesh Mistry, Mr Mark Sturrock and Miss Daniela Schlüter.

Finally I would like to thank my husband Gavin for the constant and unwavering support he has provided through the highs and lows of this project. I also would like to thank my many friends in Dundee and St Andrews and my family for all their support and encouragement.

Abstract

In silico modelling approaches are useful since they can minimise experimental costs and once set up can be used to replace animal testing for drugs. As such modelling techniques need to be developed to reduce dependence on animals for validation of pharmacological efficacy. The work within this thesis shows that computational methods can be used to model biological and medical problems effectively.

The main aim of this thesis was to investigate Cytochrome P450 enzymes and their effect on drug metabolism through the use of the Hepatic Reductase Null (HRN) mouse. This was done through using a number of computational models and compared with drug data provided by CXR Biosciences.

These models ranged from solely ODE (for comparison to experimental data) to multiscale cellular automata and spatial models when analysing the dynamics on the tumour and cellular level. Once these models were developed the parametric sensitivity was derived in order to see whether there were any needless parameters so that the models were streamlined and to test the model‘s robustness against error.

The novel three-compartment model was developed in order to explain dynamics within the Hepatic Reductase Null mouse was able to explain much of the behaviour in the supplied data. As well as this it was discovered that the transgenic mouse showed reduced speed in metabolism for many of the drugs analysed which meant that different models were sometimes necessary.

The cellular automaton program presented is applicable to other areas other than the one stated in Chapter 5. For example any area that deals with interactions between tissue media and drugs as in toxicology and drug studies. The cell cycle inside the code deals with tumour cells but this code can be re-parameterised to concentrate on other types of cell including normal cells, hepatic tissue etc.

The inclusion of spatial effects to the deterministic models like the Cytochrome P450 cycle allows for greater realism in predictions of drug passage through the body or across certain tissue media. Due to this it is useful to include both deterministic and spatial modelling with a multiscale approach in models for drug metabolism.

Chapter 1

Cytochrome P450 Enzymes

1.1 Motivation and Aims

All Cytochrome P450 enzymes are responsible for more than 90% of metabolism for all drugs (Parikh et al., 1997), which means that drug-drug interactions are very important to model prior to administration of therapy. Greater research is needed into the functionality of Cytochrome P450 in order to be able to predict the outcome with relation to the compound.

The most recent area of research related to Cytochrome P450 is that of cancer therapeutics. Their use in this area is one of metabolism, activation or inactivation. This is particularly important for prodrugs like Cyclophosphamide and Ifosfamide (Yu et al., 1999). These processes happen mostly within the hepatic system where the enzymes are most abundant. These enzymes are also found in and tumour tissue which can have positive or negative effects on anticancer drugs due to these activities (McFadyen et al., 2004). This could mean that the tumour tissue is left unaffected by the drug due to being inactivated by local CYP sources and as such ineffective.

It is due to these reasons that aim of this thesis was to concentrate on the Cytochrome P450 enzyme family and their effect on drug metabolism.

Initially this was through the use of the Hepatic Reductase Null (HRN) mice in comparison to their wild type counterparts shown in Chapter 3. This was done through using a number of different compartmental models and compared with drug data provided by CXR Biosciences. The main focus of this modelling was whether there were metabolic differences that were produced as a side effect of genetic mutation in the transgenic mouse. A three-compartment model was developed through adding time dependent excretion and a compartment that represented the fat cells in the liver that may change the dynamics of lipophilic drugs.

After this solely deterministic approach a cellular automaton was then developed in Chapter 5 to analyse how the Cytochrome P450 enzymes affect drug metabolism in general. The results were not compared to the data used in Chapter 3 as the aim was to get an indication of how the CYP enzymes would affect drug dynamics in a tumour.

In Chapter 6 a COMSOL simulation was performed on a singular cell to see whether spatial effects such as the fact that P450 enzymes are mostly found in Smooth Endoplasmic Reticulum on the cellular level would affect the drug dynamics.

The rest of this chapter will be dedicated to the location and functionality of Cytochrome P450 enzymes. In the following chapter an introduction to Drug modelling can be found. These two chapters should provide a good understanding for the modelling found within this thesis.

1.2 Introduction

Cytochrome P450 is a large class of enzymes, which constitute a superfamily of hemoproteins. The name Cytochrome P450 was first used in 1961 because of the pigment (P) having a spectral peak at 450nm when bound to carbon monoxide

(Nebert and Russell, 2002). At this point in time it was thought that there was only one enzyme but since then there have been numerous discoveries of related enzymes.

These proteins are categorised into families dependent on amino-acid correlation. There are 18 families and 42 subfamilies of CYP (Cytochrome P450) enzymes (Pirmohamed and Park, 2003). Families are defined as having more than 40% identity in genetic structure whereas subfamilies have more than 55% (de Groot, 2006). Out of the 18 families CYP1, CYP2, CYP3 and to a lesser extent CYP4 deal with drug metabolism.

There are many factors that affect the activity and functionality of Cytochrome P450 these are: age, gender, drug, smoking, alcohol, disease and polymorphisms (Cheng et al., 2009). Hepatic drug metabolism decreases with age in animals (Sotaniemi et al., 1997) and in humans age comes with diminished liver mass, blood flow and hepatic metabolising enzyme activity (Scripture et al., 2005). Although gender is thought to have an effect on P450 activity in the liver it has not yet been proven (George et al., 1995).

Excessive alcohol consumption can cause liver disease and cirrhosis, which in turn causes impaired liver function, since, for example, liver disease causes drug clearance to be reduced and cirrhosis is characterised by the replacement of normal liver tissue with scar tissue. This sometimes leads to cytotoxic chemotherapy not being offered due to the large probability of adverse drug reaction (Scripture et al., 2005). Hypoxemia can also cause diminished CYP activity due to its dependency on oxygenated conditions. This is a serious complication to a number of common diseases (Jürgens et al., 2002).

A polymorphism is a genetic variation that is present in a population (Martin and Hine, 2004). These can cause adverse drug reactions due to increased or decreased in the CYP enzyme activity with reference to any particular drug (Evans

and Relling, 1999) and therefore plays a large role in interpatient variability (Cheng et al., 2009). If the enzyme activity is decreased this could cause a longer half-life within the body before it is cleared this is known as a poor metabolism phenotype. Different alleles of the 2C9, 2C19, 2D6, 3A4, 3A5, 2A6 and 2B6 drug metabolising genes can result in failures in treatment, which can lead to toxic effects, or even death in rare cases (Meyer, 2000; Phillips et al., 2001). A list of polymorphic (shows polymorphisms) genes and the effect on certain medications were collated by Evans and Relling (1999). This paper also illuminates just how powerful a change in Cytochrome P450 enzyme panel can affect therapeutic efficacy.

1.2.1 Location

These enzymes are found in all living things with the exception of *E. coli* (Munro and Lindsay, 1996)that can be used to generate Cytochrome P450 enzymes for experimental procedures (Guengerich et al., 1997).

Cytochrome P450 enzymes are found all over the body but they are primarily located in the liver (McFadyen et al., 2004). Low levels are found in the brain, lungs, intestine and kidneys (Venkatakrishnan et al., 2001; Macé et al., 1998). On the cellular level this enzymatic system is located within the Smooth Endoplasmic Reticulum (SER) (Tsui, 2003). Human Cytochrome P450 enzyme levels are difficult to obtain due to difficulty in obtaining healthy liver tissue (Kinirons and O'Mahony, 2004) from humans. An expression study on 1A2, 2A6, 2B6, 2C, 2D6, 2E1 and 3A4 showed that (Macé et al., 1998):

Peripheral lung tissue	Bronchial Mucosa	Both
1A2 and 3A4	2C9	2C8, 2A6, 2E1 and 2B6

Table 1.1: *Study results for location of Cytochrome P450 enzymes.*

These chemicals not only occur through the normal function of systems throughout the body but also are associated with tumours. McFadyen et al. (2001) while looking at anticancer drug resistance found a link between CYP1B1 overexpression and cancer. The work of Tanaka et al. (2004) showed that the analysis of tumour tissue in cancer patients could help to predict the efficacy of anti-cancer drugs with respect to metabolism including Cytochrome P450 enzymatic reactions.

Liver

This organ is very important in drug metabolism and is the largest gland in the human body. As you can see from the figure below it is boomerang shaped and has a large vein passing through it. This allows for the blood flow to have quicker diffusion through the system since there is a large surface area connecting the tissue to the vein.

With reference to drug metabolism the drug has two chances to be cleared by the liver due to first-pass metabolism. This is where the blood flow can immediately go to the liver before the gut. Then when it escapes the hepatic system it can proceed to the gut and then return to the liver once more. This allows for drugs to be cleared from the body much quicker.

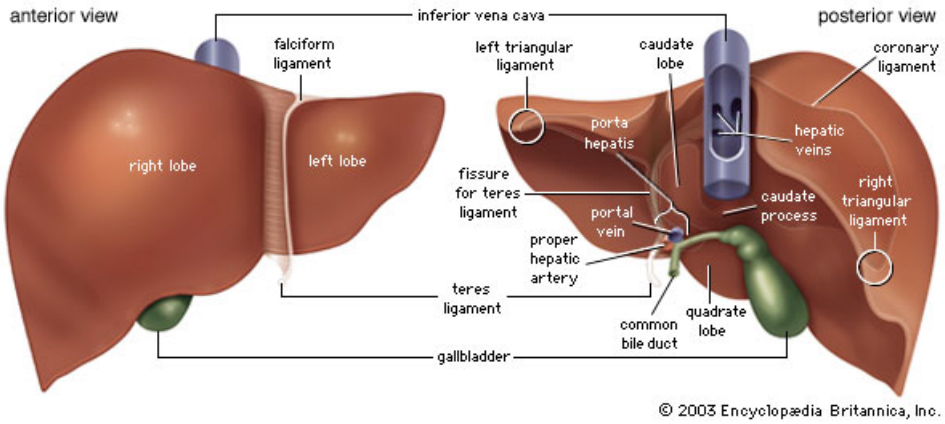

Figure 1.1: *Schematic diagram of the liver (Online., 2011a).*

The liver is one of a few organs in the body that is regenerative such that if 70% of the liver was removed it could become the whole organ again (Khan and Mudan, 2007). This is why liver transplantation usually takes the left lobe (right in the above figure) and leaves the donor with only the right lobe.
The Cytochrome P450 enzymes are found in the different liver cells for example hepatocytes and Kupffer cells (Lu and Cederbaum, 2008).

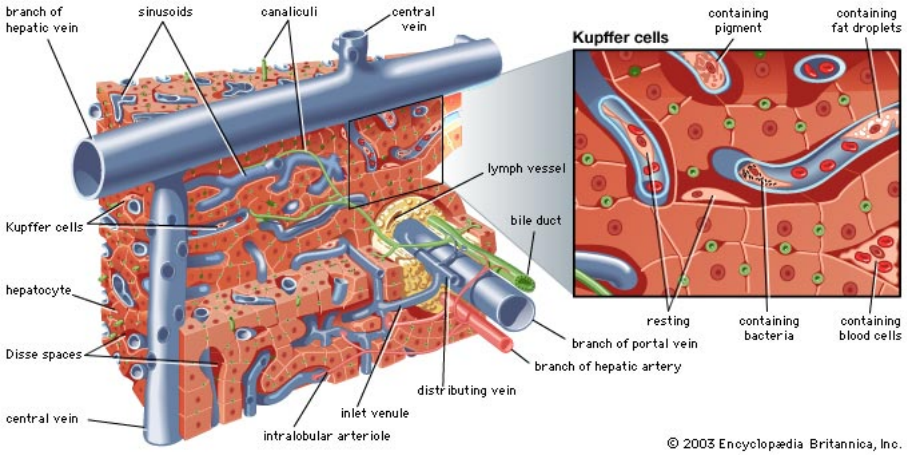

Figure 1.2: *Schematic diagram of the liver (Online., 2011b).*

This figure shows the location of these two types of cells. As they are in different areas of the liver there is a spatial dimension to drug metabolism within the liver.

1.3 Main CYP enzymes

Out of all the Cytochrome P450 enzymes that exist within the human body there are nine strains that are responsible for ninety percent of the metabolic activity (Cozza et al., 2003). These are (six major) 1A2, 3A4, 2C9, 2C19, 2D6, 2E1, (three minor) 2A6, 2B6 and 2C8.
In what follows is an explanation of specific functional details for each enzyme and known interactions with drugs. These interactions are either metabolic, inhibitory or the drug induces production of the enzyme. Some of the drugs outlined

are studied in Chapter 3 with compartment models but most are just shown to illustrate the wide range of substrates Cytochrome P450 interact with.

1.3.1 CYP1A2 enzyme

This enzyme is the predominant CYP1A form in all species (Caccia et al., 2009) that is exclusively expressed in the liver (Cozza et al., 2003) and it represents 10-15% of the organs P450 activity. The associated gene is conserved in mammals, birds and fish but not in lower eukaryotes (Schenkman and Greim, 1993). This gene is polymorphic (Tredger and Stoll, 2002) but no major phenotypes that cause adverse drug reactions have been reported currently.
It only plays a minor role in drug metabolism since it is merely responsible for 5% of therapeutically used drugs (Wolf and Smith, 1999).

Metabolism	Inhibition	Induced
Caffeine	Fluvoxamine	Omeprazole
Tamoxifen	Ciprofloxacin	

Table 1.2: *Drugs that interact with CYP1A2 (Scripture et al., 2005; Cozza et al., 2003; Tredger and Stoll, 2002).*

Since this Cytochrome P450 enzyme metabolises caffeine this drug is used as a probe for the level of CYP1A2 activity within the patient (Park et al., 1996). This enzyme‘s activity has been reported to be larger in males than in females (Caccia et al., 2009). As well as this women suffer from caffeine toxicity due to the activity of 1A2, which is not the case in males (Clewell et al., 2002).

1.3.2 CYP3A4 enzyme

CYP3A4 is the major P450 isoform in adults from the 3A family (Ingelman-Sundberg, 2001). Unlike the previous enzyme this strain is active in the liver,

gastro-intestinal tract (Holmquist, 2009) and the small intestine (Cozza et al., 2003) though it is considered to be primarily hepatic (Tredger and Stoll, 2002) and is the most abundant P450 in the liver. Although this enzyme is predominant in adult livers it is undetectable in babies (Plant, 2007) and this is the reason why blood transfusions to this age group have to be monitored for drugs. The presence of the enzyme in the small intestine although varied (Kato, 2008) causes lower bioavailability of some substrates due to first pass metabolism.

Similarly to 1A2, CYP3A4 is polymorphic (Tredger and Stoll, 2002). Various polymorphisms have been reported most are rare and of unknown function (Pirmohamed and Park, 2003). The fact that the function of these polymorphisms is unpredictable is of particular concern for the metabolism of anti-cancer agents (Rodriguez-Antona and Ingelman-Sundberg, 2006). This is because if the polymorphism results in a poor metabolism phenotype this can result in reduced clearance of cyclophosphamide and thus poorer clinical response (Ekhart et al., 2009).

CYP3A4 is responsible for metabolism of approximately 50% of drugs (Tang and Stearns, 2001) and is the major xenobiotic metabolising enzyme in humans. This enzyme has a wide range of compounds that it metabolises regardless of shape, size (Beresford et al., 2002) and lipophilicity (Lewis, 2000). The work of Zhou et al. (2005) showed how CYP3A4‘s low substrate specificity (interacts with many compounds) makes the enzyme susceptible to inhibition. This inhibition can occur to the enzyme through reversible and irreversible formation of complexes that inactivate the enzyme‘s functionality. Due to the large number of drugs that this enzyme interacts with if a patient is prescribed multiple drugs they may suffer adverse drug reactions (Marechal et al., 2006). As such overcoming the metabolism of the drug can be achieved by two means: lipophilicity reduction and functionality removal.

Metabolism	Inhibition
Midazolam	Grapefruit juice
Tamoxifen	Erythromycin
Docetaxel	
Omeprazole	

Table 1.3: *Drugs that interact with CYP3A4 (Smith et al., 2001; Hurria et al., 2006; Lewis, 2000; Miners, 2002).*

This enzyme's activity can be modelled using the Erythromycin breath test(Hurria et al., 2006).

1.3.3 CYP2C9 enzyme

This strain is found in many tissues but most of its drug metabolism activity occurs in the liver (Cozza et al., 2003). It accounts for 18% of the P450 content in the liver and this is why it is reported as primarily hepatic (Tredger and Stoll, 2002). This enzyme dominates over 2C19 (Venkatakrishnan et al., 2001) when they compete for substrates.

This enzyme also shows polymorphisms (Venkatakrishnan et al., 2001) that can complicate treatment through the presence of poor/rapid metabolism phenotypes (Rodriguez-Antona and Ingelman-Sundberg, 2006).

Metabolism	Inhibition	Induced
Diclofenac	Sulfinpyrazone	Barbiturates
Paclitaxel	Miconazole	Carbamazepine
Tamoxifen	Fluconazole	Rifampin

Table 1.4: *Drugs that interact with CYP2C9 (Scripture et al., 2005; Venkatakrishnan et al., 2001; Cozza et al., 2003; Tredger and Stoll, 2002).*

1.3.4 CYP2C19 enzyme

As with CYP2C9, this strain is found in many tissues and along with CYP2C9, is responsible for 20% of the hepatic P450 activity (Cozza et al., 2003). Out of all the factors that affect P450 activity this enzyme is affected by an age-related decrease (Scripture et al., 2005).

Polymorphisms have been recorded that are associated with deficient, reduced, normal or increased enzyme activity (Belle and Singh, 2008). These phenotypes include a poor metaboliser formulation that occurs in less than 5% of Caucasians and 12-20% of Asian populations (Venkatakrishnan et al., 2001).

Metabolism	Inhibition
Omeprazole	Fluvoxamine, Omeprazole
Tamoxifen	Fluconazole, Ticlopidine

Table 1.5: *Drugs that interact with CYP2C19 (Scripture et al., 2005; Venkatakrishnan et al., 2001; Cozza et al., 2003; Tredger and Stoll, 2002).*

For poor metabolisers Omeprazole concentration is five-fold higher and rapid metabolisers have 40% lower concentration, which can cause therapeutic failure (Belle and Singh, 2008) due to the drug levels not being high enough to be effective. Gender differences in the enzyme have been recorded in the literature but no consensus on whether males or females have greater activity has been reached (Clewell et al., 2002).

1.3.5 CYP2D6 enzyme

CYP2D6 is the only member of the CYP2D family, which functions in humans (Caccia et al., 2009). This enzyme is reported to be primarily hepatic (Tredger and Stoll, 2002) but is also found in brain, prostate, bone marrow and heart tissue (Cozza et al., 2003). 2D6 accounts for 1.5% of the P450 liver content (Cozza

et al., 2003).

As with the Cytochrome P450 enzymes described earlier this strain is also polymorphic. There are at least 75 genetic polymorphisms (Belle and Singh, 2008) ranging from deficient to ultra rapid. Approximately 8% of European and North American Caucasians have two copies of mutant CYP2D6 alleles causing the enzyme to be absent (Schenkman and Greim, 1993). This genetic defect is called debrisoquine polymorphism.

This enzyme has become a key metabolising enzyme in drug development, responsible for an estimated 25% of all drugs (Belle and Singh, 2008). It is so important to the extent that if a drug shows more than 40% of its clearance is dependent on CYP2D6 (Pirmohamed and Park, 2003), the development is halted.

Metabolism	Inhibition
Dextromethorphan	Quinidine, Fluoxetine
Tamoxifen	Paroxetine, Perplenazine
Codeine	Terbinafine, Ticlopidine

Table 1.6: *Drugs that interact with CYP2D6 (Cozza et al., 2003; Tredger and Stoll, 2002; Venkatakrishnan et al., 2001; Rang, 2003; Belle and Singh, 2008).*

For this enzyme Dextromethorphan is used as a probe drug to check activity level (Park et al., 1996).

1.3.6 CYP2E1 enzyme

This enzyme is located almost exclusively in the liver and represents 5-7% of all hepatic Cytochrome activity (Venkatakrishnan et al., 2001). 2E1 shows resistance to the toxic effects of benzene so is indicative of this enzymes role in xenobiotics metabolism (Gonzalez and Kimura, 2003). This strain was the only member of the CYP2E family in humans since CYP2E2 is only expressed in rabbits (Schenkman and Greim, 1993).

CYP2E1 has also been reported as polymorphic (Tredger and Stoll, 2002) but no actual polymorphisms have been found (Rodriguez-Antona and Ingelman-Sundberg, 2006).

Metabolism	Inhibition	Induced
Caffeine, Tamoxifen	Disulfiram	Ethanol, Isoniazid
Ethanol, Paracetamol	Diethylcarbamate	Nicotine

Table 1.7: *Drugs that interact with CYP2E1 (Scripture et al., 2005; Tredger and Stoll, 2002; Rang, 2003; Venkatakrishnan et al., 2001; Lu and Cederbaum, 2008; Dutheil et al., 2008; Lewis, 2000).*

Many substrates associated with CYP2E1 induce their own metabolism (Lu and Cederbaum, 2008).

1.3.7 CYP2A6 enzyme

This enzyme is indigenous to hepatic and extrahepatic tissues (Tredger and Stoll, 2002) and comprises 4% of liver P450 content (Venkatakrishnan et al., 2001).
CYP2A6, as with the other Cytochrome P450 enzymes, is polymorphic in humans and can lead to a reduced capacity for metabolising nicotine and a reduced risk to tobacco dependence. Experiments are underway to treat smoking dependence (Venkatakrishnan et al., 2001) in a hope to cure it.
As well as this, the polymorphisms have been linked with tobacco-induced cancers. This is due to its activity in the metabolism of nicotine and tobacco pre-carcinogens (Rodriguez-Antona et al., 2010).

1.3.8 CYP2B6 enzyme

Out of all the P450 isoforms in the hepatic system this one has low abundance (Venkatakrishnan et al., 2001) and represents less than 1% of the activity (Cozza et al., 2003). However although it is primarily hepatic (Tredger and Stoll, 2002)

it is also detected in extrahepatic tissues including the intestines, kidney, lung, skin and the brain (Miksys et al., 2003; Yengi et al., 2003). This strain shows large interindividual variance (Venkatakrishnan et al., 2001; Rodriguez-Antona and Ingelman-Sundberg, 2006) that was shown to be more than a hundred fold in a study of the activity in liver microsomes.

Metabolism
Midazolam and Tamoxifen

Table 1.8: *Drugs that interact with CYP2B6 (Tredger and Stoll, 2002).*

1.3.9 CYP2C8 enzyme

This enzyme has only a minor role in drug metabolism (Cozza et al., 2003). Polymorphisms for this enzyme exist but do not seem to be functionally important (Kirchheiner and Seeringer, 2007). However, it does affect Paclitaxel clearance (Spratlin and Sawyer, 2007).

Metabolism	Inhibition
Paclitaxel and Ibuprofen	Quercetin

Table 1.9: *Drugs that interact with CYP2C8 (Tredger and Stoll, 2002; Venkatakrishnan et al., 2001; Martínez et al., 2005).*

In a study by Martínez et al. (2005) they showed that 30% of the population carry an alternative allele CYP2C8 that interferes with ibuprofen metabolism.

1.4 Functionality

For Cytochrome P450 enzymes to function, both a substrate and a cofactor, for example NAD(P)H, are necessary. These three groups form a cyclical relationship in order to keep the enzyme working. This is shown by the fact that Cytochrome

P450 expression increases when there is more substrate to use and vice-versa. P450 systems vary greatly from species to species and this difference is mainly seen in the identity of the cofactors. In fact these changes show a prokaryotic/eukaryotic divide. This division is shown by the fact that eukaryotic systems have Cytochrome P450 reductase (CPR), FAD (flavin adenine dinucleotide) and FMN (Flavin mononucleotide) cofactors and prokaryotic systems do not. (Parikh et al., 1997; McLean et al., 2005). These eukaryotic systems are also responsible for the reduction of foreign compounds like anti-cancer drugs (Döhr et al., 2001).

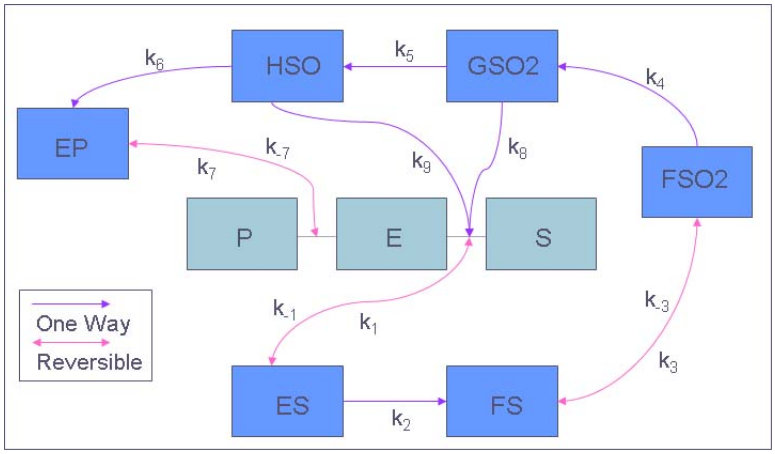

Figure 1.3: *Schematic diagram of the Cytochrome P450 cycle.*

The Cytochrome P450 cycle shown in figure 1.3 is based on a scheme discussed in a paper by Guengerich (2001). It is a simplified cycle specifically tailored for CYP1A2 enzymes. Although these enzymes only represent a small proportion of hepatic CYP activity they are conserved across higher eukaryotic species. Due to this it should be possible to relate this cycle to the other strains. The cycle starts with the unbound enzyme, E, which represents a P450 enzyme with an Iron (III) core. This then comes into contact with some substrate, S, which in this chapter is the drug variable. These two then bind together to form an enzyme-drug complex, ES. This complex is formed in equilibrium outlined in the following equation:

$$E + S \rightleftharpoons ES \tag{1.1}$$

This reaction is governed by two rate constants k_{-1} and k_1. Since this complex is in equilibrium it is still unstable and until the iron core is reduced to Iron (II) using an electron from a cofactor e.g. CPR, this is then called FS in the cycle. This part of the cycle is controlled by a rate constant, k_2, in the equation:

$$ES \rightarrow FS \tag{1.2}$$

This complex then binds with oxygen to form FSO2 as outlined by the equation:

$$FS + O_2 \rightleftharpoons FSO2 \tag{1.3}$$

This is another equilibrium with a forward and backwards reaction governed by the rate constants k_3 and k_{-3} respectively. This complex then forms GSO2 with the addition of a H^+ and an electron from a cofactor e.g. CPR or Cytochrome b5 reductase. This is shown in the equation governed by the rate constant k_4:

$$FSO2 \rightarrow GSO2 \tag{1.4}$$

This complex also breaks down as shown by the equation:

$$GSO2 \rightarrow E + S + H_2O_2. \tag{1.5}$$

This is associated with the rate constant k_8. However this reaction does not completely reduce GSO2 levels and some is converted to HSO and then a second H^+ cleaving water from the complex by the equations:

$$GSO2 \rightarrow HSO \tag{1.6}$$

$$HSO \rightarrow E + S + H_2O. \tag{1.7}$$

These equations are governed by the constants k_5 and k_9 respectively. HSO is then changed to an enzyme-product complex, EP, which is unstable:

$$HSO \rightarrow EP \tag{1.8}$$

The rate constant for this is k_6 and then the EP complex breaks down into enzyme and oxidised drug or product, P. The equation for this with constants k_7 and k_{-7} is:

$$EP \rightleftharpoons E + P \tag{1.9}$$

The interactions between Cytochrome P450 and the substrate are not always positive. Cytochrome P450 interacts with drugs to metabolise them into stable or toxic metabolites (Pirmohamed and Park, 2003). This is why greater research is needed into the functionality of Cytochrome P450 in order to be able to predict the outcome with relation to the compound.

The dependence of Cytochrome P450 enzymes on the presence of CPR has been reviewed in Omura (2010). Another cofactor that has been proposed since early studies is Cytochrome b5, which has been shown to exert various influences on P450 catalytic systems. It is unclear whether it is a physical association with the particular Cytochrome P450 or electron transfer capability (Yamazaki et al., 1996). The work of Finn et al. (2008) states that Cytochrome b5 affects CYP2C8, 2C9, 2C19, 2D6, 2E1 and 3A4 activity.

1.5 Use of Cytochrome P450 Enzymes in Pharmaceuticals

The use of Cytochrome P450 enzymes in drug development is in its early stages and has not been fully utilised yet (Guengerich, 2002). Examples of this are in the production of: chemicals that have anticarcinogenic properties like perillyl alcohol (van Beilen et al., 2005) and antibiotics using microbial CYP's.

Not only can Cytochrome be used as a drug target and a metaboliser, it can also help with drug synthesis. For example, Cytochrome P450 enzymes have been isolated from yeast and used to catalyse the biosynthesis of Taxol (Paclitaxel), an anticancer drug (Jennewein et al., 2005). A review of the use of Cytochrome P450 monooxygenases as biocatalysts can be found in Winklerb et al. (2010). This paper also classifies these enzyme systems as to their usefulness for certain substrate reactions.

In recent research it has been theorised that these enzymes can also be used to monitor drug levels in the body (Guengerich, 2002) and vice versa. For example caffeine metabolites could monitor CYP2E1 levels (Schenkman and Greim, 1993) and using this method can ensure that drug dose does not reach toxic levels The work of Roy et al. (1999) showed that there were differences in Cytochrome P450 expression profiles when under the influence of drugs like cyclophosphamide and ifosfamide.

Cytochrome P450 plays an important role in primary and secondary metabolism and drug degradation (Urlacher and Eiben, 2006). CYP1-3 are responsible for 70-80% of phase I metabolism and participate largely in the metabolism of other xenobiotics (Ingelman-Sundberg, 2004) including lipophilic chemicals (Lin and Lu, 1998). Yang et al. (2006) showed that not all CYP subfamilies are involved in the bioactivation of drugs. Only CYP1A, 2C, 2E and 3A subfamilies are

involved whereas 2B and 2D play little to no part. This set of enzymes is known to cooperate so that they can be responsible for the metabolism of all xenobiotics (Beresford et al., 2002). The effect of drugs on CYP activity is thought to be due to drug inhibition due to competition or non-competition within the liver causing toxicity (Tang and Stearns, 2001).

1.6 Chemical interactions

The work of Holmquist (2009) showed that substances entering the body can act in three ways - as a substrate, as an enzyme inhibitor or inducer. A substrate can also induce/inhibit one or more CYP450 enzymes simultaneously.
This type of enzyme acts in number of ways due to the vast number of members. The main ways it interacts with compounds in the body through the use of substrates available are - oxidation, peroxidation, epoxidation, reduction and hydroxylation (Maurer et al., 2005).
Not all drug oxidation exclusively involves the P450 system. For example, ethanol is metabolised by alcohol dehydrogenase in addition to the CYP2E1 enzyme (Rang, 2003).
These enzymes are very versatile with relation to the compounds they can interact with e.g. drugs, pollutants and plant products. However the interactions between Cytochrome P450 and the chemical are both positive and negative.

A positive example is that some mammalian CYP‘s such as 2E1 are able to metabolise low molecular weight hydrocarbons (Rodriguez-Antona and Ingelman-Sundberg, 2006) and haloalkanes. It is this ability that makes them useful in bioremediation (Guengerich, 2002)They have been used to clear up oil spills and landfill created chemicals.
Cytochrome P450 interacts with drugs to metabolise them into stable or toxic

metabolites (Pirmohamed and Park, 2003) that can cause negative side effects.

1.7 Cancer

The most recent area of research related to Cytochrome P450 is that of cancer therapeutics. Their use in this area is one of metabolism, activation or inactivation. When a precarcinogen enters the human body Cytochrome P450 is one of the main enzymes responsible for mediation of its activation and detoxification (Rodriguez-Antona and Ingelman-Sundberg, 2006). For anti-cancer drugs Cytochrome P450 participates in the activation and inactivation of the compounds, which is particularly important for prodrugs like Cyclophosphamide and Ifosfamide (Yu et al., 1999). This process happens mostly within the hepatic system where the enzymes are at their strongest in number. The presence of CYP around tumour tissue can have positive or negative effects on anticancer drugs due to its activation/inactivation protocols (McFadyen et al., 2004). This could mean that the tumour tissue is left unaffected by the drug due to being inactivated by local CYP sources.

For cancer therapy the liver system is very important but it should be understood that there is also an extrahepatic tissue configuration that is also useful. For example, CYP3A4 expression in breast tumour tissue can be used to predict the response to Docetaxel (Miyoshi et al., 2002).

Chapter 2

Drug Development and Modelling

In the pharmacological industry the cost of creating new and innovative drugs is an expensive area of research. This is due to the current methodology and approach, which consist of drug creation and testing (Grass and Sinko, 2002) without the knowledge of whether the functional groups will have the desired effect on the human body. Due to this there is a growing need for computational models investigating the metabolic and functional effect. These models should be able to minimise the percentage of new drugs that get to clinical trials but fail to make it to market due to poor bioavailability, toxicity and drug-drug interactions (Ekins et al., 2000). As well as this it should be able to stop useful drugs being rejected prematurely. This should reduce the development costs and therefore the price of the drug in general when it reaches the market.

For orally administered drugs there exists a set of rules that was developed by Lipinski in the late 1990‘s (Lipinski et al., 1997) and is known as “Lipinski’s rule of drug likeness“ or the “rule of five“ (Zhang and Wilkinson, 2007). These rules state that poor absorption/permeation are more likely when there are more than

five hydrogen bonding donor sites (e.g. hydroxyl and amine functional groups attached to the drug molecule) and more than ten acceptor sites (e.g. lone oxygen or nitrogen). As well as this the rules suggest that a large molecular weight coupled with a lipophilicity larger than five can cause poor metabolism. Compound classes that are substrates for biological transporters are exceptions to the rules. The rules are simple and easily applied in the screening of drugs but this can lead to them being misused (Zhang and Wilkinson, 2007). The other issue with these rules is that they exclude natural products and overemphasise oral bioavailability. Zhang and Wilkinson (2007) argued that such a dependence on this could mean that useful drugs may be disregarded due to poor oral bioavailability e.g. Penicillin G. This drug has to be given through an intramuscular injection to maximise efficacy. As such it should be used as a rule of thumb rather than a strict testing procedure (Ekins et al., 2000).

2.1 ADME

Pharmacokinetics is a method of characterising the processes of drugs using the headings of Absorption, Distribution, Metabolism and Elimination (ADME) (Ahmad, 2007). These four processes are able to separate the different mechanisms of action for drugs so that models can be developed.

2.1.1 Absorption

Absorption of a drug is affected by both physiological and physiochemical properties. The physiological attributes are processes such as blood flow rate and first pass metabolism in the human body that vary from species to species. Physicochemical factors are the intrinsic properties of the drugs such as lipophilicity (LogP) which do not vary across species (Lin, 1998).

This process does not affect metabolism of drugs that are given in an intravascular method e.g. intravenously (i.v.). This is due to its immediate effect on the biological system it was applied to (Ahmad, 2007).

2.1.2 Distribution

Distribution rate is what governs the speed by which the drug enters organs and tissue and is controlled by blood flow perfusion rate. It is believed that only an unbound drug can diffuse across the cellular membrane (Yang et al., 2006). Drug distribution is usually thought of in terms of volume of distribution or V_d which is defined as the ratio of drug in the body to that within the blood or plasma (Lin, 1995).

The five main physiological properties that influence the extent to which a chemical distributes through the human body are (Clewell et al., 2002) body composition, blood flow, plasma binding proteins, tissue-protein concentration and fluid pH.

2.1.3 Metabolism

Metabolism as a process is similar across species from an evolutionary standpoint due to a common ancestor, so only environmental adaptation can change this method. For example, Cytochrome P450 (CYP) enzymes have all evolved from the same ancestral gene to the present superfamily. As was shown in Chapter 1, interspecies differences do exist for CYP enzymes and the inhibition and induction preferences also differ (Lin, 1998). Out of the four processes, metabolism is the most difficult to model in silico since there are minimally a hundred (Beresford et al., 2002) drug metabolising enzymes to account for (Dickins and van de Waterbeemd, 2004).

Metabolism can be affected by drug-drug interactions since they can cause inhibition or induction of drug metabolising enzymes like CYP. This information is relevant to models since this can affect the course of the drug and the time it takes to be metabolised in the body (Ahmad, 2007).

2.1.4 Elimination

Elimination processes are the methods by which drugs and their metabolites are expelled from the human body. Examples of these are through urine and/or bile but this depends on the pharmacological nature of the drugs. Hepatic and renal processes control these and elimination can be modelled using saturable kinetics such as Michaelis-Menten (Ahmad, 2007). Saturable kinetics is usually used with enzymes since normally the substrate is dependent on the enzyme concentration and as such this can be a limiting factor. As most of these processes seem to vary across species it is understandable that extrapolation from one species to another in order to predict a drug's behaviour may not be the best approach due to limited data (Ito et al., 1998). Due to this many scientists have been trying to discover a way to scale the gap so that animal data can be used to predict drug processes in the human body and this can be done under pharmacokinetic principles (Lin, 1995).

2.2 QSAR Models

Another type of predictive model is the Quantitative Structure-Activity Relationship (QSAR) or Quantitative Structure-Property Relationship (QSPR), which provides insights into the molecular properties of drugs (Mager, 2006). For example, physicochemical and molecular properties can be correlated with drug concentrations to investigate pharmacological responses e.g. EC_{50}. These studies

have been used since the 1960s with physicochemical and biological data (van de Waterbeemd and Gifford, 2003).

These models show what happens when certain properties such as lipophilicity etc. change, and predict the binding affinity or the toxic potential of the structure. This approach has been used extensively and Lill (2007) shows how this method can be used in multidimensional studies. The method has a high throughput but only provides low level information (Cai et al., 2006) and tends to reject molecules without giving guidance on the properties needing optimisation.

2.3 Compartmental and PBPK Models

Physiologically Based Pharmacokinetics (PBPK) are models made up of a series of equations simulating the concentration of the parent compounds and metabolites in various compartments (of the body) (Flynn et al., 1996).

Hunt et al. (2006) show that drug data is usually analysed by assuming that the human body can be split into abstract compartments or in PBPK organs by compartments connected by a vascular system. This is useful since it can simplify the problem into smaller areas in which to get relevant pharmacokinetic parameters. These models integrate data from *in vitro* sources and physicochemical parameters to create a physiologically based whole body model when using an ADME basis (Lüpfert and Reichel, 2005). This is useful since it gives better realism in pharmacological studies.

Poulin and Theil (2000) developed a method of predicting the tissue:plasma partition coefficient using regression analyses. This has allowed PBPK modelling to be used in earlier stages of drug discovery. This was not possible before because predictions for new drug candidates could not be estimated as it was too time consuming and cost intensive using QSPR and *in vitro/vivo* data.

PBPK modelling can be used to quantify the potential impact of pharmacokinetic

aspects in inter-individual susceptibility (Clewell et al., 2002). The drawback to using PBPK modelling is that the data are required *a priori* in order to develop the model. If these data or other assumptions are faulty in any way, this can cause the model to be invalid.

Drug discovery is not the only area of research this methodology is used for - it is also used in risk assessment by government agencies such as the Environmental Protection Agency (EPA) in the US (Chiu et al., 2007). This is because for toxicity studies it is sometimes not possible to measure the problem directly. PBPK models are useful in these cases since they are independent of exposure route.

The advantage to this approach is that although it requires a large amount of parameters and physiological data specific to the species and compound, the model is applicable to all mammalian species (Leahy, 2004).

An example of PBPK modelling is given in the work of Keys et al. (2003) in an attempt to model Trichloroethylene (TCE) in rats and mice. A six-compartment model is used, which includes the lung, slowly and rapidly perfused tissues, fat, kidney and liver. This chemical has been extensively studied over the past 25 years and the paper covers different models used, both compartmental and PBPK.

Chapter 3

Compartment Models

3.1 Introduction

This type of modelling is widely used in pharmacokinetics, as it is a means of reducing complexity in drug metabolism problems. The simplest model is one with a single well-mixed compartment, which is used mostly to describe intravenous administrations since transfer into the blood system is assumed to be 100%. As such there is no need for an absorption phase to be taken into account such as there would be with oral or intraperitoneal administrations. This is due to the need for the oral drug to be absorbed through the Gastro-Intestinal (GI) tract membranes (Smith et al., 2001) and the intraperitoneal injection needs to pass out of the peritoneal membrane surrounding the abdominal cavity.

Recently there has been a focus on Whole Body models since this approach would give a better idea of where the metabolism takes place if all systems are taken into account (Lüpfert and Reichel, 2005). As such compartments are assigned to the lungs, heart, liver, kidney etc. and pharmacokinetic parameters for each are found experimentally or assigned arbitrarily. Techniques for retrieving this data are usually done *in vitro* with some more recent studies doing experiments *in vivo* (Lombardo et al., 2002) as well since converting parameters (Baranczewski

et al., 2006) from one to the other have been unreliable (Chiu et al., 2007). Other methods include trying to find parameters by reproducing a verified set of data (Curis et al., 2009). The other problem for this experimental data is that sometimes the particular animal used is not a good representative of the modelled animal. For example, using rat data to predict parameters for a human model (Harris and Barton, 2008) may be partially similar in mechanism in the body but the differences could cause errors in the estimation and therefore a better understanding is needed to account for these.

Grass (1997) used a two compartment STELLA (Structural Thinking Experimental Learning Laboratory with Animation) model in order to analyse the drugs ketorolac and ganciclovir. This model is a physiologically based formulation used to describe dynamics in the gastro-intestinal tract. The parameters were simulated from *in vitro* data including animal cultures and used to predict oral drug absorption in humans.

A review of modelling techniques including oral administrations with respect to metal metabolism is outlined in Curis et al. (2009). This paper outlines the advantages and disadvantages of different models as well as the need for "dummy" compartments that have no strict use as they represent the absorbed from and excreted to compartments. The paper presents the mammalian model for humans, which is generally a compartment representing blood or plasma with peripheral sections for organ systems that are relevant to the drug in question.

Doan and Boje (2000) analyse several different pharmacokinetic models with reference to the endogenous inhibitors and their effect on drug half-lives and concentration. They investigate this by using compartment models and different administration techniques for the inhibitor. This includes oral and bolus with the oral ingestion of food, which contain the inhibitor. The parameters in this case were found using data from literature sources from experiments on rats which

were given aspartame.

The oral administration of CHS 828, a cancer agent on rats, was analysed by Friberg et al. (2005) using a one-compartment model. The study investigated the effect of change of therapeutic schedule on drug efficacy on breast cancer cell lines.

Flynn et al. (1996) used a Physiologically Based Pharmacokinetic (PBPK) model with a number of compartments in order to analyse ethanol metabolism in mice after an intraperitoneal injection. This approach uses mass balance equations to track both parent and metabolite compounds over time per compartment. This allows a greater insight into the effect of certain organ systems on ethanol concentration. This approach is still used within this area of research although better parameter estimates are still needed (Ramchandani et al., 2001).

Unlike the previous example, Yu et al. (1999) used a one-compartment model for the metabolites in their experiments. They were investigating Cyclophosphamide and Ifosfamide in rats with reference to Cytochrome P450 catalysed metabolism with respect to phenbarbital pre-treatment. These drugs were given as intraperitoneal injections but since they were modelling the metabolites, the one compartment approach is equivalent to a two compartment approach since there is a phase of metabolism prior to the data used.

3.1.1 Administration techniques

The experimental data provided by CXR Biosciences were taken from procedures on both Hepatic Reductase Null (HRN) and wild type mice (three of each). The drugs were given through intraperitoneal injection and oral administration. An intraperitoneal injection is used in experiments on small rodents since they are very small and so have limited muscle mass and small veins (Fox et al., 2006). As such it is easier to inject into the peritoneum since intravenous and intramuscular

administrations are not so possible. In the case of Tamoxifen, the drug is given orally which means that all the drugs are subject to extravascular modelling and as such need more than one compartment to describe the dynamics.

3.1.2 Wild-type and Hepatic Reductase Null mouse

HRN mice are missing the hepatic Cytochrome P450 system but bred so that they are still viable and fertile. These mice are useful as they give one the opportunity to study the metabolism pathways taken by the drug. Through this method it is also possible to gain an insight as to whether the main metabolism of a drug happens in the liver, gastro-intestinal tract, extrahepatically etc. An unexpected consequence of deleting hepatic Cytochrome P450 reductase was the discovery that the P450 content of the liver was increased by approximately a factor of five. These mice help investigate the toxicokinetics of compounds which can show the side effects associated with a drug. This is especially useful when the drug has a narrow therapeutic window, for example, anti-cancer drugs (Henderson et al., 2006). Cyclophosphamide has been pharmacokinetically examined using the Cytochrome P450 reductase null mouse (Pass et al., 2005).

3.1.3 Specific Drugs

Data from experiments with the wild type and Hepatic Reductase Null mouse were made available from CXR Biosciences. This was in order to help find out the differences in metabolic properties for the two mice. There were ten sets of drug data and these were for Caffeine, Dextromethorphan, Diclofenac, Gefitinib, Imatinib, Midazolam, Omeprazole, Paclitaxel, Tamoxifen and Thalidomide.

Caffeine

Caffeine is a naturally occurring substance found in a number of food products including coffee, tea and alcoholic beverages (Wishart et al., 2006). It is also available as a drug - as a stimulant or within analgesics since it increases various numerous neurotransmitters (Kot and Daniel, 2008) and as such it can affect behaviour in terms of mood and attention. It affects many different systems in the human body causing relaxation in smooth muscle, increased heart rate through cardiac muscle stimulation and also has a diuretic affect (Wishart et al., 2006). It is metabolised by two isoforms of Cytochrome P450 (CYP) namely 1A2 (Lewis, 2000) which is found in the hepatic system. This drug was given as an intraperitoneal injection to the mice and the dose was 1 mg of caffeine per kg body mass (mg/kg).

Dextromethorphan

This drug can be found in a number of cold and flu remedies since it acts as a cough suppressant by acting on the cough centre in the medulla (Wishart et al., 2006). Dextromethorphan itself is not an addictive substance even though it is an opiate analog (Ziaee et al., 2005) but has been increasingly abused by adolescents. People who are dependent on illicit drugs like heroin and other opiates sometimes use it in combination with them. This drug is absorbed from the gastrointestinal tract quickly into the bloodstream and is subject to first pass metabolism through the hepatic portal vein. As such the availability of this drug would be quite short since its presence and that of its metabolites is short lived. The CYP enzymes associated with this drug are 3A4 and 2D6 (Felmlee et al., 2008), which are found in both hepatic and extrahepatic systems like the small intestine. The drug is given as an intraperitoneal injection of 1 mg/kg dose.

Diclofenac

This non-steroidal anti-inflammatory drug (NSAID) is used in the treatment of rheumatic diseases like arthritis and as an analgesic to help with fevers and headaches (Yang et al., 2006; Bort et al., 1999). It is supposed that its analgesic properties come from desensitising prostaglandin controlled pain receptors. It is also believed that action in the hypothalamus results in heat dissipation in the body and therefore control of fevers (Wishart et al., 2006). The enzymatic metabolism of this drug is controlled by CYP2C8 (Venkatakrishnan et al., 2001) and CYP2C9 (Lewis, 2000), which are primarily found in the hepatic system. The drug was administered by an intraperitoneal injection of 1 mg/kg.

Gefitinib

This drug is an epidermal growth factor receptor (EGFR) inhibitor and as such is used to treat many human cancers (Chang et al., 2008). In lung and breast cancers EGFR is overexpressed and this can lead to uncontrolled cell proliferation and this is why this drug is important in cancer treatment. This drug is metabolised by CYP3A4 (Scripture et al., 2005), which means this must take place in the liver or small intestine since this is where this enzyme can be found. As with the previous drugs the substance is injected into the peritoneum with a dose of 5 mg/kg.

Imatinib

This antineoplastic agent is used in the treatment of Chronic Myelogenous Leukaemia (CML) and GastroIntestinal Stromal Tumours (GISTs) (Wishart et al., 2006). It inhibits tyrosine kinase activity for Platelet Derived Growth Factor (PDGF) and Stem Cell Factor (SCF) and inhibits proliferation and induces apoptosis in GISTs (Breccia and Alimena, 2009). When it comes to metabolising enzymes

there are five that are associated with the possible breakdown of this substance and these are the CYP enzymes: 1A2, 3A4, 2C9, 2C19 and 2D6 (van Schaik, 2008; Scripture et al., 2005). The intraperitoneal injection is given with a dose level of 10 mg/kg.

Midazolam

This drug is a short-acting hypnotic-sedative drug that is commonly used in dentistry, endoscopy and in combination with local anaesthesia (Wishart et al., 2006). It is frequently used in palliative care as a sedative or anticonvulsant (Morita et al., 2003). It is supposed to be used over short periods of time with the longest time of use reported being 35 days. It is a benzodiazepine that acts as a central nervous system depressant and as such has pharmacodynamic properties including amnesia and sedation (Wishart et al., 2006). It increases (gamma)-amino butyric acid (GABA) activity, which causes a calming effect resulting in sleep. This drug is metabolised by CYP3A4 (Lewis, 2000) that is found in the liver and small intestine. As with the previously mentioned drugs this is given by intraperitoneal injection of 1 mg/kg.

Omeprazole

This drug inhibits the gastric acid secretion in order to treat gastro-duodenal ulcers (Bosch et al., 2007) and works to eradicate the *Helicobacter pylori* when combined with other drugs (Kuipers and Klinkenberg-Knol, 1999) as restriction of acid is only one attack against this bacterium. In removing this bacterium it reduces the possibility of ulcer recurrence (Wishart et al., 2006). The Cytochrome P450 enzymes associated with the metabolism of this drug are 2C19 (Lewis, 2000) and 2C8 (Martínez et al., 2005). CYP2C19 is polymorphic and as such can cause issues when it comes to drug therapy since a poor metaboliser would either have

a reduced or heightened reaction to the drug. In the case of Omeprazole the poor metabolisers have a better response when it comes to the removal of *H. pylori* (Rogers et al., 2002) since it causes the drug to have a better efficacy due to slower metabolism. This drug is given through an intraperitoneal injection of 1 mg/kg.

Paclitaxel

Paclitaxel (or Taxol) was first reported in a paper by Wani et al. (1971) and it was isolated from the pacific yew tree and the antileukemic and tumour inhibitory activity was suggested due to structure. It is associated with the therapy of ovarian, breast and various other cancers (Wishart et al., 2006). As a compound it has unfavourable properties such as low permeability and solubility and as such it is poorly absorbed from oral administration (Choi et al., 2006). The CYP enzymes associated with Paclitaxel metabolism are 3A4 (Scripture et al., 2005; Smith et al., 2001) and 2C8 (Martínez et al., 2005), which are found in the liver and small intestine (3A4). The drug is given as an intraperitoneal injection of 10 mg/kg.

Tamoxifen

According to DrugBank Tamoxifen is a multi-functional compound acting as an anti-estrogen in mammary tissue but can induce estrogen in cholesterol metabolism. As such it belongs to the selective estrogen receptor modulators (SERMs) class of drugs. This drug has been used in the fight against early and advanced breast cancer for the past thirty years and as such has become a benchmark for up and coming endocrine therapies to be measured against (Clemons et al., 2002). However this drug does have risk of developing endometrial carcinoma but this has not stopped it from being the frontline treatment for hormone-responsive breast

cancer (Singh et al., 2007). This drug is metabolised by six different CYP strains - 1A2, 3A4, 2C9, 2D6, 2E1, and 2B6 (Scripture et al., 2005; Cozza et al., 2003; Tredger and Stoll, 2002; van Schaik, 2008) - these strains are found both hepatically and extrahepatically. This drug is given by oral administration at a dose of 10 mg/kg.

Thalidomide

This compound was initially used as a non-barbiturate hypnotic but it had to be removed from distribution due to teratogenic effects. It is currently used for inflammatory and immunological disorders as it shows immunosuppressive activity (Wishart et al., 2006). In addition to this it shows anti-angiogenic activity, which might mean it can be used as part of cancer therapy. Although many of the effects of the drug have been documented there is still a lot more information about its mechanism of action required (Strasser and Ludwig, 2002). Recently there has been research with zebrafish in Japan that has isolated the protein that caused the birth defects in the children of Thalidomide patients (Ito et al., 2010). The Cytochrome P450 enzyme responsible for Thalidomide metabolism is 2C19 (Ando et al., 2002) and this is found in the liver and is subject to polymorphisms as was mentioned with reference to Omeprazole. This drug was given by intraperitoneal injection with a dose of 20 mg/kg.

3.2 Mathematical Models and Method

Three different compartment models were applied to the ten sets of drug data.

3.2.1 Model 1: One Compartment

The first model from the sequential compartment models considers only one compartment y. This compartment represents the bloodstream in a normal intravenous dosing experiment i.e. that there is 100% transference of drug into the body no loss. This assumption enables us to solve the ordinary differential equation explicitly, returning an exponential decay solution. The drug is simply eliminated at a given rate and no passage from one compartment to another takes place (since there is only one compartment).

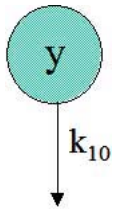

Figure 3.1: *Schematic diagram of the one compartment model.*

Using the Law of Mass Action, we obtain the following differential equation and general solution:

$$\frac{dy}{dt} = -k_{10}y \tag{3.1}$$

$$y = y(0)e^{-k_{10}t} \tag{3.2}$$

The k_{10} and $y(0)$ parameters were found using these explicit solutions with the non-linear least squares algorithm in the R statistical software. Although this is a very simplistic model, it gives a good way of evaluating the need for complexity in future models.

3.2.2 Model 2: Two Compartments

This model is slightly more accurate than the previous model, since now the drugs have an extravascular drug method either intraperitoneal or oral administration.

As such there should be an absorption phase into the bloodstream and then an elimination/excretion curve.

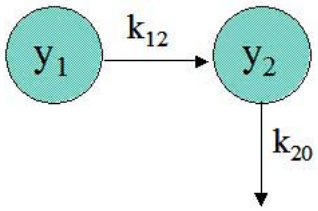

Figure 3.2: *Schematic diagram of the two compartment model.*

Once again, using the Law of Mass Action, the ordinary differential equations for the above model are:

$$\frac{dy_1}{dt} = -k_{12}y_1 \tag{3.3}$$

$$\frac{dy_2}{dt} = k_{12}y_1 - k_{20}y_2 \tag{3.4}$$

Within this model y_1 and y_2 represent the primary dosing site (e.g. mouth in oral administration) and the bloodstream respectively. The raw data is taken to represent the y_2 concentration. The explicit solutions for y_1 and y_2 are:

$$y_1(t) = y_1(0)e^{-k_{12}t} \tag{3.5}$$

$$y_2(t) = \frac{k_{12}y_1(0)(e^{-k_{20}t}e^{-k_{12}t})}{k_{12} - k_{20}} \tag{3.6}$$

This model is slightly more complicated than model 1 but it does have the right phases, which is necessitated under the dosage methods.

3.2.3 Model 3: Three Compartments

This model further extends model 2 through an extra compartment. The configuration and ordinary differential equations for this model are as follows:

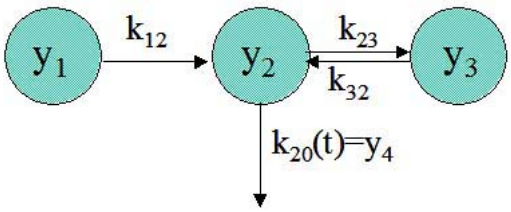

Figure 3.3: *Schematic diagram of the three compartment model.*

$$\frac{dy_1}{dt} = -k_{12}y_1 \tag{3.7}$$

$$\frac{dy_2}{dt} = k_{12}y_1 - k_{23}y_2 + k_{32}y_3 - y_4 \tag{3.8}$$

$$\frac{dy_3}{dt} = k_{23}y_2 - k_{32}y_3 \tag{3.9}$$

$$\frac{dy_4}{dt} = a \tag{3.10}$$

In this model the first and second compartments represent the same as in the previous model i.e. y_2 represents the bloodstream and y_1 the injection/dose site. As we can see there is a rate of absorption into the main compartment (y_2) indicated by k_{12}. From the main compartment there are two ways for the drug to be distributed – it can be passed into compartment three or be expelled from the system entirely. The expulsion rate from the main compartment is time dependent which means that if a is positive the rate increases as time increases and vice versa for when a is negative. Currently a is being taken as positive only. Compartment three represents lipid in the liver i.e. k_{23} is the rate at which the drug is stored and k_{32} is the rate at which it is released back into the system. The current assumption is that $k_{23} >> k_{32}$ i.e. that it is easier to get into compartment three than it is to leave.

The explicit solutions for this system are (including y_2 which was used to fit using

non-linear least squares to get the parameter values):

$$y_1(t) = y_1(0)e^{-k_{12}t} \tag{3.11}$$

$$\begin{aligned}
y_2(t) = {} & \frac{1}{2}(k_{32}+k_{23})^{-3}(-k_{32}-k_{23}+k_{12})^{-1}((2k_{23}^2e^{-(k_{32}+k_{23})t}a + 2e^{-k_{12}t}y_1(0)k_{32}^4 \\
& + 2k_{32}^3k_{12}y_1(0) + at^2k_{32}^4 - k_{32}^3at^2k_{12} - 2k_{23}k_{12}e^{-(k_{32}+k_{23})t}a + 2k_{23}^3e^{-(k_{32}+k_{23})t}k_{12}y_1(0) \\
& - 2y_1(0)k_{32}^4 - 2e^{-k_{12}t}y_1(0)k_{32}^3k_{12} + 2k_{23}e^{-(k_{32}+k_{23})t}ak_{32} + 2k_{23}atk_{32}^2 \\
& + 2k_{23}e^{-(k_{32}+k_{23})t}k_{12}y_1(0)k_{32}^2 + 4k_{23}^2e^{-(k_{32}+k_{23})t}k_{12}y_1(0)k_{32} - 2k_{23}atk_{32}k_{12} + k_{23}^3at^2k_{32} \\
& + 3k_{23}^2at^2k_{32}^2 + 3k_{23}k_{32}^3at^2 - k_{23}^2at^2k_{12}k_{32} - 2k_{23}k_{32}^2at^2k_{12} - 2k_{23}ak_{32} + 2k_{23}ak_{12} \\
& + 2ak_{23}^3t - 2ak_{23}^2 + 4ak_{32}tk_{23}^2 - 2ak_{23}^2tk_{12} - 2k_{23}^3y_1(0)k_{32} - 6y_1(0)k_{32}^3k_{23} - 6k_{23}^2y_1(0)k_{32}^2 \\
& + 2k_{23}^2k_{12}y_1(0)k_{32} + 4k_{12}y_1(0)k_{32}^2k_{23} + 6e^{-k_{12}t}k_{23}^2y_1(0)k_{32}^2 + 2e^{-k_{12}t}k_{23}^3y_1(0)k_{32} \\
& + 6e^{-k_{12}t}y_1(0)k_{32}^3k_{23} - 2k_{23}^3e^{-k_{12}t}k_{12}y_1(0) - 6k_{23}^2e^{-k_{12}t}k_{12}y_1(0)k_{32} - 6e^{-k_{12}t}k_{12}y_1(0)k_{32}^2k_{23})
\end{aligned} \tag{3.12}$$

$$\begin{aligned}
y_3(t) = {} & \frac{1}{2}(k_{32}+k_{23})^{-3}(-k_{32}-k_{23}+k_{12})^{-1}((-2y_1(0)k_{32}^3 - 2e^{-(k_{32}+k_{23})t}k_{23}a + k_{23}^3at^2 \\
& - 6k_{23}^2y_1(0)k_{32} - 2k_{23}^3y_1(0) - 2k_{23}^2at + 2k_{12}ak_{32}t - k_{12}k_{32}^2at^2 - 2k_{23}k_{32}at^2k_{12} \\
& - 2ak_{12} + 2e^{-(k_{32}+k_{23})t}k_{12}y_1(0)k_{23}^2 - 2k_{12}k_{32}^2e^{-(k_{32}+k_{23})t}y_1(0) + 2k_{23}a - 2k_{32}e^{-(k_{32}+k_{23})t}a \\
& - 2k_{32}^2at - 4k_{12}k_{32}k_{23}e^{-(k_{32}+k_{23})t}y_1(0) - 6y_1(0)k_{32}^2k_{23} + 2ak_{32} - 4k_{23}atk_{32} \\
& + 2e^{-k_{12}t}y_1(0)k_{32}^3 + 3k_{23}^2at^2k_{32} - k_{23}^2at^2k_{12} + 3k_{23}k_{32}^2at^2 + 2k_{23}ak_{12}t - 2e^{-(k_{32}+k_{23})t}ak_{12} \\
& + 4k_{32}k_{12}y_1(0)k_{23} + 6e^{-k_{12}t}k_{23}^2y_1(0)k_{32} + 6e^{-k_{12}t}k_{23}y_1(0)k_{32}^2 + 2k_{23}^2k_{12}y_1(0) \\
& + 2e^{-k_{12}t}k_{23}^3y_1(0) + 2k_{12}y_1(0)k_{32}^2 + k_{32}^3at^2)k_{23})
\end{aligned} \tag{3.13}$$

$$y_4(t) = at \tag{3.14}$$

3.3 Results

For each drug the model parameters are compared and contrasted with the Wild Type (WT) and HRN mouse. The plots show the average drug data (over three

mice) and the fitted model. The fit was assessed using the Akaikes Information Criterion (AIC) and a paired t test on each average data set compared with the each of the fitted models. The t test was also used with each mouse individually to see whether the average data was truly representative of the mice. The Akaikes Information Criterion is defined as:

$$AIC = 2k - 2log(L) \tag{3.15}$$

Where k is the number of parameters used to fit the model and L is the likelihood function. For this statistic the smaller and more negative the AIC the better the fit of the model. The paired t test is a hypothesis test using the t-distribution on the following:

$$H_0 := \bar{d} = 0 \tag{3.16}$$

$$H_1 := \bar{d} \neq 0 \tag{3.17}$$

For the purposes of this thesis the t probability values will be taken from a $t_{61-1} = t_{60}$ distribution. The test statistic is:

$$T = \frac{\bar{d}}{\frac{s.e.}{\sqrt{n}}} \tag{3.18}$$

Where $\bar{d}$ represents the average of the differences between the two data point sets, s.e. stands for the standard error of the differences and n is the number of data points. If the individual tests have similar results to that of the average then stronger conclusions can be drawn from the models than if the test statistics are very different from the average statistic. As well as these tests it was necessary to test the assumption for using non-linear least squares for fitting the parameters. This assumption is that the residuals are distributed normally and this was

assessed using a Shapiro-Wilks test in combination with a Quartile-Quartile plot (this is because the test lacks power). A runs test (which analyses systematic deviance from the model) was also run from the nls testing suite in R.

3.3.1 Caffeine

The model parameters for this drug are shown in table.

Parameters		WT	HRN	Ratio (3dp)	S-W	QQ	Runs
Model 1	y(0)	1662.21	1810	1:1.089	✓	✓	✓
	k_{10}	0.7471755	0.0517	1:0.069193918			
Model 2	$y_1(0)$	1656.924	2063.533	1:1.245	✓	✓	✓
	k_{12}	234.9226	6.631757	1:0.028			
	k_{20}	0.7471753	0.08870665	1:0.119			
Model 3	$y_1(0)$	1654.457	2035.918	1:1.231	✓	✓	✓
	k_{12}	129.4292	6.821051	1:0.053			
	k_{23}	0.7506233	0.07261716	1:0.097			
	k_{32}	0.002020398	0	1:0			
	a	0	7.6506	0:1			

Table 3.1: *Caffeine Model Parameters and outcomes at the 5% level from the Normality Assumption tests (S-W = Shapiro-Wilks Test and QQ = Quartile-Quartile Plot) and Runs Test.*

The normality assumption is satisfied in all three fitted models plus there is no evidence from the runs test of systematic deviance in the data from the fitted models.

Model 1

For model 1 there is a large difference between the k_{10} parameter values - the excretion rate is roughly 7% of the value in the HRN model than the WT. As well as this difference there is an increase in the initial value in the compartment of about 8.9% between the WT and HRN models.

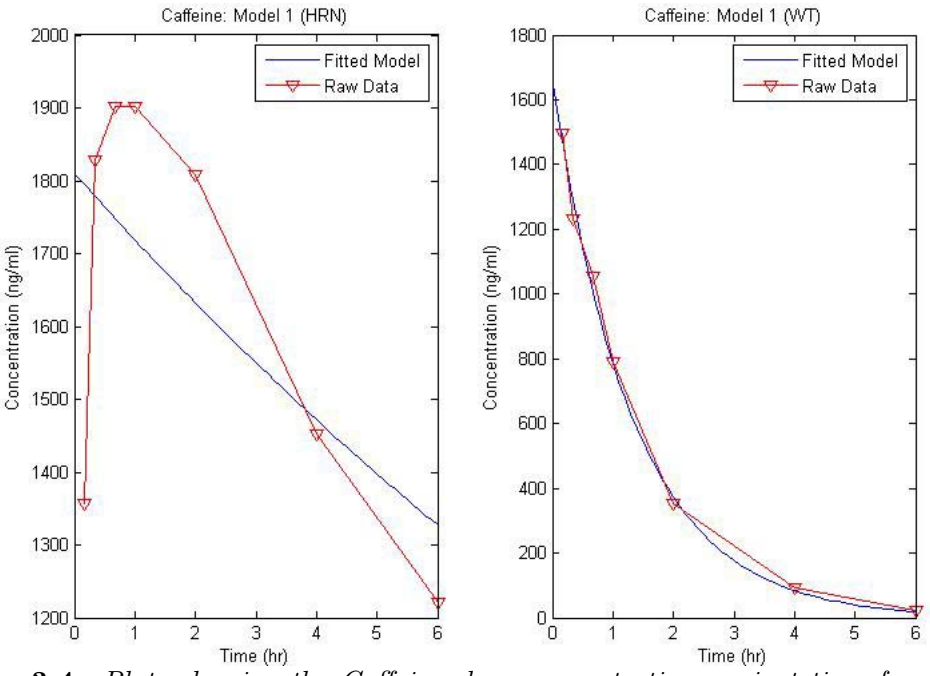

Figure 3.4: *Plots showing the Caffeine drug concentration against time for the raw data (▽) and computational simulation results (solid line) from Model 1.*

The fit for the Wild Type mouse model is much better than that of the HRN mouse. This suggests that the drug activity could be assessed as excretion only for the WT mouse but has some absorption in the HRN mouse.

Model 2

For model 2 the parameters show a large difference between the WT and HRN mouse. The transfer rate between the two compartments, which represents absorption, in the HRN is roughly 2.8% of the rate that is apparent in the WT. However the excretion rate is approximately 11.9% of the magnitude in the Hepatic Reductase Null mouse than that of the Wild Type. For the initial concentration in compartment 1 there is a 24.5% increase in value for the HRN model in comparison to the WT.

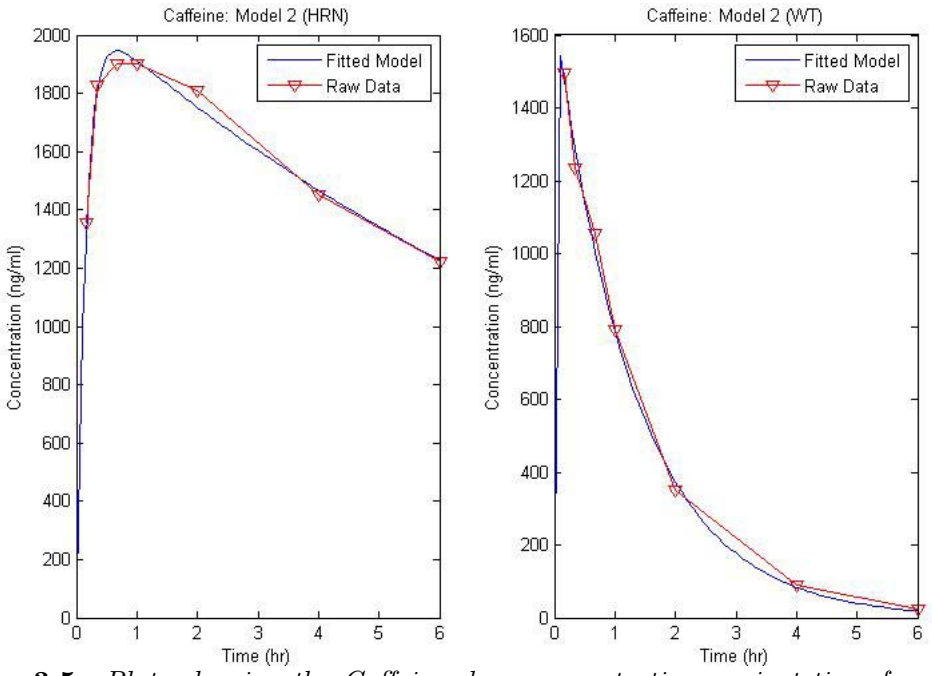

Figure 3.5: *Plots showing the Caffeine drug concentration against time for the raw data (▽) and computational simulation results (solid line) from Model 2.*

For this model, the fit for both sets of data is good but since the WT data shows a very fast absorption rate this means that the model has been fitted with a pointed peak.

Model 3

In model 3 all the parameters have been chosen so that the visual fit is better. The parameter k_{12} shows that the absorption rate in the HRN mouse is 5.3% of that of the normal WT mouse. This suggests that the absorption of Caffeine into the bloodstream (y_2) occurs at a reduced rate in the HRN mouse. The transfer rates into and away from compartment y_3 (k_{23} and k_{32}) represent a delay in the system. For k_{23} there is a marked difference being roughly a tenth of the WT value in the HRN model but for k_{32} the values are very small with the value in the HRN being zero. This means that for caffeine both mouse types show that it is easier to get into compartment y_3 than leaving it, which is the original assumptions of the model. For the time dependent excretion rate out of the bloodstream

(y_4) the parameter values have a similar shift to that of k_{32} i.e. the WT value is zero and the HRN is non-zero. As with the other two model configurations there is a difference in initial concentration for compartment 1 - in this model this change is a 23.1% increase in the HRN model.

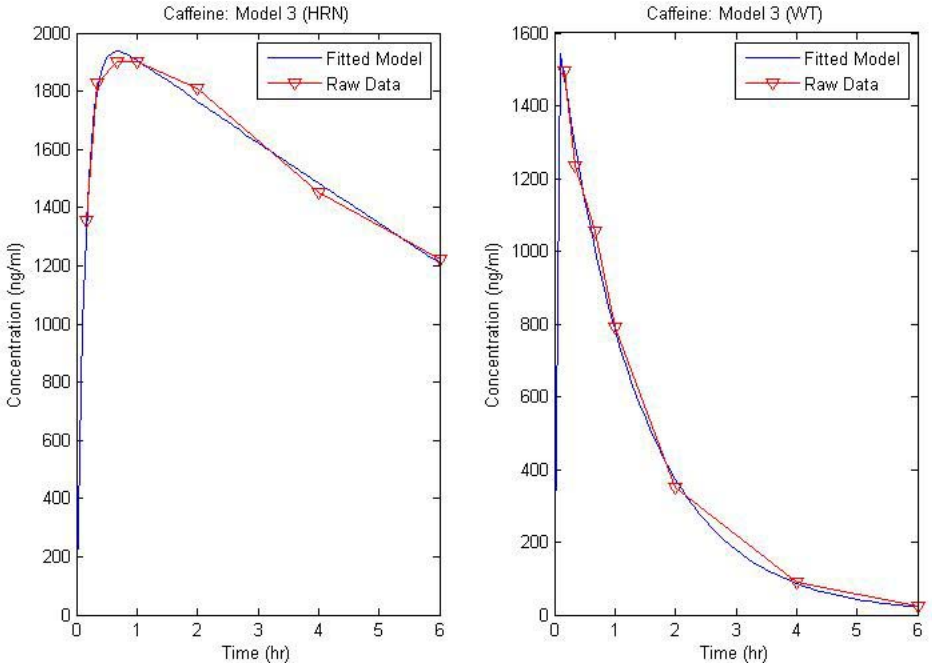

Figure 3.6: *Plots showing the Caffeine drug concentration against time for the raw data ($\bigtriangledown$) and computational simulation results (solid line) from Model 3.*

The fitted model follows the behaviour for both the wild type and HRN average mouse data quite effectively.

Data	Average	Model 1	Model 2	Model 3
HRN	-	0.99561641 *100.3834*	0.981338625 *75.63368*	0.97907404 *78.56304*
Mouse 1	0.07697907	0.149111088	0.026101267	0.026044594
Mouse 2	0.083316555	0.130935742	0.036826644	0.036278197
Mouse 3	0.836869228	0.885573384	0.778813372	0.777755126
WT	-	0.95614507 *74.46273*	0.956147316 *76.46273*	0.999998332 *80.44003*
Mouse 4	0.675740077	0.901204918	0.90120611	0.925762665
Mouse 5	0.037645727	0.010019816	0.010019833	0.011451952
Mouse 6	0.065269961	0.042006574	0.042006532	0.038551134

Table 3.2: *Caffeine - Paired t Test p-values and AIC (Akaike's Information Criterion) values.*

From this table the results of paired t tests between the average data can be seen, fitted values from each of the models and the data from each mouse either HRN or WT. The comparison test between the average data and each mouse gives an indication of how well the average data emulates the behaviour of the mice. The AIC values allow the fit to be assessed while taking into account the number of parameters used to fit the model.

For the WT mouse the model that best fits is model 1 since it has the smallest AIC value even though the paired t test shows that the data from all three fitted models show a non-significant result (do not reject $H_0 : \bar{d} = 0$) when compared to the average data. For the HRN mouse, model 2 is the best for the same reasons. From the table it can be seen that the average raw data differs significantly for mouse 5 in comparison to the WT average mouse data.

3.3.2 Dextromethorphan

The model parameters for this drug are:

Parameters		WT	HRN	Ratio (3dp)	S-W	QQ	Runs
Model 1	y(0)	71.6441	72.27797	1:1.009	✓	✓	✓
	k_{10}	0.5907	0.29669	1:0.502			
Model 2	$y_1(0)$	71.60792	78.4644	1:1.096	✓	✓	✓
	k_{12}	1169.469	9.19685	1:0.008			
	k_{20}	0.5907452	0.352626	1:0.597			
Model 3	$y_1(0)$	70.87566	2336.9234	1:32.972	✓	✓	✓
	k_{12}	263.1207	0.3181	1:0.001			
	k_{23}	0.5695108	9.6475	1:16.940			
	k_{32}	0	0	1:1			
	a	0.2565778	5.3846	1:20.986			

Table 3.3: *Dextromethorphan Model Parameters and outcomes at the 5% level from the Normality Assumption tests (S-W = Shapiro-Wilks Test and QQ = Quartile-Quartile Plot) and Runs Test.*

The normality assumption for the non-linear fitting is satisfied and the runs test shows that there is no evidence of systematic deviance in all three models.

Model 1

For model 1 the initial values are similar but with a difference of 0.9% between the HRN and wild type mouse. However for the parameter k_{10} the HRN value is 50.2% of the value suggesting that absorption is slower than in the WT.

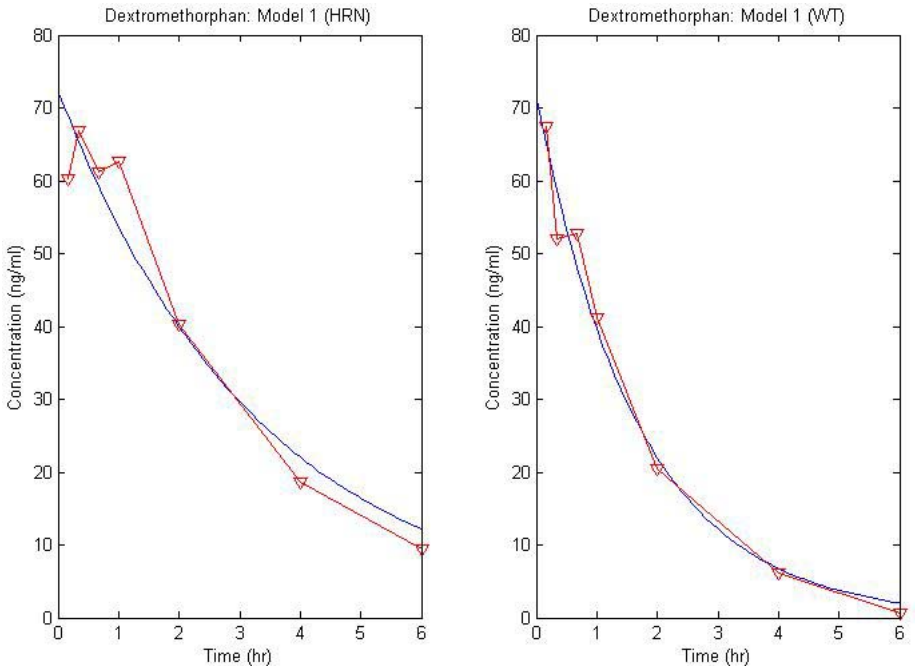

Figure 3.7: *Plots showing the Dextromethorphan drug concentration against time for the raw data (▽) and computational simulation results (solid line) from Model 1.*

The fit of this model for both sets of data is quite good however the HRN data does show an absorption phase.

Model 2

The parameters for the model show differences between the HRN and WT mice. The parameter values are all smaller for the HRN in comparison to the wild type. The initial concentrations differ by a factor of 9.6%, the absorption by 0.8% and elimination by 59.7%.

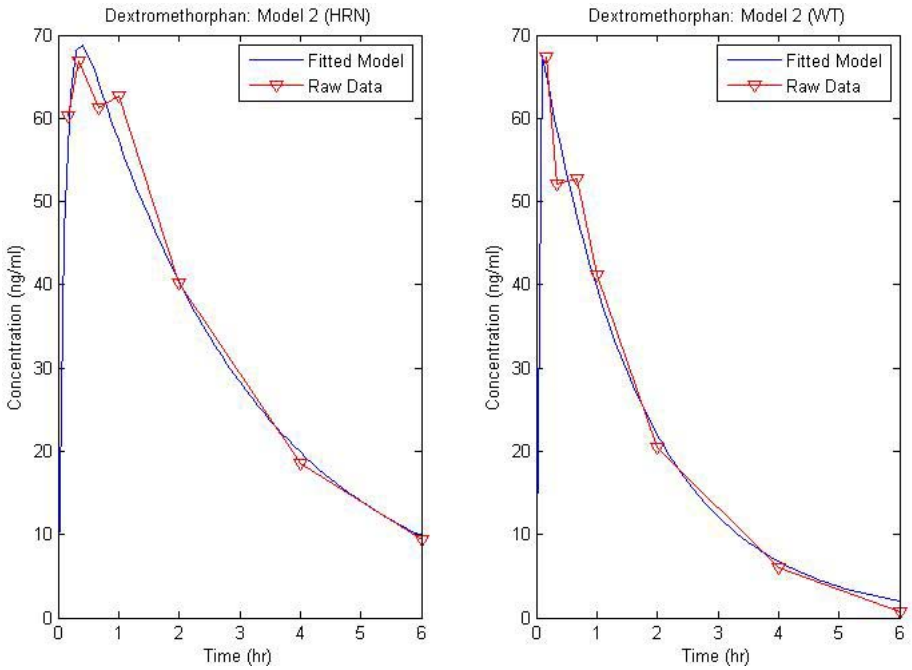

Figure 3.8: *Plots showing the Dextromethorphan drug concentration against time for the raw data (▽) and computational simulation results (solid line) from Model 2.*

The fit of these models to the raw data is good since there is similarity in behaviour.

Model 3

For the model 3 parameters the initial concentration in the HRN is roughly 33 times that of the WT and time dependent excretion is roughly 21 times. When it comes to the parameters associated with compartment 3 (k_{23} 17 times the value in HRN than in WT and k_{32} is zero in both mice. The absorption parameter k_{12} is 0.1% of the wild type value in the transgenic mouse.

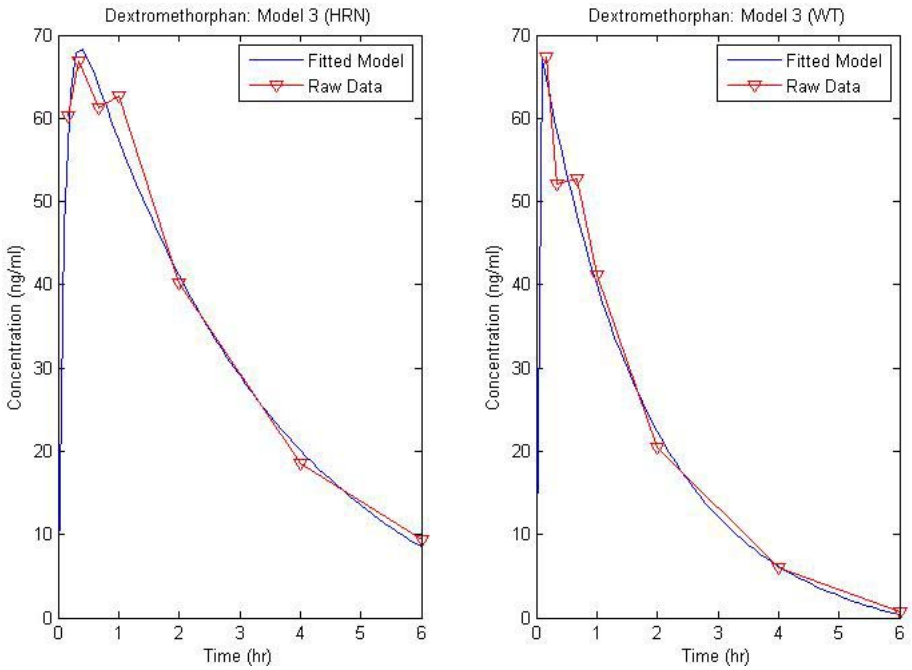

Figure 3.9: *Plots showing the Dextromethorphan drug concentration against time for the raw data (▽) and computational simulation results (solid line) from Model 3.*

The fit of this model to both mouse datasets is good. The behaviour of the averaged data shows two peaks, which is not shown through the fitted model. This shows that another time scale may be involved in the metabolism of this drug.

Data	Average	Model 1	Model 2	Model 3
HRN	-	0.880505718 *48.57802*	0.940079609 *40.85807*	0.998254187 *44.39718*
Mouse 1	0.022137418	0.039685659	0.022994648	0.02426086
Mouse 2	0.063085991	0.090636072	0.090340626	0.086546615
Mouse 3	0.1298626	0.107750331	0.090819984	0.081782114
WT	-	0.856740187 *42.85487*	0.856741514 *44.85487*	0.988181302 *48.52601*
Mouse 4	0.034496768	0.119793258	0.119793021	0.097660591
Mouse 5	0.205744262	0.223123768	0.223123853	0.254867031
Mouse 6	0.90150981	0.848116361	0.848116885	0.891413375

Table 3.4: *Dextromethorphan - Paired t Test p-values and AIC (Akaike's Information Criterion) values.*

For this drug all three fitted models show non-significant results for the paired t test at the 5% level when compared to the average data. The AIC values suggest that model 2 is best for the HRN data whereas model 1 is best for the WT data. When it comes to comparing the mice to the average data one mouse of each type fails to show similarity (mouse 1 and mouse 4).

3.3.3 Diclofenac

For this drug the model parameters are:

Parameters		WT	HRN	Ratio (3dp)	S-W	QQ	Runs
Model 1	y(0)	2550.1905	2499.7354	1:0.980	✓	✓	✓
	k_{10}	2.492	2.6666	1:1.070			
Model 2	$y_1(0)$	2508.16	2346.5682	1:0.936	✓	✓	✓
	k_{12}	147.927	42.4162	1:0.287			
	k_{20}	2.491993	2.6703	1:1.072			
Model 3	$y_1(0)$	257538799	11508.58	1:4.469E-05	✓	✓	✓
	k_{12}	3.052991	3.573899	1:1.171			
	k_{23}	286084.9	16.13086	1:5.638E-05			
	k_{32}	0.1549957	0.1641611	1:1.059			
	a	4658412	205.6111	1:4.414E-05			

Table 3.5: *Diclofenac Model Parameters and outcomes at the 5% level from the Normality Assumption tests (S-W = Shapiro-Wilks Test and QQ = Quartile-Quartile Plot) and Runs Test.*

As can be seen from the final three columns the assumption of normality is valid and the data does not show systematic deviance from any of the models.

Model 1

For model 1 the HRN mice parameter values are roughly the same as that of the WT. For the initial concentration this value is 98% of the wild type and for the excretion rate it is an increase of 7%.

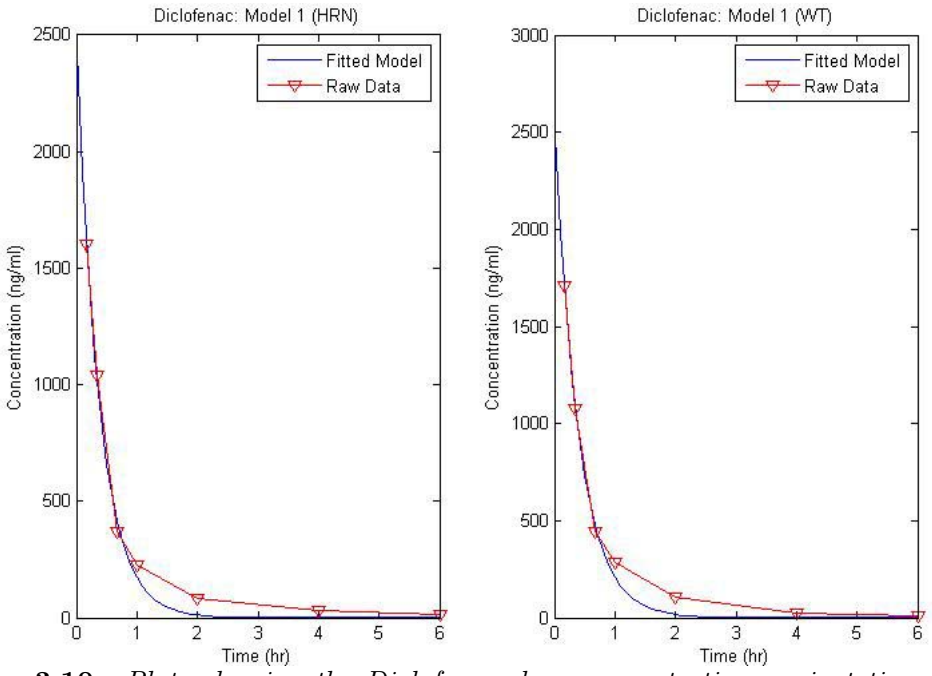

Figure 3.10: *Plots showing the Diclofenac drug concentration against time for the raw data (▽) and computational simulation results (solid line) from Model 1.*

The fit of this model is good at the start of the time period but not at the end where the fitted value is roughly half of the raw data.

Model 2

In the second model the parameters are quite different between the wild type and HRN mouse. For the initial concentrations the HRN model has a y(0), which is 93.6% of the wild type value. The HRN excretion rate however is 7.2% larger and the absorption rate is 28.7% of the wild type value.

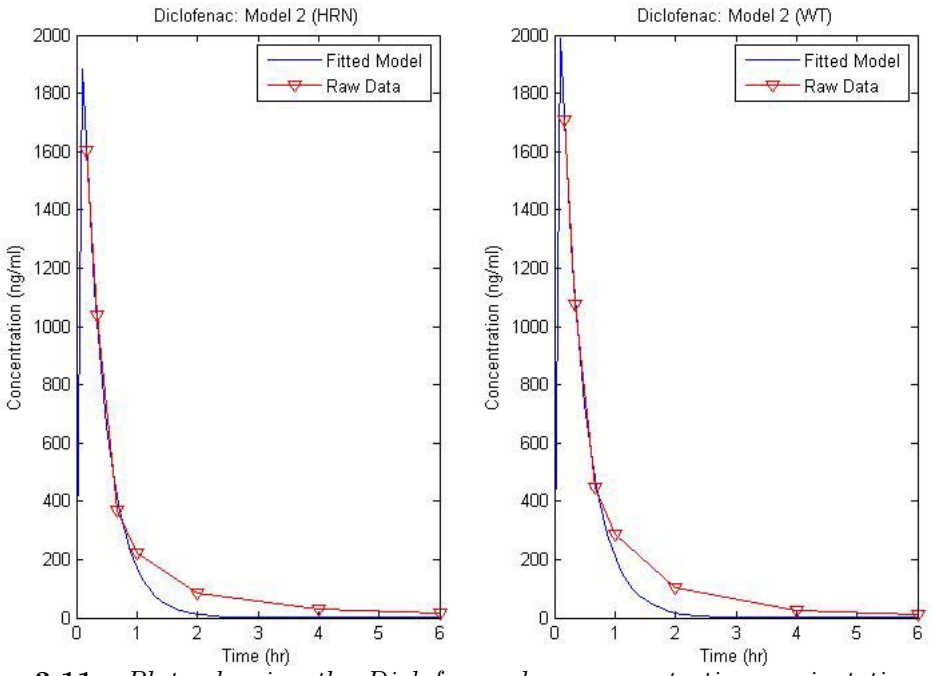

Figure 3.11: *Plots showing the Diclofenac drug concentration against time for the raw data ($\bigtriangledown$) and computational simulation results (solid line) from Model 2.*

This calculated model shows a jagged fit due to the very quick absorption and then the fit after the first hour is similar to that of model 1. This could be due to a change in time scale dynamics i.e. fast to slow.

Model 3

For the three-compartment model y(0), k_{23} and a show large differences between the sets of data. The difference between the other parameters is only slight - k_{12} changes by +17.1% and k_{32} by +5.9% from WT to HRN.

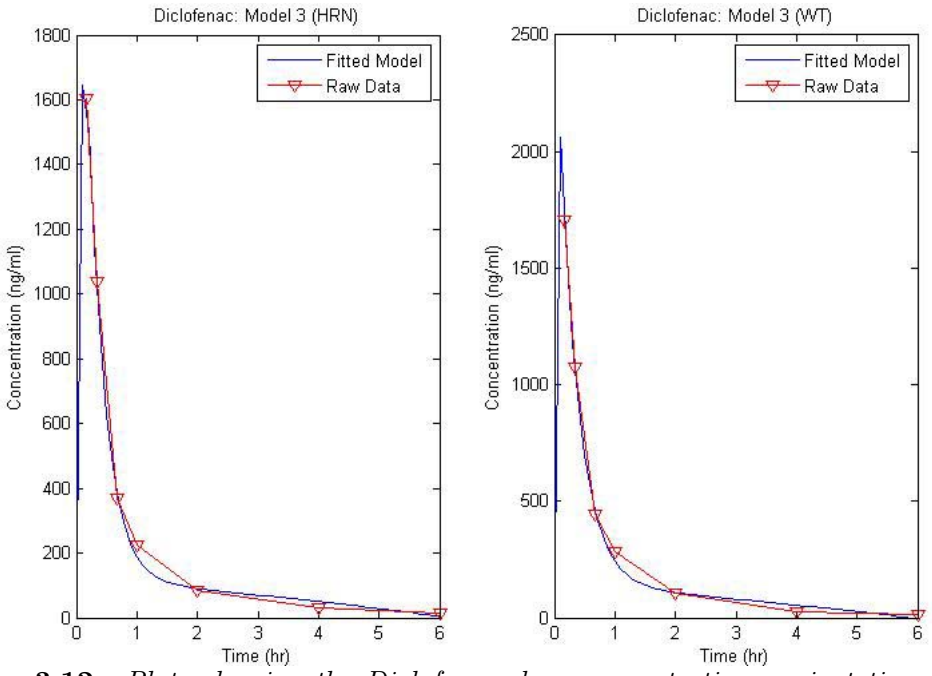

Figure 3.12: *Plots showing the Diclofenac drug concentration against time for the raw data (▽) and computational simulation results (solid line) from Model 3.*

The fit of model 3 is the best with the only deviation between the fitted model and raw data occurring between the 1-hour and 2 hours point.

Data	Average	Model 1	Model 2	Model 3
HRN	-	0.267219905 *77.7824*	0.265622061 *79.78205*	0.990714102 *72.20395*
Mouse 1	0.404437319	0.449800586	0.450939415	0.199901248
Mouse 2	0.085136337	0.14465255	0.145057985	0.042948243
Mouse 3	0.175618483	0.053122993	0.052942053	0.09035055
WT	-	0.292265579 *80.51012*	0.296993807 *82.51036*	0.989312594 *75.0641*
Mouse 4	0.033234243	0.033312079	0.0336501	0.05065298
Mouse 5	0.180834146	0.067872001	0.067994106	0.17323143
Mouse 6	0.05215308	0.181932753	0.181661341	0.062368356

Table 3.6: *Diclofenac - Paired t Test p-values and AIC (Akaike's Information Criterion) values.*

The comparison test statistics between the averages and the raw mouse data shows that for all but mouse 4 the average is similar enough to base the fitted models on. As well as this the AIC values suggest that the best model is model

3 for both sets of data, which is consistent with the visual results.

3.3.4 Gefitinib

The model parameters for this drug are:

Parameters		WT	HRN	Ratio (3dp)	S-W	QQ	Runs
Model 1	y(0)	1556.875	815.99724	1:0.524	✓	✓	✓
	k_{10}	0.4150626	0.12386	1:0.298			
Model 2	$y_1(0)$	1576.433	846.402	1:0.537	✓	✓	✓
	k_{12}	15.68056	11.28965	1:0.720			
	k_{20}	0.4466992	0.14112	1:0.316			
Model 3	$y_1(0)$	2106.7788	1162.9358	1:0.552	✓	✓	✓
	k_{12}	8.176	6.1506	1:0.752			
	k_{23}	1.2761	0.9836	1:0.771			
	k_{32}	0.5854	1.1665	1:1.993			
	a	61.0799	22.4509	1:0.368			

Table 3.7: *Gefitinib Model Parameters and outcomes at the 5% level from the Normality Assumption tests (S-W = Shapiro-Wilks Test and QQ = Quartile-Quartile Plot) and Runs Test.*

As with Diclofenac the Normality assumption tests and the systematic deviance test show that it is fine to perform non-linear least squares as a fitting mechanism.

Model 1

In the first model the initial concentration for HRN is 52.4% of WT and for the elimination parameter k_{10} this figure is 29.8%.

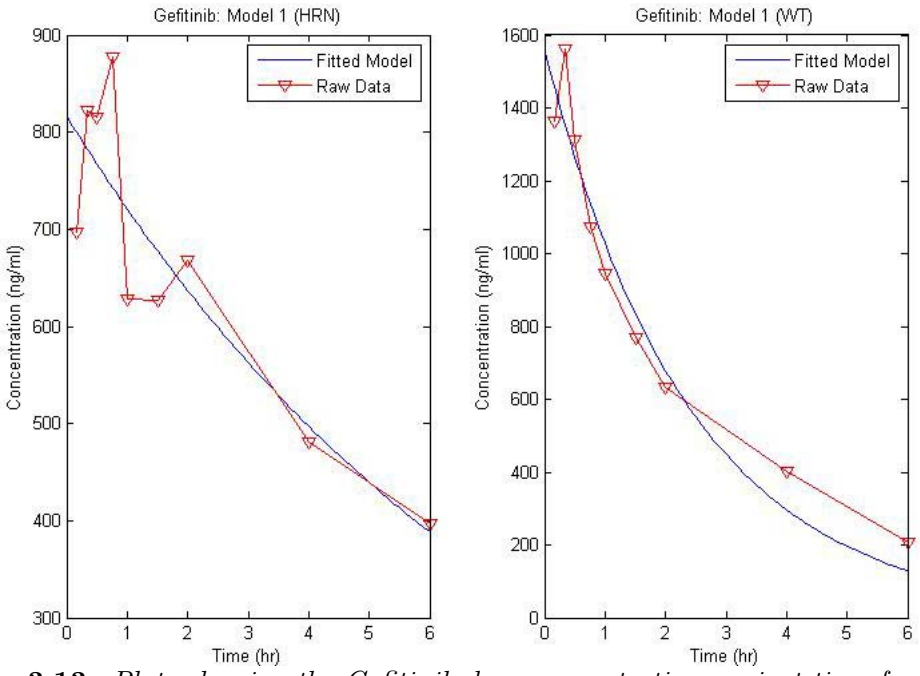

Figure 3.13: *Plots showing the Gefitinib drug concentration against time for the raw data ($\bigtriangledown$) and computational simulation results (solid line) from Model 1.*

The fit for the wild type model is far better than for the HRN mouse although both sets of data show an absorption phase, which is not present in model 1.

Model 2

For model 2 the initial concentration for the HRN mouse is 53.7% of the wild type value. For the absorption parameter, k_{12}, the value is 72% of the WT value and the elimination, k_{20}, is 31.6% of the wild type mouse.

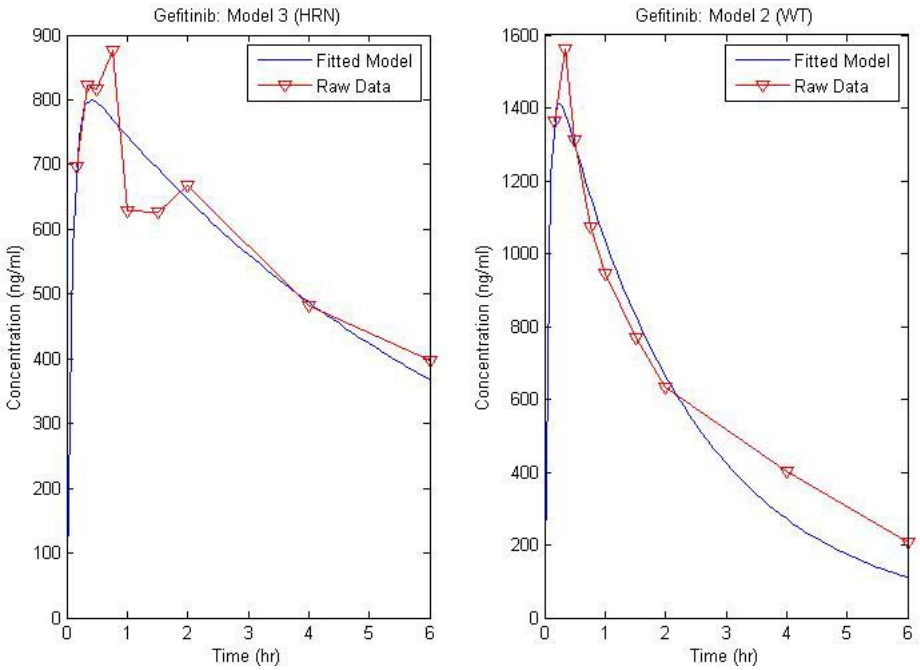

Figure 3.14: *Plots showing the Gefitinib drug concentration against time for the raw data ($\bigtriangledown$) and computational simulation results (solid line) from Model 2.*

For both these models the fit to the raw data is quite good although there are dynamics in the data not catered for in the second model.

Model 3

From inspecting the parameters for model 3 there are some differences. The initial concentration for the HRN is 55.2% of the WT value and the absorption is 75.2% of the parameter. The associated parameters to the third compartment in the HRN mouse show differences from those in the wild type: for k_{23} is 77.1% of the value whereas k_{32} is almost 2 times larger. However the time dependent excretion parameter, a, is 36.8% in the HRN mouse.

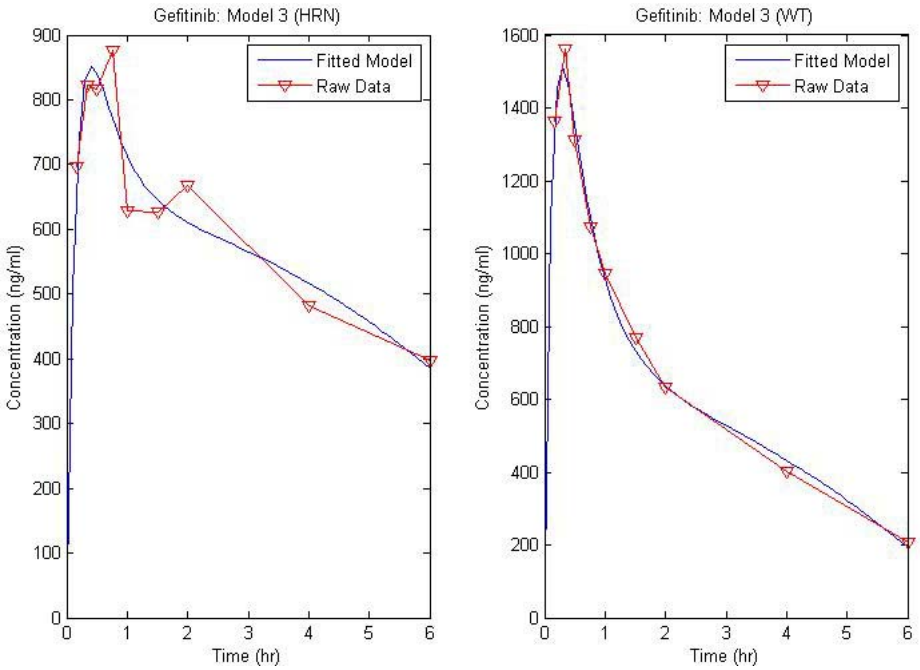

Figure 3.15: *Plots showing the Gefitinib drug concentration against time for the raw data (▽) and computational simulation results (solid line) from Model 3.*

As with model 1 the WT data is fitted much better than the HRN data but this is mainly to do with the bimodal nature of this drugs data in the transgenic mouse.

Data	Average	Model 1	Model 2	Model 3
HRN	-	0.999594586 *108.1072*	0.985005622 *107.0117*	0.988800895 *108.6244*
Mouse 1	0.080937265	0.08469173	0.121725624	0.181555724
Mouse 2	0.00148069	0.011728021	0.008528618	0.002077877
Mouse 3	0.001821999	0.024289635	0.012023015	0.006675974
WT	-	0.794259624 *114.1636*	0.703273292 *115.0288*	0.983612415 *99.98192*
Mouse 4	0.041612408	0.065304589	0.044939771	0.044394383
Mouse 5	0.21263057	0.632297258	0.675789972	0.145500062
Mouse 6	0.106517141	0.533764116	0.567128413	0.230323713

Table 3.8: *Gefitinib - Paired t Test p-values and AIC (Akaike's Information Criterion) values.*

For the average data the fit from the paired t test is good for all models but for three of the mice (mouse 2, 3 and 4) the average is not representative at

the 5% level. The AIC values suggest that the best model for the HRN mouse is model 2 whereas for the WT this is the third model. The average data for the HRN mouse shows at least two peaks, which are not features of any of the compartment models considered.

3.3.5 Imatinib

For this drug the parameters for all the models are:

Parameters		WT	HRN	Ratio (3dp)	S-W	QQ	Runs
Model 1	y(0)	7943.4099	7434.8036	1:0.936	✓(W) ✗(H)	✓	✓
	k_{10}	2.3915	2.4251	1:1.014			
Model 2	$y_1(0)$	7811.754	7021.7975	1:0.899	✓(W) ✗(H)	✓	✓
	k_{12}	144.2846	42.5696	1:0.295			
	k_{20}	2.391542	2.4282	1:1.015			
Model 3	$y_1(0)$	8672.75	7541.525	1:0.870	✓	✓	✓
	k_{12}	855075.8	16.33991	1:1.911E-05			
	k_{23}	2.83568	3.068934	1:1.082			
	k_{32}	0.1520032	0.1473011	1:0.969			
	a	179.5087	151.2954	1:0.843			

Table 3.9: *Imatinib Model Parameters and outcomes at the 5% level from the Normality Assumption tests (S-W = Shapiro-Wilks Test and QQ = Quartile-Quartile Plot) and Runs Test.*

As can be seen from the table above there is a problem with the normality assumption for the first two models applied to the HRN data. However since the test on this assumption is done in conjunction with the Quartile-Quartile plot it is still possible to use non-linear least squares to fit these data. All of the wild type models and the third HRN model obey all the assumptions.

Model 1

For model 1 the rate constant k_{10} is very similar between the two datasets with a change of only 1.4%. However the main change is between the initial concentrations where the HRN y(0) is 93.6% of the WT value.

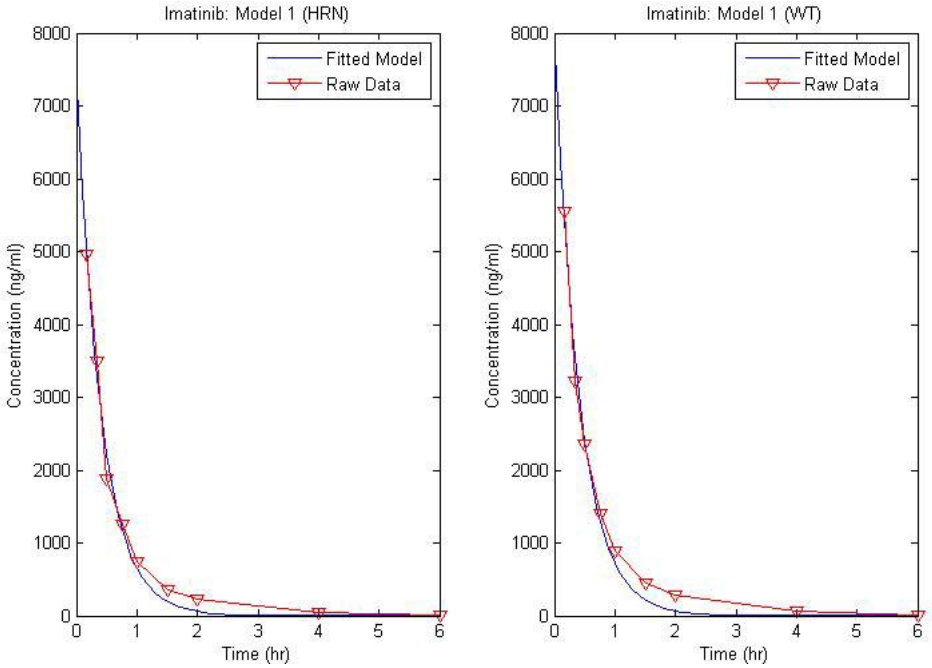

Figure 3.16: *Plots showing the Imatinib drug concentration against time for the raw data ($\bigtriangledown$) and computational simulation results (solid line) from Model 1.*

The fit of this model is fine up until the one-hour point but at the end the concentration is half what the raw data is.

Model 2

In the second model the HRN concentration at the start is 89.9% of the wild type value. The transfer rate between the two compartments, k_{12}, is calculated to be 29.5% of the WT value in the HRN mouse. However the elimination rate is very similar, the HRN being only 1.5% faster than in the wild type mouse.

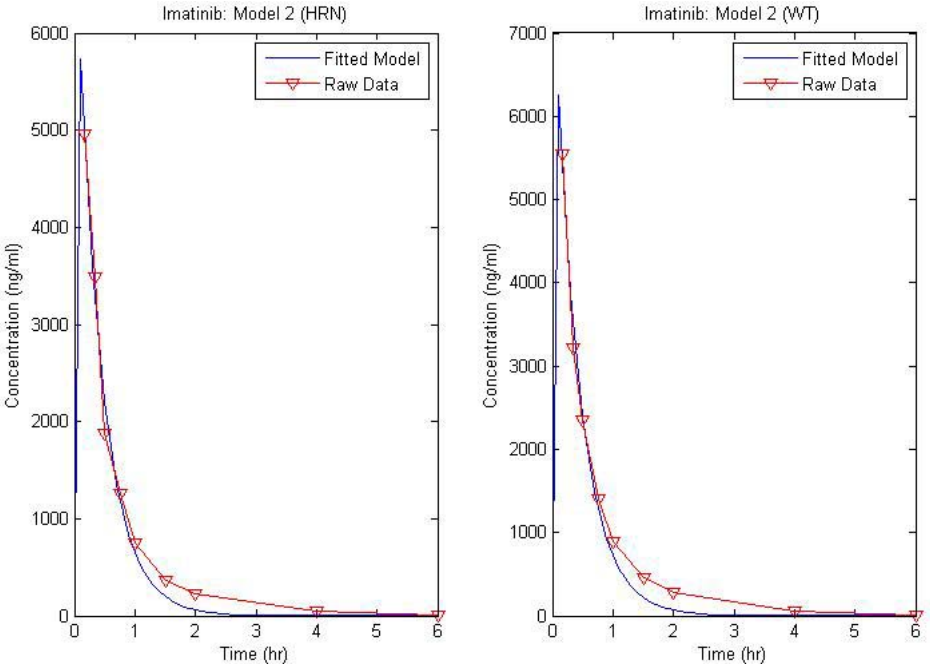

Figure 3.17: *Plots showing the Imatinib drug concentration against time for the raw data (▽) and computational simulation results (solid line) from Model 2.*

As with Diclofenac the fit of this model to the data in the first two hours is good but is poor after this point.

Model 3

For the three-compartment model the initial concentration in the transgenic mouse is 87% of the wild type level. There is a large difference in absorption rate but all other parameters do not have such a big deviation. For the third compartment parameters the input is 8.2% faster in the HRN and the output rate is a 96.9% of the wild type level. The time dependent excretion is 84.3%, this is slower than in the wild type mouse.

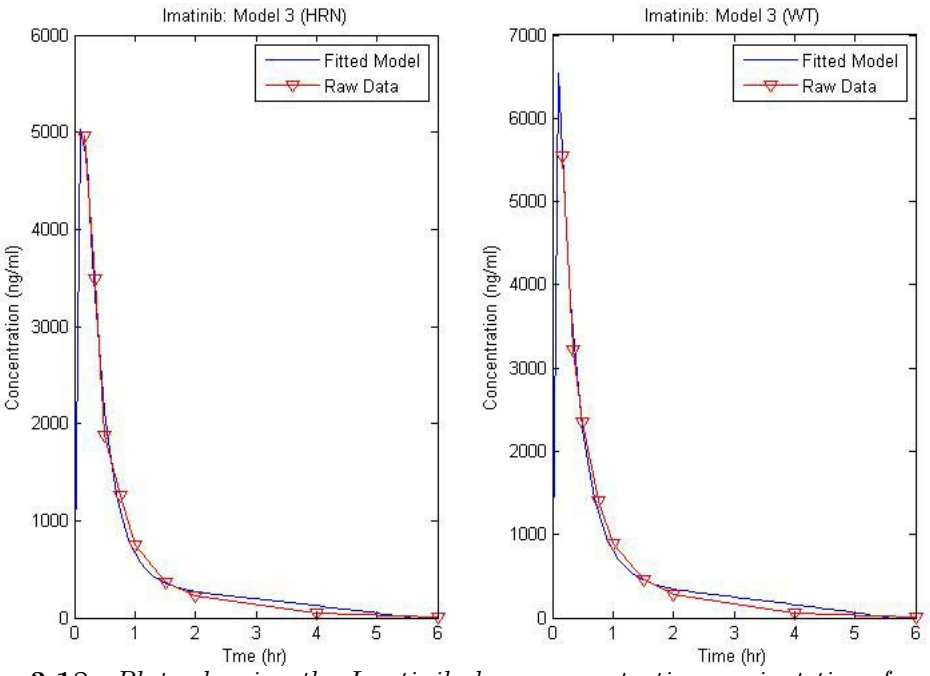

Figure 3.18: *Plots showing the Imatinib drug concentration against time for the raw data (▽) and computational simulation results (solid line) from Model 3.*

The model fit is good for both sets of data. However in the wild type plot the peak is jagged suggesting too quick a transition from absorption to elimination in the parameter set.

Data	Average	Model 1	Model 2	Model 3
HRN	-	0.450171095 *122.2021*	0.448021251 *124.2018*	0.993331183 *122.5585*
Mouse 1	0.095278266	0.059279436	0.059224358	0.096649954
Mouse 2	0.081393718	0.266882155	0.267162233	0.113754151
Mouse 3	0.123483884	0.333740222	0.334438738	0.162144015
WT	-	0.343849948 *125.8037*	0.34387883 *127.8037*	0.994015349 *123.1115*
Mouse 4	0.014543334	0.134026753	0.134024074	0.021273337
Mouse 5	0.04327831	0.010216045	0.010215945	0.035740117
Mouse 6	0.291020438	0.856229138	0.856208787	0.442361628

Table 3.10: *Imatinib - Paired t Test p-values and AIC (Akaike's Information Criterion) values.*

According to the paired t test with the average data all models are similar

to the observed data at the 5% level. When comparing the raw mice data with the average only two of the mice (mouse 4 and 5) do not show similarity in the test. The AIC values suggest that the best model for the HRN data is the first model. However since this model had a significant result in the Shapiro-Wilks test (non-normal residuals) it is better using the third model since the AIC value for this is comparable. For the wild type data the best model is the third one and this showed a good level of visual fit with the data.

3.3.6 Midazolam

For the three models for this drug we have the following parameters:

Parameters		WT	HRN	Ratio (3dp)	S-W	QQ	Runs
Model 1	y(0)	111.4156	170.2512	1:1.528	✓	✓	✓
	k_{10}	0.9694	0.3994	1:0.412			
Model 2	$y_1(0)$	130.9995	207.87443	1:1.587	✓	✓	✓
	k_{12}	8.7775	6.27233	1:0.715			
	k_{20}	1.3763	0.58136	1:0.422			
Model 3	$y_1(0)$	162.5598	212.72045	1:1.309	✓	✓	✓
	k_{12}	6.31	6.03469	1:0.956			
	k_{23}	2.0968	0.62637	1:0.299			
	k_{32}	0.1971	0.04408	1:0.224			
	a	3.2448	1.36268	1:0.420			

Table 3.11: *Midazolam Model Parameters and outcomes at the 5% level from the Normality Assumption tests (S-W = Shapiro-Wilks Test and QQ = Quartile-Quartile Plot) and Runs Test.*

All three columns showing the results from the assumption check agree that non-linear least squares can be used to fit these models to the data.

Model 1

As the ratio for the initial concentration for model 1 suggests the HRN mouse has 1.528 times the amount of Midazolam starting in compartment 1. However

with respect to the parameter k_{10} it is 41.2% of the value, suggesting a slower excretion rate.

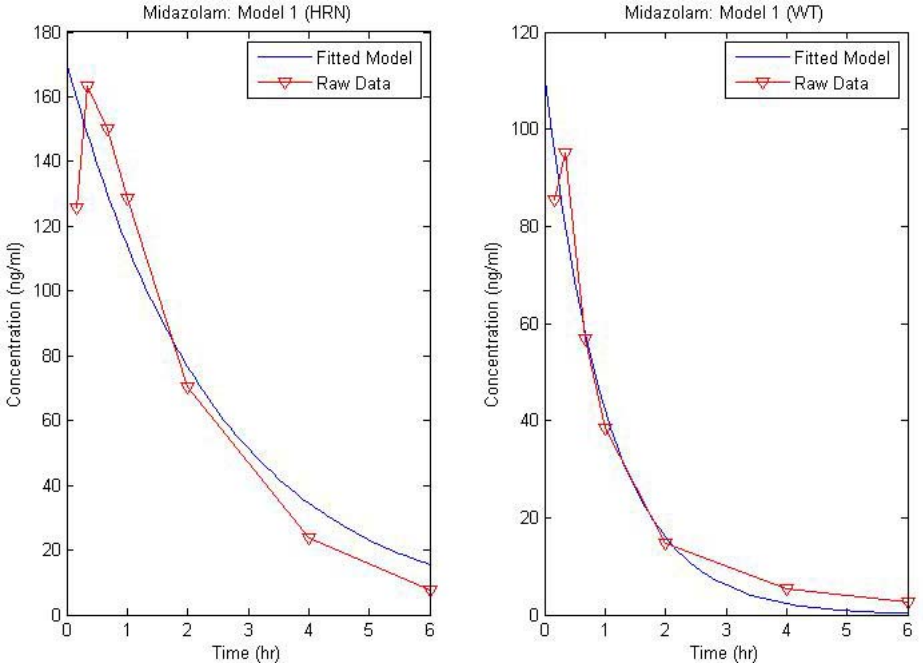

Figure 3.19: *Plots showing the Midazolam drug concentration against time for the raw data ($\bigtriangledown$) and computational simulation results (solid line) from Model 1.*

The fit of the model to this data is reasonable although there is definitely an absorption phase that should be accounted for as per the second model.

Model 2

The transgenic mouse initial concentration is 1.587 times that of the wild type. The HRN values for k_{12} and k_{20} are 71.5% and 42.2% of the WT respectively.

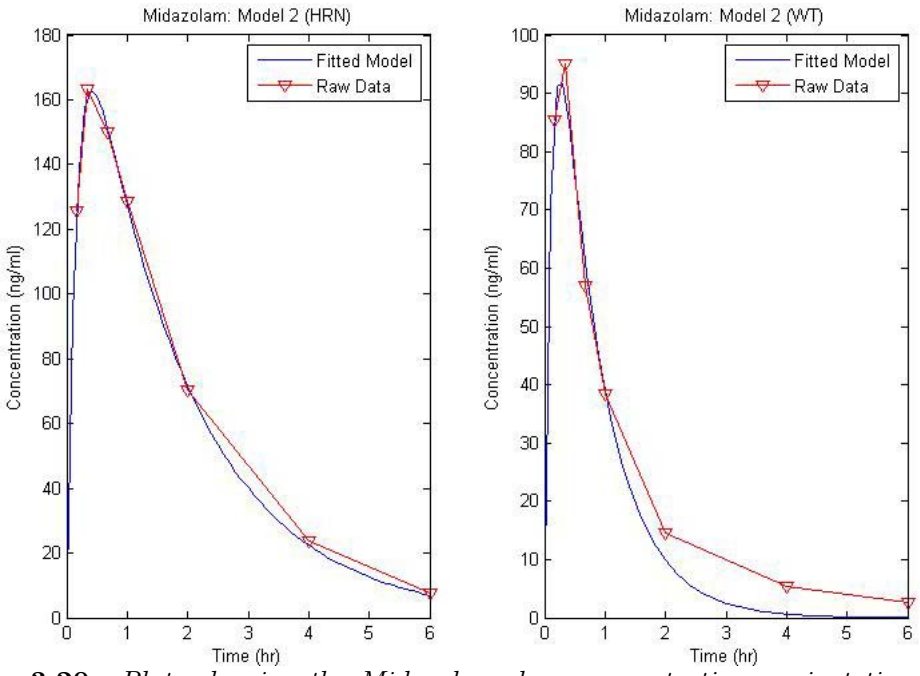

Figure 3.20: *Plots showing the Midazolam drug concentration against time for the raw data (▽) and computational simulation results (solid line) from Model 2.*

Although there is an absorption phase demonstrated by the data this behaviour is not mimicked closely enough by the fitted model especially after the one-hour point.

Model 3

For the initial concentrations the difference is +30.9% from the WT to the HRN values. The absorption parameter, k_{12}, is nearly identical in the HRN and wild type mouse since it is 95.6% the value. According to the ratios both compartment 3 parameters are smaller for the HRN mouse. It is a 29.9% the size for k_{23} and 22.4% for k_{32}. The a parameter is also smaller in the HRN mouse at 44% the wild type level.

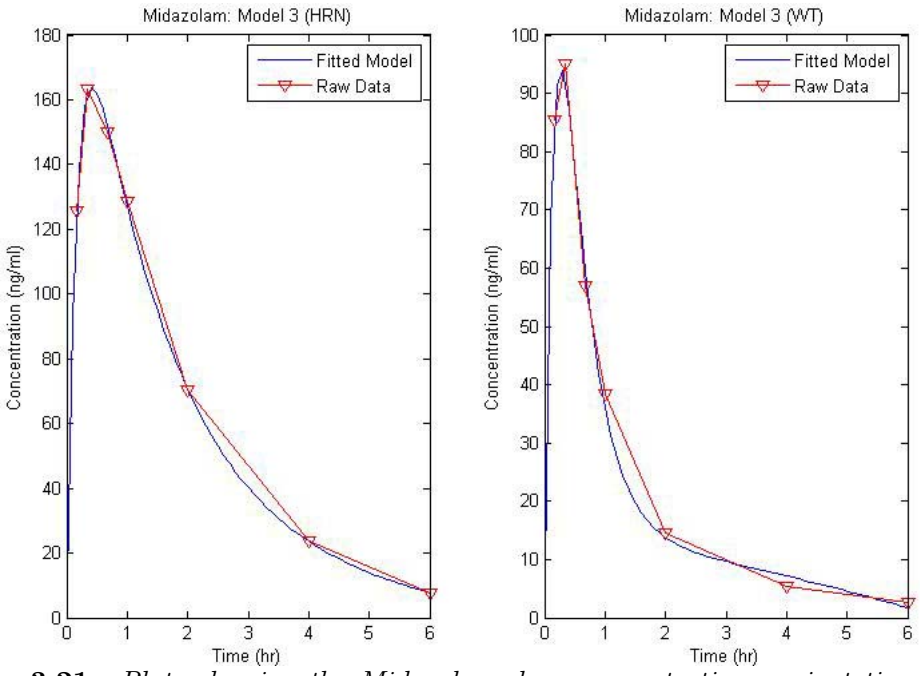

Figure 3.21: *Plots showing the Midazolam drug concentration against time for the raw data (▽) and computational simulation results (solid line) from Model 3.*

The model results in a good fit to the data with a slight difference only occurring between the 2hr and 4hr points in the HRN and 1hr and 2hr points in the wild type.

Data	Average	Model 1	Model 2	Model 3
HRN	-	0.845128727 *65.92079*	0.868274293 *35.40085*	0.962974603 *37.86993*
Mouse 1	0.008537834	0.160864989	0.007911405	0.008793906
Mouse 2	0.346047952	0.751822893	0.283365543	0.303815977
Mouse 3	0.019639363	0.016451803	0.023642364	0.022096791
WT	-	0.869871134 *52.84141*	0.406401416 *46.82994*	0.978943436 *42.34225*
Mouse 4	0.175962694	0.253692084	0.117791101	0.19005748
Mouse 5	0.01630903	0.163253623	0.078725595	0.00441406
Mouse 6	0.718358027	0.774532791	0.915624061	0.723533972

Table 3.12: *Midazolam - Paired t Test p-values and AIC (Akaike's Information Criterion) values.*

For these sets of data the goodness-of-fit test show that for mouse 1, mouse 3 and mouse 5 the average data does not emulate the same behaviour. However all

three models fit the average data well according to the paired t test comparison. According to the AIC values model 2 is the best for the HRN data and model 3 shows the best fit from the three models examined for the wild type.

3.3.7 Omeprazole

This drug has the following model parameters:

Parameters		WT	HRN	Ratio (3dp)	S-W	QQ	Runs
Model 1	y(0)	626.18439	941.0905	1:1.503	✓	✓	✓
	k_{10}	5.45408	1.2607	1:0.231			
Model 2	$y_1(0)$	525.1421	5642.2077	1:10.744	✓	✓	✓
	k_{12}	28.8632	1.742	1:0.060			
	k_{20}	5.5588	8.9964	1:1.618			
Model 3	$y_1(0)$	532.74888	1127.2856	1:2.116	✓	✓	✓
	k_{12}	20.27684	8.5388	1:0.421			
	k_{23}	6.0252	1.858	1:0.308			
	k_{32}	0.02656	0.0421	1:1.585			
	a	2.14976	8.5514	1:3.978			

Table 3.13: *Omeprazole Model Parameters and outcomes at the 5% level from the Normality Assumption tests (S-W = Shapiro-Wilks Test and QQ = Quartile-Quartile Plot) and Runs Test.*

As with Midazolam in the previous section the non-linear least squares algorithm can be used due to residual normality and systematic deviation assumptions being satisfied.

Model 1

In model 1 there is a large difference between the calculated initial concentrations since HRN has a value about 1.5 times the WT constant. The k_{10} parameter is smaller at 23.1% of the WT value.

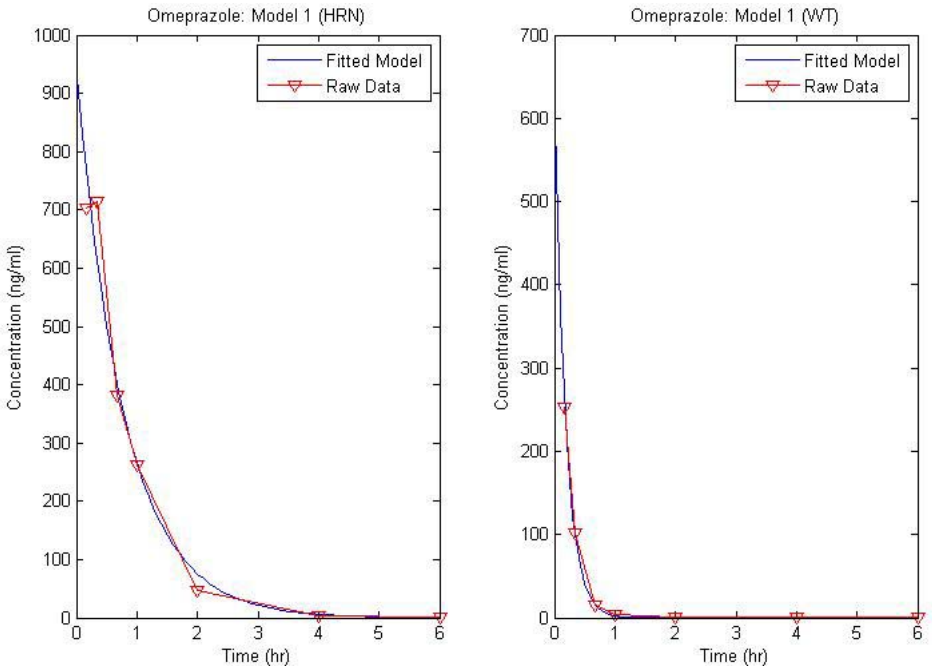

Figure 3.22: *Plots showing the Omeprazole drug concentration against time for the raw data ($\bigtriangledown$) and computational simulation results (solid line) from Model 1.*

For the HRN data the fit of this model is reasonable but there is an indication of an absorption phase. For the wild type mouse the fit of this model to the data is good.

Model 2

For this model the calculated starting values seem unusual since the wild type value is comparatively small at 525.1421ng/mol whereas the HRN value is 10.744 times this according to the ratio. The two rate parameters are different as well - k_{12} is 6% of the wild type value and k_{20} is 1.618 times in magnitude.

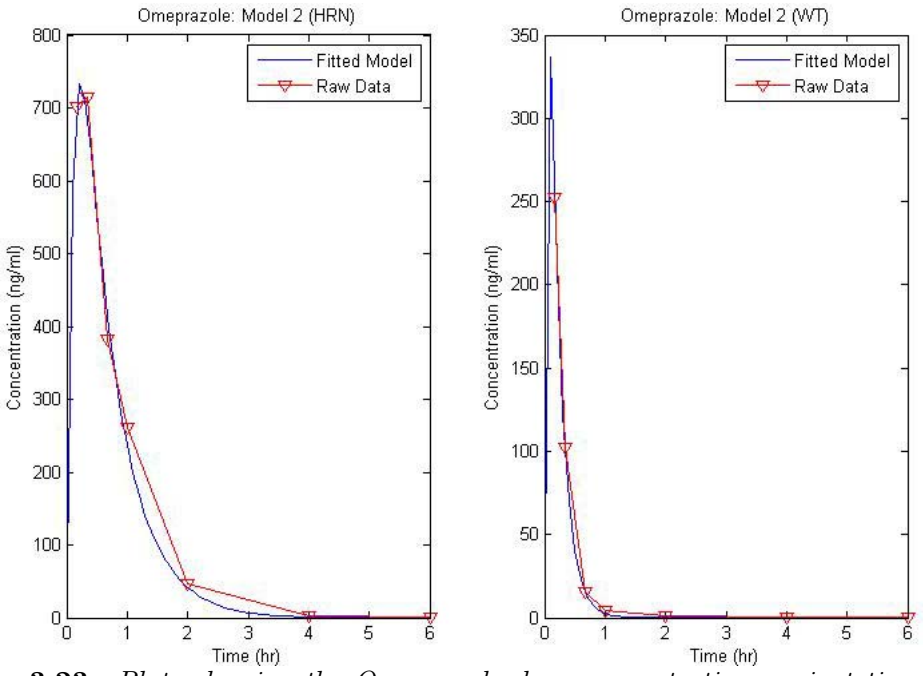

Figure 3.23: *Plots showing the Omeprazole drug concentration against time for the raw data (▽) and computational simulation results (solid line) from Model 2.*

The fit for both sets of data is good, especially in the wild type plot.

Model 3

The starting values for this model differ by a factor of 2.116 in the HRN favour. The other parameter that is increased is a showing roughly a four fold increase. The absorption parameter k_{12} is 42.1% and k_{23} is 30.8% of their WT counterparts. Whereas k_{32} is 1.585 times larger than its wild type equivalent.

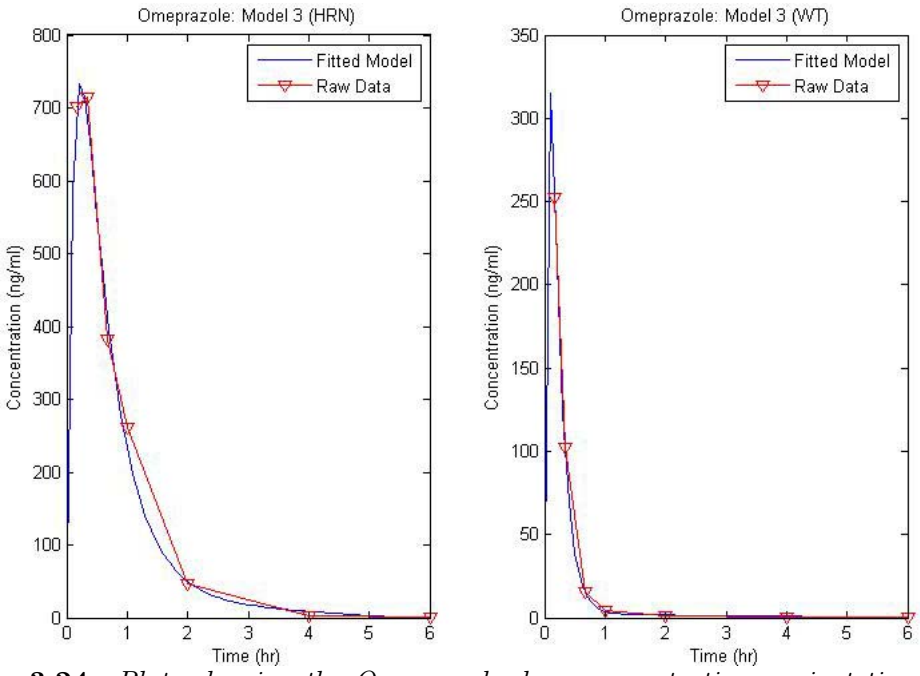

Figure 3.24: *Plots showing the Omeprazole drug concentration against time for the raw data (▽) and computational simulation results (solid line) from Model 3.*

The fitted model for the WT mouse is better than the HRN since in its plot it has a gaps between the two lines in the time period 1-2 hrs.

Data	Average	Model 1	Model 2	Model 3
HRN	-	0.854680191 *79.20484*	0.877093755 *69.5871*	0.989060612 *73.1831*
Mouse 1	0.561316659	0.967884949	0.540672452	0.628406255
Mouse 2	0.033634637	0.076531815	0.045814346	0.034233958
Mouse 3	0.036175825	0.254645058	0.080387231	0.097132208
WT	-	0.285873511 *26.15958*	0.192530647 *27.80053*	0.995394603 *20.80836*
Mouse 4	0.175784132	0.168025764	0.166611719	0.17576973
Mouse 5	0.132644192	0.145028751	0.147134361	0.132716795
Mouse 6	0.257919396	0.28146986	0.285949807	0.258179914

Table 3.14: *Omeprazole - Paired t Test p-values and AIC (Akaike's Information Criterion) values.*

With reference to the paired t test all the wild type and mouse 1 from the HRN mice show similarity with the average data. The best model for the wild

type data is model 3 whereas for the HRN mouse the second model is the top.

3.3.8 Paclitaxel

For this drug the model parameters are:

Parameters		WT	HRN	Ratio (3dp)	S-W	QQ	Runs
Model 1	y(0)	694.34851	476.45113	1:0.686	✓	✓	✓(W) ✗(H)
	k_{10}	0.07061	0.03066	1:0.434			
Model 2	$y_1(0)$	694.285	812.4896	1:1.170	✓	✓	✓
	k_{12}	805.5993	1.276029	1:0.002			
	k_{20}	0.07060922	0.07387129	1:1.046			
Model 3	$y_1(0)$	3266.985	1448.483	1:0.443	✓	✓	✓(W) ✗(H)
	k_{12}	0.4601999	0.6898806	1:1.499			
	k_{23}	0.460518	0.4584039	1:0.995			
	k_{32}	0	0.2703421	0:1			
	a	0.04483011	10.65818	1:237.746			

Table 3.15: *Paclitaxel Model Parameters and outcomes at the 5% level from the Normality Assumption tests (S-W = Shapiro-Wilks Test and QQ = Quartile-Quartile Plot) and Runs Test.*

With respect to the normality of the residuals all models for both sets of data are fine. However the runs test has a significant result at the 5% level for the HRN model 1 and 3, which suggests that the data systematically deviates from the models.

Model 1

From the table above the parameters for model 1 are different between HRN and WT. The initial concentration is 68.6% of the WT value and for k_{10} this level is 43.4%.

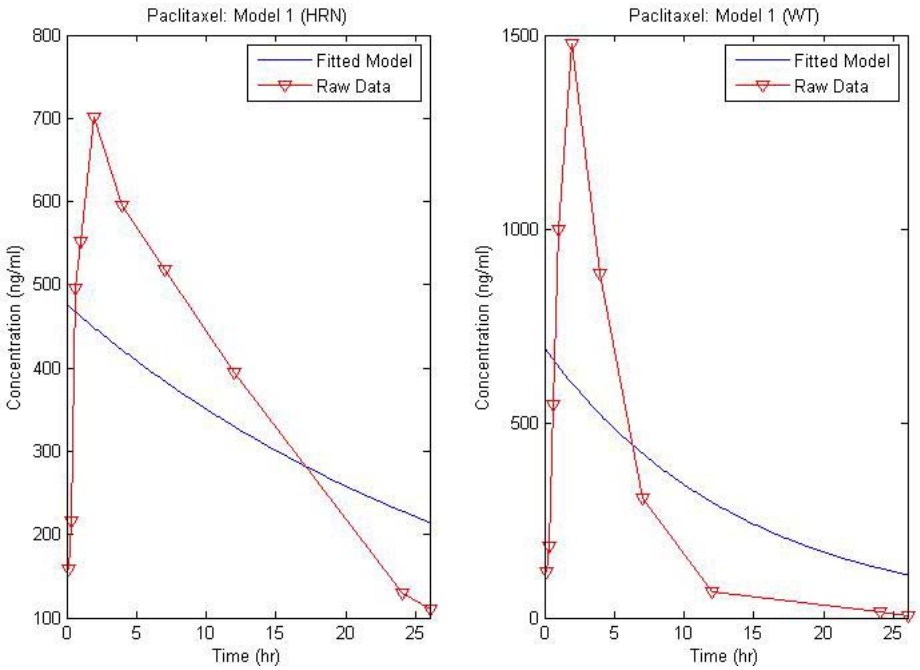

Figure 3.25: *Plots showing the Paclitaxel drug concentration against time for the raw data ($\bigtriangledown$) and computational simulation results (solid line) from Model 1.*

Since both these plots show an absorption phase this model does not provide a good enough fit.

Model 2

The initial concentration for the HRN mouse is 1.17 times the WT and k_{20} is also larger by 4.6%. For k_{12} the parameter is smaller since this value is 0.2% of the WT value in the HRN mouse.

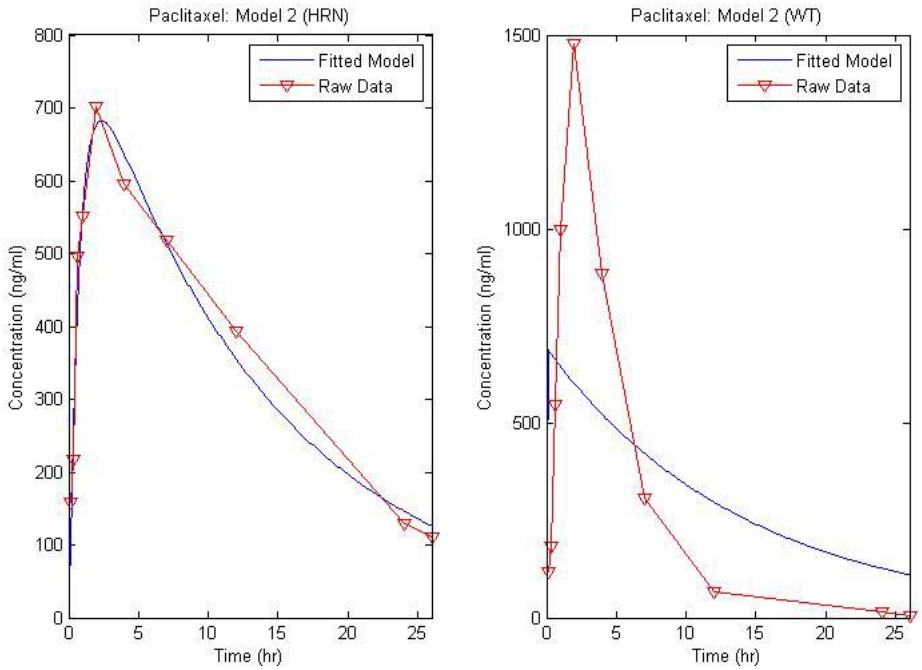

Figure 3.26: *Plots showing the Paclitaxel drug concentration against time for the raw data (▽) and computational simulation results (solid line) from Model 2.*

For the HRN mouse the fit is a lot better in comparison to model 1 but the elimination part of the curve still differs. For the wild type the fit seems poor since the curve does not follow the behaviour of the data.

Model 3

In model 3 the HRN initial value is 44.3% of the WT constant. The only parameter other than this showing a reduction in value is k_{23}, which is 99.5% of the WT level. The k_{12} parameter is +49.9% and a is 237.746 times the WT value. The k_{32} value is different between the two mice as it is zero in the wild type and 0.27 in the HRN mouse.

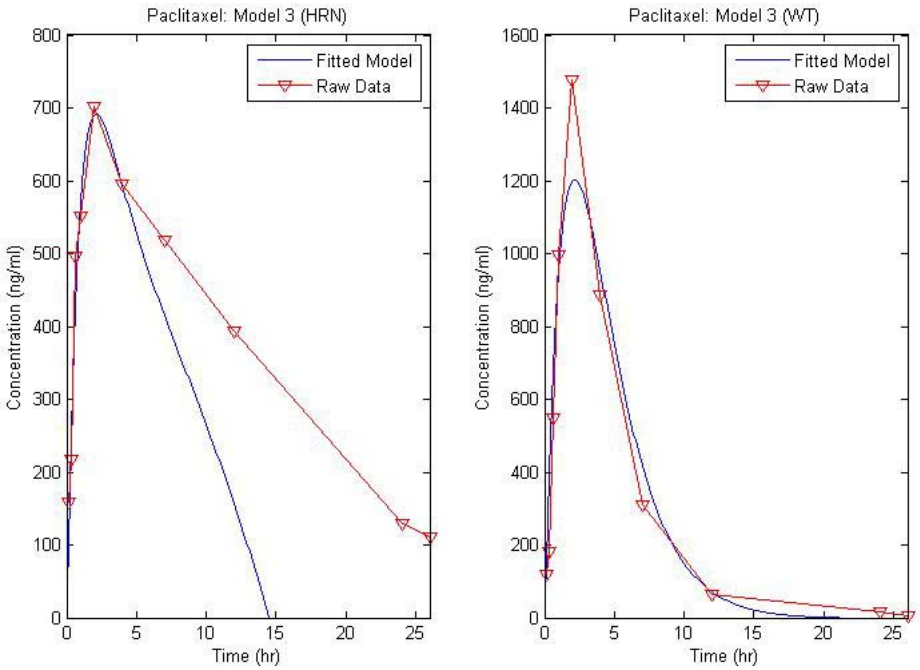

Figure 3.27: *Plots showing the Paclitaxel drug concentration against time for the raw data (▽) and computational simulation results (solid line) from Model 3.*

Given these changes in parameter value the WT model seems to fit the corresponding data better than the HRN although neither gives a very good fit.

Data	Average	Model 1	Model 2	Model 3
HRN	-	0.962195496 *137.7816*	0.793552517 *105.5475*	0.893191317 *106.0508*
Mouse 1	0.251939365	0.23068858	0.215916235	0.234643429
Mouse 2	0.0630742	0.513246421	0.089454806	0.069459408
Mouse 3	0.786460194	0.936184518	0.867490755	0.831785634
WT	-	0.914061936 *154.7613*	0.914056865 *156.7613*	0.436215134 *139.792*
Mouse 4	0.068164909	0.713677412	0.713672297	0.129054034
Mouse 5	0.192315621	0.958616557	0.95862171	0.761125341
Mouse 6	0.284894945	0.982517343	0.98251257	0.638383344

Table 3.16: *Paclitaxel - Paired t Test p-values and AIC (Akaike's Information Criterion) values.*

All the models and mice show similarity to the average data in the paired t test at the 5% level. According to the AIC values the best model for the HRN data is the second model and for the WT it is the third. This is congruent with

the visual fit of these models and the fact that the first and third models are unsuitable for the HRN data due to the significant Runs test.

3.3.9 Tamoxifen

The model parameters for this drug are shown in the following table:

Parameters		WT	HRN	Ratio (3dp)	S-W	QQ	Runs
Model 1	y(0)	105.58456	55.37275	1:0.524	✓	✓	✓(W) ✗(H)
	k_{10}	0.2125	0.02592	1:0.122			
Model 2	$y_1(0)$	120.28051	132.8924	1:1.105	✓	✓	✓
	k_{12}	6.15138	0.8996	1:0.146			
	k_{20}	0.27348	0.1695	1:0.620			
Model 3	$y_1(0)$	129.3104	213.5103	1:1.651	✓	✓	✓
	k_{12}	5.27876	0.5576164	1:0.106			
	k_{23}	0.3712349	0.4473217	1:1.205			
	k_{32}	0.05571804	0.1092564	1:1.961			
	a	0	0.3575627	0:1			

Table 3.17: *Tamoxifen Model Parameters and outcomes at the 5% level from the Normality Assumption tests (S-W = Shapiro-Wilks Test and QQ = Quartile-Quartile Plot) and Runs Test.*

As with Paclitaxel, Tamoxifen HRN data shows systematic deviation from model 1.

Model 1

For the first model the parameters are all lower in value for HRN in comparison to WT. The initial concentration is 52.4% of the level and k_{10} is 12.2% of the rate.

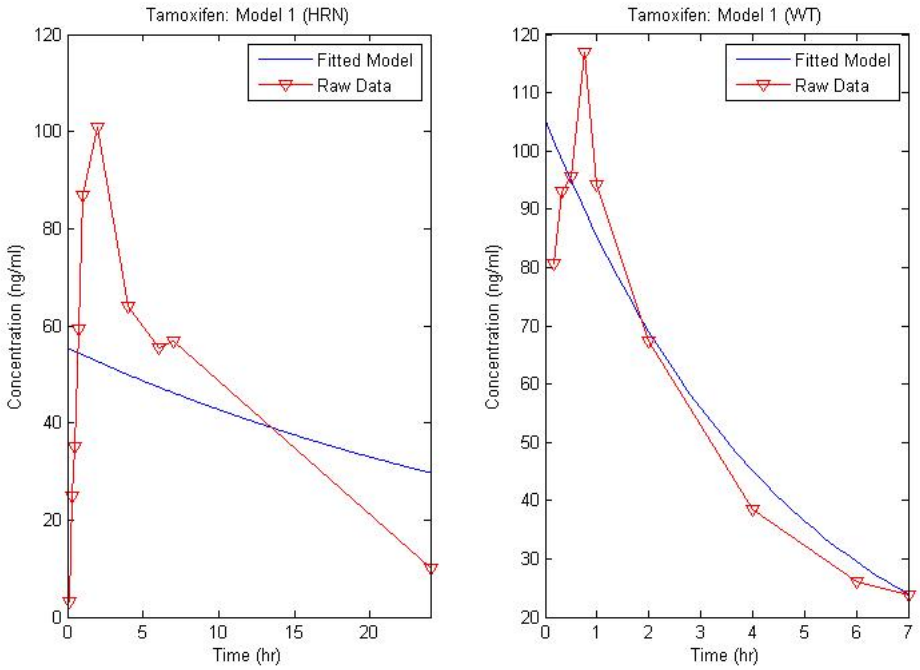

Figure 3.28: *Plots showing the Tamoxifen drug concentration against time for the raw data (▽) and computational simulation results (solid line) from Model 1.*

The fit for the WT model is reasonable although the formulation does not allow the absorption phase shown in the data. The HRN model however has a poor fit for the data.

Model 2

For this model the HRN model starts with a concentration 1.105 times that of the WT starting value. The absorption parameter, k_{12}, is 14.6% of the wild type value and the elimination rate is 62%.

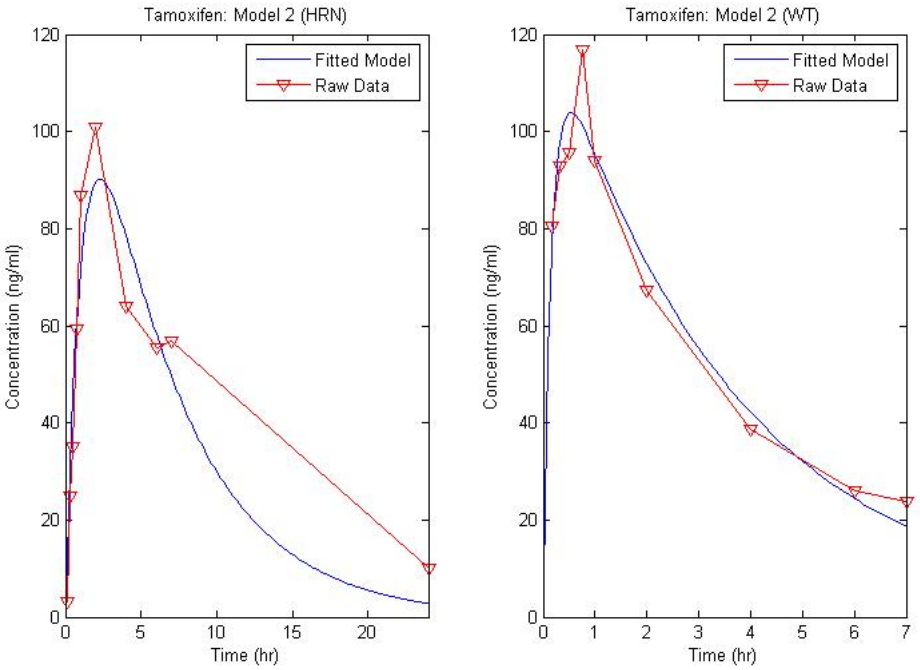

Figure 3.29: *Plots showing the Tamoxifen drug concentration against time for the raw data (▽) and computational simulation results (solid line) from Model 2.*

The fit for the WT data is better than that for the HRN data. There is disparity between the HRN model and the raw data between the 7hr and 24hr points but this is more due to a lack of points between.

Model 3

Initially the HRN third model starts with 65.1% more Tamoxifen in the first compartment. The wild type model has a transfer rate between the first and second compartment that is ten times that of the HRN. When it comes to the third section the rate of transfer into it is +20.5% of the WT value and the opposite flow is also quicker by 96.1%. In the wild type mouse the time dependent elimination is zero but it is larger in the HRN mouse with a level of 0.34.

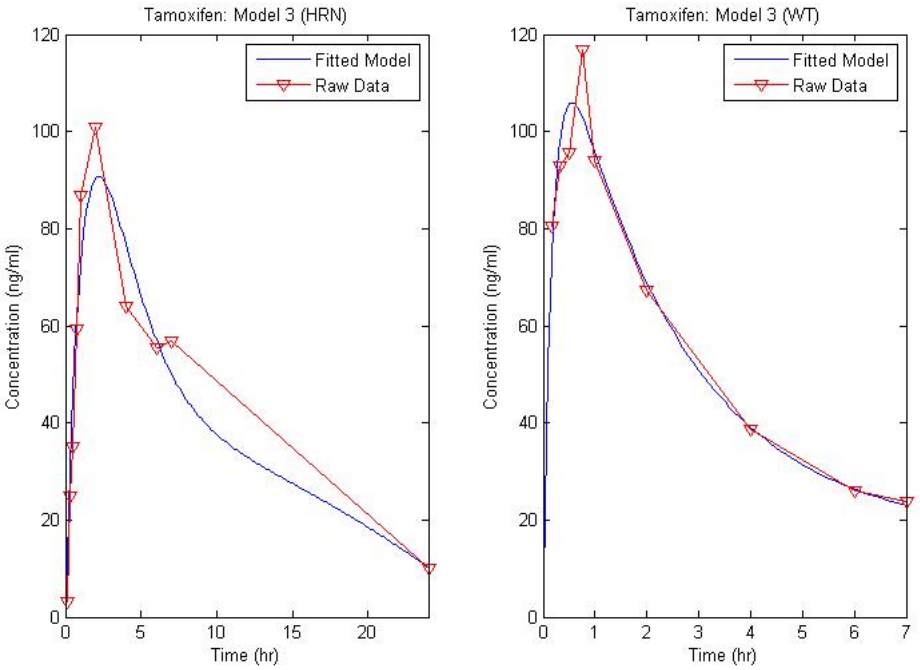

Figure 3.30: *Plots showing the Tamoxifen drug concentration against time for the raw data (▽) and computational simulation results (solid line) from Model 3.*

The fit of these models to the datasets is quite good since the general behaviour seems to be mimicked by the model.

Data	Average	Model 1	Model 2	Model 3
HRN	-	0.98239315 *101.4413*	0.723754161 *83.39319*	0.533049756 *85.95446*
Mouse 1	0.912719662	0.993406559	0.87235823	0.758075348
Mouse 2	0.476351664	0.848469337	0.334221281	0.224672664
Mouse 3	0.664126381	0.891435861	0.977396816	0.861637272
WT	-	0.865898958 *76.55137*	0.888208185 *68.72095*	0.940834517 *71.51396*
Mouse 4	0.000410784	0.000207095	0.000388317	0.000376994
Mouse 5	0.000340973	0.000639792	0.000441549	0.000429731
Mouse 6	0.00035478	0.000404869	0.000293569	0.00031208

Table 3.18: *Tamoxifen - Paired t Test p-values and AIC (Akaike's Information Criterion) values.*

For all the wild type mice the average data has a significant p-value and therefore the average difference is non-zero. This is not the case with the HRN

data where the average is significantly similar for all the mice. The AIC values suggest that the best model for the transgenic mice is the second model and this is also the case in the wild type.

3.3.10 Thalidomide

For this drug the model parameters are:

Parameters		WT	HRN	Ratio (3dp)	S-W	QQ	Runs
Model 1	y(0)	7844.8679	14208.76	1:1.811	✓	✓	✓
	k_{10}	0.3168	0.0975811	1:0.308			
Model 2	$y_1(0)$	11126.53	24408.25	1:2.194	✓	✓	✓
	k_{12}	3.907653	2.126012	1:0.544			
	k_{20}	0.5605251	0.283173	1:0.505			
Model 3	$y_1(0)$	10938.48	35847.56	1:3.277	✓	✓	✓
	k_{12}	4.024039	1.443215	1:0.359			
	k_{23}	0.5415965	0.8693192	1:1.605			
	k_{32}	0.03747103	0.5505027	1:14.691			
	a	103.8998	1006.862	1:9.691			

Table 3.19: *Thalidomide Model Parameters and outcomes at the 5% level from the Normality Assumption tests (S-W = Shapiro-Wilks Test and QQ = Quartile-Quartile Plot) and Runs Test.*

For the Thalidomide data it is fine to assume normality in the residuals and none of the models show systematic deviation from the data.

Model 1

The first model shows an increase in initial concentration from WT to HRN by 81.1%. This is coupled with a decrease in elimination rate with the value being 30.8% of the wild type flow.

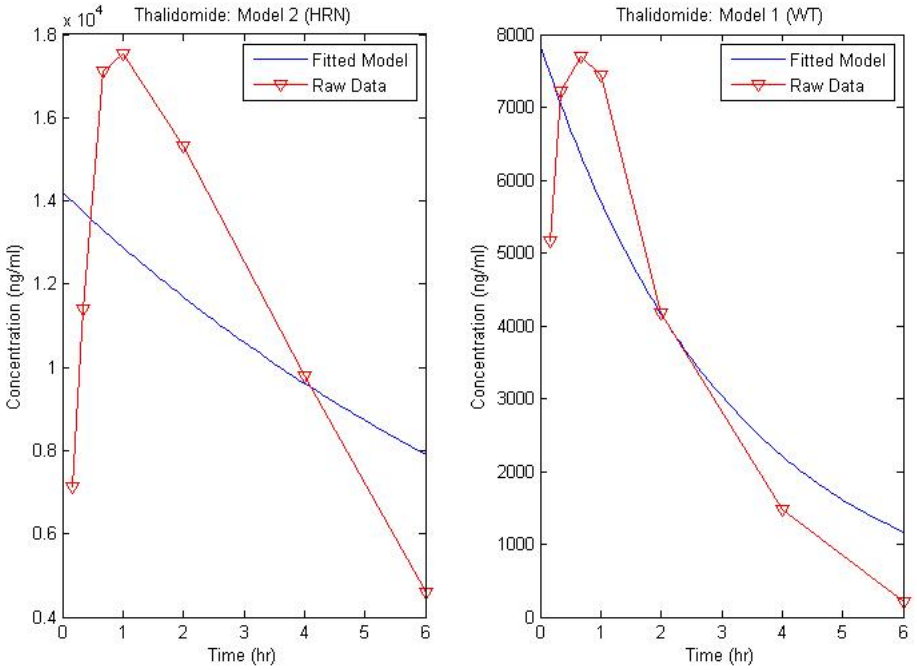

Figure 3.31: *Plots showing the Thalidomide drug concentration against time for the raw data (▽) and computational simulation results (solid line) from Model 1.*

The fit of this one compartment model to the average data is not good since it does not include an absorption phase.

Model 2

For the second model the difference between the wild type and HRN model shows an increase in the starting concentration by 2.194 times. The absorption and the elimination parameters, k_{12} and k_{20}, however, are smaller than the wild type at 54.4% and 50.5% of the value respectively.

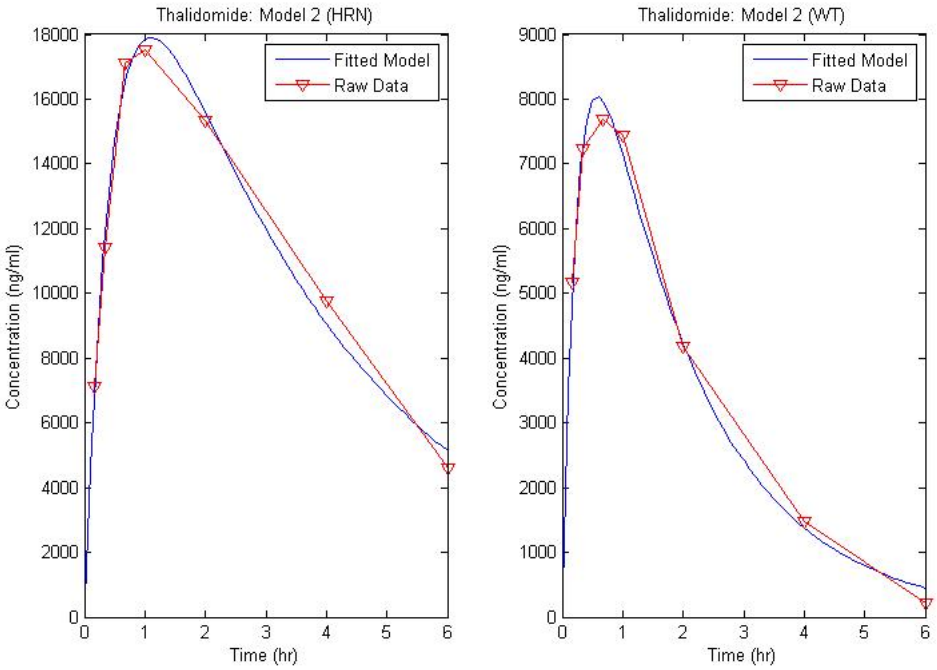

Figure 3.32: *Plots showing the Thalidomide drug concentration against time for the raw data (▽) and computational simulation results (solid line) from Model 2.*

The fit of this model to these data points is good but the peaks are not similar in shape.

Model 3

For this model the starting value of HRN is 3.277 times bigger than the wild type parameter. With the exception of k_{12} (35.9% the size) all the parameters are larger in the HRN mouse - k_{23} is +60.5%, a is 9.691 times bigger and k_{32} is 14.691 times larger.

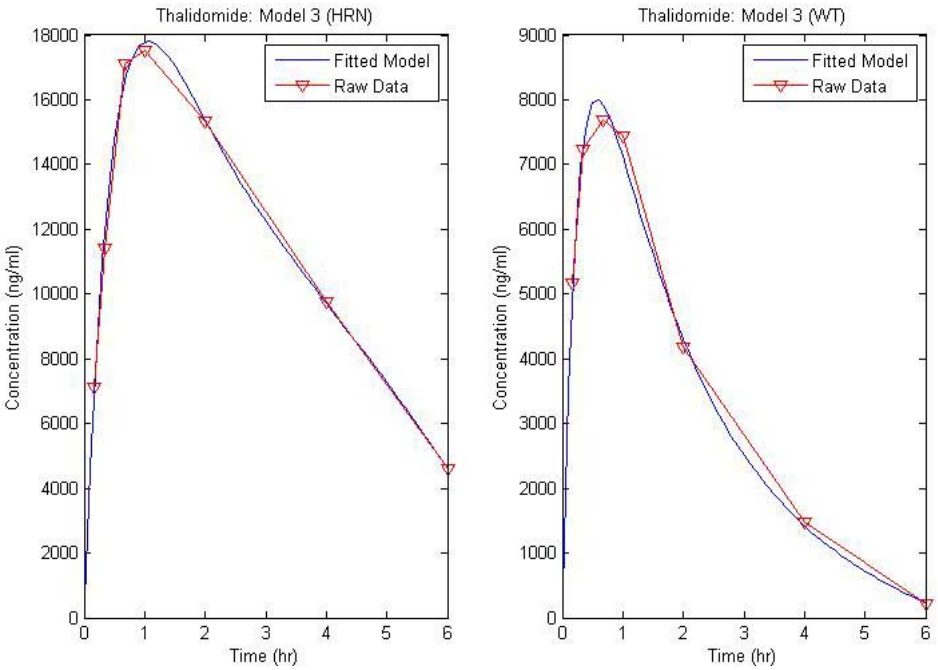

Figure 3.33: *Plots showing the Thalidomide drug concentration against time for the raw data (▽) and computational simulation results (solid line) from Model 3.*

The visual fit of the model is good for the data although there is still a disparity in peak shape for both mice.

Data	Average	Model 1	Model 2	Model 3
HRN	-	0.980441293 *142.0342*	0.917512018 *114.0037*	0.922990225 *111.3868*
Mouse 1	0.0041872	0.187357181	0.003430427	0.00285762
Mouse 2	0.13911992	0.644791545	0.166101494	0.157164959
Mouse 3	0.00480581	0.553649658	0.032930053	0.01660397
WT	-	0.851221037 *125.982*	0.857263377 *100.7898*	0.95076315 *102.8101*
Mouse 4	0.002257028	0.011975152	0.001897443	0.002564998
Mouse 5	0.001589166	0.059113262	0.002565842	0.001939229
Mouse 6	0.010637094	0.117544203	0.005813605	0.009099098

Table 3.20: *Thalidomide - Paired t Test p-values and AIC (Akaike's Information Criterion) values.*

All except mouse 2 show a significant result in the paired t test with the average data suggesting that for these mice the average is not representative. As such the agreement between the model fits and the real data is not good especially

with respect to model 2 and 3. The AIC values suggest that the best model for the HRN data is the third model and for the WT it is the second.

3.4 Discussion

When fitting the first model to the caffeine data the initial values were found to be similar whereas the absorption rate was much slower in the HRN mouse than in the WT. This is due to the absorption phase exhibited by the HRN data not being a feature of a one compartment pharmacokinetic model.

For the second caffeine model there is a marked difference between the two parameter sets in the different mice. With both parameters the rates are much faster in the wild type mouse than in the HRN. This suggests either that the transgenic mouse has a slower metabolism than the wild type or the second model allows too much complexity not exhibited by the wild type data leading to errors.

In the third model parameter sets there are rates that are set to zero. In the HRN the $k_{32} = 0$ which means that any drug entering the third compartment cannot leave. In the wild type it is a that is zero that means the excretion rate does not change over time and since it is initially set to zero no excretion takes place. Biologically speaking both these scenarios are unrealistic so the third model is wrong for these data sets.

For both the HRN and wild type mice the third caffeine model has the better visual fit for the data. However, when it comes to the AIC statistic deems model 1 as the best for the WT data and model 2 for the HRN data.

Due to its mechanism of action and enzyme metabolism it can be understood why there might be a short or unmeasured absorption period. Since the injection is into the peritoneum this causes the drug to be close to its metabolising enzymes in the small intestine and liver.

With respect to the first Dextromethorphan model the fit is good for the wild

type data but not for the HRN since it shows an absorption phase. The initial values for the model are similar between the two mice although the elimination rate is 50% slower in the HRN mouse. This could suggest a slower transport through the gut in the transgenic mouse.

For the second model the fit is good for the both sets of data although in the wild type mouse the fitted peak is jagged since there is no data supporting an absorption phase. The initial concentrations are similar but the other two parameters are not. The absorption and elimination parameters for the HRN mouse are 0.8% and 60% of the size of the wild type parameter respectively. The absorption parameter difference is explainable by the lack of data but the elimination being less in the HRN than the WT concurs with model 1 which suggests evidence of physical difference.

Even though the third model for both the mice shows good fit the k_{32} parameter is zero for both datasets. This would mean there is a compartment in the model which once entered can never be exited which is biologically unreasonable. Due to this and the fact that the parameters show a large variation between the two mice the model 3 is not a good model for this data.

As with the caffeine data the AIC statistic deems model 1 as the best for the WT data and model 2 for the HRN data.

For both the wild type and HRN first Diclofenac models the parameters are very similar in both mice. The fit of this model was good at the start of the time period for both sets of the data.

In the second model the initial concentrations and excretion parameters are similar between the wild type and HRN mice. The main difference between the two models is in the absorption parameter where the HRN value is roughly 30% of the wild type value. This calculated model shows a jagged fit due to the very quick absorption and then the fit after the first hour is similar to that of model

1. This could be due to a change in time scale dynamics i.e. fast to slow.

For the three-compartment model y(0), k_{23} and a show large differences between the sets of data. The fit of the model is the best out of the three visually with the only problem area being the shaping of the peak, which is jagged.

The AIC values suggest that the best model is model 3 for both sets of data, which is consistent with the visual results.

For the first Gefitinib model there is a marked difference between the parameters associated with the data sets. Both the initial concentration and excretion rate are much lower (52.4% and 29.8% respectively) in the HRN mouse. The fit however is good although both data sets show an absorption phase, which is not included in this model.

In the second model the parameters all are lower in the HRN mouse (53.7% for initial concentration, 72% for absorption and 31.6% for excretion) when compared with the wild type mouse. The fit for this model is good for both the HRN and wild type.

The model 3 parameters also showed differences between the HRN and WT fitted parameters. Unlike the previous two models there is a parameter that is larger in the HRN than the WT - k_{32}. This fact indicates that compartment 3 in the HRN mouse is less like a "fatty liver" as was intended since it is easier to leave than enter. All the other parameters are smaller in the HRN indicating an inherent slower absorption and metabolism of this drug within the mouse.

The average data for Gefitinib in the mice show very different behaviour between HRN and WT, which is visible from the multiple peaks in the HRN plot. Even though it shows more difference from the models the HRN test statistics show more similarity than all the WT model values.

The AIC values suggest that the best model for the HRN mouse is model 2 whereas for the WT this is the third model.

With Imatinib there was uncertainty around the normality assumption for model 1 and 2 related to the HRN data. Due to the Quartile-Quartile plot showing linearity it was still possible to use the non-linear least squares method to fit the data for these models.

With the first Imatinib model both parameters are similar for the HRN and WT data. The model only partially fit with the dynamics exhibited by the datasets suggesting more complexity was needed.

For the second model the initial concentration and elimination were similar in the two mice (difference of 10.1% and 1.5% respectively) whereas the absorption rate was a third of the wild type rate in the HRN. This means that absorption of this drug is much slower in this mouse. As with the previous model the fit is partially good as the dynamics after the first two hours are not the same as the data.

As with the second model the parameters in model 3 show little deviation between the wild type and transgenic mouse. This is the case for all but the absorption rate parameter, which has a very large difference. The model fit is good for both sets of data. However in the wild type plot the peak is jagged suggesting too quick a transition from absorption to elimination in the parameter set.

The AIC values suggested that the best model for the wild type data is the third model and for the HRN this was also the case after the first model was ruled out due to the normality assumption.

A more complex model may be needed to explain the metabolism since there are five CYP enzymes associated. This might mean that there are different sites of metabolism since they are located in both the hepatic system and small intestine. As with the previous drugs this explains the very short absorption phase exhibited by the data.

The one compartment Midazolam model with respect to this drug when fitted to

the two sets of data showed marked differences in parameter values. The differences between them for the initial concentration and excretion were +52.8% and 41.2% (HRN compared to the WT) respectively. This means that the excretion rate is much lower in the transgenic than in the wild type. The fit of this model is fine although the data shows an absorption phase not fitted by the model.

For the second model the whole parameter set showed deviation between the two data sets although with the exception of the initial concentration the values are reduced in the HRN. The fit for this data is better in the HRN than the WT although both models fail to mimic the behaviour after the one-hour point.

In the third model the initial concentration is once again larger in the HRN than the WT with all other parameters being smaller. The absorption parameter is nearly identical in both models suggesting that this is not a source of difference between the mice. Out of the three models this one shows the best visual fit to the data sets.

The AIC values showed that the HRN and wild type data were fitted best by the model 2 and model 3 respectively. Through all three model fittings the parameters for this drug were smaller with respect to the HRN mouse than the wild type suggesting a physiological or metabolic difference. For both of the Midazolam data sets model 3 is the best fit both visually and numerically. The fact that this model fits well could be due to this drug being associated with only one CYP enzyme located in the liver and small intestine.

For the first Omeprazole model there are large differences between the fitted parameter sets the HRN initial concentration is 1.5 times larger than the wild type although the corresponding excretion rate is only 23.1%. As with other data sets the HRN shows an absorption phase, which is not catered for within the one compartment model. The wild type data model shows a good fit throughout the time period.

Although all of the Omeprazole models do not fit well when using the χ^2 test but out of all of them the third model shows the most similarity. This drug is metabolised by two CYP enzymes that are located within the liver, which explains the absorption phase being slower due to the movement from the peritoneum.

Within the second model there are large differences in the parameter values including the initial concentration. This value is ten times higher in the transgenic mouse and the excretion is 1.6 times larger but the absorption is only 6% of the wild type value. These mean that the mouse has slow absorption and fast excretion but starts out with a much higher amount of drug which is unusual since the dose was the same in both mice. The fit to the data is good for both the wild type and transgenic mice.

For the third model the parameter sets show large deviations as with the previous two models especially in the initial concentration, which is double the wild type value in the transgenic mouse. For the rate parameters, k_{12}, k_{23} and k_{32} are 42.1% smaller, 30.8% smaller and 1.585 times larger than the values in the wild type respectively. The a parameter is also larger at roughly 4 times the WT value. The "fatty liver" compartment still holds for both sets of data as $k_{23} >> k_{32}$. The fit of this model is the best visually for both sets of data although the peaks are jagged in shape.

The chosen models using the AIC values are the third model for the wild type data and the second model for the HRN data.

For the first and third Paclitaxel model in the Hepatic Reductase Null mouse the data shows significant systematic deviation from the fitted models. This agrees with the fact that for both these models the line fits the data poorly in the HRN mouse. As such the only model left for parameter comparison is the two compartment model. The parameters in the second model show differences in the initial concentration (+17%) and excretion rate (+4.6%) are larger in the transgenic

mouse and the reverse is true for the absorption (0.2%). The AIC deems the second model the best for the HRN and the third for the WT. This is congruent with the visual fit of these models and the fact that the first and third models are unsuitable for the HRN data due to the significant Runs test.

With regards to Tamoxifen the metabolism must be quite complex since it is an oral administration and associated with six CYP enzymes. The data for this drug go from 24 hours in the HRN and only for 7 for the WT. As such it is difficult to compare fit between the two. There is a large gap between the 7 and 24-hour point and as such fitting the models is difficult.

As with Paclitaxel, Tamoxifen HRN data shows systematic deviation but only in regards to model 1. Since the Tamoxifen data shows an absorption phase this model is not going to show the same behaviour.

For model 2 the initial concentrations between the two mice are similar whereas the rate parameters representing absorption and excretion are smaller. The k_{12} parameter is 14.6% and the elimination is 62% of the wild type suggesting that these processes are slower within the transgenic mouse. The fit of this model is better for the WT data than that for the HRN data. There is disparity between the HRN model and the raw data between the 7hr and 24hr points but this is more due to a lack of points between.

In the third model the most worrying parameter difference is that the time dependent elimination is zero in the wild type mouse i.e. $\frac{dy_4}{dt} = 0$ and since the initial value for y_4 is zero there is no excretion of this drug. The initial concentration in the transgenic mouse is 65.1% higher than in the wild type but all the absorption parameter is smaller so this phase is slower. The influx and outflow from the third compartment are larger in the HRN than in the WT and this could indicate the presence of a larger compartment or liver with a higher concentration of fat cells. The AIC values suggest that the best model for the transgenic mice is the second

model and this is also the case in the wild type. This means that the third compartment is not necessary for a good fit to the data. The data for both the wild type and HRN mouse showed absorption and thus the first Thalidomide model was not a good fit. Although the initial concentration for the second model was roughly double in the HRN mouse the rate parameters associated were both half the wild type rate. This suggests that physiologically the absorption and elimination of the transgenic mouse was much slower than a normal mouse metabolising Thalidomide. The visual fit of this model to the data sets was good with the exception of the peak area.

For the third model there was large differences in the parameter values with all being greater in the HRN with the exception of k_{12} which was a third of the WT rate. The visual fit of the model is good for the data although there is still a disparity in peak shape for both mice.

The AIC values suggest that the best model for the HRN data is the third model and for the WT it is the second. This drug is only associated with one CYP enzyme in the liver which should mean a less complex model is best which is the case in the wild type mouse.

Throughout this chapter the same three models have been fitted to the data sets with varying amount of success. The reasons for this varied from the need of an absorption phase i.e. model 1 is unsuitable to more peaks exhibited by the data than are allowed in the model formulation. It shows that although the traditional one compartment (model 1) and two compartment (model 2) fit well to the data sometimes a more complex model is necessary. The complex behaviour could stem from the need for multiple time scales this could mean multiple Cytochrome P450 enzymes are acting on the drug. The novel model 3 outlined in this chapter takes a step towards addressing this need for more complexity.

When the parameters for the HRN and wild type mice were compared for most

of the data sets the HRN rates were slower than their counterpart. This could mean there is a metabolic difference between the two mice stemming from the genetic knockout. Since metabolism is dependent on a number of factors it is difficult to pin this down to one physiological parameter. Within the Tamoxifen model 3 there was evidence supporting the observation that the knockout caused a liver filled with a higher proportion of lipid cells.

The problem with fitting the compartment models to these sets of data is generated by experimental constraints. It would be easier if more data were available instead of just three mice of each type for each drug. This would mean that the average would be statistically more representative which would aid in providing a better fit.

Other than the number of mice it would be useful if more samples could be taken or at least they could be more regular. However this is unfeasible since the volume of blood in a mouse is finite and takes a while to replenish. It is due to these constraints that sampling is prioritised within the first hour after the dose. For some of the drugs shown in this chapter earlier sampling is needed in order to record concentrations during fast processes such as absorption e.g. Caffeine.

Chapter 4

Sensitivity Analysis

4.1 Introduction

Sensitivity analysis is a method of investigating the effect of parameter change on the solution of models (Turanyi, 1990) that can be anything from kinetic to stochastic models in science and engineering (Varma et al., 1999). This is useful for optimising the parameters in order to fit real data or finding out if there are any parameters that have little or no effect so they can be left out of the next formulation of the model. Also to analyse the robustness of the model to errors in parameter estimation and experimental error.

There are numerous ways of getting sensitivity measures including local and global techniques. Local methods produce gradients with relation to the parameter at time points along the domain. When looking for the global sensitivity it finds parametric importance over the parameter space in question (Rabitz et al., 1983).

Examples of local sensitivity methods are (Rabitz et al., 1983; Turanyi, 1990)- Finite difference methods, Curve fitting and derivative extraction, Direct differential methods, Green‘s Function Method (GFM) and Analytically Integrated Magnus (AIM method. The first three in this list give accurate sensitivities (to

different degrees) and have a low computational cost. When the number of parameters gets large in comparison to the number of variables, then the GFM or AIM are advised (Turanyi, 1990) to get the sensitivity gradient.

Global techniques for sensitivity analysis are - Stochastic Sensitivity Analysis, Fourier Amplitude Sensitivity Test (FAST), Walsh Amplitude Sensitivity Procedure (WASP), Monte Carlo and Latin hypercube methods. Global methods are more computationally intensive and therefore it is more difficult to attain these sensitivities. As such local measures are used more often in the literature due to these constraints.

Some of these techniques (either local or global) are more popular in the literature than others, for example, FAST and Monte Carlo methods are popular global techniques, whereas, for the local methods finite difference is most often used. Some good reviews of these methods can be found in Rabitz et al. (1983), Kramer and Leis (1988), Turanyi (1990) and Saltelli et al. (2005).

4.2 Sensitivity Analysis Theory

4.2.1 Sensitivity Coefficients

Local Techniques

Finite difference methods are sometimes thought of as a brute force or indirect method and the application of this is using the following equation (Turanyi, 1990):

$$\frac{\partial c(t_2)}{\partial k_j(t_1)} \simeq \frac{c(t_2, k_j + \Delta k_j) - c(t_2, k_j)}{\Delta k_j},$$

with reference to the differential equation:

$$\frac{dc}{dt} = f(c, k).$$

This method is used frequently since a normal ODE solver is the only code needed to solve for the sensitivity coefficients.

Takors et al. (2004) used the finite difference method to simplify complex kinetic models explaining metabolic pathways concerning glycolysis in *E. Coli*. This model started out with 122 parameters and using sensitivity analysis they were able to minimise this number to 73 parameters.

Zak et al. (2005) used this method while investigating models explaining cell cycle and circadian dynamics. Since these models deal with situations that show oscillations, it is more difficult to tell whether the sensitivity is to do with the behaviour of the system or parameter changes.

For biophysical models, Gunawan et al. (2005) compared deterministic (finite difference method) and stochastic (Monte Carlo) approaches to calculating the sensitivity coefficients.

Global Techniques

Saltelli et al. (2005) compare the results from local (Taylor expansion) and global methods (FAST, Monte Carlo and Latin Hypercube sampling). It uses theoretical chemical reactions in order to investigate issues with computer use and outcome quality. These were calculated on SIMLAB and therefore it is easier to compare computational cost.

In Gertner and Xu (2008) the FAST method is investigated through a number of test cases and is compared to an ANOVA (ANalysis Of VAriance) method. One of the main uses for the FAST method in this paper was to account for correlated and uncorrelated parameters.

Monte Carlo methods include Markov Chain Monte Carlo (MCMC) that can be seen in Jayawardhana et al. (2008) and Calvetti et al. (2008). In the Jayawardhana et al. (2008) paper MCMC is used in conjunction with Bayesian inference

to investigate parametric estimation in glycolytic and pyruvate pathways. This paper shows a method that uses steady state data and copes with outside factors that affect the variables but are not present in the equations. Calvetti's paper also uses a Bayesian framework to analyse dynamic compartment based models dealing with myocardial metabolism. Due to the size of the model it draws some conclusions about the pathway but ends pretty inconclusively.

Ancheyta and Alcázar (2007) use Monte Carlo methods for parameter estimation as does Kramer and Snowling (2001) and Horenko et al. (2005). They all use the Monte Carlo method to pick estimates from a probability density function and simulate the model through time to see how change in parameters changes the model solution.

4.2.2 Analysis of the Difference between the Percentile and Normal Drug Uptake Curves

In order to test the effects caused by altering parameters it is necessary to choose how big a change is required to obtain a significant change. In the current literature there are large differences in the size of change ranging from 1% to 50%. Some have worked with a 1% change either side of the chosen parameter value Yang et al. (1997), Rieger et al. (2005), Gunawan et al. (2005) and Zak et al. (2005). There are examples of larger differences showing a 10% change - Ancheyta and Alcázar (2007), Gertner and Xu (2007), Brugnach (2005) and Gertner and Xu (2008). Finally Ancheyta and Alcázar (2007) and Saltelli et al. (2005) show that up to a 20% change is feasible and for second order derivatives a 50% change holds (Saltelli et al., 2005).

4.3 Sensitivity Analysis Method

4.3.1 Sensitivity Test

Using *sens_sys.m* developed by Mollá and Padilla (2002) for MATLAB as a replacement for ODE15s as its base the sensitivity coefficients $\frac{dy}{du}$ were calculated where y is the variable and u is the parameter. This function requires a system of vectorised equations, initial and parameter values in order to calculate the derivative over time with respect to the parameter. *Sens_sys.m* uses an iterative approximation in order to find the derivatives (Mollá and Padilla, 2002).

Once the sensitivity coefficients have been found it is useful to plot them over time and examine their effect on the variable, which can be either: positive, negative, both and none. As well as this inspection a look at the maximum and minimum value and therefore the range helps to find the parameters that have the most effect on the variable in question.

In the previous chapter where compartment models were applied to the CXR Biosciences data sets the model parameters showed both small and large differences between the HRN and wild type mice. The smallest deviation for the Midazolam data used in this chapter was 4.4% and the largest was 77.6%. Due to this and from the evidence outlined in the previous section a 10% deviation was chosen as a big enough change to ensure response is significant for the sensitivity test.

4.3.2 Magnitude Measure

The magnitude measure is the following test statistic:

$$\sum \frac{(y_{norm\pm 10\%} - y_{norm})^2}{(p_{norm\pm 10\%} - p_{norm})}$$

It can be seen that this equation is based on a least-squared approach, since if there is little difference between the curves this value will be small. The denominator compensates for the magnitude of the 10% difference to allow comparison between parameters.

Once this sum has been calculated the maximum is found. As it is possible that many parameters could have a similar strength of sensitivity the parameters that have a similar effect in size are included. This is achieved by tabulating all the parameters with a result within the following range:

$$[10^{-3} \sum \frac{(y_{norm\pm 10\%} - y_{norm})^2}{(p_{norm\pm 10\%} - p_{norm})}, 10^{3} \sum \frac{(y_{norm\pm 10\%} - y_{norm})^2}{(p_{norm\pm 10\%} - p_{norm})}] \tag{4.1}$$

As well as this measure a paired t test was used to analyse the differences between the data sets as explained in section 3.3.

4.3.3 Extended Sensitivity Testing

Using a random number from a gamma distribution dependent on the mean and variance being the original value and +/- 10% respectively. The gamma distribution was chosen due to it being characterised as wholly positive and only bound at zero. The mean and variance for this distribution are defined as:

$$\bar{x} = \frac{\alpha}{\lambda} \qquad\qquad \sigma^2 = \frac{\alpha}{\lambda^2} \tag{4.2}$$

Using these equations the correct parameter for the distribution associated with the original model parameter values. Rearranging and solving simultaneously the

above equations using a variance of 10%-(-10%) = 20% the equations become:

$$\alpha = \lambda\bar{x} = 0.2\lambda^2 \tag{4.3}$$

$$\Rightarrow \lambda = 5\bar{x} \tag{4.4}$$

$$\Rightarrow \alpha = 5\bar{x}^2 \tag{4.5}$$

After the distribution parameters are found as above the model is run with one hundred random values from the appropriate distribution. At each time point the minimum and maximum value was taken and from these a range is calculated.

4.4 Results

For the first three models the parameter values are taken from the fitted models to Midazolam (Wild Type) data as shown in table 3.11. For Cytochrome P450 (CYP) cycle and model the initial values of enzyme and drug are 3 and 5 respectively and the parameters are shown in Tables 5.3 and 5.4.

4.4.1 Model 1

This model has the following equation and initial value:

$$\frac{dy}{dt} = -k_{10}y$$

When changing the parameter k_{10} by 10% the graph of the function and the associated sensitivity graph for y shows:

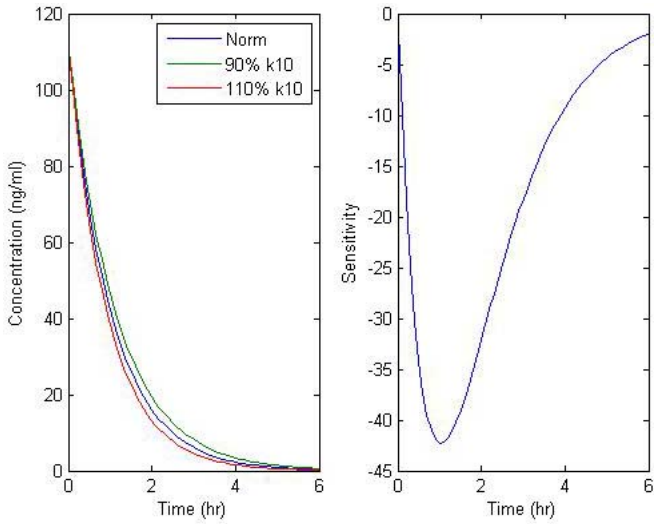

Figure 4.1: *The left hand plot shows the difference between the fitted model in comparison with a 10% difference in Model 1 with the k_{10} parameter over time. The right hand plot shows the calculated sensitivity from sens_sys.m for the parameter and variable over time.*

It can be observed that the parameter has a large effect at around the one-hour point. This is consistent with the ten percent graph above as the only difference shown is initiated around this time point. The fact that the sensitivity graph is negative means that as the parameter value gets larger the variable should be smaller. This is also shown in the ten percent plot, as the "110% k10" line is smaller than the "norm" line, which is less than the "90% k10"line.

The results of the magnitude and paired t test p values are:

Model1		k_{10}
Σ	110%	3858.10121
	90%	2857.983479
t	110%	2.14899E-16
	90%	2.12118E-14

Table 4.1: *Model 1 - t Test p values and Magnitude Test Statistics.*

As the p values for the paired t test are much less than 0.05 the null hypothesis is rejected in favour the alternative that is the value of y is independent of the change in parameter k_{10}. The magnitude result is large but this is expected since it is the only parameter. The parameter k_{10} has an associated gamma distribution of

Γ(4.6986818,4.847). The maximum range from the extended sensitivity analysis is 78.58821432 for k_{10}. The different curves are shown in the following plot:

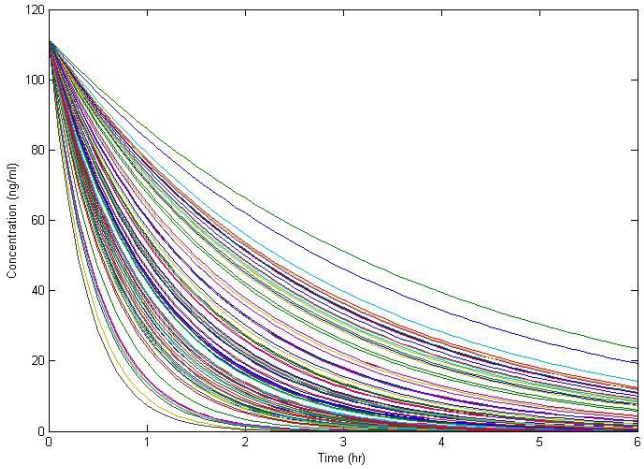

Figure 4.2: *Plot showing the impact of using a random value from a probability density function for the parameter k_{10} in Model 1.*

It can be observed from this that the change in parameter value can make a large difference, which confirms the results from the previous tests.

4.4.2 Model 2

The equations for this model are:

$$\frac{dy_1}{dt} = -k_{12}y_1 \tag{4.6}$$

$$\frac{dy_2}{dt} = k_{12}y_1 - k_{20}y_2 \tag{4.7}$$

The explicit solutions to this system of equation show that the following relationship between the variables and parameters should hold:

Model2	k_{12}	k_{20}
y_1	✓	✗
y_2	✓	✓

Table 4.2: *Model 2 Explicit Solution Relationship with Parametric Sensitivity.*

The three ten percent graphs (since y_1 and k_{20} show no sensitivity as shown

in the table above) associated with the change in parameter value for both k_{12} and k_{20} are:

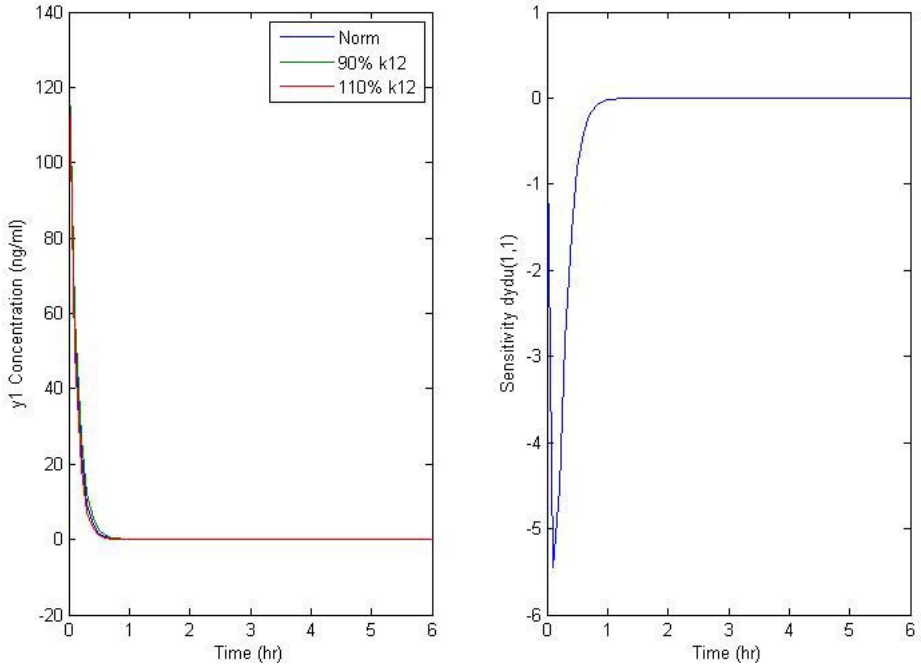

Figure 4.3: *The left hand plot shows the difference between the fitted model in comparison with a 10% difference in Model 2 with the k_{12} parameter with respect to y_1 over time. The right hand plot shows the calculated sensitivity from sens_sys.m for the parameter and variable over time.*

This plot shows sensitivity in the first hour and is negative, therefore the larger the parameter value is for k_{12} the smaller y_1 should be and the ten percent plot shows this.

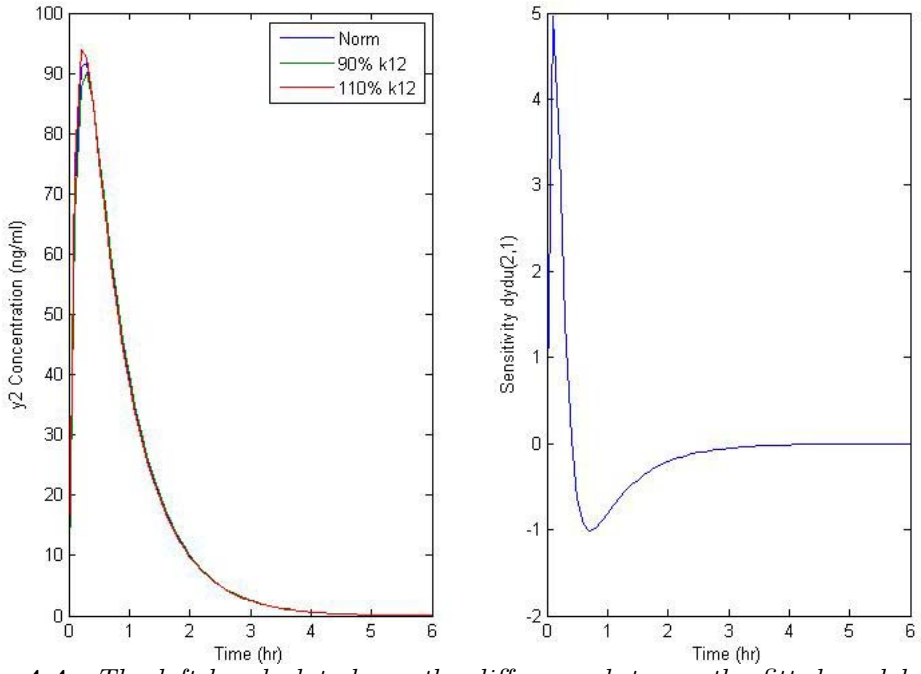

Figure 4.4: *The left hand plot shows the difference between the fitted model in comparison with a 10% difference in Model 2 with the k_{12} parameter with respect to y_2 over time. The right hand plot shows the calculated sensitivity from sens_sys.m for the parameter and variable over time.*

These plots show that y_2 is sensitive to k_{12} for the first 3 hours. The first 0.5 hour the graph shows a positive sensitivity which means that the larger k_{12} is, the larger y2 is, but then after this point y_2 is negatively sensitive to k_{12} i.e. the larger k_{12} causes a smaller y_2 value.

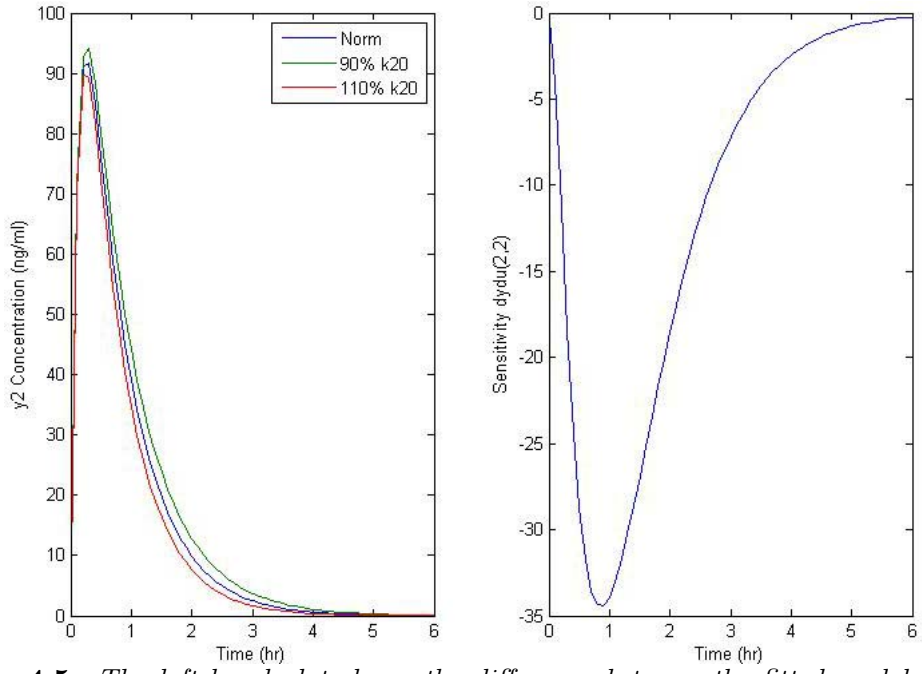

Figure 4.5: *The left hand plot shows the difference between the fitted model in comparison with a 10% difference in Model 2 with the k_{20} parameter with respect to y_2 over time. The right hand plot shows the calculated sensitivity from sens_sys.m for the parameter and variable over time.*

This plot shows sensitivity over the entire time period and is negative so that the larger the parameter value is for k_{20} the smaller y_2 should be and the ten percent plot shows this.

The results for the magnitude are:

Model2		k_{12}	k_{20}
y_1	110%	46.42571648	4.10729E-11
	90%	63.43745506	3.97125E-11
y_2	110%	34.60459351	1921.869627
	90%	46.15739087	2604.567308

Table 4.3: *Model 2 - Σ Test Statistics.*

And for the paired t test:

Model2		k_{12}	k_{20}
y_1	110%	0.999999616	0.042932943
	90%	0.034748543	0.039667563
y_2	110%	0.870438539	1.22367E-09
	90%	0.886952553	8.39084E-11

Table 4.4: *Model 2 - Paired t Test p values.*

In order to find out the most effective parameter for each y it is useful to look at the magnitude and t test jointly. For y_1 and y_2, k_{12} and k_{20} are the most effective parameters respectively.

The extended sensitivity analysis showed parameter distribution and maximum ranges as follows:

Model2	k_{12}	k_{20}
p.d.f	Γ(385.2225313, 43.8875)	Γ(9.47100845, 6.8815)
y_1	13.29368206	1.78471E-05
y_2	12.11069991	74.79936767

Table 4.5: *The ranges and Probability Density Functions with respect to the parameters and variables for Model 2.*

The effect of the change of values k_{12} on y_1 is shown in the following plot:

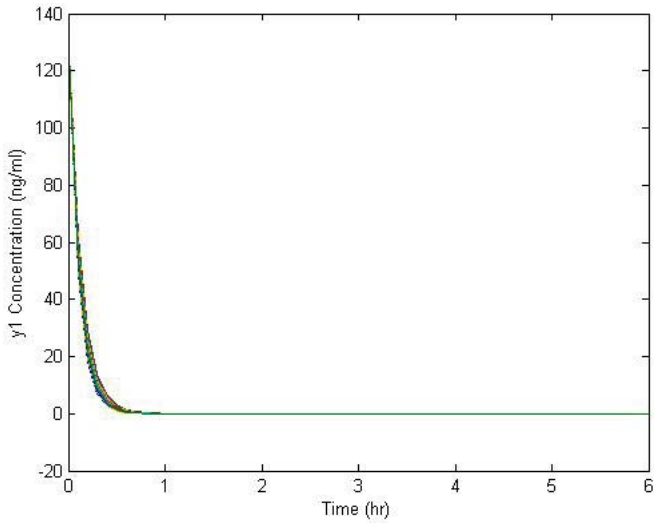

Figure 4.6: *Plot showing the impact of using a random value from a probability density function for the parameter k_{12} with respect to y_1 in Model 2.*

From this plot and the range value in the table shows that k_{12} has an effect

on the value of y_1 over the first hour. For y_2 the parameter k_{12} has less of an effect shown by the range values and the plot is:

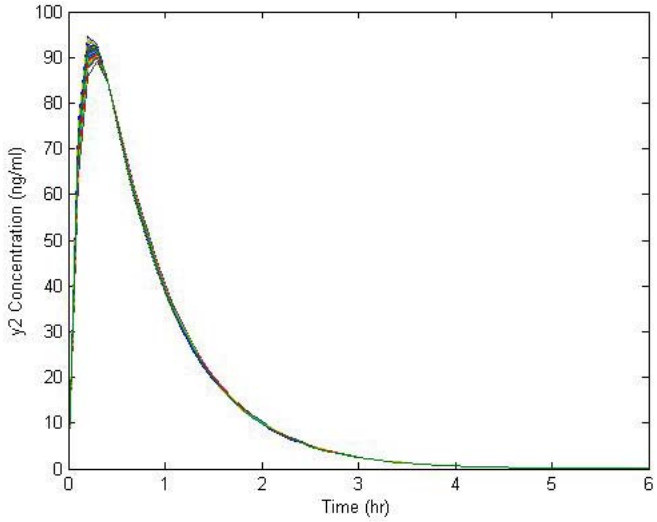

Figure 4.7: *Plot showing the impact of using a random value from a probability density function for the parameter k_{12} with respect to y_2 in Model 2.*

Both variables are affected by k_{12} to a similar extent and over the first three hours. This confirms the results from the t test p values and the magnitude test statistics. For k_{20}, from all previous tests, shows that it has a large effect on y_2 and the plot is:

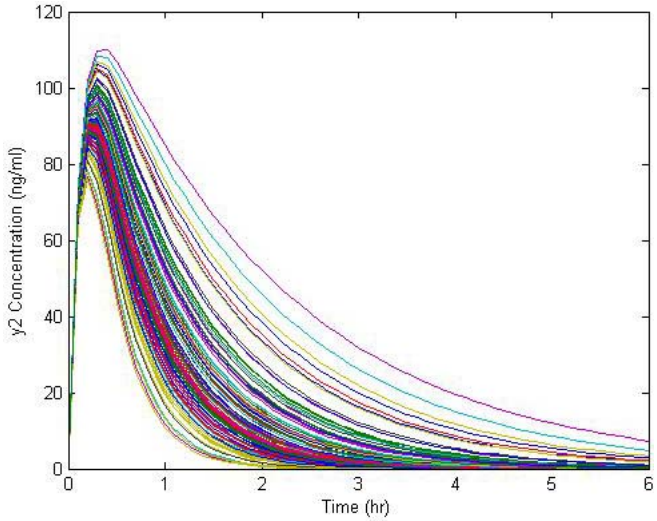

Figure 4.8: *Plot showing the impact of using a random value from a probability density function for the parameter k_{20} with respect to y_2 in Model 2.*

This shows a wide range in resultant curves for y_2 at least beyond the 0.5-hour

point.

4.4.3 Model 3

The equations for this model are:

$$\frac{dy_1}{dt} = -k_{12}y_1 \tag{4.8}$$
$$\frac{dy_2}{dt} = k_{12}y_1 - k_{23}y_2 + k_{32}y_3 - y_4 \tag{4.9}$$
$$\frac{dy_3}{dt} = k_{23}y_2 - k_{32}y_3 \tag{4.10}$$
$$\frac{dy_4}{dt} = a \tag{4.11}$$

The explicit solutions to this system of equation show that the following relationship between the variables and parameters should hold:

Model3	k_{12}	k_{23}	k_{32}	a
y_1	✓	✗	✗	✗
y_2	✓	✓	✓	✓
y_3	✓	✓	✓	✓
y_4	✗	✗	✗	✓

Table 4.6: *Model 3 Explicit Solution Relationship with Parametric Sensitivity.*

The ten percent graphs for this model are (again if the table above shows no sensitivity the plot is not shown):

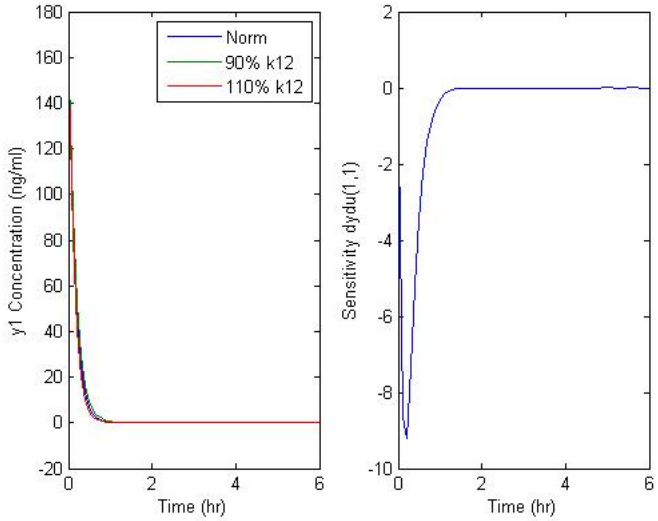

Figure 4.9: *The left hand plot shows the difference between the fitted model in comparison with a 10% difference in Model 3 with the k_{12} parameter with respect to y_1 over time. The right hand plot shows the calculated sensitivity from sens_sys.m for the parameter and variable over time.*

It is unclear from the ten percent plot, which way the parameter difference affects the y_1 value but from the sensitivity graph it shows that as k_{12} increases y_1 decreases, but the sensitivity is only prevalent in the first hour.

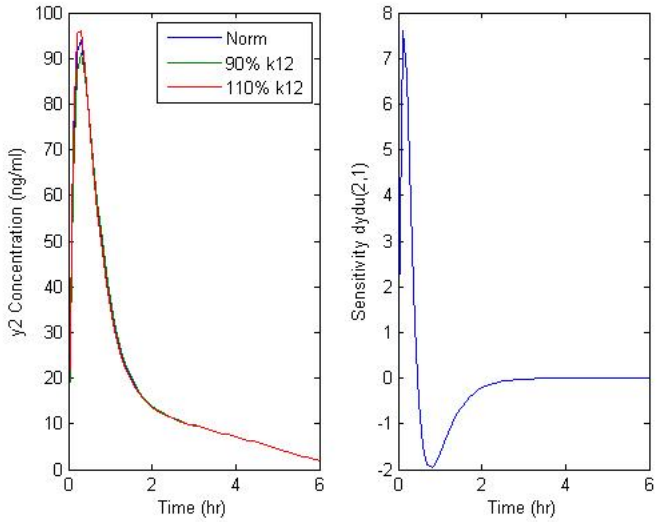

Figure 4.10: *The left hand plot shows the difference between the fitted model in comparison with a 10% difference in Model 3 with the k_{12} parameter with respect to y_2 over time. The right hand plot shows the calculated sensitivity from sens_sys.m for the parameter and variable over time.*

At the start of the time period the effect of k_{12} on y_2 is positive and then after 0.5 hours the sensitivity curve becomes negative. After the 3-hour point the variable is no longer sensitive to the parameter change.

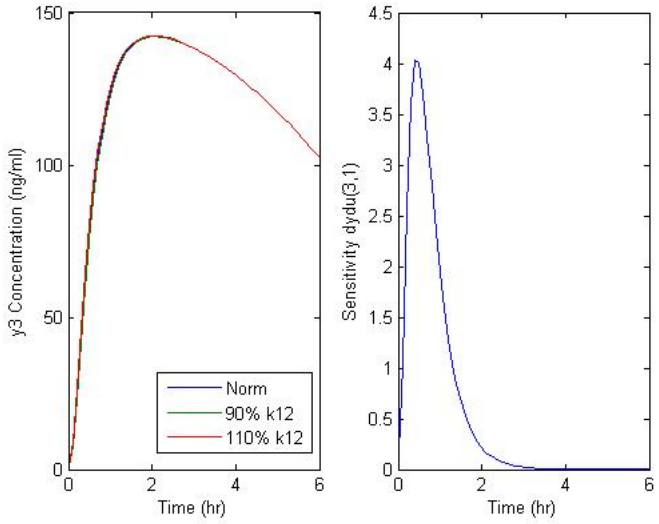

Figure 4.11: *The left hand plot shows the difference between the fitted model in comparison with a 10% difference in Model 3 with the k_{12} parameter with respect to y_3 over time. The right hand plot shows the calculated sensitivity from sens_sys.m for the parameter and variable over time.*

Within the first two hours the "norm +10%" curve will be bigger than the norm due to a positive sensitivity but this lessens by the 2hr point.

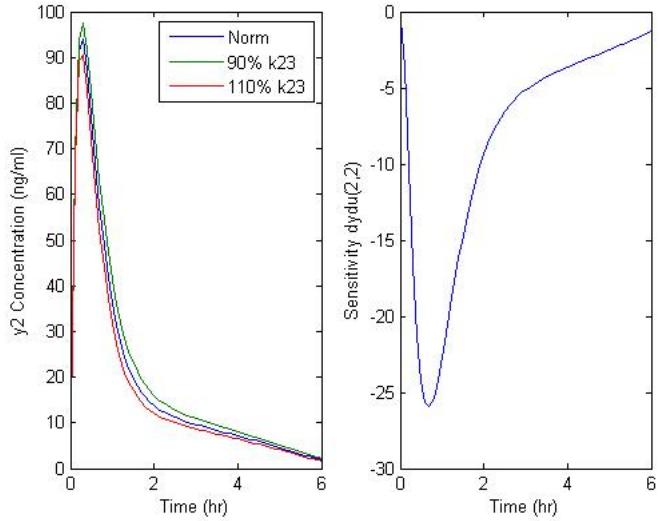

Figure 4.12: *The left hand plot shows the difference between the fitted model in comparison with a 10% difference in Model 3 with the k_{23} parameter with respect to y_2 over time. The right hand plot shows the calculated sensitivity from sens_sys.m for the parameter and variable over time.*

The sensitivity plot shows a negative effect of the parameter k_{23} on y_2, which means that if k_{23} is bigger than the norm of the model it causes y_2 to be smaller than the norm curve.

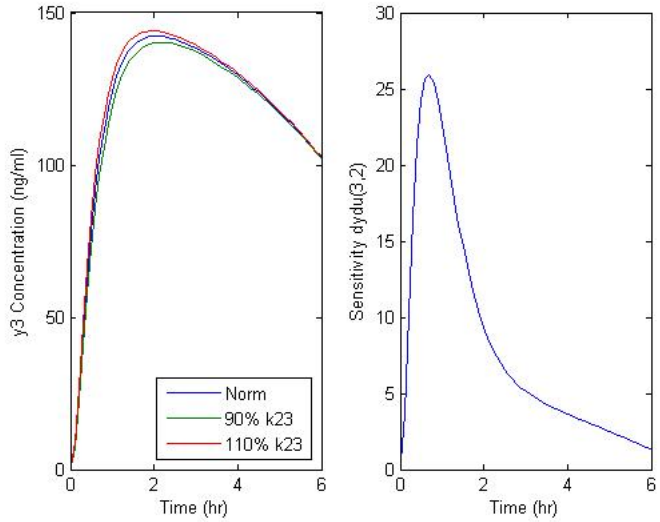

Figure 4.13: *The left hand plot shows the difference between the fitted model in comparison with a 10% difference in Model 3 with the k_{23} parameter with respect to y_3 over time. The right hand plot shows the calculated sensitivity from sens_sys.m for the parameter and variable over time.*

k_{23} has a positive effect on y_3 over the entire period which means that if k_{23} is larger then y_3 will be larger too.

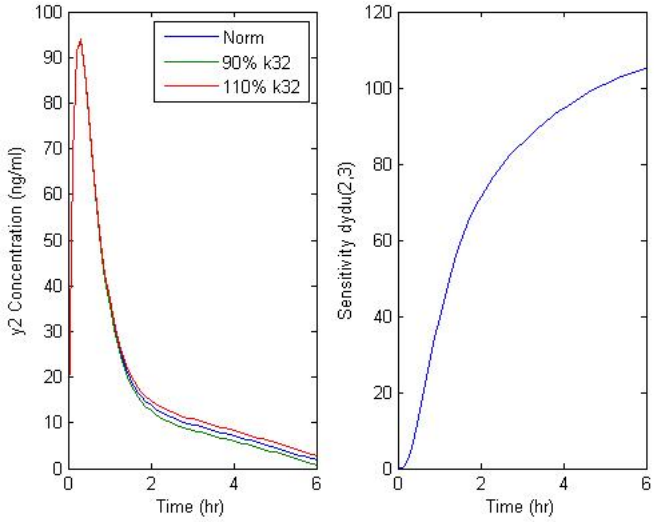

Figure 4.14: *The left hand plot shows the difference between the fitted model in comparison with a 10% difference in Model 3 with the k_{32} parameter with respect to y_2 over time. The right hand plot shows the calculated sensitivity from sens_sys.m for the parameter and variable over time.*

k_{32} has a positive effect on y_2 over the entire period which means that if k_{32} is larger then y_2 will be larger too.

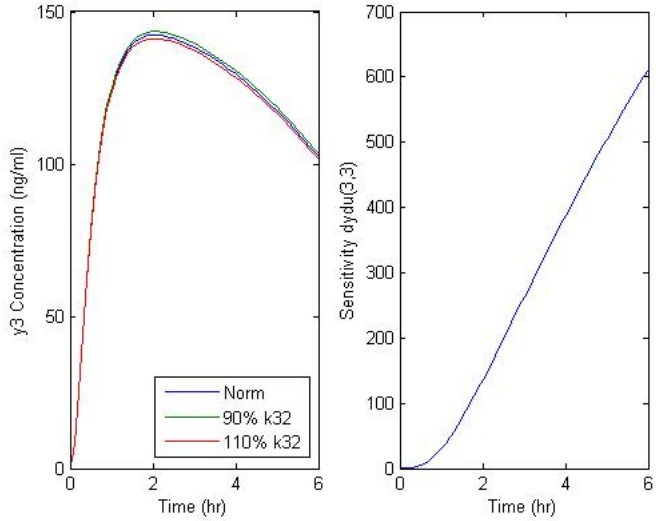

Figure 4.15: *The left hand plot shows the difference between the fitted model in comparison with a 10% difference in Model 3 with the k_{32} parameter with respect to y_3 over time. The right hand plot shows the calculated sensitivity from sens_sys.m for the parameter and variable over time.*

k_{32} has a positive effect on y_3 over the entire period which means that if k_{32} increases, y_3 will do the same.

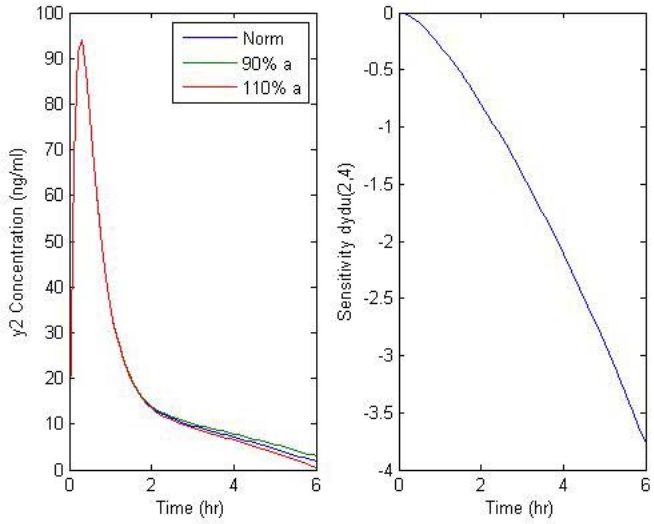

Figure 4.16: *The left hand plot shows the difference between the fitted model in comparison with a 10% difference in Model 3 with the a parameter with respect to y_2 over time. The right hand plot shows the calculated sensitivity from sens_sys.m for the parameter and variable over time.*

The sensitivity plot shows a negative effect of the parameter a on y_2 which

means that if a is bigger than the norm of the model it causes y_2 to be smaller than the norm curve especially at the end of the period since that is when the sensitivity is higher.

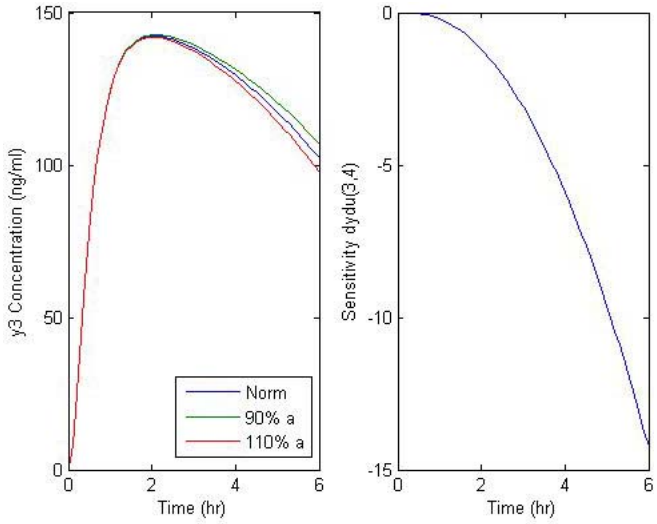

Figure 4.17: *The left hand plot shows the difference between the fitted model in comparison with a 10% difference in Model 3 with the a parameter with respect to y_3 over time. The right hand plot shows the calculated sensitivity from sens_sys.m for the parameter and variable over time.*

The sensitivity plot shows a negative effect of the parameter a on y_3. This is similar to the effect a has on y_2.

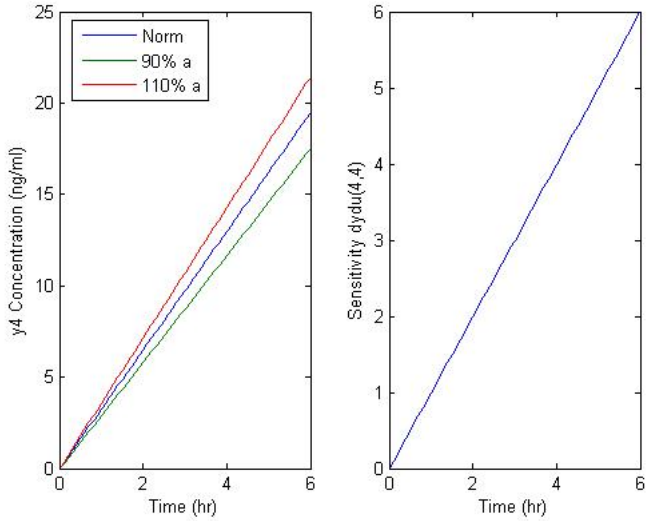

Figure 4.18: *The left hand plot shows the difference between the fitted model in comparison with a 10% difference in Model 3 with the a parameter with respect to y_4 over time. The right hand plot shows the calculated sensitivity from sens_sys.m for the parameter and variable over time.*

The parameter a has a positive effect on y_4 over the entire period which means that if a is larger then y_4 will be larger too this is understandable since it is directly proportional to the gradient in the model equations.

The magnitude results are:

Model3		k_{12}	k_{23}	k_{32}	a
y_1	110%	142.0500983	1.03102E-11	1.66127E-12	1.81789E-16
	90%	192.5731239	1.92793E-11	1.59893E-12	4.75816E-17
y_2	110%	77.85633289	1358.358575	3093.936724	73.76749612
	90%	100.3570105	1848.135197	3196.142832	73.7674949
y_3	110%	53.87347289	1358.353019	3093.938887	771.0636614
	90%	77.44943342	1848.128794	3196.145423	771.0636694
y_4	110%	3.97087E-27	3.40951E-27	7.77754E-26	239.498688
	90%	1.46177E-27	5.77218E-27	8.26689E-26	239.498688

Table 4.7: *Model 3 - Σ Test Statistics.*

And the paired t test p values are:

Model3		k_{12}	k_{23}	k_{32}	a
y_1	110%	0.015781416	0.676968011	0.262424501	0.003326071
	90%	0.010518866	0.34072817	0.449552078	0.000741898
y_2	110%	0.867849815	1.40703E-11	2.66665E-30	2.84028E-15
	90%	0.840208799	1.95825E-12	3.13127E-30	2.84028E-15
y_3	110%	0.000115989	1.40715E-11	2.66663E-30	4.20416E-11
	90%	8.15396E-05	1.95843E-12	3.13125E-30	4.20415E-11
y_4	110%	6.03094E-06	0.705790135	0.004538659	2.13912E-19
	90%	0.717919965	0.084834393	2.48321E-05	2.13912E-19

Table 4.8: *Model 3 - Paired t Test p values.*

Most of the paired t test p values in the table are significant at the 5% level with the exception of k_{23}:y_1, k_{23}:y_4 and k_{12}:y_4(90%). Due to this it is better to draw conclusions from both statistics jointly. y_2 by k_{32}; y_3 by k_{32} and y_4 by a in both result sets. For y_1, the magnitude results show that it is primarily affected by k_{12}. However the paired t test suggests that a is the most significant which is odd since the explicit solution for y_1 does not contain a. From the magnitude results it can be seen that k_{23} also has an effect on y_2 and y_3 but not as great as k_{32}.

For the extended sensitivity analysis the probability densities and ranges are as follows:

Model3	k_{12}	k_{23}
p.d.f	Γ(199.0805,31.55)	Γ(21.9828512,10.484)
y_1	18.16077958	6.95738E-06
y_2	15.3054356	49.30430778
y_3	7.9238265	49.30425246
y_4	4.9738E-14	4.9738E-14
Model3	k_{32}	a
p.d.f	Γ(0.19424205,0.9855)	Γ(52.6436352,16.224)
y_1	1.90479E-05	2.35617E-08
y_2	88.17826511	9.226851326
y_3	88.17827273	34.89966143
y_4	9.9476E-14	14.70883874

Table 4.9: *The ranges and Probability Density Functions with respect to the parameters and variables for Model 3.*

For k_{12} the variable y_1 is sensitive just as the following plot shows:

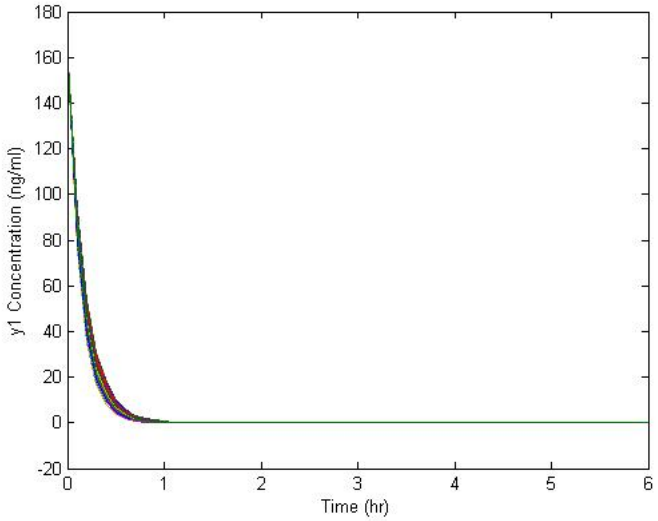

Figure 4.19: *Plot showing the impact of using a random value from a probability density function for the parameter k_{12} with respect to y_1 in Model 3.*

However the sensitivity is only in effect for the first two hours as was shown on the ten percent plot. y_2's reaction to change in the parameter k_{12} is shown as follows:

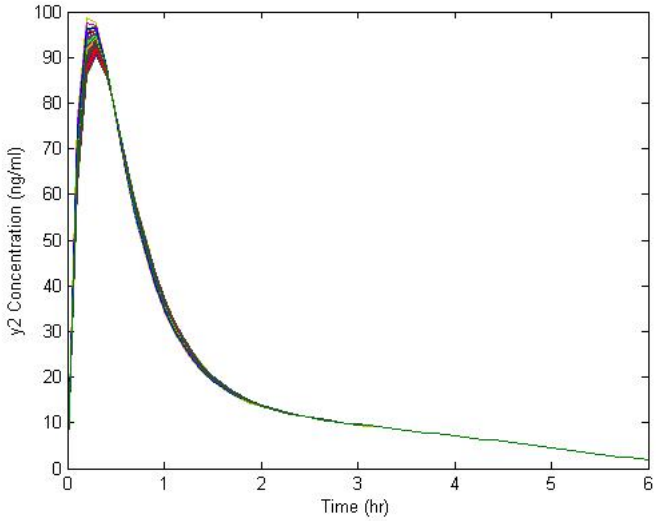

Figure 4.20: *Plot showing the impact of using a random value from a probability density function for the parameter k_{12} with respect to y_2 in Model 3.*

From this plot that the sensitivity is slightly larger than the previous plot occurs across the entire time period. For y_3 the extended sensitivity plot is:

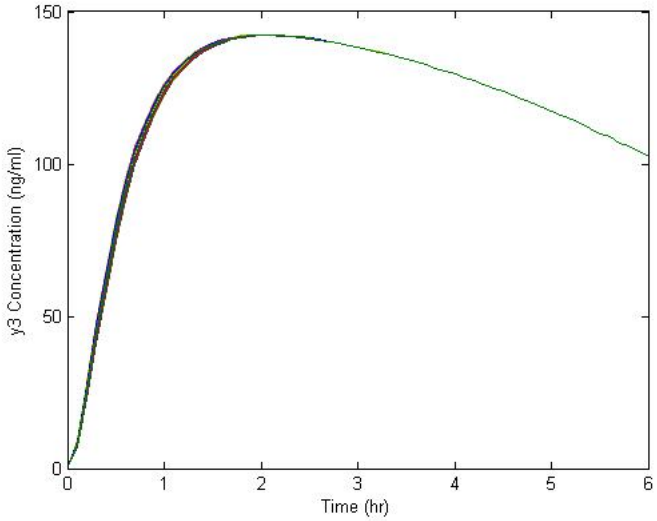

Figure 4.21: *Plot showing the impact of using a random value from a probability density function for the parameter k_{12} with respect to y_3 in Model 3.*

This plot shows a low sensitivity but looks very similar in banding to the last plot.

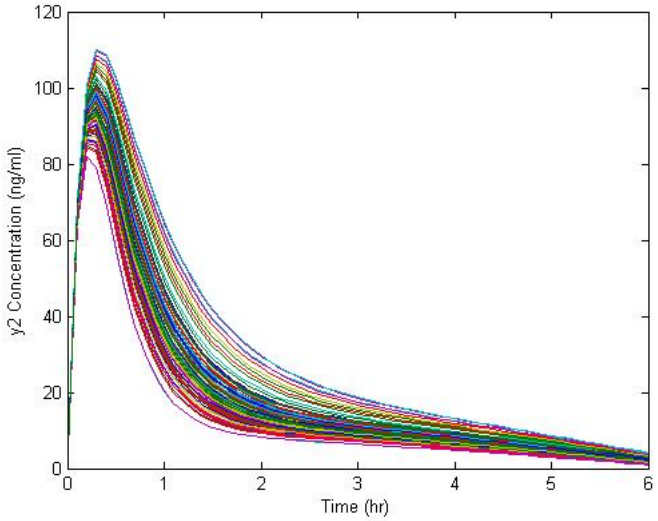

Figure 4.22: *Plot showing the impact of using a random value from a probability density function for the parameter k_{23} with respect to y_2 in Model 3.*

The parameter k_{23} effect on y_2 shown above, indicates the large sensitivity; which is in line with the other tests of sensitivity.

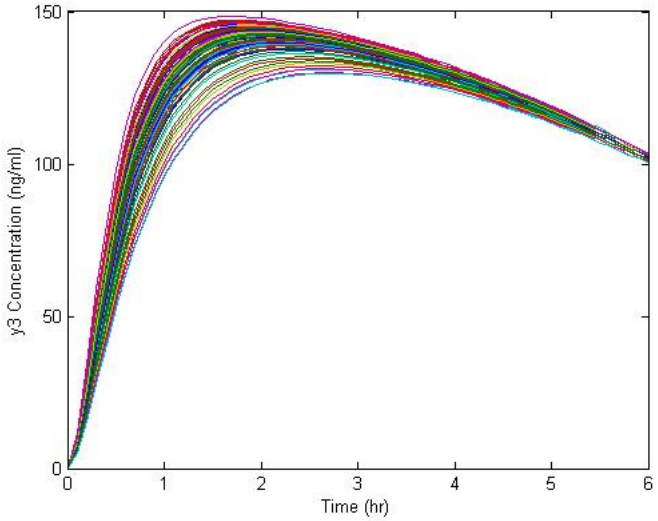

Figure 4.23: *Plot showing the impact of using a random value from a probability density function for the parameter k_{23} with respect to y_3 in Model 3.*

The interaction between k_{23} and y_3 is similar in range size and magnitude statistic as that of y_2.

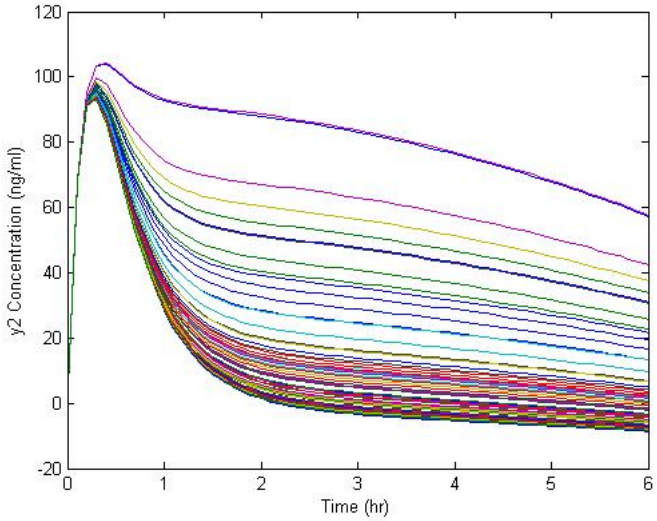

Figure 4.24: *Plot showing the impact of using a random value from a probability density function for the parameter k_{32} with respect to y_2 in Model 3.*

The above plot shows the effect of change in k_{32} value on y_2 in the model. This shows that this parameter can be the difference in the curviness of the profile after the 0.5-hour point.

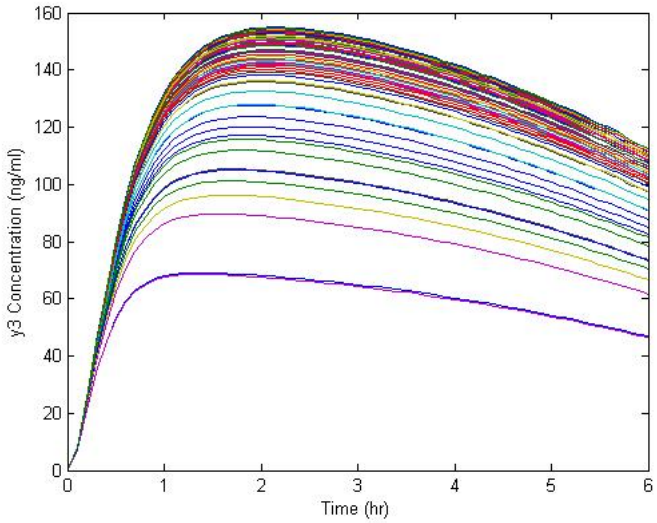

Figure 4.25: *Plot showing the impact of using a random value from a probability density function for the parameter k_{32} with respect to y_3 in Model 3.*

As with k_{23} the effect on y_2 and y_3 is very similar in magnitude. However in the case for k_{32} the reaction is larger for y_3 than for y_2.

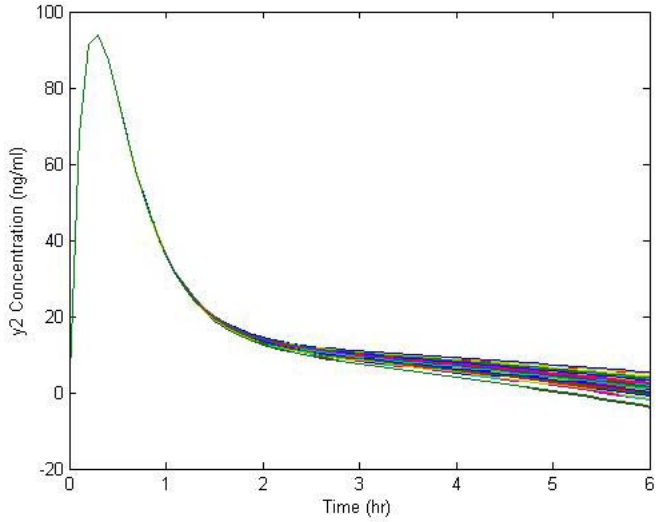

Figure 4.26: *Plot showing the impact of using a random value from a probability density function for the parameter a with respect to y_2 in Model 3.*

The parameter a causes differences in the profile after the two hour point. Although this parameter has an effect on the variable y_2 it is not the largest range over the variables.

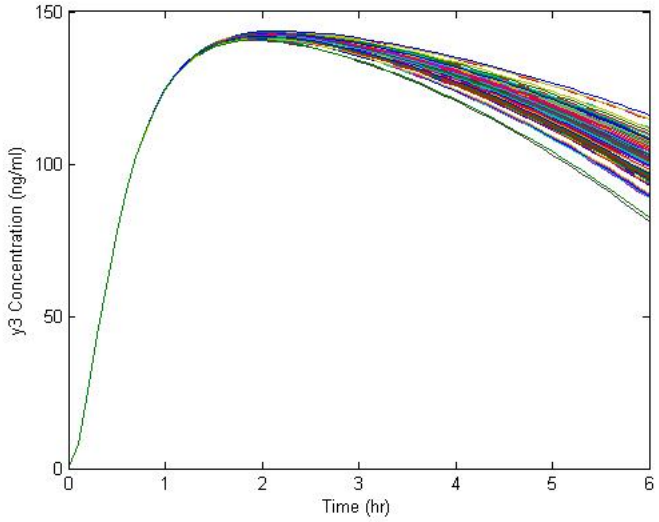

Figure 4.27: *Plot showing the impact of using a random value from a probability density function for the parameter a with respect to y_3 in Model 3.*

For the variable y_3 the parameter a has a similar effect in size to y_2 and the location of the difference is the same for both variables.

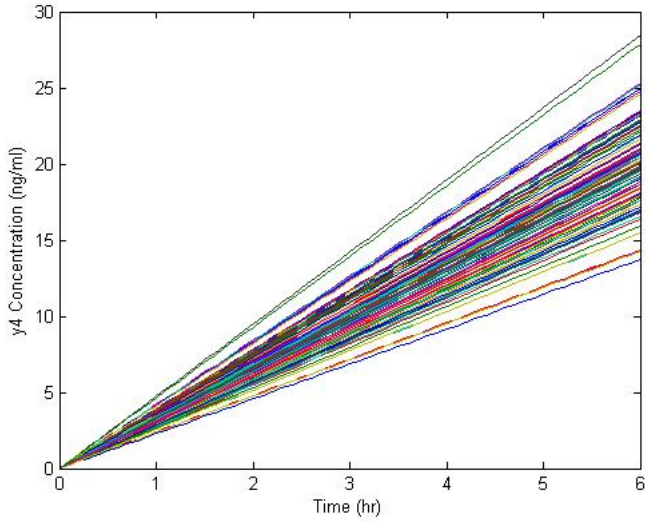

Figure 4.28: *Plot showing the impact of using a random value from a probability density function for the parameter a with respect to y_4 in Model 3.*

As can be seen from the equations for this model the parameter a should have the most effect on y_4. A summary of the test results are shown in the following table:

Variable	Magnitude Parameters	t test	Maximum Range
y_1	k_{12}	a	k_{12}
y_2	k_{12}, k_{23}, k_{32}, a	k_{32}	k_{32}
y_3	k_{12}, k_{23}, k_{32}, a	k_{32}	k_{32}
y_4	a	a	a

Table 4.10: *The most prominent parameters for the Model 3.*

The table above shows that the extended sensitivity analysis, paired t test and magnitude tests all show similar answers for y_4. For y_1 the tests show a dependence on the parameter a where due to the explicit solution there should be very little effect.

4.4.4 Cytochrome P450 Cycle

This cycle relates to the equilibria outlined in section 1.4 and is used within the cellular automata model in Chapter 5. Please refer to these sections for greater

detail of the model assumptions. The model equations are:

$$\frac{d[E]}{dt} = k_{-1}[ES] + k_7[EP] + k_8[GSO2] + k_9[HSO] - (k_1 + k_{-7})[E] \tag{4.12}$$

$$\frac{d[S]}{dt} = k_{-1}[ES] + k_8[GSO2] + k_9[HSO] - k_1[S] \tag{4.13}$$

$$\frac{d[ES]}{dt} = k_1[E][S] - (k_{-1} + k_2)[ES] \tag{4.14}$$

$$\frac{d[FS]}{dt} = k_2[ES] + k_{-3}[FSO2] - k_3[FS] \tag{4.15}$$

$$\frac{d[FSO2]}{dt} = k_3[FS][O2] - (k_{-3} + k_4)[FSO2] \tag{4.16}$$

$$\frac{d[GSO2]}{dt} = k_4[FSO2] - (k_5 + k_8)[GSO2] \tag{4.17}$$

$$\frac{d[HSO]}{dt} = k_5[GSO2] - (k_6 + k_9)[HSO] \tag{4.18}$$

$$\frac{d[EP]}{dt} = k_6[HSO] + k_{-7}[E][P] - k_7[EP] \tag{4.19}$$

$$\frac{d[P]}{dt} = k_7[EP] - k_{-7}[P] \tag{4.20}$$

The parameter values used for this model are as outlined in table 5.4.The ranges of sensitivity for this model for each parameter with relation to the variables are:

CYP cycle		k_{-1}	k_1	k_2	k_{-3}	k_3	k_4
$[E]$	Min	-8.48723E-07	-1.00438E-08	-1.0688E-06	-4.73323E-08	0	0
	Max	0	0	4.04429E-07	0	5.2854E-05	4.06096E-07
	Range	8.48723E-07	1.00438E-08	1.47323E-06	4.73323E-08	5.2854E-05	4.06096E-07
$[S]$	Min	-8.50811E-07	-9.66988E-09	-1.12746E-06	-4.95532E-09	-7.43136E-06	-5.71147E-08
	Max	3.94056E-09	5.13128E-10	4.18353E-08	6.63778E-09	5.53345E-06	4.25154E-08
	Range	8.54751E-07	1.0183E-08	1.1693E-06	1.15931E-08	1.29648E-05	9.96301E-08
$[ES]$	Min	-1.81948E-05	-8.07874E-08	-2.09474E-05	-9.28224E-11	-8.19708E-08	-6.29275E-10
	Max	5.52001E-09	1.19008E-10	6.55486E-09	7.40078E-11	9.98387E-08	7.63734E-10
	Range	1.82004E-05	8.09064E-08	2.0954E-05	1.6683E-10	1.81809E-07	1.39301E-09
$[FS]$	Min	-0.005325095	-0.00020216	0	0	-0.647192547	-0.004894885
	Max	0	0	0.08081187	0.000578772	0	0
	Range	0.005325095	0.00020216	0.08081187	0.000578772	0.647192547	0.004894885
$[FSO2]$	Min	-4.76604E-06	-1.80982E-07	0	-8.69975E-06	0	-1.25808E-05
	Max	0	0	7.23696E-05	0	0.009723469	0
	Range	4.76604E-06	1.80982E-07	7.23696E-05	8.69975E-06	0.009723469	1.25808E-05
$[GSO2]$	Min	-2.04406E-05	-7.75802E-07	0	-3.67335E-05	0	0
	Max	0	0	0.000310131	0	0.041018531	0.00031516
	Range	2.04406E-05	7.75802E-07	0.000310131	3.67335E-05	0.041018531	0.00031516
$[HSO]$	Min	-2.66359E-05	-1.01094E-06	0	-4.72782E-05	0	0
	Max	0	0	0.000404127	0	0.052794462	0.000405638
	Range	2.66359E-05	1.01094E-06	0.000404127	4.72782E-05	0.052794462	0.000405638
$[EP]$	Min	-1.46498E-07	-5.56027E-09	0	-2.6003E-07	0	0
	Max	0	0	2.22271E-06	0	0.00029037	2.23102E-06
	Range	1.46498E-07	5.56027E-09	2.22271E-06	2.6003E-07	0.00029037	2.23102E-06
$[P]$	Min	-1.33169E-06	-5.05435E-08	0	-2.36354E-06	0	0
	Max	0	0	2.02047E-05	0	0.002639319	2.02788E-05
	Range	1.33169E-06	5.05435E-08	2.02047E-05	2.36354E-06	0.002639319	2.02788E-05

Table 4.11: *CYP Cycle - Sensitivity Ranges - k_{-1} to k_4.*

CYP cycle		k_5	k_6	k_{-7}	k_7	k_8	k_9
$[E]$	Min	-2.59589E-09	-8.90243E-09	-1.40962E-08	-1.40846E-12	-1.66867E-08	-9.16012E-09
	Max	1.72144E-07	8.89731E-07	0	1.04484E-10	1.17979E-06	9.01987E-07
	Range	1.7474E-07	8.98634E-07	1.40962E-08	1.05892E-10	1.19648E-06	9.11147E-07
$[S]$	Min	0	-1.62534E-06	-8.08783E-09	-1.02555E-14	-2.25566E-06	0
	Max	1.07157E-06	0	3.69802E-10	8.72911E-15	0	1.36901E-06
	Range	1.07157E-06	1.62534E-06	8.45763E-09	1.89846E-14	2.25566E-06	1.36901E-06
$[ES]$	Min	-9.54638E-09	-1.45044E-08	-1.55576E-07	-2.06604E-13	-8.13148E-09	-1.44273E-08
	Max	4.55421E-09	1.40355E-09	7.50191E-11	1.75815E-13	1.91969E-09	1.53198E-09
	Range	1.41006E-08	1.5908E-08	1.55651E-07	3.82419E-13	1.00512E-08	1.59593E-08
$[FS]$	Min	-8.83991E-08	-1.63462E-07	-0.000536392	-2.33864E-12	-9.42117E-08	-1.60318E-07
	Max	1.63718E-08	3.33934E-09	0	1.38207E-12	3.41169E-09	3.98733E-09
	Range	1.04771E-07	1.66801E-07	0.000536392	3.72071E-12	9.76234E-08	1.64305E-07
$[FSO2]$	Min	-7.93332E-11	-1.59185E-10	-4.8025E-07	-4.41409E-14	-8.51968E-11	-1.52457E-10
	Max	1.7174E-11	9.66394E-13	0	3.16641E-14	9.99865E-13	2.38926E-12
	Range	9.65072E-11	1.60151E-10	4.8025E-07	7.5805E-14	8.61967E-11	1.54846E-10
$[GSO2]$	Min	-0.00155864	-6.80677E-10	-2.05849E-06	-2.89561E-13	-0.00155864	-6.10741E-10
	Max	0	3.97465E-12	0	9.86462E-16	0	5.74921E-12
	Range	0.00155864	6.84651E-10	2.05849E-06	2.90547E-13	0.00155864	6.1649E-10
$[HSO]$	Min	0	-0.00390236	-2.68238E-06	-8.95601E-14	-0.002037023	-0.00390236
	Max	0.001063359	0	0	2.49853E-14	0	0
	Range	0.001063359	0.00390236	2.68238E-06	1.14545E-13	0.002037023	0.00390236
$[EP]$	Min	0	0	-1.47533E-08	-2.99168E-07	-1.12037E-05	-2.14631E-05
	Max	5.8484E-06	3.48231E-05	0	0	0	0
	Range	5.8484E-06	3.48231E-05	1.47533E-08	2.99168E-07	1.12037E-05	2.14631E-05
$[P]$	Min	0	0	-2.48548E-05	-2.54313E-10	-0.000101846	-0.0001951
	Max	5.30795E-05	0.000316421	0	1.87564E-08	0	0
	Range	5.30795E-05	0.000316421	2.48548E-05	1.90107E-08	0.000101846	0.0001951

Table 4.12: *CYP Cycle - Sensitivity Ranges - k_5 to k_9.*

The [E] concentration is mostly affected by k_2, k_3 and k_8. However, all other parameters show sensitivity for this variable to a lesser extent. The parameters with a positive effect (i.e. the larger the parameter the larger the variable's value) are: k_3 and k_4. The parameters with a negative effect are k_{-1}, k_1, k_{-3} and k_{-7}. All other parameters have both a positive and negative effect.

The concentration of [S] is primarily affected by the same parameters as [E] as well as k_5, k_6 and k_9. The sensitivities for k_{-1} to k_4, k_7 and k_{-7} all have both positive and negative effect, k_5 and k_9 have positive sensitivity whereas k_6 and k_8 have a negative effect.

The primary parameters for [ES] are k_{-1} and k_2. All the sensitivities for this variable are ones with a positive and negative effect over the time period.

The variable [FS] is primarily affected by k_2 and k_3. The parameters with a positive effect are: k_{-1}, k_1, k_3, k_4 and k_{-7}. The parameters with a negative effect are: k_2 and k_{-3}. All others have a positive and negative effect.

The [FSO2] concentration is primarily affected by k_2 and k_4. The split of positive and negative sensitivities are the same for this variable as with the last with the exception of k_{-3} and k_3 which are the reverse i.e. k_{-3} has a negative effect and k_3 a positive one.

Variable [GSO2] is highly sensitive to k_3, k_5 and k_8. The parameters with a negative effect are: k_{-1}, k_1, k_{-3}, k_5, k_{-7} and k_8. The parameters with a positive effect are: k_2, k_3 and k_4. All others have a positive and negative effect.

The [HSO] concentration is primarily affected by k_3, k_5, k_6, k_8 and k_9. All the sensitivities are similar in effect as [GSO2] with the exception of k_5, k_6 and k_9 k_5 has a positive effect rather than negative, k_6 has a negative rather than both and k_9 has a straight negative effect rather than varying from positive and negative.

The enzyme-product complex [EP] is primarily affected by k_3, k_6, k_8 and k_9. The parameters have a similar effect on this variable as it did with the last with the

exception of k_6 and k_7. For k_6 the variable is positively sensitive and k_7 has negative sensitivity rather than both positive and negative.

The product concentration [P] is affected by k_2, k_4, k_5, k_{-7} and k_9. The sensitivities are comparable to the [EP] effects but k_7 has both a negative and positive effect rather than just negative.

The magnitude, paired t test and extended sensitivity results are:

CYP cycle		k_{-1}	k_1	k_2	k_{-3}	k_3	k_4
$[E]$	110%	3.67465E-12	1.18675E-13	1.01484E-11	9.18758E-13	1.33315E-09	9.06499E-12
	90%	1.7294E-11	2.08741E-13	1.1118E-11	1.28742E-12	1.36306E-09	9.70036E-12
$[S]$	110%	3.4199E-12	1.45639E-14	1.39907E-12	1.03706E-14	1.41327E-11	9.88166E-14
	90%	1.6973E-11	2.95188E-14	1.78718E-12	1.3653E-14	1.52286E-11	1.23036E-13
$[ES]$	110%	1.42001E-09	9.63548E-13	4.51458E-10	4.11917E-14	2.80356E-10	4.12243E-13
	90%	8.90647E-09	1.89523E-12	5.81527E-10	2.78623E-13	4.33072E-11	3.17165E-12
$[FS]$	110%	0.012568005	0.00035899	0.418903154	6.04814E-05	0.089204768	0.000573997
	90%	0.020579086	0.000615509	0.441802696	8.59116E-05	0.089966863	0.000602359
$[FSO2]$	110%	1.00803E-08	2.87943E-10	3.36004E-07	3.41281E-08	4.9922E-05	7.92068E-09
	90%	1.65053E-08	4.93696E-10	3.54371E-07	4.83226E-08	5.05619E-05	8.34569E-09
$[GSO2]$	110%	1.75911E-07	5.03348E-09	5.87614E-06	5.96982E-07	0.000875021	5.90903E-06
	90%	2.87646E-07	8.62008E-09	6.19866E-06	8.45293E-07	0.000885892	6.22744E-06
$[HSO]$	110%	2.55375E-07	7.32304E-09	8.54742E-06	8.71731E-07	0.001279483	8.63891E-06
	90%	4.18386E-07	1.25496E-08	9.01734E-06	1.23556E-06	0.001293901	9.09484E-06
$[EP]$	110%	7.70717E-12	2.21128E-13	2.57952E-10	2.63144E-11	3.86269E-08	2.60811E-10
	90%	1.26277E-11	3.78959E-13	2.72157E-10	3.73008E-11	3.9059E-08	2.74574E-10
$[P]$	110%	6.24005E-10	1.79078E-11	2.0888E-08	2.13256E-09	3.13113E-06	2.1141E-08
	90%	1.02249E-09	3.0688E-11	2.20392E-08	3.02349E-09	3.16547E-06	2.22522E-08

Table 4.13: *CYP Cycle - Magnitude Test Statistics - k_{-1} to k_4.*

CYP cycle		k_5	k_6	k_{-7}	k_7	k_8	k_9
$[E]$	110%	6.11351E-14	6.36299E-13	2.80553E-15	8.74099E-19	1.17382E-12	9.49202E-13
	90%	6.99262E-14	7.2042E-13	1.77713E-15	1.32336E-18	1.26404E-12	1.1472E-12
$[S]$	110%	9.10919E-12	5.24269E-12	8.4755E-16	6.80931E-23	2.03737E-11	5.7206E-12
	90%	1.19033E-11	5.82067E-12	8.22157E-17	2.28033E-22	2.26972E-11	7.22206E-12
$[ES]$	110%	1.47433E-12	6.03813E-12	3.28096E-13	2.84108E-20	3.98593E-12	4.00727E-12
	90%	2.47714E-13	5.96413E-12	2.94298E-14	9.51736E-20	3.94985E-12	3.92347E-12
$[FS]$	110%	1.43534E-10	6.00315E-10	1.7868E-05	8.77018E-19	4.01596E-10	3.99998E-10
	90%	1.84901E-11	6.05982E-10	1.7894E-05	1.48154E-18	3.95347E-10	3.95648E-10
$[FSO2]$	110%	1.14803E-16	4.80799E-16	1.43318E-11	7.01847E-25	3.21605E-16	3.20353E-16
	90%	1.48131E-17	4.8528E-16	1.43527E-11	1.18561E-24	3.16634E-16	3.16856E-16
$[GSO2]$	110%	1.95175E-05	1.65585E-14	2.50806E-10	4.15556E-22	9.49456E-06	1.09813E-14
	90%	2.53499E-05	1.80249E-14	2.50899E-10	1.4255E-21	1.06902E-05	1.16625E-14
$[HSO]$	110%	8.23772E-06	2.96417E-05	3.65708E-10	2.69102E-20	1.36854E-05	4.3381E-05
	90%	1.06987E-05	3.40423E-05	3.65011E-10	9.22479E-20	1.53967E-05	5.35111E-05
$[EP]$	110%	2.48778E-10	2.95061E-09	1.08787E-14	3.39329E-11	4.12906E-10	1.30868E-09
	90%	3.2309E-10	3.39923E-09	1.10275E-14	5.06678E-11	4.64797E-10	1.61469E-09
$[P]$	110%	2.02234E-08	2.39578E-07	2.48305E-08	2.87195E-14	3.33706E-08	1.05518E-07
	90%	2.6261E-08	2.75936E-07	3.69313E-08	4.28968E-14	3.75571E-08	1.30097E-07

Table 4.14: *CYP Cycle - Magnitude Test Statistics - k_5 to k_9.*

CYP cycle		k_{-1}	k_1	k_2	k_{-3}	k_3	k_4
$[E]$	110%	0.002212019	4.89232E-30	5.67215E-19	1.27318E-34	4.64505E-35	4.93215E-35
	90%	0.028333201	7.10167E-29	9.05544E-18	8.39852E-35	7.60307E-35	1.05884E-34
$[S]$	110%	0.270137522	0.033590894	0.937059854	1.94991E-05	5.11388E-05	2.02154E-05
	90%	0.291446758	0.043233061	0.926754891	5.5259E-05	1.80886E-05	1.0082E-05
$[ES]$	110%	0.32250993	0.281628335	0.304997395	0.317399733	0.168685127	0.691495177
	90%	0.323014646	0.330990634	0.376955941	0.171206841	0.329674052	0.097899636
$[FS]$	110%	5.0992E-55	5.09394E-55	5.10333E-55	3.71016E-20	3.06139E-20	1.22877E-19
	90%	5.09888E-55	5.10484E-55	5.09661E-55	3.53701E-20	3.32642E-20	1.32007E-19
$[FSO2]$	110%	5.08513E-55	5.09026E-55	5.10265E-55	2.43508E-54	3.71261E-54	6.64874E-49
	90%	5.07891E-55	5.10089E-55	5.09577E-55	3.676E-54	2.34943E-54	1.15918E-48
$[GSO2]$	110%	4.07282E-43	1.74072E-43	8.57348E-44	1.19598E-43	4.51126E-44	4.02053E-44
	90%	5.09674E-43	2.0227E-43	8.6371E-44	1.29692E-43	5.02779E-44	4.52108E-44
$[HSO]$	110%	6.6944E-30	4.49377E-30	3.02962E-30	2.46018E-30	1.51069E-30	1.44431E-30
	90%	5.9121E-30	3.96699E-30	3.1821E-30	2.34204E-30	1.7299E-30	1.64359E-30
$[EP]$	110%	1.02848E-29	7.16791E-30	4.623E-30	3.80675E-30	2.35687E-30	2.25539E-30
	90%	8.86875E-30	6.00465E-30	4.9255E-30	3.63227E-30	2.69002E-30	2.56164E-30
$[P]$	110%	3.2433E-28	2.34596E-28	1.5493E-28	1.31831E-28	8.62232E-29	8.29002E-29
	90%	2.74746E-28	1.95393E-28	1.65662E-28	1.26528E-28	9.68797E-29	9.27311E-29

Table 4.15: *CYP Cycle - Paired t test p values - k_{-1} to k_4.*

CYP cycle		k_5	k_6	k_{-7}	k_7	k_8	k_9
$[E]$	110%	1.41011E-06	1.14759E-09	4.59818E-15	9.26206E-07	1.12218E-06	6.98251E-10
	90%	1.3355E-08	3.20142E-11	1.05979E-29	9.12667E-07	1.66563E-07	2.68034E-11
$[S]$	110%	6.84494E-36	1.11826E-22	0.193688028	0.526941488	1.73983E-40	4.9207E-35
	90%	4.21385E-35	6.78049E-23	0.063085592	0.6742349	2.23699E-40	2.13387E-34
$[ES]$	110%	0.120323075	0.295931897	0.184994714	0.521627027	0.277981104	0.290378601
	90%	0.401840019	0.268075342	0.344728616	0.666434976	0.28472117	0.27650262
$[FS]$	110%	1.50783E-09	7.8476E-07	4.82883E-55	5.98752E-22	7.63638E-07	8.88636E-07
	90%	5.50359E-23	8.32398E-07	5.09875E-55	1.2249E-17	8.67852E-07	7.31132E-07
$[FSO2]$	110%	1.64984E-09	8.31381E-07	4.8261E-55	6.88415E-22	8.09502E-07	9.41344E-07
	90%	6.77768E-23	8.83008E-07	5.0959E-55	1.29592E-17	9.2007E-07	7.75589E-07
$[GSO2]$	110%	2.07814E-34	1.27617E-09	1.35646E-43	0.636991356	3.2245E-34	1.02709E-09
	90%	1.15941E-33	5.7416E-09	1.32505E-43	0.191920933	7.03197E-34	5.70287E-09
$[HSO]$	110%	2.44704E-37	4.23216E-23	4.27063E-30	0.395926067	1.76171E-25	3.53924E-23
	90%	1.09213E-36	8.80951E-23	3.74489E-30	0.378340644	2.83455E-25	1.07634E-22
$[EP]$	110%	5.11603E-37	1.67434E-33	5.04939E-30	7.59011E-30	2.37009E-25	4.53515E-23
	90%	2.20728E-36	4.99614E-33	5.66945E-30	8.26357E-30	3.82601E-25	1.37196E-22
$[P]$	110%	1.21872E-34	1.41013E-31	3.01501E-27	6.36932E-07	2.90103E-24	3.74825E-22
	90%	4.3259E-34	3.68746E-31	5.33909E-27	6.36188E-07	4.50702E-24	1.04874E-21

Table 4.16: *CYP Cycle - Paired t test p values - k_5 to k_9.*

CYP cycle	k_{-1}	k_1	k_2	k_{-3}	k_3	k_4
p.d.f	Γ(200000,2000)	Γ(80000000,40000)	Γ(2722.37778,233.34)	Γ(200000,2000)	Γ(0.2,2)	Γ(2722.37778,233.34)
$[E]$	1.1831E-06	1.70254E-08	1.17653E-06	6.56419E-08	5.85586E-05	5.17815E-07
$[S]$	1.18602E-06	1.42568E-08	1.24126E-06	1.86169E-08	9.81965E-06	7.11372E-08
$[ES]$	2.53511E-05	2.84536E-07	2.30833E-05	2.85895E-07	2.31532E-06	4.03507E-07
$[FS]$	0.007417851	0.000240301	0.0892153	0.000636393	0.629942199	0.006099786
$[FSO2]$	6.63936E-06	2.15128E-07	7.98951E-05	9.57914E-06	0.013131568	1.56867E-05
$[GSO2]$	2.86558E-05	9.24E-07	0.000342475	4.04477E-05	0.049284681	0.000392701
$[HSO]$	3.72924E-05	1.26127E-06	0.000446143	5.2055E-05	0.058190479	0.000505482
$[EP]$	2.04954E-07	7.22001E-09	2.45385E-06	2.8628E-07	0.000320084	2.78015E-06
$[P]$	1.86501E-06	6.60004E-08	2.23098E-05	2.60186E-06	0.002907356	2.52745E-05
CYP cycle	k_5	k_6	k_{-7}	k_7	k_8	k_9
p.d.f	Γ(67.19778,36.66)	Γ(6.05,11)	Γ(2420,220)	Γ(200000,2000)	Γ(13.87778,16.66)	Γ(13.87778,16.66)
$[E]$	2.19683E-07	9.98826E-07	1.97185E-08	3.17796E-10	1.28303E-06	1.04205E-06
$[S]$	1.40306E-06	1.7939E-06	1.42044E-08	2.95704E-10	2.42419E-06	1.62305E-06
$[ES]$	1.60851E-06	1.28862E-06	2.84705E-07	9.65064E-10	1.22926E-06	1.35337E-06
$[FS]$	3.66253E-06	4.0582E-06	0.000651515	1.97206E-09	4.29624E-06	4.06717E-06
$[FSO2]$	3.30502E-09	3.63478E-09	5.83324E-07	1.73975E-12	3.84864E-09	3.64352E-09
$[GSO2]$	0.002012383	7.06457E-08	2.50768E-06	1.17233E-10	0.001670643	1.82378E-07
$[HSO]$	0.001362757	0.004296598	3.26739E-06	5.71721E-10	0.002184306	0.004955985
$[EP]$	7.49434E-06	3.79129E-05	1.79621E-08	2.95713E-07	1.20135E-05	2.72573E-05
$[P]$	6.80261E-05	0.000344523	3.06007E-05	1.85396E-08	0.000109209	0.000247685

Table 4.17: *CYP Cycle - Extended Sensitivity Analysis.*

Variable	Magnitude Parameters	t-test	Maximum Range
[E]	k_{-1}, k_2, k_3, k_4	k_3	k_3
[S]	k_{-1}, k_1 (90%), k_2, k_3, k_4, k_5, k_6, k_8, k_9	k_8	k_3
[ES]	k_{-1}, k_2, k_3, k_5 (110%), k_6 (110%), k_8 (110%), k_9 (110%)	k_5 (110%) k_4 (90%)	k_{-1}
[FS]	k_{-1}, k_1 (90%), k_2, k_3, k_4	k_{-7}	k_3
[FSO2]	k_2, k_3	k_{-7} (110%) k_{-1} (90%)	k_3
[GSO2]	k_2, k_3, k_4, k_5, k_8	k_4	k_3
[HSO]	k_2, k_3, k_4, k_5, k_6, k_8, k_9	k_5	k_3
[EP]	k_2, k_3, k_4, k_5, k_6, k_7 (110%), k_8, k_9	k_5	k_3
[P]	k_2, k_3, k_4, k_5, k_6, k_{-7}, k_8, k_9	k_5	k_3

Table 4.18: *The most prominent parameters for the CYP Cycle.*

The magnitude table shows that the most prominent parameters are as shown in the table. It can be seen from this table that there is coherence between the prominent parameters mostly that k_3 affects the most variables.

4.4.5 Cytochrome P450 Model

This model is used within the cellular automata outlined in Chapter 5 specifically in section 5.2.2. Please refer to this section for greater detail of the model

assumptions. The parameters are shown in table 5.4. The model equations are:

$$\frac{dy_1}{dt} = -k_{12}y_1 \tag{4.21}$$
$$\frac{dy_2}{dt} = k_{32}[S] + k_{12}y_1 - k_{23}y_2 - y_3 \tag{4.22}$$
$$\frac{dy_3}{dt} = a \tag{4.23}$$
$$\frac{d[E]}{dt} = k_{-1}[ES] + k_7[EP] + k_8[GSO2] + k_9[HSO] - (k_1 + k_{-7})[E] \tag{4.24}$$
$$\frac{d[S]}{dt} = k_{23}y_2 + k_{-1}[ES] + k_8[GSO2] + k_9[HSO] - (k_1 + k_{32})[S] \tag{4.25}$$
$$\frac{d[ES]}{dt} = k_1[E][S] - (k_{-1} + k_2)[ES] \tag{4.26}$$
$$\frac{d[FS]}{dt} = k_2[ES] + k_{-3}[FSO2] - k_3[FS] \tag{4.27}$$
$$\frac{d[FSO2]}{dt} = k_3[FS][O2] - (k_{-3} + k_4)[FSO2] \tag{4.28}$$
$$\frac{d[GSO2]}{dt} = k_4[FSO2] - (k_5 + k_8)[GSO2] \tag{4.29}$$
$$\frac{d[HSO]}{dt} = k_5[GSO2] - (k_6 + k_9)[HSO] \tag{4.30}$$
$$\frac{d[EP]}{dt} = k_6[HSO] + k_{-7}[E][P] - k_7[EP] \tag{4.31}$$
$$\frac{d[P]}{dt} = k_7[EP] - k_{-7}[P] \tag{4.32}$$

The parameter values used as a basis for the sensitivity analysis are outlined in Table 5.4. The sensitivity for the variables can be summarised in the following table:

Variable	Primarily affected	Positive	Negative	Both	None
y_1	k_{12}	-	k_{12}	-	All but k_{12}
y_2	k_{12}, k_{23} , k_{32}, a	k_1	a, k_7 and k_8	all other	-
y_3	a	a	-	-	All but a
[E]	all but a, k_1 and k_{-3}	k_{12}, k_{23} and k_2	k_{32}, a and k_1	all other	-
[S]	k_{12}, k_{23} , k_{32}, a and k_{-1}	-	a and k_7	all other	-
[ES]	all but k_{-3} and k_{-7}	-	-	all other	-
[FS]	k_{12}, k_{23}, k_{-1}, k_2, k_{-3}, k_3, k_4 and k_7	-	a	all other	-
[FSO2]	k_{12}, k_{23}, k_{32}, k_{-1}, k_2, k_3, k_4 and k_7	-	a	all other	-
[GSO2]	k_{12}, k_{23}, k_{32}, k_{-1}, k_2, k_3, k_4, k_5 and k_7	k_{12}, k_{23} and k_2	k_{32}, a, k_{-1}, k_1, k_5, k_7 and k_8	all other	-
[HSO]	k_{12}, k_{23}, k_{32}, k_{-1}, k_2, k_3, k_4, k_5, k_6 and k_7	k_{12}, k_{23} and k_2	k_{32}, a, k_{-1}, k_1, k_6, k_7, k_8 and k_9	all other	-
[EP]	all but a, k_1 and k_{-3}	k_{12}, k_{23} and k_2	k_{32}, a, k_{-1}, k_1, k_{-7}, k_7, k_8 and k_9	all other	-
[P]	all but a, k_1 and k_{-3}	k_{12}, k_{23} and k_2	k_{32}, a, k_{-1}, k_1, k_7, k_8 and k_9	all other	-

Table 4.19: *The most prominent parameters in the CYP model according to the* $\frac{dy}{du}$ *statistic.*

CYP model		k_{12}	k_{23}	k_{32}	a	k_{-1}	k_1	k_2	k_{-3}
y_1	110%	0.337541216	3.57322E-16	3.00122E-21	9.15869E-17	1.79923E-14	1.40168E-20	1.01492E-22	1.46176E-27
	90%	0.456268658	2.41138E-11	3.00077E-21	8.6348E-17	6.44148E-14	6.4504E-15	1.02047E-22	2.704E-27
y_2	110%	0.268987589	12.63665691	7.00664E-05	31.77022087	5.78987E-08	3.06364E-20	1.22469E-19	4.1637E-25
	90%	0.355518792	15.74214588	7.00791E-05	31.77022024	8.64052E-08	1.07289E-14	1.22711E-19	6.339E-25
y_3	110%	3.49441E-29	1.79712E-28	2.89537E-27	22.143	6.98881E-31	5.49121E-32	1.96822E-29	1.39776E-30
	90%	3.49441E-29	2.59585E-28	1.4976E-27	22.143	1.39871E-30	1.44815E-31	4.27874E-30	1.39776E-30
$[E]$	110%	2.00419E-17	6.45526E-17	4.53251E-23	9.22463E-25	2.66998E-15	1.33354E-20	2.83372E-18	1.41643E-22
	90%	3.59669E-15	2.78403E-14	4.50253E-23	9.68673E-25	2.44594E-16	8.14603E-18	2.84126E-18	2.20348E-22
$[S]$	110%	6.72817E-06	0.000657564	3.47547E-09	0.000787533	4.52683E-06	4.27038E-20	6.90543E-18	5.76413E-22
	90%	8.88385E-06	0.000740494	3.47645E-09	0.000787533	6.75704E-06	1.24517E-15	6.92358E-18	8.88085E-22
$[ES]$	110%	5.35917E-21	1.19784E-21	1.92928E-26	1.90934E-25	3.56325E-21	3.1315E-22	1.94906E-24	2.85042E-29
	90%	1.3377E-15	1.07292E-14	1.93006E-26	1.90962E-25	1.61791E-17	2.90576E-18	1.95978E-24	4.39703E-29
$[FS]$	110%	3.08129E-20	2.57704E-19	2.07983E-25	7.9779E-27	7.71164E-22	4.06287E-23	1.09773E-20	8.93789E-21
	90%	1.90658E-17	1.52487E-16	2.08019E-25	7.9793E-27	9.68025E-19	5.64083E-20	1.10055E-20	3.53318E-20
$[FSO2]$	110%	1.23069E-14	1.02186E-13	7.28854E-20	9.72432E-22	2.25206E-16	2.05574E-17	4.33834E-15	6.80452E-18
	90%	1.10506E-14	9.12726E-14	7.2896E-20	9.72432E-22	2.81838E-16	3.40956E-17	4.34994E-15	1.02093E-17
$[GSO2]$	110%	9.99998E-14	8.28591E-13	5.50955E-19	7.00951E-21	1.43268E-15	1.64575E-16	3.51688E-14	4.80915E-18
	90%	9.34775E-14	7.70931E-13	5.51032E-19	7.00951E-21	1.71554E-15	2.62257E-16	3.52624E-14	7.60364E-18
$[HSO]$	110%	7.18877E-14	5.95578E-13	3.9577E-19	5.1224E-21	1.02734E-15	1.18268E-16	2.5279E-14	6.91358E-19
	90%	6.66739E-14	5.49937E-13	3.95825E-19	5.12206E-21	1.24071E-15	1.89742E-16	2.53462E-14	1.03046E-18
$[EP]$	110%	1.76309E-16	1.4607E-15	9.70663E-22	1.25822E-23	2.51964E-18	2.9006E-19	6.19986E-17	1.43899E-21
	90%	1.63505E-16	1.34864E-15	9.70798E-22	1.25811E-23	3.0432E-18	4.65392E-19	6.21633E-17	2.14739E-21
$[P]$	110%	2.13284E-18	1.76703E-17	1.17423E-23	1.52228E-25	3.04806E-20	3.50891E-21	7.50009E-19	1.73671E-23
	90%	1.97795E-18	1.63147E-17	1.17439E-23	1.52214E-25	3.68141E-20	5.62994E-21	7.52001E-19	2.59203E-23

Table 4.20: *CYP Model - Magnitude Test Statistics - k_{12} to k_{-3}.*

CYP model		k_3	k_4	k_5	k_6	k_{-7}	k_7	k_8	k_9
y_1	110%	1.01877E-26	2.44553E-27	8.98175E-30	6.76119E-29	3.43911E-28	1.70691E-13	7.56959E-27	1.31778E-26
	90%	1.08828E-25	1.93856E-27	6.19634E-27	2.078E-27	9.77672E-28	1.55724E-14	3.36419E-27	3.04861E-29
y_2	110%	2.42052E-24	2.70914E-22	6.1212E-21	7.35809E-20	3.19302E-27	6.57701E-12	6.43985E-20	8.98331E-20
	90%	8.82536E-25	3.98685E-22	7.98469E-21	8.46778E-20	3.19196E-26	3.953E-14	7.12654E-20	1.09316E-19
y_3	110%	1.39776E-27	1.19805E-29	2.83235E-28	2.54139E-28	1.27155E-29	2.99521E-31	1.67912E-28	1.67912E-28
	90%	1.19903E-27	3.423E-30	7.62555E-29	2.54139E-28	1.27069E-29	7.98722E-31	1.67799E-28	4.79425E-29
$[E]$	110%	1.05448E-23	7.84493E-20	1.47953E-19	1.03866E-18	2.90713E-21	2.91376E-15	6.06255E-18	2.08042E-18
	90%	1.07036E-23	1.05714E-19	1.75347E-19	1.1148E-18	4.17894E-21	4.04571E-16	6.41538E-18	2.31006E-18
$[S]$	110%	2.46755E-23	2.78607E-19	3.56381E-19	3.79147E-18	7.17896E-25	3.88721E-15	2.24062E-17	1.01275E-17
	90%	3.7246E-23	3.68647E-19	4.54616E-19	4.30381E-18	1.07851E-24	8.31531E-17	2.36988E-17	1.14916E-17
$[ES]$	110%	3.22139E-30	2.1485E-26	9.16326E-26	6.21138E-25	1.77655E-27	3.69279E-18	2.54072E-24	1.22543E-24
	90%	3.02842E-30	3.14626E-26	1.07863E-25	6.64468E-25	2.58339E-27	6.43487E-21	2.71686E-24	1.35896E-24
$[FS]$	110%	6.5226E-19	4.45566E-21	1.26584E-27	8.58571E-27	2.45092E-29	1.0492E-19	3.49458E-26	1.69368E-26
	90%	6.52332E-19	5.97616E-21	1.49015E-27	9.18513E-27	3.56312E-29	7.17944E-21	3.73787E-26	1.87834E-26
$[FSO2]$	110%	1.16961E-19	4.39945E-15	8.56316E-26	5.90484E-25	1.59189E-27	8.46392E-16	2.23817E-24	1.15962E-24
	90%	1.16982E-19	5.93884E-15	1.01188E-25	6.3271E-25	2.32558E-27	1.35498E-15	2.40296E-24	1.28953E-24
$[GSO2]$	110%	3.99909E-19	2.95833E-15	5.71566E-14	7.24405E-24	1.45795E-26	6.49947E-15	2.74459E-14	1.39052E-23
	90%	3.99972E-19	3.86157E-15	7.05572E-14	7.8534E-24	2.1625E-26	9.89554E-15	3.02001E-14	1.57585E-23
$[HSO]$	110%	5.10265E-20	3.70573E-16	3.63165E-14	5.49834E-14	9.19933E-27	4.65095E-15	2.78211E-14	8.07092E-14
	90%	5.1029E-20	5.29788E-16	4.39764E-14	6.24064E-14	1.38424E-26	7.10958E-15	3.10704E-14	9.77823E-14
$[EP]$	110%	1.1276E-22	8.14247E-19	8.65559E-17	7.14742E-16	5.43526E-17	1.14064E-17	6.87973E-17	2.00277E-16
	90%	1.12763E-22	1.17378E-18	1.05261E-16	7.86617E-16	8.06746E-17	1.74371E-17	7.686E-17	2.42789E-16
$[P]$	110%	1.36236E-24	9.83751E-21	1.04672E-18	8.6453E-18	1.16062E-20	3.70342E-19	8.32337E-19	2.42313E-18
	90%	1.3624E-24	1.41823E-20	1.27298E-18	9.51489E-18	1.66847E-20	7.07846E-19	9.29886E-19	2.93749E-18

Table 4.21: *CYP Model - Magnitude Test Statistics - k_3 to k_9.*

CYP model		k_{12}	k_{23}	k_{32}	a	k_{-1}	k_1	k_2	k_{-3}
y_1	110%	0.001716791	0.185718901	0.012775453	0.068853522	0.016316584	0.2299796	0.197513858	0.020955248
	90%	0.000897064	0.203223414	0.012617626	0.106501027	0.010066157	0.007683909	0.19818231	0.022052658
y_2	110%	0.868850118	2.93957E-11	2.66854E-12	3.0367E-14	2.35067E-12	0.0004972	0.000226006	0.689029406
	90%	0.847909587	2.28717E-13	2.68146E-12	3.0367E-14	2.30403E-12	0.293088281	0.000233627	0.797439954
y_3	110%	8.17843E-05	0.002055402	0.000228222	2.13912E-19	0.007077009	0.000581686	0.000211426	8.17843E-05
	90%	8.17843E-05	0.000158923	4.16047E-05	2.13912E-19	9.36821E-05	0.000248599	0.181871631	8.17843E-05
$[E]$	110%	0.006145401	1.17817E-06	2.05559E-05	9.20754E-08	0.313795791	1.5457E-05	9.54939E-07	0.779205292
	90%	0.281945979	0.30014915	1.80258E-05	1.54236E-07	0.679166295	0.149040344	9.55043E-07	0.806754611
$[S]$	110%	0.851189989	0.19568081	0.232863389	3.31577E-14	0.017356372	0.005071051	6.16821E-06	0.838075482
	90%	0.832462502	0.269309849	0.23279037	3.31577E-14	0.017122075	0.28043315	6.16883E-06	0.859974877
$[ES]$	110%	0.503815511	0.055925938	0.164112097	1.53299E-08	0.338804848	0.306163894	2.54873E-05	0.357561419
	90%	0.329973011	0.327721181	0.164242324	1.53575E-08	0.314725619	0.331783772	2.55209E-05	0.383704742
$[FS]$	110%	0.197368576	0.201661374	0.21196454	6.11138E-05	0.215477833	0.195115081	0.200978821	0.261836317
	90%	0.276512046	0.286307584	0.211961071	6.11678E-05	0.291022207	0.279382223	0.201373069	0.280241391
$[FSO2]$	110%	0.169125726	0.169225466	0.169173063	0.148896775	0.169130189	0.16925036	0.169214576	0.164807953
	90%	0.173474865	0.173632512	0.169173087	0.148896225	0.16149076	0.165318077	0.169219374	0.162320802
$[GSO2]$	110%	0.001912769	0.001912121	0.001870542	0.001306098	0.001776382	0.001904794	0.00191162	0.638677615
	90%	0.002000082	0.001995145	0.001870539	0.001305166	0.001676664	0.001832825	0.001911745	0.675683597
$[HSO]$	110%	1.79428E-07	1.79517E-07	1.79439E-07	2.61852E-07	1.7967E-07	1.79431E-07	1.79409E-07	0.991979675
	90%	1.82066E-07	1.81239E-07	1.79439E-07	2.63003E-07	1.77287E-07	1.77298E-07	1.79429E-07	0.989935177
$[EP]$	110%	1.28169E-07	1.28246E-07	1.28281E-07	2.26625E-07	1.28544E-07	1.28198E-07	1.28163E-07	0.991927457
	90%	1.29921E-07	1.29284E-07	1.28283E-07	2.27922E-07	1.26945E-07	1.26771E-07	1.28178E-07	0.992253646
$[P]$	110%	1.27776E-07	1.27853E-07	1.27885E-07	2.30312E-07	1.28127E-07	1.27805E-07	1.27771E-07	0.993481253
	90%	1.29523E-07	1.28882E-07	1.27887E-07	2.31646E-07	1.2653E-07	1.26382E-07	1.27785E-07	0.993930426

Table 4.22: *CYP Model - Paired t test p values - k_{12} to k_{-3}.*

CYP model		k_3	k_4	k_5	k_6	k_{-7}	k_7	k_8	k_9
y_1	110%	0.256327816	0.03851696	0.784843524	0.064278082	0.022817286	0.142559452	0.035613733	0.024875644
	90%	0.02374135	0.04703425	0.024143121	0.132338009	0.033434579	0.032747235	0.388072667	0.216419127
y_2	110%	0.061108295	0.651890383	2.89403E-21	3.66595E-22	8.74471E-05	8.84084E-09	3.63976E-05	2.91507E-12
	90%	0.187601589	0.651642251	2.04712E-21	2.32491E-22	0.004465565	0.076499032	2.84974E-05	5.42879E-13
y_3	110%	8.17843E-05	8.17843E-05	3.94771E-05	8.17843E-05	9.36821E-05	0.083220957	9.36821E-05	9.36821E-05
	90%	0.000348452	0.044545113	8.17843E-05	8.17843E-05	8.17843E-05	0.003823599	8.17843E-05	0.044545113
$[E]$	110%	0.977522161	0.990888446	0.993175621	0.97190591	0.996455305	0.257675483	0.99708666	0.975234852
	90%	0.968861497	0.994514806	0.991820122	0.964215549	0.996515096	0.505608081	0.996764935	0.964732166
$[S]$	110%	0.791806261	0.993999869	6.75177E-09	2.41715E-11	0.264356335	0.981451071	0.314786893	0.00397943
	90%	0.956561832	0.9924152	3.17663E-09	8.40951E-12	0.394241448	0.062418274	0.298028472	0.002155222
$[ES]$	110%	0.927012915	0.809386674	0.099510064	0.01729721	0.341587504	0.356558036	0.602000172	0.028789282
	90%	0.855564015	0.885208917	0.076981985	0.012900132	0.315855923	0.32173888	0.557355214	0.018730772
$[FS]$	110%	0.168602426	0.073308458	0.099133874	0.017213702	0.340589357	0.249063007	0.601083202	0.028682525
	90%	0.168641378	0.058231396	0.076689806	0.012837886	0.315181461	0.219060279	0.556423158	0.018660381
$[FSO2]$	110%	0.380805381	0.079773736	0.088253104	0.014636263	0.314668547	0.170857474	0.575537297	0.024627187
	90%	0.380781782	0.06342341	0.067769772	0.010845209	0.290305835	0.169104475	0.530001899	0.01584884
$[GSO2]$	110%	0.994186731	0.957454318	3.88187E-05	0.002118439	0.144875061	0.00190148	3.27464E-05	0.004251612
	90%	0.994182433	0.965110618	1.93539E-05	0.001435025	0.127992781	0.001850465	2.38999E-05	0.002371546
$[HSO]$	110%	0.991751941	0.991169265	0.002570667	2.34648E-11	0.013419763	1.80068E-07	5.65444E-09	2.99271E-11
	90%	0.9917516	0.992000368	0.001601952	8.1431E-12	0.010311021	1.79256E-07	4.01193E-09	6.00203E-12
$[EP]$	110%	0.997149168	0.99646287	0.001989758	6.32709E-05	9.83305E-08	1.28637E-07	4.3982E-09	2.40799E-11
	90%	0.997158553	0.996525023	0.001240212	3.32057E-05	8.71755E-08	1.28145E-07	3.12979E-09	4.89485E-12
$[P]$	110%	0.997657012	0.997170425	0.001984757	6.30705E-05	0.997144181	1.27871E-07	4.38807E-09	2.40951E-11
	90%	0.997666044	0.997113802	0.001237022	3.30959E-05	0.997072226	1.27458E-07	3.12293E-09	4.90675E-12

Table 4.23: *CYP Model - Paired t test p values - k_3 to k_9.*

When a parameter has a "Both" effect on the variable it means that there are both positive and negative effects from the parameter during the time period. This could mean that the plots show cycling, or it only has a small positive/negative effect for part of the time period and then it crosses the t-axis to cause a negative/positive effect. The extended sensitivity ranges and probability density functions are as follows:

Parameter	p.d.f	Parameter	p.d.f
k_{12}	Γ(320,80)	k_{23}	Γ(5,10)
k_{32}	Γ(0.2,2)	a	Γ(1.8,6)
k_{-1}	Γ(200000,2000)	k_1	Γ(80000000,40000)
k_2	Γ(2722.37778,233.34)	k_{-3}	Γ(200000,2000)
k_3	Γ(0.2,2)	k_4	Γ(2722.37778,233.34)
k_5	Γ(67.19778,36.66)	k_6	Γ(6.05,11)
k_{-7}	Γ(2420,220)	k_7	Γ(200000,2000)
k_8	Γ(13.87778,16.66)	k_9	Γ(13.87778,16.66)

Table 4.24: *The Probability Density Functions with respect to the parameters for the CYP Model.*

CYP model	k_{12}	k_{23}	k_{32}	a	k_{-1}	k_1	k_2	k_{-3}
y_1	0.554629036	6.32366E-07	3.17129E-10	1.75229E-07	2.88183E-08	5.20006E-12	6.2601E-12	3.01981E-14
y_2	0.512827092	2.995910662	0.018710964	9.412212643	1.87512E-05	9.34008E-12	1.8566E-10	1.9984E-13
y_3	3.9968E-15	3.9968E-15	3.9968E-15	6.883517979	3.9968E-15	3.9968E-15	3.9968E-15	3.9968E-15
$[E]$	3.68487E-08	3.91044E-08	2.60393E-11	2.50693E-12	1.57723E-08	3.69353E-12	6.37311E-10	3.75021E-12
$[S]$	0.002538125	0.028791852	0.000170617	0.046905191	0.000204774	1.08009E-11	1.14331E-09	7.72204E-12
$[ES]$	2.36296E-08	2.37069E-08	1.34511E-12	1.43762E-12	2.64543E-11	1.87389E-12	5.63724E-13	1.37592E-15
$[FS]$	2.92004E-09	2.89071E-09	5.02302E-12	4.7974E-13	1.1156E-11	5.74373E-13	1.15288E-10	4.03113E-11
$[FSO2]$	1.98224E-07	1.35166E-06	2.8683E-09	1.96046E-10	5.21073E-09	4.01395E-10	7.04323E-08	8.49714E-10
$[GSO2]$	3.10213E-07	2.10277E-06	4.30991E-09	2.87425E-10	7.10356E-09	6.19992E-10	1.0953E-07	6.81449E-10
$[HSO]$	1.60111E-07	1.08673E-06	2.22482E-09	1.48355E-10	3.65705E-09	3.20337E-10	5.661E-08	1.63102E-10
$[EP]$	7.85224E-09	5.32952E-08	1.09101E-10	7.28261E-12	1.79746E-10	1.57096E-11	2.77624E-09	6.79403E-12
$[P]$	8.6348E-10	5.86302E-09	1.20141E-11	8.02099E-13	1.97942E-11	1.72858E-12	3.05423E-10	7.52215E-13
CYP model	k_3	k_4	k_5	k_6	k_{-7}	k_7	k_8	k_9
y_1	3.01981E-14	3.01981E-14	3.01981E-14	4.9738E-14	1.9984E-14	3.6904E-08	1.10134E-13	3.9968E-14
y_2	9.99645E-13	7.70006E-12	4.23999E-11	1.99948E-10	1.60316E-13	3.73645E-08	3.5101E-10	2.6328E-10
y_3	3.9968E-15	3.9968E-15	3.9968E-15	3.9968E-15	3.9968E-15	3.9968E-15	3.9968E-15	3.9968E-15
$[E]$	2.51506E-11	2.31812E-10	4.21547E-10	1.44915E-09	3.38619E-11	2.02152E-08	5.77032E-09	1.91214E-09
$[S]$	4.8092E-11	4.47387E-10	4.61017E-10	1.9206E-09	5.99E-13	2.12485E-09	1.16886E-08	4.30323E-09
$[ES]$	1.29301E-14	1.06529E-13	3.80393E-13	1.32004E-12	2.92585E-14	5.9264E-11	3.60261E-12	1.72574E-12
$[FS]$	8.57161E-09	5.56914E-11	4.45851E-14	1.55747E-13	3.4392E-15	2.72161E-11	4.1507E-13	2.03056E-13
$[FSO2]$	2.40901E-09	5.79512E-08	3.5843E-13	1.26237E-12	2.64542E-14	1.39178E-08	3.17259E-12	1.6418E-12
$[GSO2]$	5.6311E-09	5.0331E-08	2.43286E-07	3.87491E-12	6.80748E-14	2.06472E-08	2.60041E-07	4.93448E-12
$[HSO]$	1.32224E-09	1.14309E-08	2.11444E-07	2.30896E-07	4.49502E-14	1.06564E-08	1.95461E-07	2.54081E-07
$[EP]$	5.78204E-11	5.00244E-10	1.01189E-08	3.65204E-08	2.99285E-09	5.22596E-10	9.67272E-09	1.26222E-08
$[P]$	6.40935E-12	5.55962E-11	1.11658E-09	4.02533E-09	6.79794E-11	9.87373E-11	1.06319E-09	1.38907E-09

Table 4.25: *The ranges associated with the Extended Sensitivity analysis with respect to the parameters and variables for the CYP Model.*

Variable	Magnitude Parameters	t test	Maximum Range
y_1	k_{12}	k_{12}	k_{12}
y_2	k_{12}, k_{23}, a	k_6	a
y_3	a	a	a
[E]	k_{12}, k_{23}, k_{-1}, k_7, k_8 (90%)	a	k_{23}
[S]	k_{12}, k_{23}, a, k_{-1}	a	a
[ES]	k_{12}, k_{23} (90%), k_{-1} (110%), k_7 (110%)	a	k_{23}
[FS]	k_{12}, k_{23}, k_{-1}, k_2 (90%), k_{-3} (90%), k_3 (110%), k_4 (110%), k_7 (110%)	a	k_3
[FSO2]	k_{12}, k_{23}, k_{-1}, k_2, k_{-3} (90%), k_4, k_7	k_6	k_{23}
[GSO2]	k_{12}, k_{23}, k_{-1}, k_2, k_4, k_5, k_7, k_8	k_8 (110%) k_5 (90%)	k_{23}
[HSO]	k_{12}, k_{23}, k_{-1}, k_2, k_5, k_6, k_7, k_8, k_9	k_6 (110%) k_9 (90%)	k_{23}
[EP]	k_{12}, k_{23}, k_{-1}, k_2, k_5, k_6, k_{-7}, k_7, k_8, k_9	k_9	k_{23}
[P]	k_{12}, k_{23}, k_{-1}, k_2, k_5, k_6, k_{-7} (90%), k_7, k_8, k_9	k_9	k_{23}

Table 4.26: *The most prominent parameters for the CYP model.*

The three tests seem to concur over the parameter with the highest sensitivity for the variable.

4.5 Discussion

For model 1 it is understandable that within a 'one variable - one parameter system that this would have an effect, so this was to test if the methodology worked correctly.

In model 2 there are two parameters and variables and the tests concurred with the plots. This means that the parameters with the most effect k_{12}:y_1 and k_{20}:y_2. The extended sensitivity analysis also shows this conclusion is valid. It is understandable that these parameters have the biggest effect on the variable since they

are the excretion/removal rate for the compartment in question.

The third model has four variables and parameters and the parameters that have the most effect are k_{12}:y_1, k_{32}:y_2, k_{32}:y_3 and a:y_4. It is surprising that the parameter a has less effect on y2 than others considering affects the main excretion out of this compartment.

The y_3 is supposed to represent a fatty liver or compartment where it is easier to enter than to leave. It is interesting that it is primarily affected by its removal rate k_{32} which is smaller in parameter value than its influx rate k_{23}.

The y_4 variable being primarily affected by a is not very surprising due to the fact that this is the only parameter that affects this variable in the equations. This should be the same for y_1 and k_{12} but according to the paired t test this variable is also affected by a. This outcome could be due to very small difference average being divided by a tiny standard error leading to a large T statistic causing a false positive.

For the Cytochrome P450 cycle within the first few variables it is not easy to see which parameters have a larger effect even though the primary parameters would have an effect right away i.e. k_1, k_{-1}, k_2 etc but the later variables like [FSO2] the issue becomes clearer with only two out of the twelve parameters being highlighted. In order to try and see through this issue it would be necessary to run the cycle for longer in order for the difference to truly become clear.

The sensitivity ranges show smaller one parameter being outlined but sometimes the one selected does not have a direct effect on the concentration like k_3:[E] and k_3:[S] etc. These can be explained by a rolling effect i.e. k_3 affects [FS] which in turn influences the [GSO2] level and [HSO] level and so on.

The extended sensitivity shows that k_3 is a controlling factor although this does not affect all the variables directly. The t test by contrast shows that k_5 is also a parameter that has and effect on multiple variables. Due to this model being a

cycle it is difficult to know what parameters truly affect each variable the most unless the model is run for much longer or a stronger measure of sensitivity is used.

The Cytochrome P450 model is an amalgamation of the last two models so it is thought that the same sensitivities would be held with slight adjustments due to model 3's y_3 disappearing and joining with the drug level [S].

The y_1 and y_3's sensitivity to parameters are left the same from model 3 (y_3 is the same as y_4) but y_2 is now affected by k_6 which is due to the joining with the CYP cycle. As with the previous model the fuzziness in the parameter sensitivity comes at the end. This means that if the last model needed longer then this one does as well.

The extended sensitivity analysis shows that k_{23} is a prominent parameter, which is sensible as it regulates transfer between y_2 and [S]. For the paired t test the prominent parameters are k_6 and k_9 which control the passage from HSO to EP and E respectively. The variables for which the Magnitude test seems to have worked in minimising the parameter effect to 1-4 parameters are y_1, y_2, y_3 and [S]. For these concentrations the rates that were singled out were accurate since all the parameters directly affect the variable.

The analysis outlined in this chapter allows for prominent parameters to be isolated and to see how robust the models are to experimental error and parameter estimation. For the first three models the parameters that have the greatest sensitivity are easily found and there is agreement between the tests performed. Unfortunately for the larger models these tests do not agree and as such for all but a few variables it is unclear what parameters are powerful.

The first three models were applied to experimental data in Chapter 3. The analysis in this chapter shows with respect to model 2 the shifts between the HRN and WT parameter sets are most visible in y_2 if the excretion rate k_{20} changes. For

model 3 this is the k_{32} parameter representing the influx from the third compartment or "fatty liver". This particular change is visible in the Tamoxifen models, which can be found in section 3.3.9. The techniques for finding the sensitive parameters outlined in this chapter are easily applied and return good results so long as the model is simple enough. It is possible that the difference taken of 10% in the parameters is too small to gain insight into the larger models.

Chapter 5

Cellular Automaton Models

5.1 Introduction

Cellular Automaton (CA) models have been used for a number of years now since John von Neumann and Stanislaw Ulam first introduced them in the middle of the last century. These models are a mathematical representation of real life systems usually in physics and biology where space and time are discretised. This is done using a lattice and each site takes on specific values corresponding to rules laid down by the programmer, which include boundary conditions and neighbourhood searching. The algorithm is evaluated at discrete time steps in order to update sites simultaneously (Wolfram, 1983). Cellular Automata can use 1D, 2D and even 3D lattices which allow for greater complexity in the model (Sigmund, 1993).

Rules are used to define state values in step $t+1$ dependent on nearest neighbour values in step t (Wolf-Gladrow, 2000). As such there are numerous rules that can be used in order to do this since there is no restriction on the type they can use (Raabe, 2004). In one dimension it can be shown that if you have eight different states with two options (on or off) there are 256 rules used in the cellular automaton.

In Wolfram (1984) four classes of 1D cellular automata and their corresponding rule set were outlined. The class 1 cellular automata evolve to a homogeneous state in a finite number of steps. Class 2 and class 3 show periodic and aperiodic behaviour respectively. In the final class the cellular automaton creates periodic and propagating stable structures, which can exist for arbitrary lengths of time Although four classes were defined, only three have been found (Bak, 1997) - the other being propagating complex patterns forever. This is an area of much debate and it has been proposed that a better classification system maybe needed (Barbosa et al., 2006).

Different types of cellular automata

Traditional cellular automaton models are deterministic but due to the rules being unrestricted this allows for greater variation. For example the lattice can be triangular, square or hexagonal in shape. The other part of the definition that can be different is the neighbourhood searching algorithm. This can be either von Neumann or Moore which gives either a diamond or square shape respectively to the cells on the lattice when they propagate.

For processes in physics like fluid dynamics it is better to use a more specific cellular automaton like Lattice Gas (Kutrib et al., 1997). The HPP (Hardy, de Pazzis and Pomeau) lattice gas model is an important model in physical systems using statistical properties of particles (Wolf-Gladrow, 2000; Bandini et al., 2001). Lattice Boltzmann models are useful in fluid dynamics as well, although this is due to the automaton having a continuous state space. As such this type of model cannot be thought of as a strict cellular automaton model (Bandini et al., 2001). Biological problems were the reason for the first cellular automaton to be designed (Bandini et al., 2001). These models have been used to model a wide range of applications from fluids in physics to cell growth in biology and medical studies.

Tumour growth has been a focus of cellular automaton modelling in recent years. For example, Dormann and Deutsch (2002) used a hybrid lattice-gas cellular automaton in order to model pattern formation in multicellular tumour spheroids. They showed that the self-organized growth of the cells caused a three layer formation within the sphere. These layers represented a necrotic core with a quiescent layer and proliferating rim around it. There was no cell flow towards the core only outwards towards nutrients since all cells in the core were in the resting phase. This paper also shows that it is necessary to include interaction with more than just the cell‘s nearest neighbours.

Using an extended Potts model, Turner and Sherratt (2002) investigated malignant invasion to see how cell adhesion at its core affects invasiveness. In Ghaemi and Shahrokhi (2006) an attempt was made to combine a cellular Potts model and Lattice-Gas cellular automaton to simulate avascular tumour growth.

Ward and King (2003) also studied multicellular spheroids using a purely PDE based model. They studied the difference in survival rates between a spheroid and a monolayer when a drug was applied. As can be expected the survival rate was higher in the spheroid since drug penetration was lower.

Another case where a cellular automaton model has been used to investigate drug therapy on tumour cells was shown in Ribba et al. (2004). While studying non-Hodgkins Lymphoma a vascular network was included in their algorithm. This allowed for blood flow to have an effect on the drug treatment. However, the tumour growth was found to be unstable which caused oscillations in cell colony number.

Multi-scale models have been used in the literature in order to account for both cell-cycle dynamics and diffusion of therapeutic drugs. In Alarcon et al. (2004) a model for tumour growth was proposed which included blood flow and cell-cycle dynamics with vascular adaption. Ribba et al. (2006) also developed a multi-scale

model but this time of avascular tumour growth, which included spatial tumour dynamics using Darcy's law. It also included radiosensitivity due to cell cycle phase.

Sinek et al. (2009)use a multicompartment Pharmacokinetic-Pharmacodynamic (PKPD) model to investigate the efficacy of Doxorubicin and Cisplatin. They suggest that spatial heterogeneity in nutrient and oxygen distribution is necessary for realism. This is due to microenvironments exist within tumour spheroids.

In Frieboes et al. (2009) a mathematical model was presented that included a three dimensional physical morphology to tumour growth. This allowed them to investigate the different physical scales in order to predict the response to breast cancer drugs e.g. Doxorubicin.

In Bearer et al. (2009) a multiscale tumour growth model was proposed which included morphology, genotype and phenotype as well as nutrient and oxygen heterogeneity. This 3D model showed that tumours to exhibit morphological instability resulting in finger shaped protrusions which are found *in vivo*.

Ermentrout and Edelstein-Keshet (1993) produced a good review of models from biologically inspired cellular automata, which include areas such as neuroscience and population biology. Another good review of cellular automaton theory that provides a good background is by Kari (2005).

In this chapter a traditional cellular automaton is used with an on-lattice approach. It is a multi-scale model with individual cells on the lattice having an internal cell cycle and also a Cytochrome P450 cycle. In the following sections is held a description for both the cell cycle and the P450 cycle models.

5.2 Background Theory to the Multiscale Model

The background to the Cytochrome P450 cycle and functionality can be found in section 1.4.

5.2.1 The Eukaryotic Cell Cycle

The cell cycle is a biological mechanism that describes the stages an individual cell goes through in order to divide and produce daughter cells.

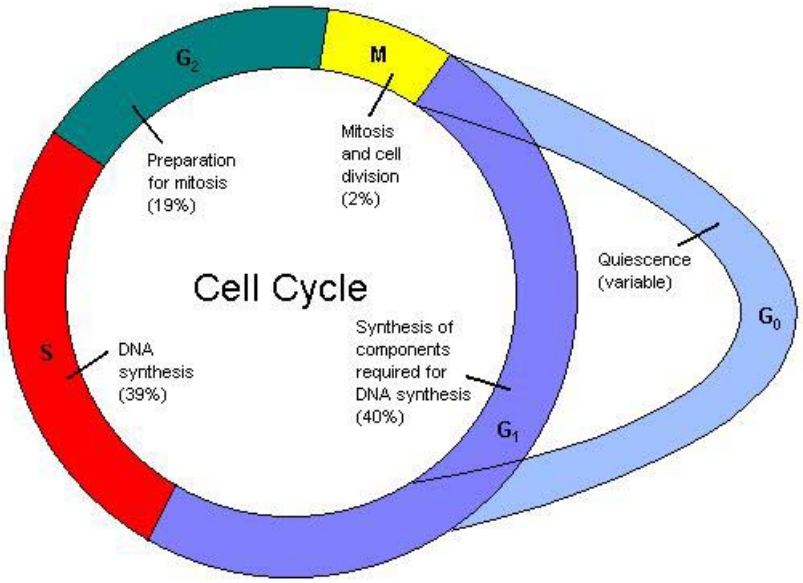

Figure 5.1: *Schematic diagram of the cell cycle.*

The cell cycle is usually divided into four stages (shown in figure 5.1), which are known as the M, G1, S and G2 phases. The M phase represents Mitosis where nuclear division occurs and two identical daughter cells are created. The G1 phase is the part of the cell cycle concerned with growth and biosynthesis whereas G2 is mostly just growth. DNA replication happens in the Synthesis (S) phase, which occurs between the G1 and G2 phases. The other state shown in the cycle is that of the resting phase G0. This is where the cells, which are not proliferating or dormant, are categorised. The length of stay in the G0 phase can be of any length.

Mathematical models have been created over the years with varying levels of complexity. The model by Novak and Tyson (2004) includes eighteen differential equations for the eukaryotic cell. The cell cycle used in this chapter is a previous

less complex version and is governed by the six differential equations in a model proposed by Tyson and Novak (2001). The six components include differential equations for the Cdk-CyclinB complex (CycB), APC-Cdh1 complex (Cdh1), the Plk1 protein (Plk1), the cell mass (mass) and the p55cdc-APC complex - both the active and total levels (B=$p55cdc_A$ and A=$p55cdc_T$ respectively).

The CycB complex can be expressed in the following equation:

$$\frac{d[CycB]}{dt} = K_1 - (K_2^{'} + K_2^{''}[Cdh1])[CycB] \tag{5.1}$$

The complex is decayed both naturally and based on the Cdh1 complex level.

$$\frac{d[Cdh1]}{dt} = \frac{(K_3^{'} + K_3^{''}[B])(1 - [Cdh1])}{J_3 + 1 - [Cdh1]} - \frac{K_4 m[CycB][Cdh1]}{J_4 + [Cdh1]} \tag{5.2}$$

The equation for [Cdh1] shows Michaelis-Menten dynamics for both activation and inactivation of the complex. It is activated by the active version of $p55cdc_A$ and inactivated by [CycB].

$$\frac{d[A]}{dt} = K_5^{'} + K_5^{''} \frac{([CycB][mass])^n}{J_5^n + ([CycB][mass])^n} - K_6[A] \tag{5.3}$$

The total p55cdc has a Hill function in the equation explaining the transcription of total p55cdc turned on by [CycB] and other than that it is naturally degraded.

$$\frac{d[B]}{dt} = \frac{K_7[Plk1]([A] - [B])}{J_7 + [A] - [B]} - \frac{K_8[Mad][B]}{J_8 + [B]} - K_6[B] \tag{5.4}$$

Just like [Cdh1] the equation for active p55cdc contains Michaelis-Menten dynamics to explain the activation and inactivation of inactive and active p55cdc respectively. Protein [Plk1] activates inactive p55cdc and Mad genes inactivate active p55cdc.

$$\frac{d[Plk1]}{dt} = K_9[mass][CycB](1 - [Plk1]) - K_{10}[Plk1] \tag{5.5}$$

The [Plk1] protein equation shows a mass proportional inactivation of [CycB] and a natural degradation.

$$\frac{d[mass]}{dt} = \mu[mass](1 - \frac{[mass]}{m_*}) \tag{5.6}$$

The final equation of the cell cycle six component model governs the cell mass by a logistic growth equation with maximum cell mass m_*.

As the cells are tumour cells the cell cycle needed to be longer than the 63.05mins outlined in the paper. Cancer cells have cell cycle lengths, which vary from 15 hours to 10 days. Smith and Martin (1973) proposed that the difference in cell cycle length was due to the length of stay in the G0 phase. This means that if there was no stay in the G0 phase the cell cycle length would be shorter and vice versa. In Novak and Tyson (2004) the rate constants were changed from min^{-1} to hr^{-1} changing the time scale to be changed to hours as well. This allows the change of cell cycle length to 63.05 hours for the following model, which is within the range for human cancers.

The parameters used for the cell cycle model are outlined in table 5.1.

Component	Rate Constants (hr^{-1})	Dimensionless Constants
[CycB]	K_1=0.04, $K_2^{'}$=0.04, $K_2^{''}$=1	$[CycB]_{threshold}$=0.1
[Cdh1]	$K_3^{'}$=1, $K_3^{''}$=10, K_4=35	J_3=0.04, J_4=0.04
[A]	$K_5^{'}$=0.005, $K_5^{''}$=0.2, K_6=0.1	J_5=0.3, n=4
[B]	K_7=1, K_8=0.5	J_7=0.001, J_8=0.001, [Mad]=1
[Plk1]	K_9=0.1, K_{10}=0.02	-
[mass]	μ =0.01	m_*=10

Table 5.1: *Cell Cycle Parameters.*

In order to include variability affecting the cell growth rates white noise was added to μ shown in the following equation. The variable μ is a measure of nutrient, oxygen and growth factor level for the grid point.

$$\mu = \mu^{+} + \varepsilon\widehat{\mu} \tag{5.7}$$

Where $\mu^{+} = 0.01$, ε=0.005 and $\widehat{\mu} \sim U(-1, 1)$. This allows for cells to divide faster or slower than the general population on the lattice. This equation shows that μ varies from 0.005 to 0.015 if the cell was experiencing normal cell growth due to the presence of ample nutrient, oxygen and growth factor. However if the cell has no space around it the μ parameter is set to zero meaning that these levels have dropped.

5.2.2 The Cytochrome P450 Cycle

As seen from the previous section, the Cytochrome P450 cycle is characterised by chemical equilibria (1.1) to (1.9). Using the law of mass action it is possible to transfer these equilibria to a set of ordinary differential equations. For example, while focussing on the variable [E] that represents enzyme concentration, the reactions involving this are:

Equation	Rate Constants
$E + S \rightarrow ES$	k_1
$ES \rightarrow E + S$	k_{-1}
$EP \rightarrow E + P$	k_7
$E + P \rightarrow EP$	k_{-7}
$GSO2 \rightarrow E + S + H2O2$	k_8
$HSO \rightarrow E + S + H2O$	k_9

Table 5.2: *P450 Enzyme Equations.*

This means that the differential equation describing the rate of change of enzyme concentration is:

$$\begin{aligned}\frac{d[E]}{dt} &= k_{-1}[ES] + k_7[EP] + k_8[GSO2] + k_9[HSO] - k_1[E] - k_{-7}[E] \\ &= k_{-1}[ES] + k_7[EP] + k_8[GSO2] + k_9[HSO] - (k_1 + k_{-7})[E] \quad (5.8)\end{aligned}$$

Using the same methodology with the rest of the variables, the following system of ordinary differential equations is obtained:

$$\frac{d[S]}{dt} = k_{-1}[ES] + k_8[GSO2] + k_9[HSO] - k_1[S] \quad (5.9)$$

$$\frac{d[ES]}{dt} = k_1[E][S] - (k_{-1} + k_2)[ES] \quad (5.10)$$

$$\frac{d[FS]}{dt} = k_2[ES] + k_{-3}[FSO2] - k_3[FS] \quad (5.11)$$

$$\frac{d[FSO2]}{dt} = k_3[FS][O2] - (k_{-3} + k_4)[FSO2] \quad (5.12)$$

$$\frac{d[GSO2]}{dt} = k_4[FSO2] - (k_5 + k_8)[GSO2] \quad (5.13)$$

$$\frac{d[HSO]}{dt} = k_5[GSO2] - (k_6 + k_9)[HSO] \quad (5.14)$$

$$\frac{d[EP]}{dt} = k_6[HSO] + k_{-7}[E][P] - k_7[EP] \quad (5.15)$$

$$\frac{d[P]}{dt} = k_7[EP] - k_{-7}[P] \quad (5.16)$$

The parameters in the original paper of Guengerich (2001) have units min^{-1}. These had to be adjusted to match the units in the cell cycle model which are hr^{-1}. Table 5.3 below shows the converted values.

Parameter	Value (hr^{-1})	Parameter	Value (hr^{-1})
k_1, k_{-3}, k_7	$6000 * 60 = 360000$	k_{-1}	$120000 * 60 = 7200000$
k_2, k_4	$700 * 60 = 42000$	k_3	$6 * 60 = 360$
k_5	$110 * 60 = 6600$	k_6	$33 * 60 = 1980$
k_{-7}	$660 * 60 = 39600$	k_8, k_9	$50 * 60 = 3000$

Table 5.3: *P450 Cycle Parameters.*

The substrate used for this cycle is taken to be an externally administered drug.

Cytochrome P450 Model

In order to achieve this a hybrid model was adopted which combined the model 3 shown in section 3.2.3 configuration with the Cytochrome P450 cycle. This model had the following equations:

$$\frac{dy_1}{dt} = -k_{12}y_1 \tag{5.17}$$
$$\frac{dy_2}{dt} = k_{32}[S] + k_{12}y_1 - k_{23}y_2 - y_3 \tag{5.18}$$
$$\frac{dy_3}{dt} = a \tag{5.19}$$
$$\frac{d[E]}{dt} = k_{-1}[ES] + k_7[EP] + k_8[GSO2] + k_9[HSO] - (k_1 + k_{-7})[E] \tag{5.20}$$
$$\frac{d[S]}{dt} = k_{23}y_2 + k_{-1}[ES] + k_8[GSO2] + k_9[HSO] - (k_1 + k_{32})[S] \tag{5.21}$$
$$\frac{d[ES]}{dt} = k_1[E][S] - (k_{-1} + k_2)[ES] \tag{5.22}$$
$$\frac{d[FS]}{dt} = k_2[ES] + k_{-3}[FSO2] - k_3[FS] \tag{5.23}$$
$$\frac{d[FSO2]}{dt} = k_3[FS][O2] - (k_{-3} + k_4)[FSO2] \tag{5.24}$$
$$\frac{d[GSO2]}{dt} = k_4[FSO2] - (k_5 + k_8)[GSO2] \tag{5.25}$$
$$\frac{d[HSO]}{dt} = k_5[GSO2] - (k_6 + k_9)[HSO] \tag{5.26}$$
$$\frac{d[EP]}{dt} = k_6[HSO] + k_{-7}[E][P] - k_7[EP] \tag{5.27}$$
$$\frac{d[P]}{dt} = k_7[EP] - k_{-7}[P] \tag{5.28}$$
$$\tag{5.29}$$

The parameters used are outlined in the following table:

Parameter	Value
k_{12}	1
k_{23}	0.4
k_{32}	0.175
a	0.4

Table 5.4: *Cytochrome P450 Model Parameters.*

For this model the cell killing protocol was transferred to the level of y_2 instead of [S]. The plots of the growing tumour are shown in figure 5.20.

5.2.3 Computational Simulation Method

The cellular automaton model was coded in Java, which means it can be run on any platform. This model starts with an empty grid of 51 by 51 squares with $\Delta l = 0.04mm$ and a cell in G1 phase in the middle as shown in figure 5.3. The grid point size is within the size range set out in the work in Melicow (1982). This paper stated that normal cancer cells have a range of 10100 μm and the Δl is within this. The grid is a regular square lattice and each grid point contains either a empty space or a cell. The cell can take five different states: G1, S, G2, M, or G0. The levels and progression is shown in the following figure:

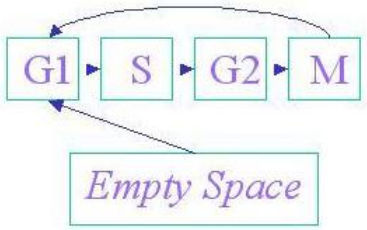

Figure 5.2: *Schematic diagram of the possible states for a cell in the cellular automaton.*

This gives four states in all that each grid point can take.

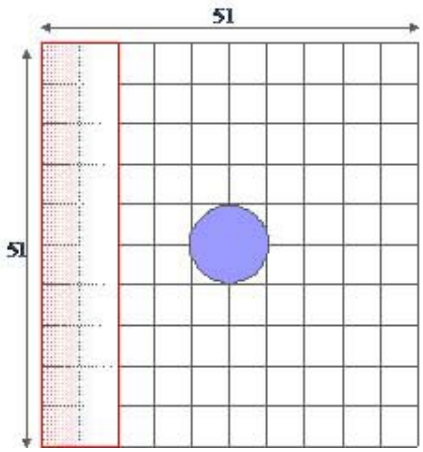

Figure 5.3: *Schematic diagram of the configuration of cells on the cellular automaton grid.*

A fourth order Runga-Kutta algorithm was used at each time step to get the intercellular protein levels in each cell using the model outlined in equations (5.1) to (5.6). Within the program there are 1000 time steps for each hour of simulation. This is the same for both the Cytochrome P450 cycle and cell cycle. After this, the phase of the cell and division signal is added to the grid square information. The cell is marked for division when $[CycB] > 0.1$ and then the $mass$ is halved. The threshold for the [CycB] protein was calculated from numerical simulations of the cell cycle model shown in the work by Gordon (2006). The work showed that this protein dips below 0.1 just before the mitosis phase begins. If this happens then neighbourhood searching techniques are used to find space and if no space is found a marker is added to the grid point and this causes μ to be zeroed and the cell to enter G0 phase. Even if the cell has not been marked for division, the code checks for space to the order of three spaces away from the cell. In order to avoid the artificial effect of the grid structure on the growth of the tumour, the cancer cells grow and spread using the Moore algorithm and von Neumann algorithm alternately i.e. at one time step the Moore algorithm is used and at the next time the von Neumann algorithm is used and so on. As was mentioned in the introduction these two neighbourhood searching techniques

have different shape outcomes due to the number of neighbours analysed. Moore looks at all eight neighbours leading to a square shape and von Neumann the 4 neighbours to the north, south, east and west, which gives a diamond shape. The alternation between these two techniques result in a more circular shape for the tumour growth.

The external substrate (i.e. the drug), [S], diffuses from the right boundary across the domain according to the following equation:

$$\frac{\delta[S]}{\delta t} = d\frac{\delta^2[S]}{\delta x^2} - \lambda[S] \tag{5.30}$$

where d is the (constant) diffusion coefficient and λ is the decay rate of the drug. This equation is used in conjunction with equation (5.9) in order to control the drug level. The diffusion coefficient used was $d = 0.1875$ and the decay rate $\lambda = 0.005$. This equation is solved by a forward-time-central-space finite difference method.

The P450 cycle only acts when there is a cell present in the square on the grid and these cells start with an enzyme level of 3. The other variable in the model is that of the oxygen level. The default is $[O2] = 1$ per grid square with $\frac{d[O2]}{dt} = 0$. Drug induced cell death is programmed through identifying the drug level in the cell and if this value is greater than the active concentration set there is a probability for this grid point to be emptied or "killed". The drug algorithm includes a cell cycle phase-specific anti-cancer drug, which kills cells with a probability of 0.8. It is currently assumed that a cell in M-phase (which is found using the grid square information) is probably killed if the drug concentration is above 0.0001. Once the drug level drops below this threshold the tumour grows unhindered.

5.3 Computational Simulation Results

Initially, the tumour is allowed to grow and develop for two hundred hours (using the cell-cycle equations). After this time, the drug is delivered by one of the three delivery regimes and undergoes diffusion according to equation (5.30).

Three dosing regimens were applied to the tumour that was grown to, these were: (i) a single dose of drug released from the first two leftmost columns ($2*51 = 102$ squares) of the grid, (ii) a constant infusion of drug released from only the first leftmost column on the grid, and (iii) a single dose of drug released from the central ten by ten square which is equivalent in size to the side dose.

As well as the three different dose regimes, the time of delivery was changed between -10, +0 and +10 hours after the tumour had grown for the side and central dose regimes.

Plots of the growing tumour are made at +5, +15, +25, +35 and +45 hours after drug dosage time and these pictures are shown in figures 5.5, 5.7, 5.9, 5.11, 5.13, 5.15 and 5.17. From figures 5.8, 5.12 and 5.16 it can be observed that there is a difference when using the P450 cycle which is carried through the entire period of the algorithm. For the central and side dosing regimens the dosage time was changed in order to analyse how a shift of 10 hours could affect the efficacy of the drug. The drug curves relating to this are shown in figures 5.14 and 5.10 respectively In the plots of the growing tumour, the blue cells represent those in G1 phase, green cells are those in S-G2-M phase and black are in the resting phase G0.

5.3.1 Effect of Changing the Drug Diffusion Coefficient

To see the impact on the growing tumour through changing the value of the drug diffusion coefficient, the value was changed by a factor of ten from a baseline value i.e. we carried out computational simulations with $d = 0.0025, 0.025, 0.25$.

The drug uptake curve for these three scenarios is shown in figure 5.4. The plots in figure 5.5 show the effect on the growing tumour.

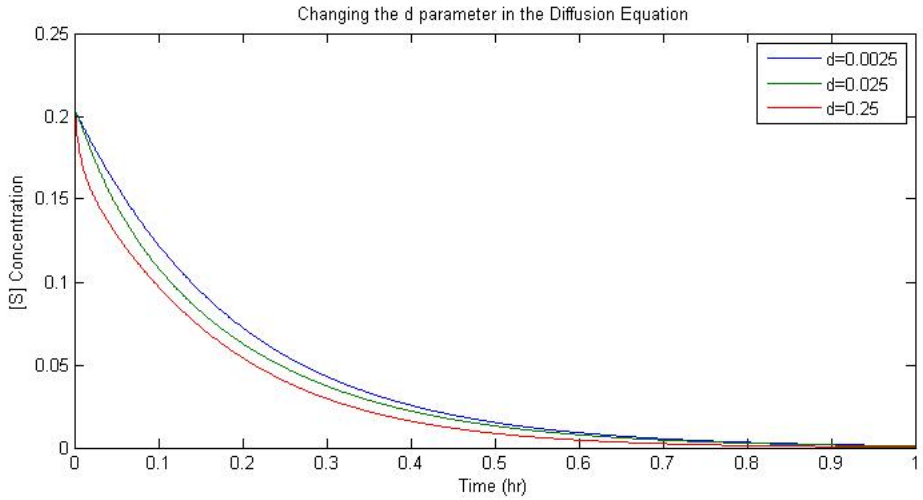

Figure 5.4: *Plots of average drug concentration over time with different drug diffusion coefficients d.*

The plots of the drug curve show that as the diffusion parameter increases the drug concentration is reduced. This means that the active drug is around for a shorter period of time when d is larger which suggests that it diffuses away too quickly to have as much effect on the cells.

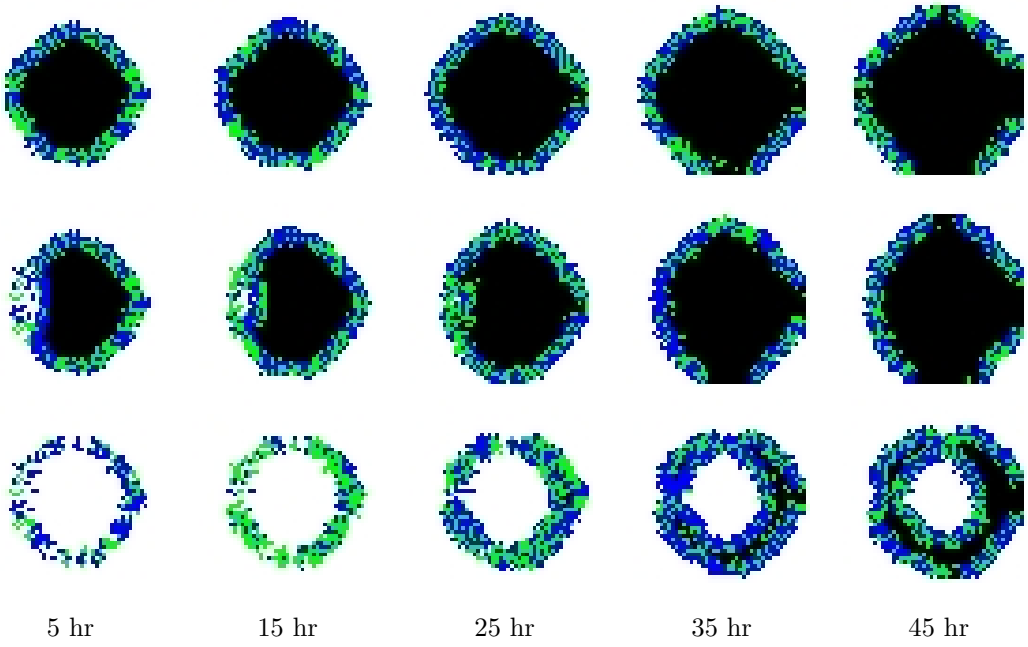

Figure 5.5: *Plots showing the effect on the growing tumour of changing the drug diffusion coefficient d - $d = 0.0025$ (top), $d = 0.025$ (middle) and $d = 0.25$ (bottom). Blue cells represent those in G1 phase, green cells are those in S-G2-M phase and black are in the resting phase G0.*

Although it seems that it is cells in the resting phase G0 are being destroyed this is not the case. This effect is caused by the cells being killed while in M phase and the cells left alive ending up in G0 due to lack of resources near the centre. The top two lines of tumour snapshots showed that the drug has not been able to diffuse to the cells at the lower diffusion parameter values. This is an interesting result since this suggests that the decay section of the diffusion equation in 5.30 affects the curve more when the diffusion parameter is smaller i.e. $d\frac{\delta^2[S]}{\delta x^2} << \lambda[S]$. This is related to the diffusive length, which is defined as:

$$L = \sqrt{\frac{d}{\lambda}} \tag{5.31}$$

From this equation it can be seen that if the diffusion is doubled the diffusion length increases by a factor of $\sqrt{2}$. This property would explain why the last line is the only one that shows cell death across the tumour. As such if the

diffusion parameter is less than 0.25 with a decay rate of 0.005 the tumour is more susceptible to a lower drug concentration (less than active threshold) and when this occurs the tumour grows unheeded.

5.3.2 Effect of Changing the Drug Decay Rate

To see the impact on the growing tumour through changing the value of the drug decay rate λ, the value was changed by a factor of ten from a baseline value i.e. carried out computational simulations with $\lambda = 0.0005, 0.005, 0.05$. The corresponding drug uptake curves are shown in figure 5.6. The plots in figure 5.7 show the effect on the growing tumour.

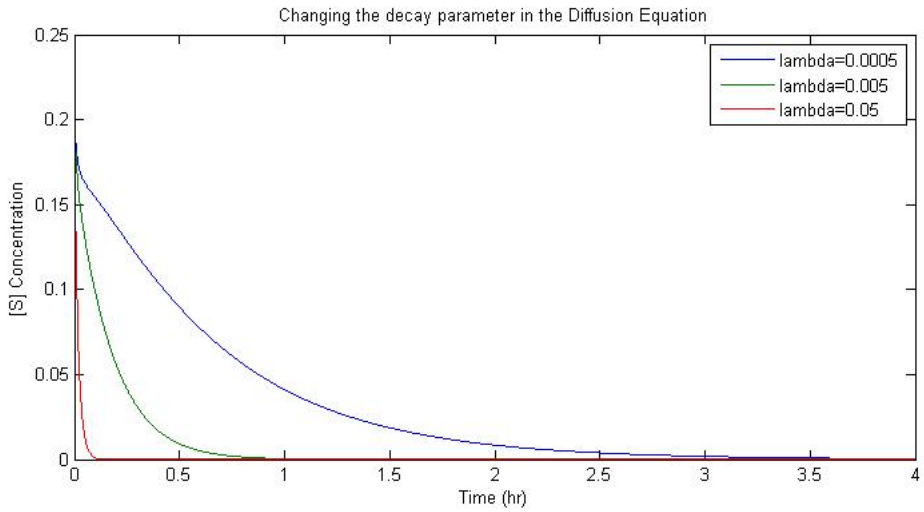

Figure 5.6: *Plots of average drug concentration over time with different drug decay rate λ.*

The drug concentration curves show that as the decay parameter increases there is less drug in the system. This means that when drug decay is large it has less killing effect on the tumour.

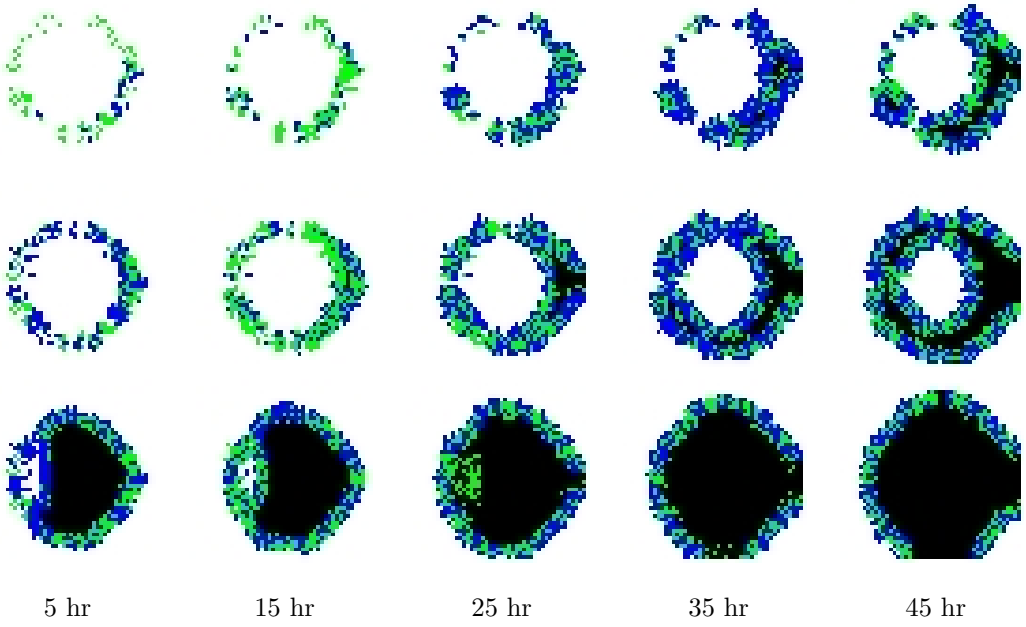

Figure 5.7: *Plots showing the effect on the growing tumour of changing in the decay parameter – $\lambda = 0.0005$ (top), $\lambda = 0.005$ (middle) and $\lambda = 0.05$ (bottom). Blue cells represent those in G1 phase, green cells are those in S-G2-M phase and black are in the resting phase G0.*

The plots of the snapshots of the tumour mass show that as the decay parameter increases the tumour is bigger since there is a lower drug concentration around to have a killing effect. Although this is understandable due to the nature of a decay component of an equation i.e. as the parameter gets bigger the decay gets larger. However due to this not being the only component in the equation the decay would have to be large enough in order to counter-balance the diffusive nature of the equation. This is why the drug concentration level seems to have no effect in the final line of figure 5.7 $d\frac{\delta^2[S]}{\delta x^2} >> \lambda[S]$. As before when related to the diffusion length an double in the value of λ in equation 5.31 equates to a shortening of diffusive length by a factor of $\sqrt{2}$.

5.3.3 Application of the Drug via a Single Dose Released from the Boundary

For this dosing regimen the drug uptake curve is shown in figure 5.8.

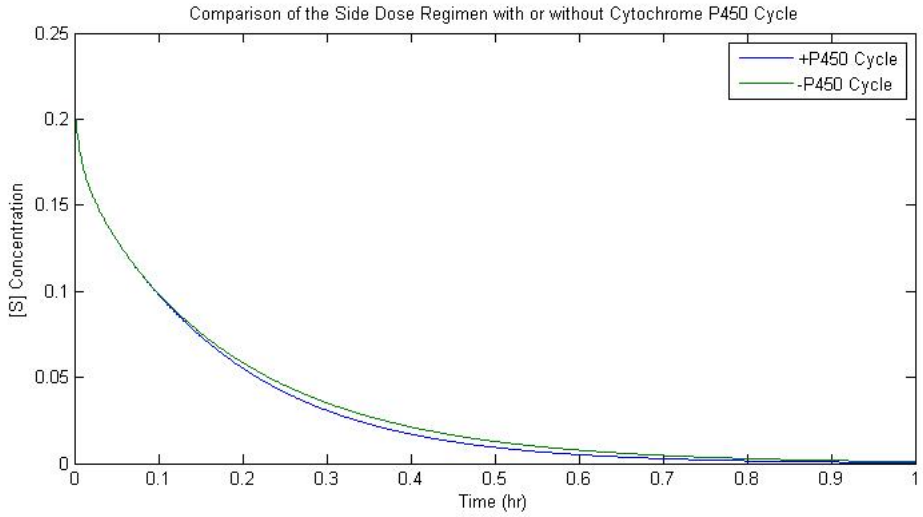

Figure 5.8: *Comparison of average drug concentration with and without the P450 Cycle under the single dose release from the boundary.*

It can be seen from this plot that there is a difference in the curves when the CYP cycle is included in the program. The two curves show similar dynamics although after the 0.1 hour point the "+P450 Cycle" curve drops below the "-P450 Cycle" curve. This is probably to do with the cycle equations (5.8) to (5.16) because the drug level is related to enzyme and enzyme-drug complex level. The equilibrium in equation (1.1) shows how these three chemicals are related. The inclusion of the Cytochrome P450 enzymatic cycle in the program allows for an added level of complexity that has resulted in interesting outcomes.

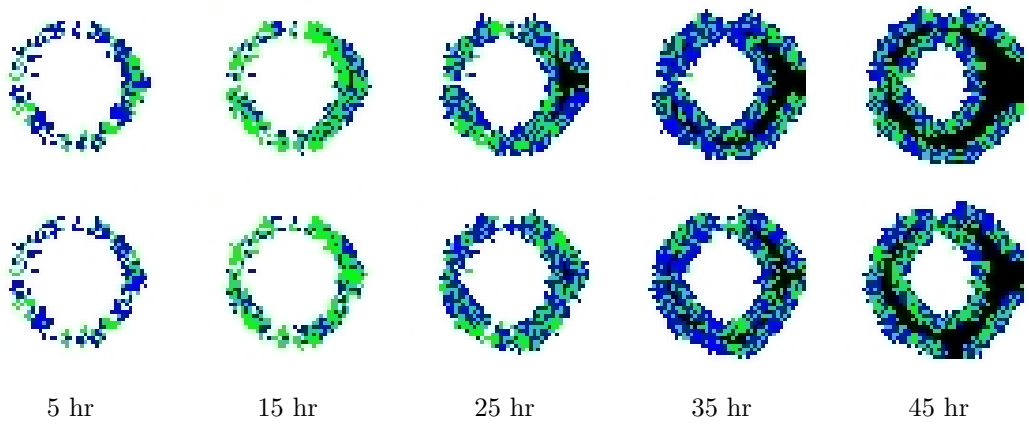

Figure 5.9: *Plots showing the tumour mass at various times for the single dose release from the boundary: With (top) and Without (bottom) P450 Cycle. Blue cells represent those in G1 phase, green cells are those in S-G2-M phase and black are in the resting phase G0.*

The change between the top and bottom rows are due to the inclusion of the enzymatic cycle and the plots shown in figure 5.9 outline the effect of the drug level on the tumour cells. The top row shows that the tumour is slightly smaller with the P450 cycle. However the black cells (resting phase, G0) appear earlier in the top row than in the bottom row and the last picture shows the largest amount of them in both rows. The morphology of the tumours are different between the two lines and this is attributable to the kill and regrowth mechanism inherent to the program. The right hand side of the tumours in the top line is a lot wider due to cell proliferation that has been left untouched by the cell killing algorithm.

Effect of Changing the Time of Dose

The plot showing the different drug curves for the changes in time of dosing is given in figure 5.10.

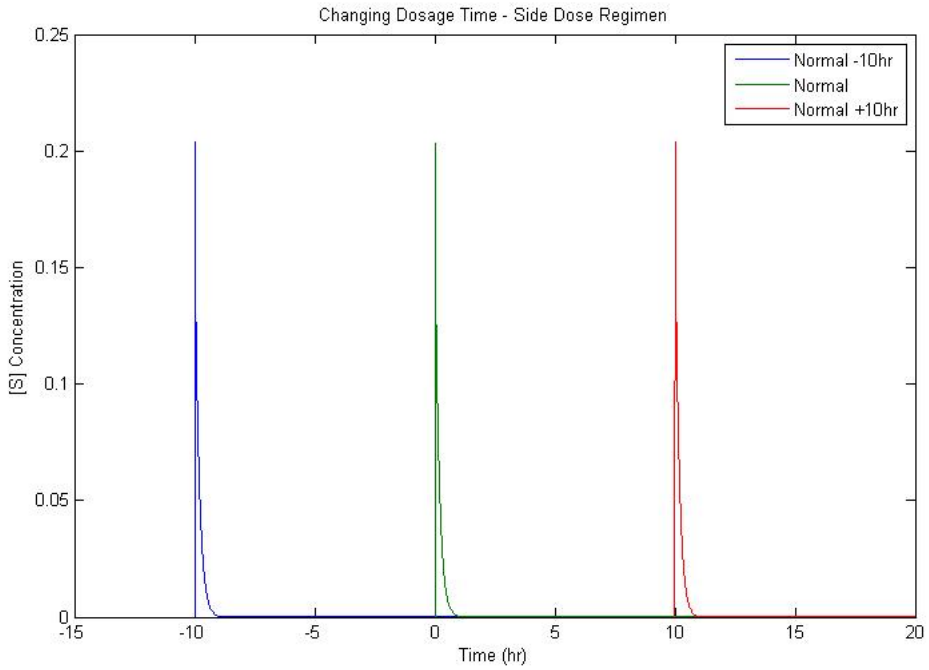

Figure 5.10: *Plots of average drug concentration over time with three different times of dose application.*

The plot shows that although the dosing time was changed the shape and peak height of the curve remains unchanged. This does not mean however that there would not be differences in the shape of the tumour due to the timing of the dose since the drug would be more effective on a smaller tumour and vice versa.

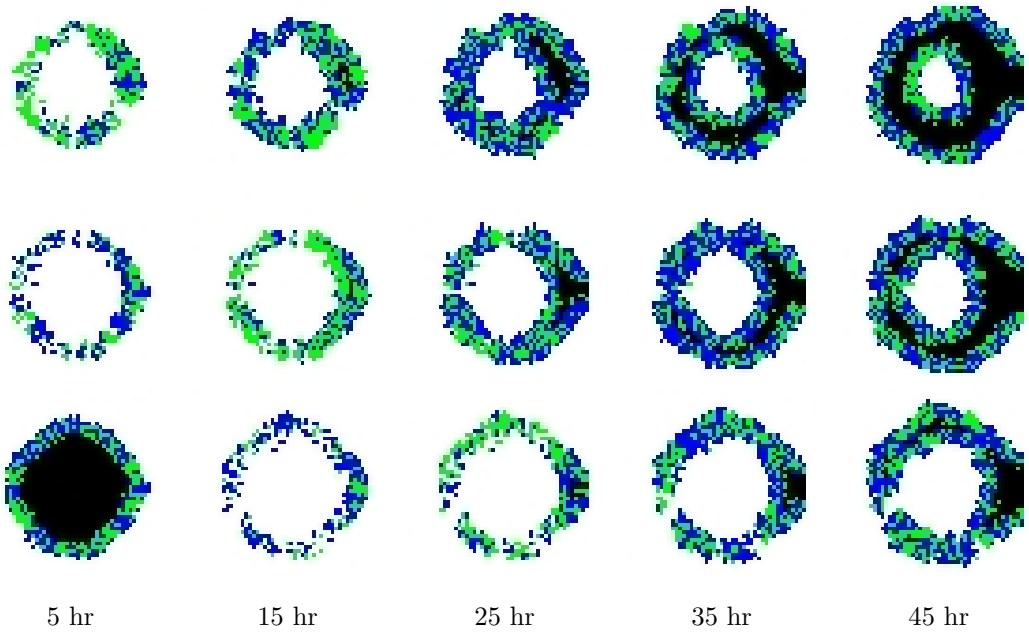

Figure 5.11: *Plots showing the effect on the growing tumour of changing the time of dosage: -10 hours (top), +0 hours (middle) and +10 hours (bottom). Blue cells represent those in G1 phase, green cells are those in S-G2-M phase and black are in the resting phase G0.*

The plots of the tumour cells are shown in figure 5.11 and the rows are what would be expected of a time shift of ten hours (-10, +0 and +10 hours). The other result is that as the time of drug dose is earlier or delayed, the tumour changes size. This could be more to do with the fact that the tumour the drug is applied to is not fully grown. Since the drug curves are similar in shape the drug pressure would be similar in each line but occurring at different points before the start of row 1, start of row 2 and after picture 1 in row 3. The G0 cells appear to be more prevalent in the -10 hours and +0 hours snapshots, which could be due to regrowth after the cells had been killed, or the drug level has dropped below the active threshold. This is an interesting result as it shows how the tumour cells proliferate with or without the drug being present.

5.3.4 Application of the Drug via a Single Dose Released from the Centre of the Domain

For this dosing regimen the drug uptake curve is shown in figure 5.12 and there are marked differences between this plot and the one for side dose (figure 5.8). These are probably to do with the fact that the P450 cycle is active straight away so causes the peak and dip in comparison to the '-P450' curve.

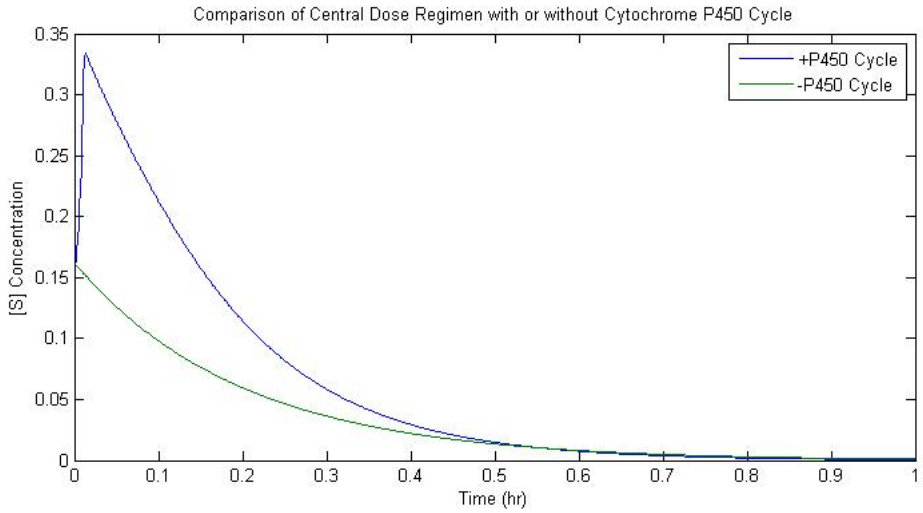

Figure 5.12: *Comparison of With and Without P450 Cycle average drug concentration with the Central Dose Regimen.*

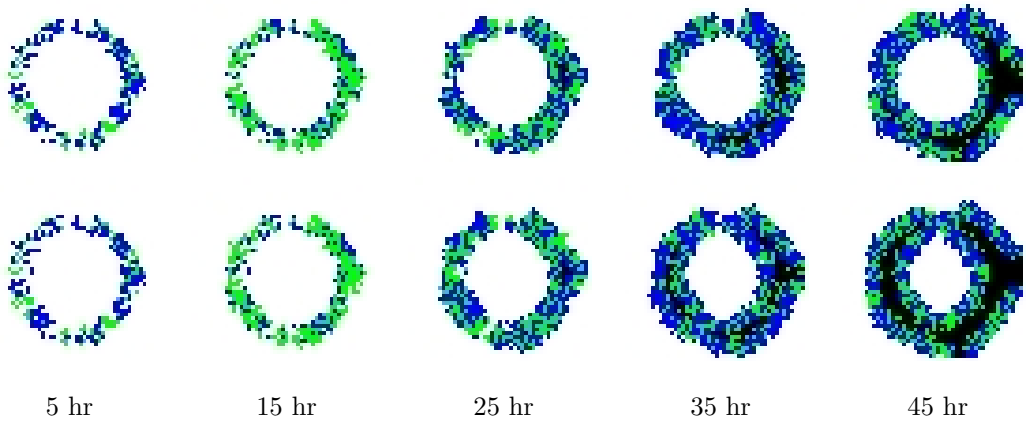

Figure 5.13: *Tumour snapshots for the Central Dose Regimen: With (top) and Without P450 Cycle (bottom). Blue cells represent those in G1 phase, green cells are those in S-G2-M phase and black are in the resting phase G0.*

The plots shown in figure 5.13 demonstrate what the drug level does to the tumour cells. There is similarity between the two rows for the first three snapshots but for the last two there are significant differences. The final snapshots in the bottom row show a less circular shape on the outside than the corresponding pictures in the top row. This would suggest that the cells are growing outwards as well as inwards. This is interesting as it would be easy to assume that the tumour would try to strengthen the inner core before expanding as was seen in the top row of 5.11. Although the snapshots are only 2D it may show another aspect of tumour cell regrowth when looking in 3D models.

Effect of Changing the Time of Dose

The plot showing the different drug curves for the changes in time of dosing is in figure 5.14.

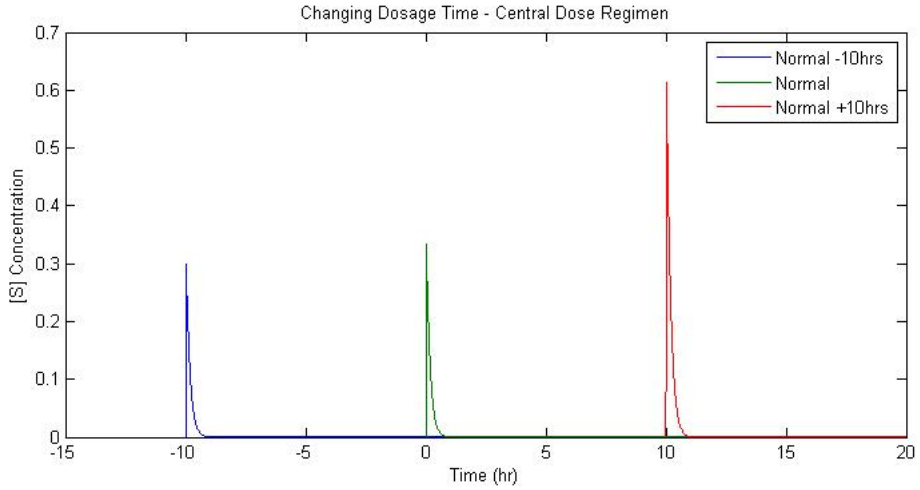

Figure 5.14: *Plots of average drug concentration over time with three different times of dose application.*

The curve for '+10 hrs' curve is much higher than '+0 hrs' but this difference is much larger than the distance between '-10 hrs' and '+0 hrs'.

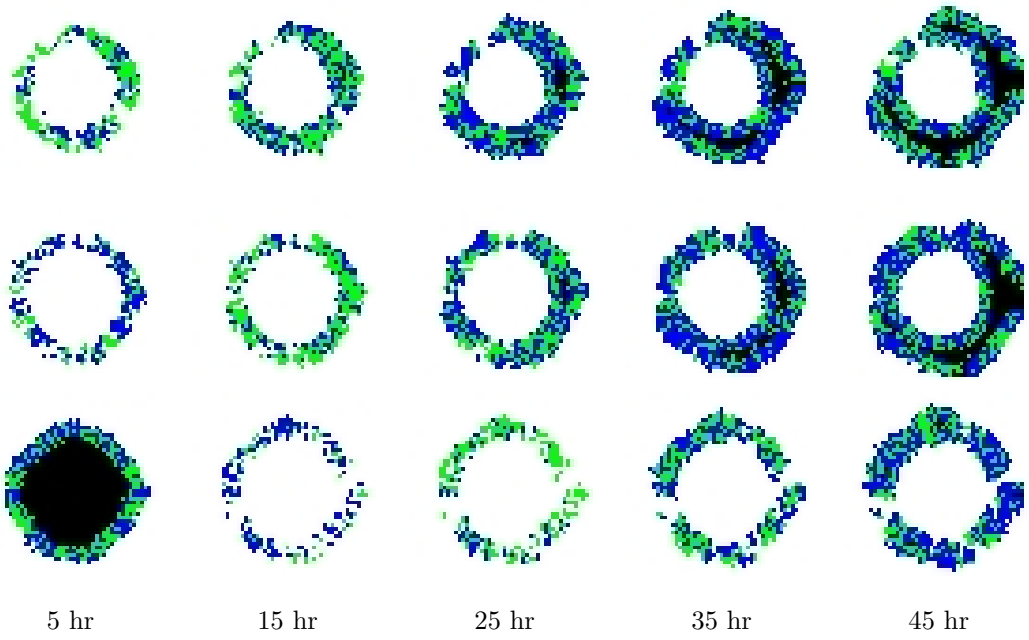

Figure 5.15: *Plots showing the effect on the growing tumour of changing the time of dosage: -10 hours (top), +0 hours (middle) and +10 hours (bottom). Blue cells represent those in G1 phase, green cells are those in S-G2-M phase and black are in the resting phase G0.*

The snapshots of the cell grid are shown in figure 5.15 and the three rows have similar pictures but shifted horizontally since the dosing time is different for each row. This is similar to the side dose time change shown in section 5.3.3 but there is a difference in the shape of the tumours due to the location of the drug dose. In the top line there is a higher proportion of G0 cells in the final snapshot and although there are these cell types in the other two lines it is not as pronounced. It was expected that if the tumour had more time to grow in the absence of drug it would cause the size to be bigger. This does not seem to be the case with the central dose since the tumour seems to be fragmented in the final line but no larger. This could be due to the peak level in the drug concentration being greater for the later dose times and as such the cells are killed more effectively.

5.3.5 Application of the Drug via a Constant Dose Released from the Boundary

The uptake curve for the drug in the case of constant dose released from the boundary is shown in figure 5.16.

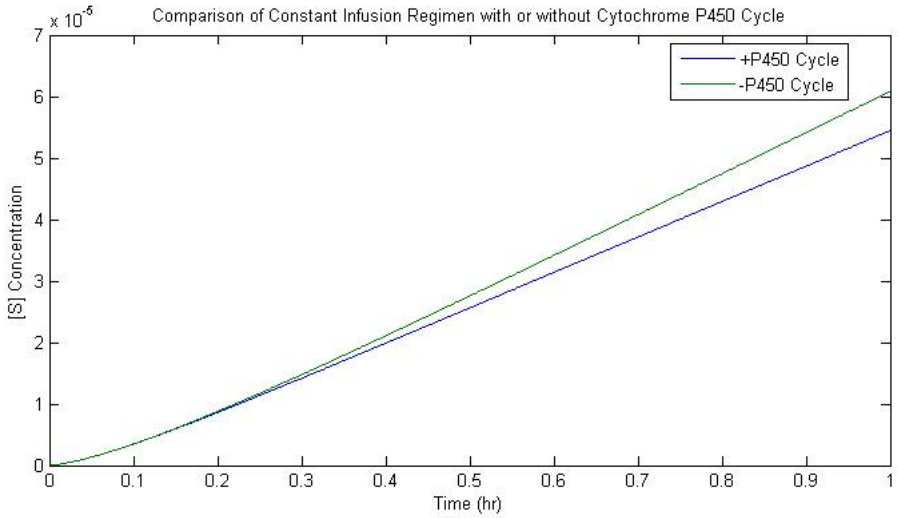

Figure 5.16: *Plots showing average drug uptake With and Without P450 Cycle in the case of a constant dose released from the boundary.*

The graph has the same time axis as the other two dosing regimes in order to aid in comparison between them. This curve is different to the plots for the other dosing regimens shown in figures 5.8 and 5.12 since the drug level continues to increase over the entire fifty hour stretch of code time (one hour = 1000 time steps).

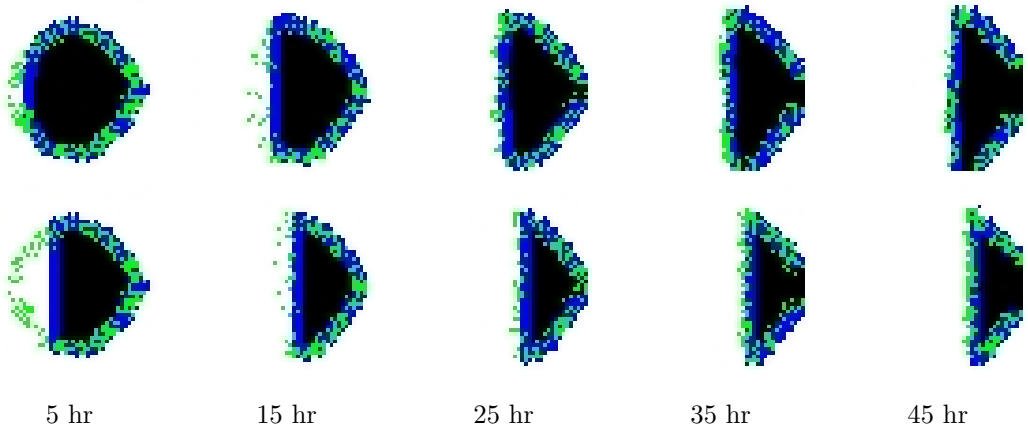

Figure 5.17: *Tumour snapshots for the Constant Side Infusion Regimen: With (top) and Without (bottom) P450 Cycle. Blue cells represent those in G1 phase, green cells are those in S-G2-M phase and black are in the resting phase G0.*

The plots of the growing tumour are shown in figure 5.17 and it is easy to see the effect of the P450 cycle on the tumour. As with the previous simulations the CYP cycle causes the drug level to be lower over time and as such the tumours tend to be bigger. For the two rows the drug interaction with the tumour cells is one of annihilation, which has resulted in half moon shaped tumours especially in the bottom row. This suggests that the tumour cells do not have the ability to regrow due to the constant pressure of the program‘s kill command.

5.3.6 Effect of Changing the Oxygen Level

Three different oxygen levels were used - 0.3333, 0.6667 and 1 in order to investigate the impact of the oxygenation on the P450 cycle. The product concentration curve was used for the three levels since the drug level for each showed no change and these curves are shown in figure 5.18. The snapshots in figure 5.19 show the different effects on the tumour cells.

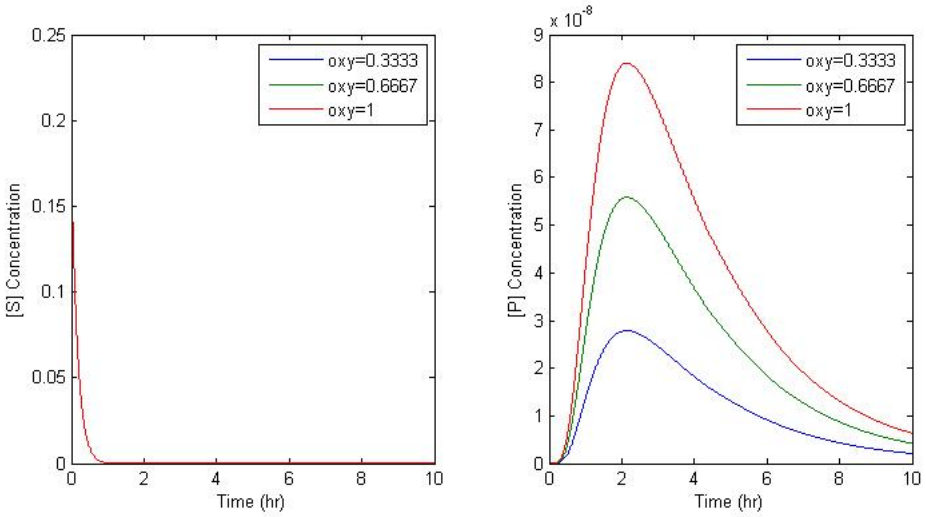

Figure 5.18: *Plot showing the effect of oxygen level change on the average drug and product concentration.*

The curves show that even though the change in oxygen level across the grid has little to no effect on the drug ([S]) level it has an effect on the product ([P]). The effect on the product is due to a knock-on effect from the FSO2 level in the cell - the higher oxygen level causes more product to be produced.

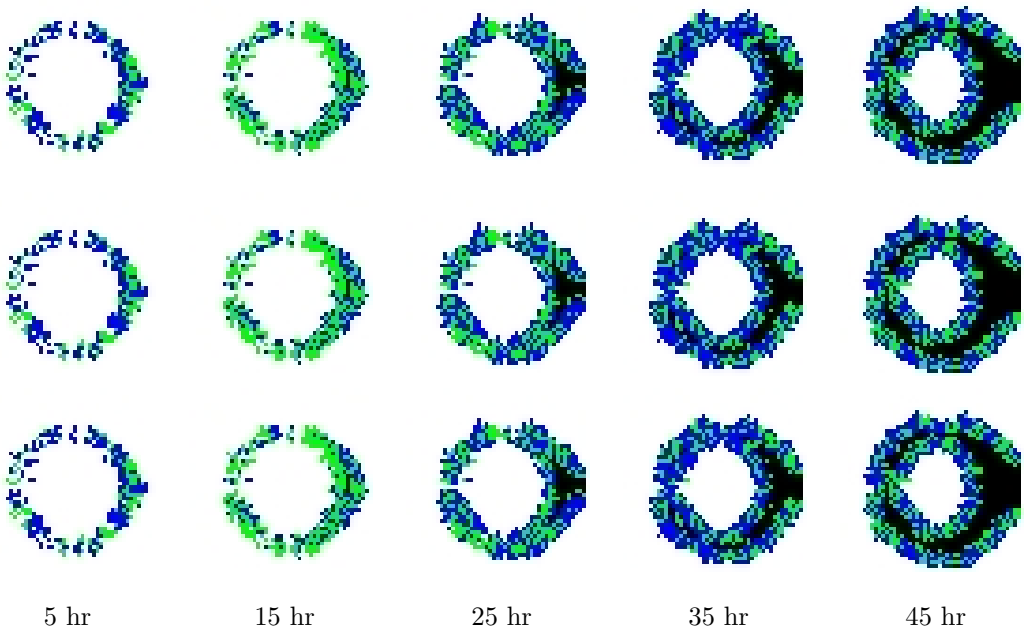

Figure 5.19: *Plots showing the effect on the growing tumour of changing the time of dosage: oxy=0.3333 (top), oxy=0.6667 (middle) and oxy=1 (bottom). Blue cells represent those in G1 phase, green cells are those in S-G2-M phase and black are in the resting phase G0.*

The snapshots show very little variation between the rows and this is due to the drug level not being dependent on the oxygen level change as shown in figure 5.18. Since the killing of cells is dependent on the drug level being above the active threshold the only randomness comes from the probability of death (p=0.8) and this has caused the variation seen in the snapshots.

5.3.7 Extended Cytochrome P450 Model for Drug Metabolism

Since the drug level in the program seemed to dissipate quite quickly (one hour) an attempt to add a delay to the Cytochrome P450 cycle was made.

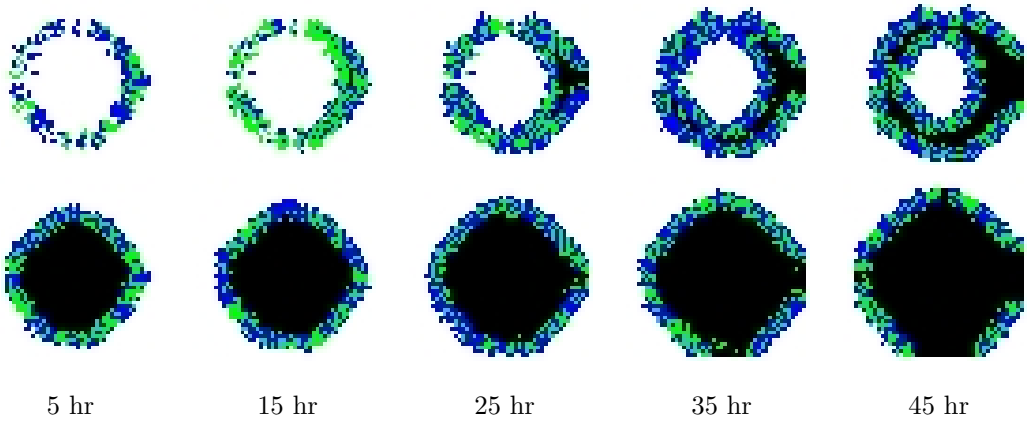

Figure 5.20: *Tumour snapshots comparing CYP cycle (top) and CYP model (bottom). Blue cells represent those in G1 phase, green cells are those in S-G2-M phase and black are in the resting phase G0.*

Due to the bottom row of the tumour snapshots showing little or no drug induced cell death it shows that the drug level must not rise above the active threshold for very long.

5.4 Discussion

This chapter has presented a multiscale mathematical model of solid tumour growth. It combined a cellular automaton model for the growing tumour cells with ordinary differential equations governing internal concentrations of proteins, the cell cycle and the P450 enzymatic cycle. Each individual automaton cell represented a single tumour cell. The effect of treating the tumour with a drug was considered and was allowed to diffuse across the spatial domain in different ways. The curves shown in this chapter are averages across grid curve rather than on a particular grid square. It would be useful to know what happens on each grid square but it is computationally demanding.

The changes in the Drug diffusion coefficient and the decay showed results, which are related to the diffusion length. This means that as d increases or λ decreases the length of diffusion extends by a factor of $\sqrt{2}$ meaning more cells across the

tumour are killed by the program.

The different regimens have shown a number of aspects of the model's applicability. The side and central dosing regimes results differ due to proximity of tumour tissue to the dose squares. The central dose is more efficient at killing the cells in the centre of the grid, which is understandable due to its definition. Other than this difference there is a change in drug level since when the drug is on a grid square where a cell is present the P450 cycle acts and temporarily heightens the drug level. However this is short lived as the P450 cycle causes the drug to be lower than without the cycle.

The constant side infusion works well to kill the tumour but is not feasible since it is not possible to set up in real life. In real life chemotherapy the dosing strategy tries to limit the amount of systemic damage caused by the cytotoxic drugs. This is done by locating the tumour and injecting as close as possible, which would be analogous to the central dose if close and the side dose if the drug has to diffuse towards the tumour.

The oxygen level affects the tumour‘s growth in two different ways through the cell cycle where nutrient levels affect protein and the P450 cycle in the step described by equation 1.3. In the cell cycle this is controlled by the variation in the μ parameter which can be affected by lack of space within the tumour this is what can cause the generation of the necrotic core. The oxygen component in the P450 cycle affects the product level but not the drug itself since the reaction it is involved in is later on in the cycle. This means that if the program was used for a prodrug where the [P] level is important the oxygen level would play a larger role in determining efficacy.

The drug curves unfortunately are very short in duration for this system, which is not useful since only a few drugs have a short half life in the human body. The half life of the curve being about 20-30 minutes is comparable to drugs like

Cisplatin (Zahra et al., 2008).

In order to fix the brevity of the drug concentration the Cytochrome P450 model was proposed as a way of delaying the transport of the drug through the tumour. The Cytochrome P450 model is a useful application since it delays the drug level change but the parameters and dose level need adjusting since it does not rise high enough to kill many tumour cells. It is possible that the model needs a different parameter set or more complexity in order to delay the drug elimination.

The drug diffusion, dose and decay are currently arbitrary and therefore not related to any drug in particular. It is intended to make this more realistic by relating these parameters to known properties of actual drugs using half lives obtained through *in vitro* and *in vivo* diffusion experiments. Diffusion coefficients are related to both the size of the molecule and the functional groups. It is difficult to estimate this coefficient since these two properties vary between chemicals. Diffusion experiments with agar are difficult to compare with different tissue media. Functional group specificity can cause issues in prediction since it can mean the drug reacts in the wrong part of the organism.

The tumour snapshots shown within this chapter have confirmed that a rotation of Moore and von Neumann algorithms for neighbourhood searching gave a rounder tumour. The only pictures that seem to refute this are when the tumour has grown large enough to meet the sides of the grid giving a diamond shaped tumour (e.g. Figure 5.5).

This program is applicable to other areas other than the one stated here. For example any area that deals with interactions between tissue media and drugs like in toxicology and drug studies.

The cell cycle inside the code deals with tumour cells but this code can be reparametised to concentrate on other types of cell including normal cells, hepatic tissue etc.

Instead of a mammalian cell structure it could be a yeast cell or a xylem cell in order to investigate growing structures in the plant kingdom as well as the animal. As such it could be used as part of a multi-system approach to drug metabolism if the action of the drug is roughly known.

Other enzymatic systems can be used instead of or as well as Cytochrome P450 e.g. UDP glycosyltransferases (UGTs). This would allow for greater flexibility in substrate use as many drugs use multiple enzyme systems for their metabolism.

Chapter 6

Mathematical Modelling of a Drug Uptake in a Single Cell

In the previous chapters the temporal and spatial effects of the Cytochrome P450 (CYP) enzymes have been investigated and the current chapter focuses on the effect of the cycle on the cellular level. As such it is the size of one point from the 51 by 51 grid. As mentioned in chapter 1 the CYP enzyme system is located in the smooth endoplasmic reticulum (SER) (Tsui, 2003). A diagram of a eukaryotic cell is shown in figure 6.1 and shows the location of the SER.

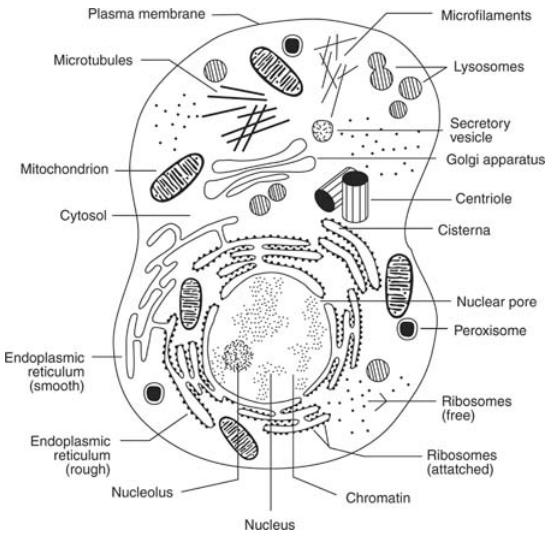

Figure 6.1: *Schematic diagram of a eukaryotic cell (CliffNotes.com, 2011).*

Using COMSOL to model the CYP enzyme system on the cellular level a basic cell of size 40 μm in diameter was set up as shown in figure 6.2. Using a very basic cell allows for a better inspection of the cellular level of the enzymatic cycles effect on drug metabolism since it allows for added complexity to be included in the enzyme equations. The formulation was solved using Finite-Element Method on triangles that have been drawn in order to form a fine mesh across the basic cell setup.

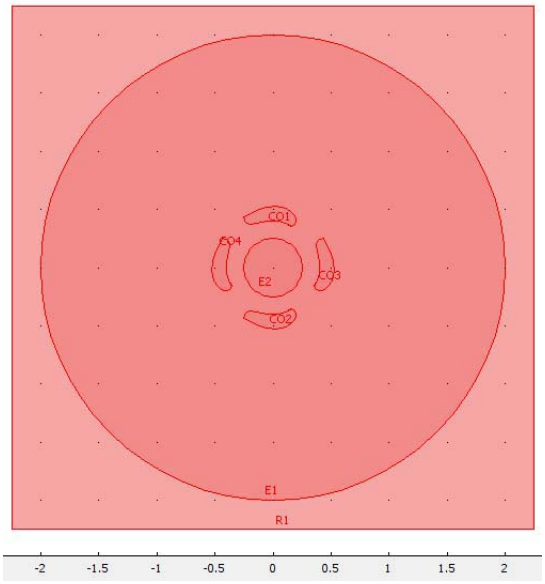

Figure 6.2: *Plot showing the "mathematical cell" used in the simulations - the figure shows the different compartments considered i.e. the exterior of the cell, the cytoplasm, the smooth endoplasmic reticulum and the nucleus.*

Region 1 (R1) represents a drug reservoir that has zero-flux conditions on the external boundaries whereas all the internal boundaries use continuation of flow principles. The drug, [S], diffuses across the reservoir using the following equation:

$$\frac{\delta[S]}{\delta t} = D\nabla^2[S] - \lambda[S]$$

The drug starts off in this section and diffuses towards the cell wall, which is represented by the boundary of E1 (cytoplasm). All of the objects within this boundary have the same diffusion equation with a diffusion coefficient of E instead of D, which is set to a tenth of the value. This is due to the fact that within the cell wall the medium is denser than the outside.

The four kidney shaped objects encircling the nucleus represent the smooth endoplasmic reticulum (CO1 to CO4 in figure 6.2) and as such this is where the P450 cycle equations will be in effect. As has been outlined before the P450 cycle equations are:

$$\frac{d[E]}{dt} = k_{-1}[ES] + k_7[EP] + k_8[GSO2] + k_9[HSO] - (k_1 + k_{-7})[E] \tag{6.1}$$

$$\frac{d[S]}{dt} = k_{-1}[ES] + k_8[GSO2] + k_9[HSO] - k_1[S] \tag{6.2}$$

$$\frac{d[ES]}{dt} = k_1[E][S] - (k_{-1} + k_2)[ES] \tag{6.3}$$

$$\frac{d[FS]}{dt} = k_2[ES] + k_{-3}[FSO2] - k_3[FS] \tag{6.4}$$

$$\frac{d[FSO2]}{dt} = k_3[FS][O2] - (k_{-3} + k_4)[FSO2] \tag{6.5}$$

$$\frac{d[GSO2]}{dt} = k_4[FSO2] - (k_5 + k_8)[GSO2] \tag{6.6}$$

$$\frac{d[HSO]}{dt} = k_5[GSO2] - (k_6 + k_9)[HSO] \tag{6.7}$$

$$\frac{d[EP]}{dt} = k_6[HSO] + k_{-7}[E][P] - k_7[EP] \tag{6.8}$$

$$\frac{d[P]}{dt} = k_7[EP] - k_{-7}[P] \tag{6.9}$$

The only other object in the basic COMSOL cell is the nucleus (E2) and since some drugs on the market attack this part of the cell it would be interesting to see how drug level in this area is affected. The parameters for the P450 cycle and the initial conditions are outlined in the following table:

CYP Parameter	**Value** min^{-1}	**CYP Parameter**	**Value** min^{-1}
k_1, k_{-3}, k_7	$\frac{360000}{60*51^2} = 2.306805$	k_{-1}	$\frac{7200000}{60*51^2} = 46.136101$
k_2, k_4	$\frac{42000}{60*51^2} = 0.269127$	k_3	$\frac{360}{60*51^2} = 0.002307$
k_5	$\frac{6600}{60*51^2} = 0.042291$	k_6	$\frac{1980}{60*51^2} = 0.012687$
k_{-7}	$\frac{39600}{60*51^2} = 0.253749$	k_8, k_9	$\frac{3000}{60*51^2} = 0.019223$
Spatial Parameter	**Value**	**Spatial Parameter**	**Value**
$[S]_0$ in R1	5	$[E]_0$,$[ES]_0$	3
λ	0.009	D	2.5

Table 6.1: *Parameters and initial conditions.*

From table 6.1 it is visible that the parameters associated with the CYP cycle

are much smaller than those cited in table 5.3. This is due to a reduction in value since the equations are reference a single grid point rather than a whole grid so each parameter is divided by the grid size.

6.1 Results

In figure 6.3 the pictures show a flow of drug into the cytoplasm across the cell wall and toward the nucleus.

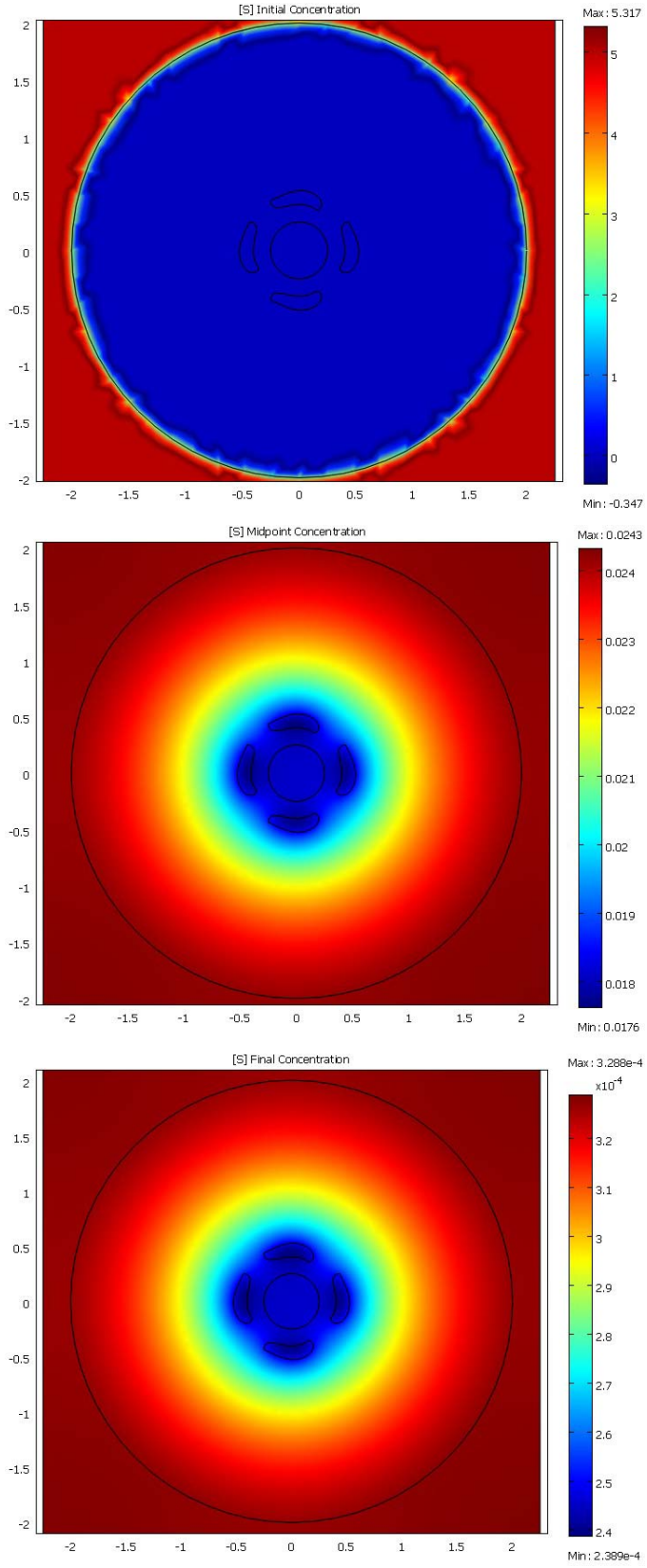

Figure 6.3: *Plots showing the concentration of drug in the cell at times t = 0 (top), t = 3 (middle) and t=6 (bottom).*

For the set of surfaces shown in figure 6.5 the images represent the initial and final levels of the drug [S]. The surface plot in figure 6.4 shows the initial Enzyme [E] level.

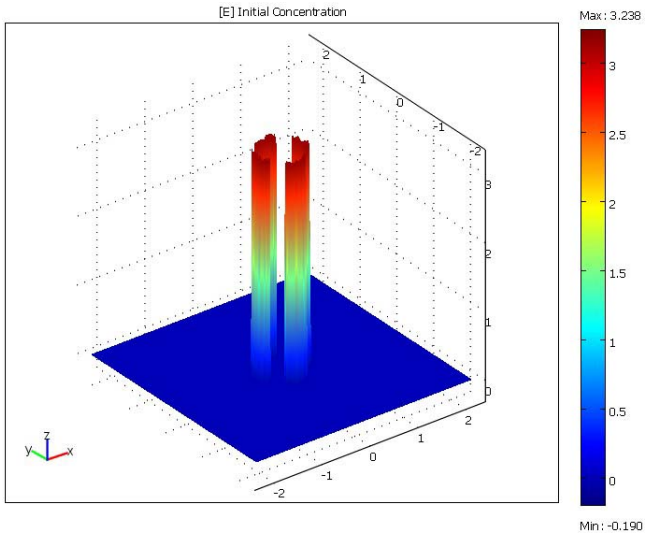

Figure 6.4: *Plots showing the initial concentration profile of enzyme [E].*

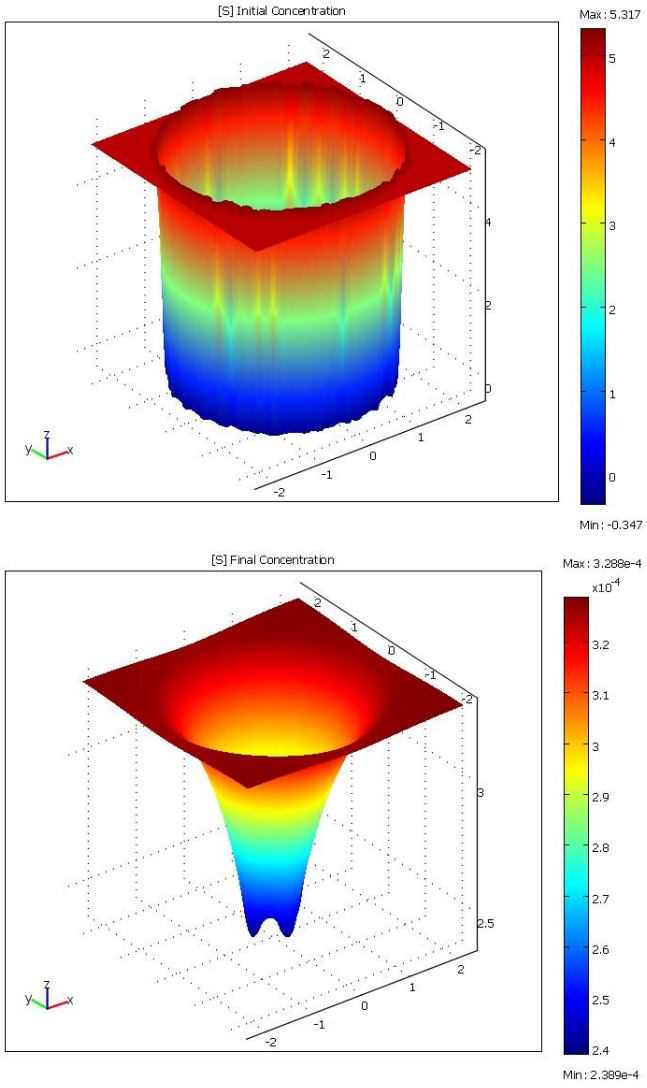

Figure 6.5: *Plots showing the initial concentration profile of drug [S] (top) and final concentration profile of drug [S] (bottom).*

The final drug surface shows a bucket shape, which is understandable as the drug is stored outside the cell and it is gradually diffusing into the cell where it is metabolised in the SER causing the curved sides.

As well as the surfaces it is also of interest to look at integrated solutions across the domains i.e. the Nucleus (figure 6.7), Cytoplasm (figure 6.6) and the Smooth Endoplasmic Reticulum (SER) (figures 6.8 to 6.16). These can give a better idea of the drug level curve in each internal cell structure and the effect of the CYP

cycle in the SER.

Drug level (S) in the cytoplasm is shown in figure 6.6.

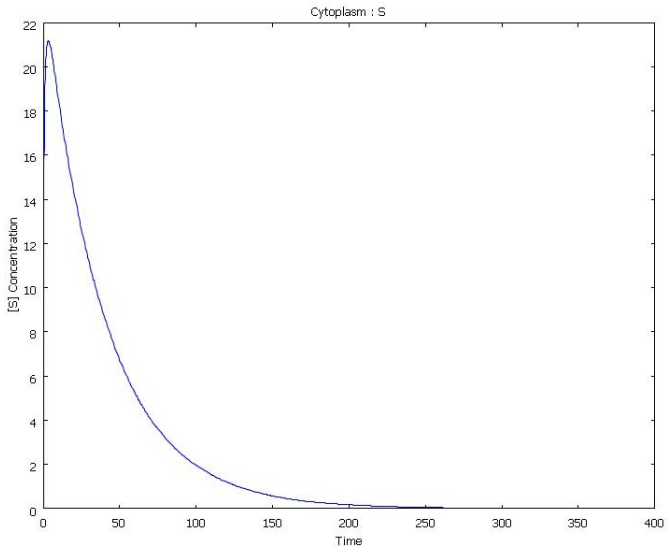

Figure 6.6: *Plot showing the drug uptake curve over time in the Cytoplasm.*

This figure shows that the peak in drug for this area of the cell occurs just before the one-hour point. The shape of the uptake curve shows an absorption period, which represents the time taken to get from the outside region across the cell wall and into the cytoplasm.

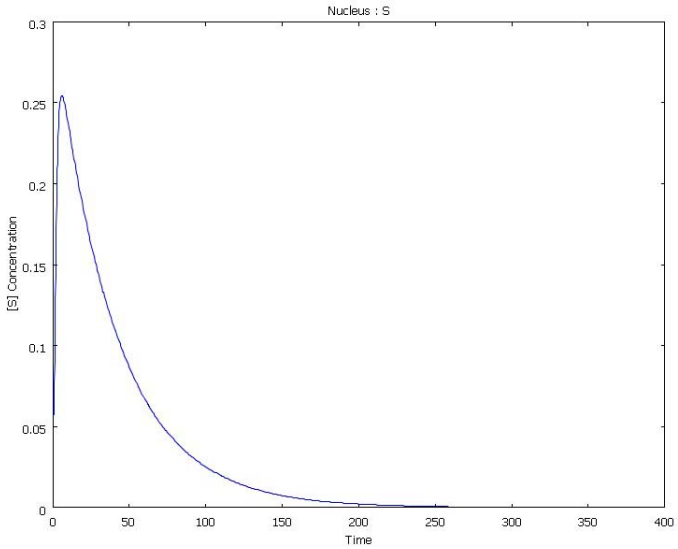

Figure 6.7: *Plot showing the drug uptake curve over time in the Nucleus.*

The nucleus plot shows a early peak, which could suggest pulses of substrate moving through the cell. The initial peak represents the drug that has made it through the gap in between the SER modules.
In the SER the P450 cycle is in action so the following integration plots refer to this structure within the cell.

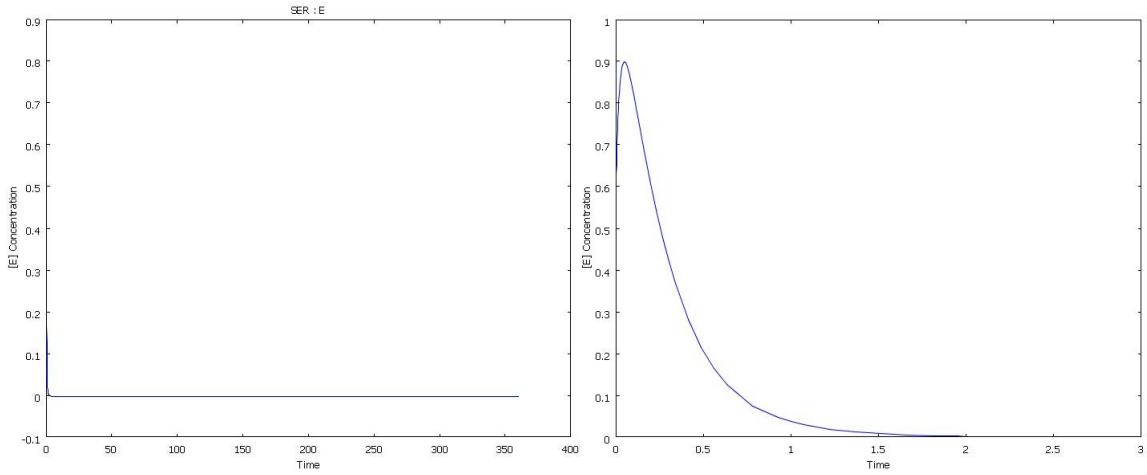

Figure 6.8: *Plot showing the enzyme level over entire time in the Smooth Endoplasmic Reticulum (left) and the enzyme level for the first burst (right).*

The enzyme level drops very quickly in the cell and does not recover within the time period. The only other dynamic affecting the drug is through the decay rate in the diffusion equation.

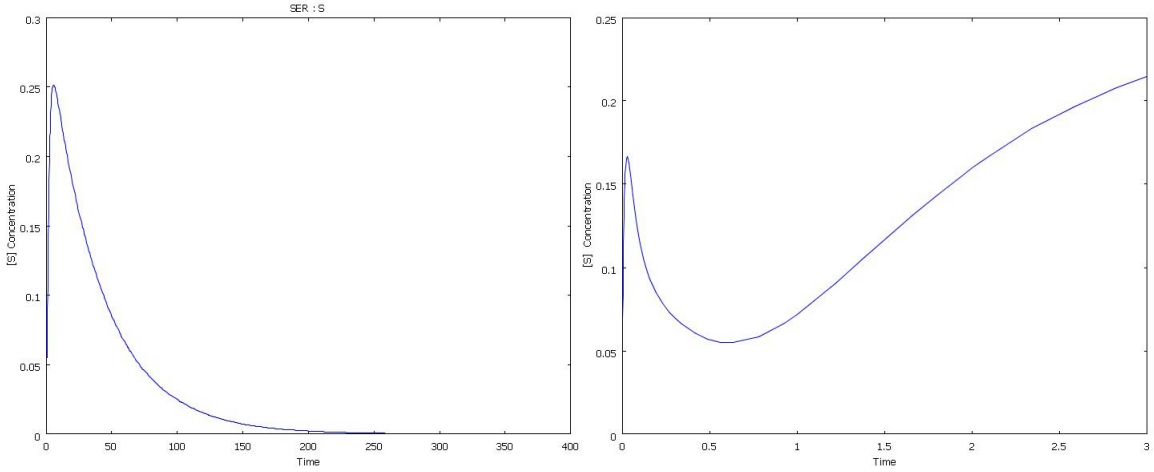

Figure 6.9: *Plot showing the drug uptake curve over time in the Smooth Endoplasmic Reticulum (left) and the drug uptake during the first enzyme burst (right).*

During the first enzyme burst the drug shows an absorption period followed by elimination/complex creation. After this time the drug level shows a levelling until the enzyme can return to a high enough level for more metabolism.

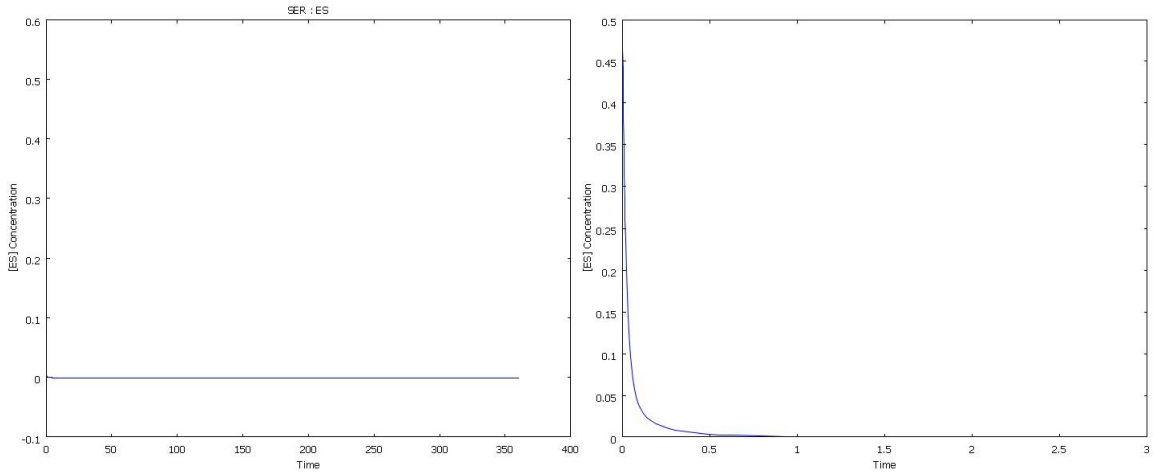

Figure 6.10: *Plot showing the enzyme-drug complex ES with Iron (III) core over time in the Smooth Endoplasmic Reticulum (left) and the ES level during the first enzyme burst (right).*

The ES level drops from its initial value very quickly during the enzyme burst never recovering. This is due to an irreversible transition from ES to FS in the model equations. This means that the only process by which the complex can be

made is if the enzyme and drug level are high enough to produce it. As the enzyme level is recovering by the end of the time it is quite likely that this complex will too.

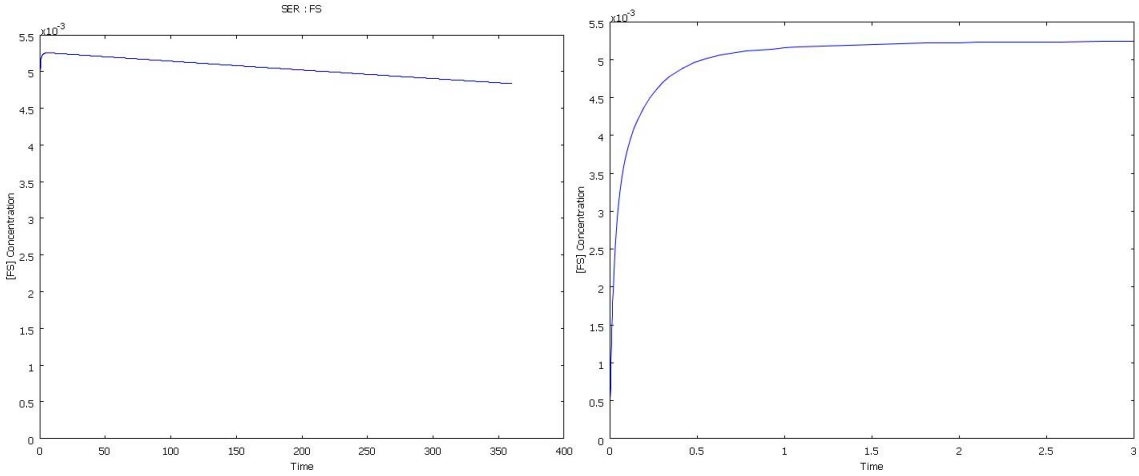

Figure 6.11: *Plot showing the enzyme-drug complex FS with Iron (II) core over time in the Smooth Endoplasmic Reticulum (left) and the FS level during the first enzyme burst (right).*

The FS level peaks during the first enzyme burst and then steadily drops through reversible oxygenation to FSO2.

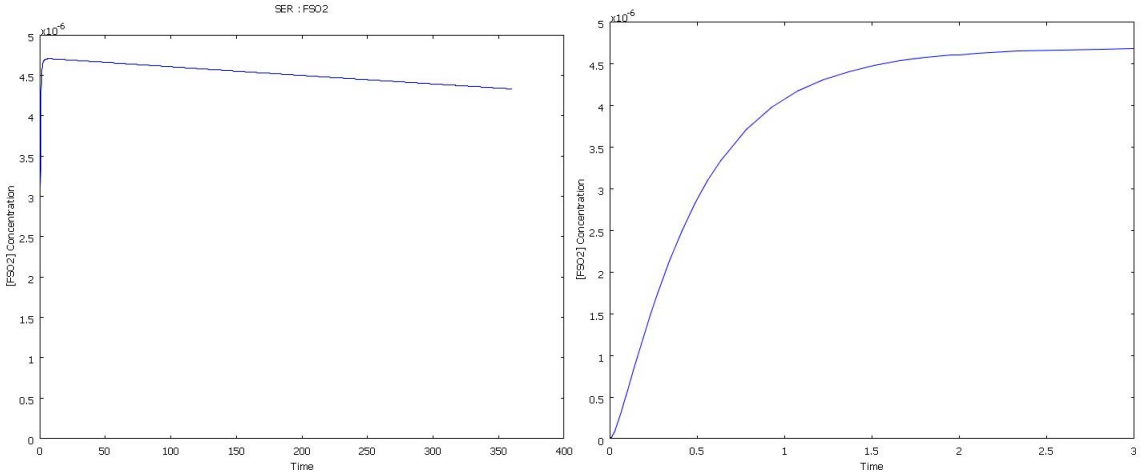

Figure 6.12: *Plot showing the oxygenated enzyme-drug complex, FSO2, with Iron (II) core over time in the Smooth Endoplasmic Reticulum (left) and the FSO2 level during the first enzyme burst (right).*

As with the ES level the FSO2 level drops off during the first enzyme burst but never recovers due to irreversible creation of GSO2.

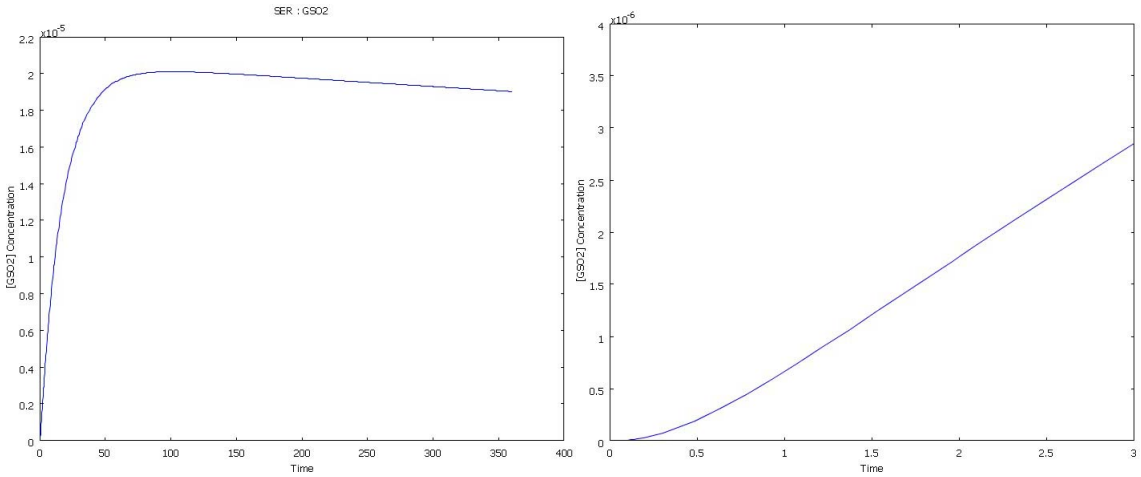

Figure 6.13: *Plot showing the oxygenated enzyme-drug complex, GSO2, with Iron (III) core over time in the Smooth Endoplasmic Reticulum (left) and the GSO2 level during the first enzyme burst (right).*

Although the GSO2 level is fairly constant during the first enzyme burst it is eliminated by the two-hour point through creation of HSO or breaking down into the enzyme and drug with by-products.

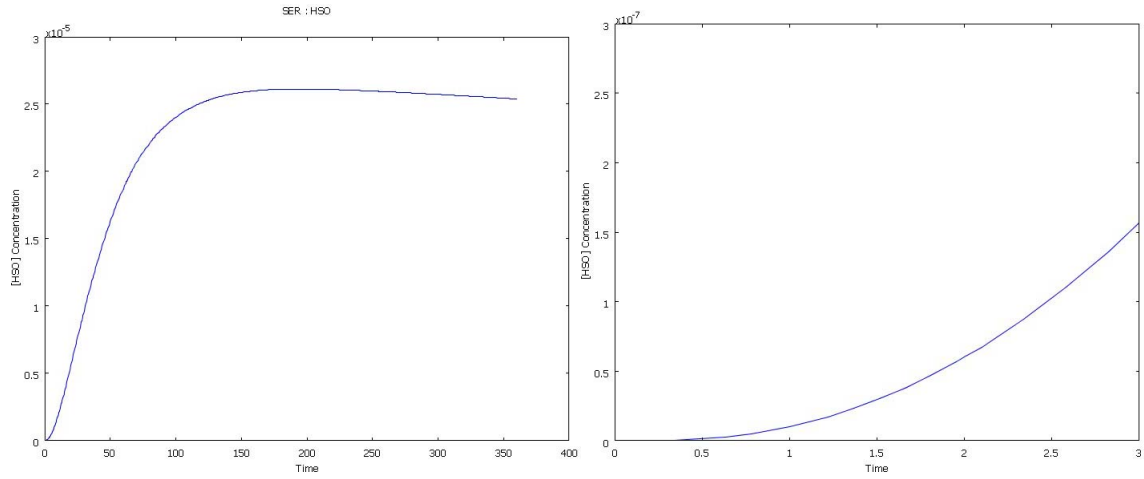

Figure 6.14: *Plot showing the oxygenated enzyme-drug complex after the loss of water, HSO, with Iron (III) core over time in the Smooth Endoplasmic Reticulum (left) and the HSO level during the first enzyme burst (right).*

The HSO level drops off by the 3 hour point but unlike the GSO2 plots this complex shows a creation phase from the GSO2 to HSO reaction in equation 1.6. This also shows elimination due to the transfer to the enzyme-product complex or breaking down into enzyme and drug with by-products through equation 1.7.

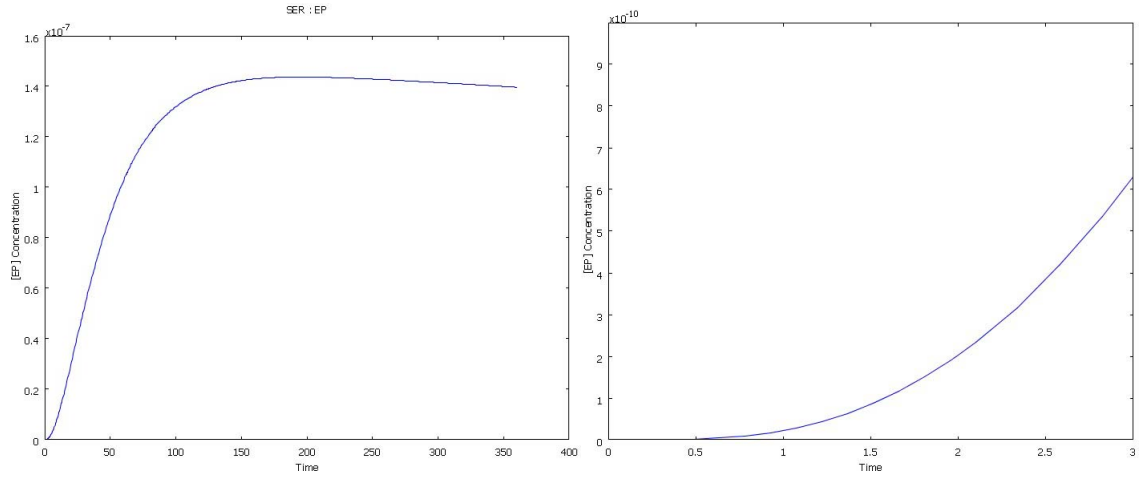

Figure 6.15: *Plot showing the Enzyme-Product complex, EP, over time in the Smooth Endoplasmic Reticulum (left) and the EP level during the first enzyme burst (right).*

The initial EP levels drop during the first enzyme burst and shows no recovery

during the time period. This is due to the need for enzyme to be present for its creation in equation 1.9.

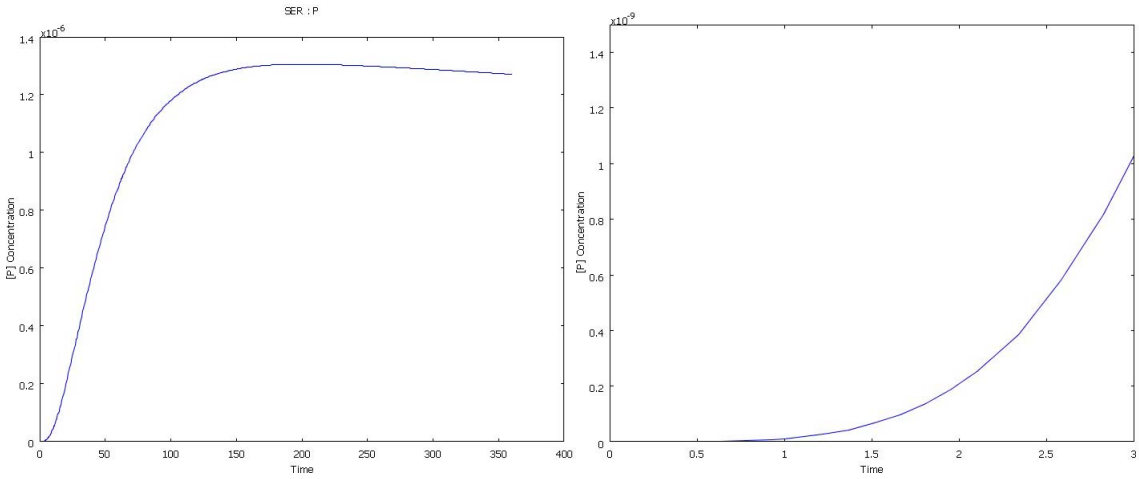

Figure 6.16: *Plot showing the Product level curve over time in the Smooth Endoplasmic Reticulum (left) and the Product level during the first enzyme burst (right).*

This plot shows that the Product is created at the same time as the first enzyme burst but after a very short period the level drops. This is due to the level being decayed by the creation rate of the enzyme-product complex since this is a reversible equilibrium.

6.2 Discussion

In this chapter we have considered a model of a drug diffusing into a single cell where it is acted upon by the P450 cycle that allows for more realism to be included. The drug was successfully diffused across the cell wall boundary and then proceeded to be either metabolised within the Smooth Endoplasmic Reticulum or built up in the Nucleus.

At the end of the simulation the shape of the cell was like a bucket since the lowest drug level was in the SER and highest in the drug reservoir around the cell. The associated integration curve showed an absorption period, which represents

the time taken to get from the outside region across the cell wall and into the cytoplasm.

During the only enzyme peak the drug shows an absorption period followed by elimination/complex creation. After this time the drug level shows a levelling until the enzyme can return to a high enough level for more metabolism.

Both the enzyme and enzyme-drug complex level show a very quick drop in level within the first hour of simulation and shows no recovery during the time period. The ES complex level reduction is due to irreversible transition to the FS that peaks at the same time as the ES dips. The FS is then steadily oxygenated into FSO2, which in turn is irreversibly changed to GSO2.

Both the GSO2 and HSO level are eliminated within the SER due to breaking down into by-products and enzyme-product complex creation in the HSO case. This plot shows that the Product is created at the same time as the first enzyme burst but after a very short period the level drops. This is due to the level being decayed by the creation rate of the enzyme-product complex since this is a reversible equilibrium.

This simulation has shown how spatial effects need to be included in order to become more realistic. The other point of this simulation was to look at the dynamics at a finer scale and it seems that the dynamics are similar to the cellular automata in so far as the drug level within the SER drops very quickly. The drug level is accumulated in the nucleus and if there was a killing protocol within the COMSOL program the cell would be dead very early on as the peak is 0.25 which is much greater than the cellular automata‘s 0.00001 active threshold.

Chapter 7

Conclusions and Further Work

7.1 Aims

The main aim of this thesis was to investigate Cytochrome P450 enzymes and their effect on drug metabolism.

Initially this was through the use of the Hepatic Reductase Null (HRN) mice in comparison to their wild type counterparts shown in Chapter 3. This was done through using a number of different compartmental models and compared with drug data provided by CXR Biosciences. The main focus of this modelling was whether there were metabolic differences that were produced as a side effect of genetic mutation in the transgenic mouse. A three compartment model was developed through adding time dependent excretion and a compartment that represented the fat cells in the liver that may change the dynamics of lipophilic drugs.

After this solely deterministic approach in conjunction with experimental data a cellular automaton was then developed in Chapter 5 to analyse how the Cytochrome P450 enzymes affect drug metabolism in general. The results were not compared to the data used in Chapter 3 as the aim was to get an indication of how the CYP enzymes would affect drug dynamics in a tumour.

In Chapter 6 a COMSOL simulation was performed on a singular cell to see whether spatial effects such as the fact that P450 enzymes are mostly found in Smooth Endoplasmic Reticulum on the cellular level would affect the drug dynamics.

7.2 Compartment Models

The compartment models developed in chapter 3 show the variability in drug metabolism between the wild type and transgenic (HRN) mouse. The problem with fitting the compartment models to these sets of data is generated by experimental constraints. It would be easier if more data were available instead of just three mice of each type for each drug. This would mean that the average would be statistically more representative which would aid in providing a better fit.
Other than the number of mice it would be useful if more samples could be taken or at least they could be more regular. However this is unfeasible since the volume of blood in a mouse is finite and takes a while to replenish. It is due to these constraints that sampling is prioritised within the first hour after the dose. For some of the drugs shown in this chapter earlier sampling is needed in order to record concentrations during fast processes such as absorption e.g. Caffeine.
A table summarising the success in fitting the models to the CXR Bioscience data:

Drug	Wild Type	Hepatic Reductase Null
Caffeine, Dextromethorphan	1	2
Tamoxifen	2	2
Thalidomide	2	3
Gefitinib, Omeprazole Paclitaxel	3	2
Diclofenac, Imatinib Midazolam	3	3

Table 7.1: *Summary of Compartmental Models chosen for each CXR Bioscience Experiment.*

Since all three models developed were fitted using the non-linear least squares in R the results are comparable. From the table above it is visible that all three models were used to fit the wild type mice whereas just models 2 and 3 were used for the transgenic mouse.

This area of modelling is useful since the curves generated are able to mimic real life. The only drawback to the work shown in Chapter 3 was that even though the models emulated some of the drug behaviour but sometimes more complexity was needed in order to fully explain the mechanism of action in the wild type and HRN mice. If it was possible to fully explain the action of the drug for both types of mouse it would be easier to show the specific metabolic differences between the transgenic and wild type. From the work presented it can be seen that the HRN mouse has a slower metabolism than the wild type and with respect to the Tamoxifen models the liver is physiologically different.

7.3 Sensitivity Analysis

The sensitivity analysis for the models shown in Chapter 4 was useful to see which are the powerful parameters for each system in order to check for robustness to errors in estimation. The analysis from this method is less clear as the models get more complex. For example model 1 only has one parameter so it is very clear

that this affects the model more than anything else whereas for the Cytochrome P450 cycle and model this is very unclear. In these two models the parameters affecting one variable are carried over to other connected variables.

The techniques for finding the sensitive parameters outlined in this chapter are easily applied and return good results so long as the model is simple enough. It is possible that the difference taken of 10% in the parameters is too small to gain insight into the larger models. When the magnitude test was unclear it was useful to have the extended sensitivity analysis plots or ranges to illuminate the power of each parameter this was particularly useful for the larger models.

7.4 Multiscale Cellular Automaton

In chapter 5 a multiscale model was developed that models a growing solid tumour that combines the cell cycle, the Cytochrome P450 enzymatic cycle with drug diffusion. The model incorporates spatial and deterministic models allowing for a more realistic approach to death through drug level and growth of cancer cells. As such it is possible to analyse dosing strategy whether it be level or location.

The different regimens have shown a number of aspects of the model's applicability. The side and central dosing regimes results differ due to proximity of tumour tissue to the dose squares. The constant side infusion works well to kill the tumour but is not feasible since it is not possible to set up in real life. In real life chemotherapy the dosing strategy tries to limit the amount of systemic damage caused by the cytotoxic drugs. This is done by locating the tumour and injecting as close as possible, which would be analogous to the central dose if close and the side dose if the drug has to diffuse towards the tumour.

The oxygen level affects both the cell and P450 cycle, which in turn affects tumour

growth. In the cell cycle this is controlled by the variation in the μ parameter which can be affected by lack of space within the tumour this is what can cause the generation of the necrotic core. The oxygen component in the P450 cycle affects the product level but not the drug itself. This means that if the program was used for a prodrug where the [P] level is important the oxygen level would also matter.

The Cytochrome P450 model is a useful application since it delays the drug level change but the parameters need adjusting since it does not rise high enough to kill many tumour cells.

The drug diffusion, dose and decay are currently arbitrary and therefore not related to any drug in particular. It is intended to make this more realistic by relating these parameters to known properties of actual drugs using half lives obtained through *in vitro* and *in vivo* diffusion experiments. Diffusion coefficients are related to both the size of the molecule and the functional groups. It is difficult to estimate this coefficient since these two properties vary between chemicals. Diffusion experiments with agar are difficult to compare with different tissue media. Functional group specificity can cause issues in prediction since it can mean the drug reacts in the wrong part of the organism.

This program is applicable to other areas other than the one stated here. For example any area that deals with interactions between tissue media and drugs like in toxicology and drug studies. The cell cycle inside the code deals with tumour cells but this code can be re-parameterised to concentrate on other types of cell including normal cells, hepatic tissue etc.

As such it could be used as part of a multi-system approach to drug metabolism if the action of the drug is roughly known. Other enzymatic systems can be used instead of or as well as CYP e.g. UDP glycosyltransferases (UGTs). This would allow for greater flexibility in substrate use as many drugs use multiple enzyme

systems for their metabolism.

7.5 Drug Uptake in a Single Cell

The model of a drug diffusing into a single cell where it is acted upon by the P450 cycle created a more realistic view of the inner metabolism of a cell. The drug was successfully diffused across the cell wall boundary and then proceeded to be either metabolised within the Smooth Endoplasmic Reticulum or built up in the Nucleus.

This is interesting since it is what would be expected of a cell surrounded by a drug reservoir i.e. that the drug would diffuse in and then have to pass through the internal cell structures at a slower rate to reach the nucleus.

This simulation has shown how spatial effects need to be included in order to become more realistic. The other point of this simulation was to look at the dynamics at a finer scale and it seems that the dynamics are similar to the cellular automata in so far as the drug level within the SER drops very quickly. The drug level is accumulated in the nucleus and if there was a killing protocol within the COMSOL program the cell would be dead very early on as the peak is 0.25, which is much greater than the 0.00001 active threshold.

In the future more cell structures could be added e.g. the rough endoplasmic reticulum, the mitochondrion and Golgi apparatus. Although Cytochrome P450 enzymes have not been discovered within them it would give an idea of the time it would take to diffuse through them since the tissue media may differ within them.

The other extension to this model is that the basic cell could be of a different type e.g. hepatocyte, Kupffer or tumour cell.

7.6 Future Work

In silico modelling approaches are useful since they can minimise experimental costs and once set up can be used to replace animal testing for drugs. As such modelling techniques need to be developed to reduce dependence on animals for validation of pharmacological efficacy. The work within this thesis shows that computational methods can be used to model biological and medical problems effectively,

The compartment models were able to analyse the difference between the normal and the transgenic mouse with an impaired hepatic Cytochrome P450 system. It was possible from these models to see that metabolism of the drugs was reduced in the HRN mouse. For some of the drugs the models need improving by the addition of more compartments or the use of more physiologically based approaches. This is due to the fact that it is unclear in the current models where the area of disposition for the drug is.

The spatial models outlined in this project (Multiscale Cellular Automaton and Diffusion into a Single Cell) have added a useful dimension to this area of research. The cell cycle model included in the Cellular Automaton model is a six-component model. This could be changed to a more complex model like the 13 component model as described in Csikász-Nagy et al. (2006) or a more complex method of nutrient heterogeneity as shown in Frieboes et al. (2009). As well as the cell cycle the Cytochrome P450 cycle could be changed as it currently only relates to one strain CYP1A2. This could just mean a change in the parameter set rather than the model equations but it depends on the substrate specificity of the strain. Another way of changing the CYP dynamics is to include a mechanism for multiple strains interacting within the metabolism, which has not been included in this project.

The inclusion of spatial effects to the deterministic models like the Cytochrome

P450 cycle allows for greater realism in predictions of drug passage through the body or across certain tissue media.

Bibliography

Ahmad, A. M., 2007. Recent advances in pharmacokinetic modeling. Biopharmaceutics & Drug Disposition 28, 135–143.

Alarcon, T., Byrne, H., Maini, P., 2004. Towards whole-organ modelling of tumour growth. Progress in Biophysics & Molecular Biology 85, 451–472.

Ancheyta, J., Alcázar, L., 2007. Sensitivity analysis based methodology to estimate the best set of parameters for heterogeneous kinetic models. Chemical Engineering Journal 128, 85–93.

Ando, Y., Fuse, E., Figg, W. D., Jun 2002. Thalidomide metabolism by the cyp2c subfamily. Clinical Cancer Research 8 (6), 1964–1973.

Bak, P., 1997. How Nature Works: The Science of Self-Organized Criticality. Springer.

Bandini, S., Mauri, G., Serra, R., 2001. Cellular automata: From a theoretical parallel computational model to its application to complex systems. Parallel Computing 27, 539–553.

Baranczewski, P., Stańczak, A., Sundberg, K., Svensson, R., Wallin, A., Jansson, J., Garberg, P., Postlind, H., 2006. Introduction to in vitro estimation of metabolic stability and drug interactions of new chemical entities in drug discovery and development. Pharmacological Reports 58, 453–472.

Barbosa, V., Miranda, F., Agostini, M., 2006. Cell-centric heuristics for the classification of cellular automata. Parallel Computing 32, 44–66.

Bearer, E., Lowengrub, J., Frieboes, H., Chuang, Y., Jin, F., Wise, S., Ferrari, M., Agus, D., Cristini, V., 2009. Multiparameter computational modeling of tumor invasion. Cancer Research 69, 4493–4501.

Belle, D. J., Singh, H., Jun 2008. Genetic factors in drug metabolism. American Family Physician 77 (11), 1553–1560.

Beresford, A., Selick, H., Tarbit, M., 2002. The emerging importance of predictive adme simulation in drug discovery. Drug Discovery Today 7, 109–116.

Bort, R., Macé, K., Boobis, A., Gómez-Lechón, M. J., Pfeifer, A., Castell, J., 1999. Hepatic metabolism of diclofenac: role of human cyp in the minor oxidative pathways. Biochemical Pharmacology 58, 787–796.

Bosch, M. E., Snchez, A. J. R., Rojas, F. S., Ojeda, C. B., 2007. Analytical methodologies for the determination of omeprazole: an overview. Journal of Pharmaceutical and Biomedical Analysis 44, 831–844.

Breccia, M., Alimena, G., 2009. The metabolic consequences of imatinib mesylate: Changes on glucose, lypidic and bone metabolism. Leukemia Research 33, 871–875.

Brugnach, M., 2005. Process level sensitivity analysis for complex ecological models. Ecological Modelling 187, 99–120.

Caccia, S., Garattini, S., Pasina, L., Nobili, A., 2009. Predicting the clinical relevance of drug interactions from pre-approval studies. Drug Safety 32, 1017–1039.

Cai, H., Stoner, C., Reddy, A., Freiwald, S., Smith, D., Winters, R., Stankovic, C., Surendran, N., 2006. Evaluation of an integrated in vitro-in silico pbpk (physiologically based pharmacokinetic) model to provide estimates of human bioavailability. International Journal of Pharmaceutics 308, 133–139.

Calvetti, D., Hageman, R., Occhipinti, R., Somersalo, E., 2008. Dynamic bayesian sensitivity analysis of a myocardial metabolic model. Mathematical Biosciences 212, 1–21.

Chang, G.-C., Yu, C.-T. R., Tsai, C.-H., Tsai, J.-R., Chen, J.-C., Wu, C.-C., Wu, W.-J., Hsu, S.-L., 2008. An epidermal growth factor inhibitor, gefitinib, induces apoptosis through a p53-dependent upregulation of pro-apoptotic molecules and downregulation of anti-apoptotic molecules in human lung adenocarcinoma a549 cells. European Journal of Pharmacology 600, 37–44.

Cheng, J., Frishman, W., Aronow, W., 2009. Updates on cytochrome p450-mediated cardiovascular drug interactions. American Journal of Therapeutics 16, 155–163.

Chiu, W. A., Barton, H. A., DeWoskin, R. S., Schlosser, P., Thompson, C. M., Sonawane, B., Lipscomb, J. C., Krishnan, K., 2007. Evaluation of physiologically based pharmacokinetic models for use in risk assessment. Journal of Applied Toxicology 27, 218–237.

Choi, B.-C., Choi, J.-S., Han, H.-K., 2006. Altered pharmacokinetics of paclitaxel by the concomitant use of morin in rats. International Journal of Pharmaceutics 323, 81–85.

Clemons, M., Danson, S., Howell, A., 2002. Tamoxifen ("nolvadex"): a review. Cancer Treatment Reviews 28, 165–180.

Clewell, H., Teeguarden, J., McDonald, T., Sarangapani, R., Lawrence, G., Covington, T., Gentry, R., Shipp, A., 2002. Review and evaluation of the potential impact of age- and gender-specific pharmacokinetic differences on tissue dosimetry. Critical Reviews in Toxicology 32, 329–389.

CliffNotes.com, 2011. Prokaryote and Eukaryote Cell Structure.
URL $http : //www.cliffsnotes.com/study\_guide/topicArticleId - 8741, articleId - 8587.html$

Cozza, K., Armstrong, S., Oesterheld, J., 2003. Drug Interaction Principles for Medical Practice, 2nd Edition. American Psychiatric Publishing Inc.

Csikász-Nagy, A., Battogtokh, D., Chen, K. C., Novák, B., Tyson, J. J., 2006. Analysis of a generic model of eukaryotic cell-cycle regulation. Biophysical Journal 90, 4361–4379.

Curis, E., Nicolis, I., Bensaci, J., Deschamps, P., Bénazeth, S., 2009. Mathematical modeling in metal metabolism: overview and perspectives. Biochimie 91, 1238–1254.

de Groot, M., 2006. Designing better drugs: predicting cytochrome p450 metabolism. Drug Discovery Today 11, 601–606.

Dickins, M., van de Waterbeemd, H., 2004. Simulation models for drug disposition and drug interactions. Drug Discovery Today BIOSILICO 2, 38–45.

Doan, K. M. M., Boje, K. M., 2000. Theoretical pharmacokinetic and pharmacodynamic simulations of drug delivery mediated by blood–brain barrier transporters. Biopharmaceutics & Drug Disposition 21, 261–278.

Döhr, O., Paine, M. J., Friedberg, T., Roberts, G. C., Wolf, C. R., 2001. Engineering of a functional human nadh-dependent cytochrome p450 system. Proceedings of the National Academy of Sciences 98, 81–86.

Dormann, S., Deutsch, A., 2002. Modeling of self-organized avascular tumor growth with a hybrid cellular automaton. In Silico Biology 2, 35–44.

Dutheil, F., Beaune, P., Loriot, M., 2008. Xenobiotic metabolizing enzymes in the central nervous system: Contribution of cytochrome p450 enzymes in normal and pathological human brain. Biochimie 90, 426–436.

Ekhart, C., Rodenhuis, S., Smits, P., Beijnen, J., Huitema, A., 2009. An overview of the relations between polymorphisms in drug metabolising enzymes and drug transporters and survival after cancer drug treatment. Cancer Treatment Reviews 35, 1831.

Ekins, S., Waller, C. L., Swaan, P. W., Cruciani, G., Wrighton, S. A., Wikel, J. H., 2000. Progress in predicting human adme parameters in silico. Journal of Pharmacological and Toxicological Methods 44 (1), 251–272.

Ermentrout, G., Edelstein-Keshet, L., 1993. Cellular automata approaches to biological modelling. Journal of Theoretical Biology 160, 97–133.

Evans, W., Relling, M., 1999. Pharmacogenomics: Translating functional genomics into rational therapeutics. Science 286, 487–491.

Felmlee, M. A., Lon, H.-K., Gonzalez, F. J., Yu, A.-M., 2008. Cytochrome p450 expression and regulation in cyp3a4/cyp2d6 double transgenic humanized mice. Drug Metabolism and Disposition 36, 435–441.

Finn, R., McLaughlin, L., Ronseaux, S., Rosewell, I., Houston, J., Henderson, C., Wolf, C., 2008. Defining the in vivo role for cytochrome b5 in cytochrome p450 function through the conditional hepatic deletion of microsomal cytochrome b5. Journal of Biological Chemistry 283, 3138531393.

Flynn, E., Pastino, G., Sultatos, L., 1996. Development and application of a physiologically based pharmacokinetic model for ethanol in the mouse. Alcohol & Alcoholism 31 (4), 365–374.

Fox, J., Barthold, S., Davisson, M., Newcomer, C., Quimby, F., Smith, A. (Eds.), 2006. The Mouse in Biomedical Research: Normative Biology, Husbandry, and Models. Academic Press.

Friberg, L. E., Hassan, S. B., Lindhagen, E., Larsson, R., Karlsson, M. O., 2005. Pharmacokinetic-pharmacodynamic modelling of the schedule-dependent effect of the anti-cancer agent chs 828 in a rat hollow fibre model. European Journal of Pharmaceutical Sciences 25, 163–173.

Frieboes, H., Edgerton, M., Fruehauf, J., Rose, F., Worrall, L., Gatenby, R., Ferrari, M., Cristini, V., 2009. Prediction of drug response in breast cancer using intergrative experimental/computational modeling. Cancer Research 69, 4484–4492.

George, J., Byth, K., Farrell, G. C., 1995. Age but not gender selectively affects expression of individual cytochrome p450 proteins in human liver. Biochemical Pharmacology 50, 727–730.

Gertner, G., Xu, C., 2007. Extending a global sensitivity analysis technique to models with correlated parameters. Computational Statistics and Data Analysis 51, 5579–5590.

Gertner, G., Xu, C., 2008. A general first-order global sensitivity analysis method. Reliability Engineering and System Safety 93, 1060–1071.

Ghaemi, M., Shahrokhi, A., 2006. Combination of the cellular potts model and lattice gas cellular automata for simulating the avascular cancer growth. Lecture Notes in Computer Science 4173, 297–303.

Gonzalez, F. J., Kimura, S., 2003. Study of p450 function using gene knockout and transgenic mice. Archives of Biochemistry and Biophysics 409, 153–158.

Gordon, K., 2006. Mathematical modelling of cell-cycle-dependent chemotherapy drugs: Implications for cancer treatment. Ph.D. thesis, Division of Mathematics, University of Dundee.

Grass, G., 1997. Simulation models to predict oral drug absorption. Advanced Drug Delivery Review 23, 199–219.

Grass, G. M., Sinko, P. J., 2002. Physiologically-based pharmacokinetic simulation modelling. Advanced Drug Delivery Review 54, 433–451.

Guengerich, F. P., 2001. Common and uncommon cytochrome p450 reactions related to metabolism and chemical toxicity. Chemical Research in Toxicology 14, 611–650.

Guengerich, F. P., 2002. Cytochrome p450 enzymes in the generation of commercial products. Nature Reviews Drug Discovery 1, 359–366.

Guengerich, F. P., Parikh, A., Johnson, E. F., Richardson, T. H., von Wachenfeldt, C., Cosme, J., Jung, F., Strassburg, C. P., Manns, M. P., Tukey, R. H., Pritchard, M., Fournel-Gigleux, S., Burchell, B., 1997. Heterologous expression of human drug-metabolizing enzymes. Drug Metabolism and Disposition 25, 1234–1241.

Gunawan, R., Cao, Y., Petzold, L., Doyle III, F., 2005. Sensitivity analysis of discrete stochastic systems. Biophysical Journal 88, 2530–2540.

Harris, L. A., Barton, H. A., 2008. Comparing single and repeated dosimetry data for perfluorooctane sulfonate in rats. Toxicology Letters 181, 148–156.

Henderson, C. J., Pass, G. J., Wolf, C. R., 2006. The hepatic cytochrome p450 reductase null mouse as a tool to identify a successful candidate entity. Toxicology Letters 162, 111–117.

Holmquist, G., 2009. Opioid metabolism and effects of cytochrome p450. Pain Medicine 10, S20–S29.

Horenko, I., Lorenz, S., Schuütte, C., Huisinga, W., 2005. Adaptive approach for nonlinear sensitivity analysis of reaction kinetics. Journal of Computational Chemistry 26, 941–948.

Hunt, C. A., Ropella, G. E. P., Yan, L., Hung, D. Y., Roberts, M. S., 2006. Physiologically based synthetic models of hepatic disposition. Journal of Pharmacokinetics and Pharmacodynamics 33, 737–772.

Hurria, A., Fleming, M., Baker, S., Kelly, K., Cutchall, K., Panageas, K., 2006. Pharmacokinetics and toxicity of weekly docetaxel in older patients. Clinical Cancer Research 12, 6100–6105.

Ingelman-Sundberg, M., 2001. Pharmacogenetics: an opportunity for a safer and more efficient pharmacotherapy. Journal of Internal Medicine 250, 186–200.

Ingelman-Sundberg, M., 2004. Pharmacogenetics of cytochrome p450 and its applications in drug therapy: the past, present and future. Trends in Pharmacological Sciences 25, 193–200.

Ito, K., Iwatsubo, T., Kanamitsu, S., Nakajima, Y., Sugiyama, Y., 1998. Quantitative prediction of in vivo drug clearance and drug interactions from in vitro data on metabolism, together with binding and transport. Annual Review of Pharmacology and Toxicology 38, 461–499.

Ito, T., Ando, H., Suzuki, T., Ogura, T., Hotta, K., Imamura, Y., Yamaguchi, Y., Handa, H., 2010. Identification of a primary target of thalidomide teratogenicity. Science 327, 1345–1350.

Jayawardhana, B., Kell, D., Rattray, M., 2008. Bayesian inference of the sites of perturbations in metabolic pathways via markov chain monte carlo. Bioinformatics 24, 1191–1197.

Jennewein, S., Park, H., DeJong, J. M., Long, R. M., Bollon, A. P., Croteau, R. B., 2005. Coexpression in yeast of taxus cytochrome p450 reductase with cytochrome p450 oxygenases involved in taxol biosynthesis. Biotechnology and Bioengineering 89, 588–598.

Jürgens, G., Christensen, H. R., Brsen, K., Sonne, J., Loft, S., Olsen, N. V., 2002. Acute hypoxia and cytochrome p450-mediated hepatic drug metabolism in humans. Clinical Pharmacology & Therapeutics 71, 214–220.

Kari, J., 2005. Theory of cellular automata: A survey. Theoretical Computer Science 334, 333.

Kato, M., 2008. Intestinal first-pass metabolism of cyp3a4 substrates. Drug Metabolism and Pharmacokinetics 23, 8794.

Keys, D. A., Bruckner, J. V., Muralidhara, S., Fisher, J. W., 2003. Tissue dosimetry expansion and cross-validation of rat and mouse physiologically based pharmacokinetic models for trichloroethylene. Toxicological Sciences 76, 35–50.

Khan, A. Z., Mudan, S. S., 2007. Liver regeneration: mechanisms, mysteries and more. ANZ Journal of Surgery 77, 9–14.

Kinirons, M. T., O'Mahony, M. S., May 2004. Drug metabolism and ageing. British Journal of Clinical Pharmacology 57 (5), 540–544.

Kirchheiner, J., Seeringer, A., 2007. Clinical implications of pharmacogenetics of cytochrome p450 drug metabolizing enzymes. Biochimica et Biophysica Acta 1770, 489494.

Kot, M., Daniel, W., Apr 2008. Relative contribution of rat cytochrome p450 isoforms to the metabolism of caffeine: the pathway and concentration dependence. Biochemical Pharmacology 75 (7), 1538–1549.

Kramer, J., Snowling, S., 2001. Evaluating modelling uncertainty for model selection. Ecological Modelling 138, 17–30.

Kramer, M. A., Leis, J. R., 1988. Simultaneous solution and sensitivity analysis of systems described by ordinary differential equations. ACM Transactions on Mathematical Software 14, 45–60.

Kuipers, E. J., Klinkenberg-Knol, E. C., 1999. Helicobacter pylori, acid, and omeprazole revisited: bacterial eradication and rebound hypersecretion. Gastroenterology 116, 479–483.

Kutrib, M., Vollmar, R., Worsch, T., 1997. Introduction to a special issue on cellular automata. Parallel Computing 23, 1567–1576.

Leahy, D. E., 2004. Drug discovery information integration: virtual humans for pharmacokinetics. Drug Discovery Today BIOSILICO 2, 78–84.

Lewis, D., 2000. On the recognition of mammalian microsomal cytochrome p450 substrates and their characteristics. Biochemical Pharmacology 60, 293306.

Lill, M. A., 2007. Multi-dimensional qsar in drug discovery. Drug Discovery Today 12, 1013–1017.

Lin, J., 1995. Species simularities and differences in pharmacokinetics. Drug Metabolism and Disposition 23, 1008–1021.

Lin, J. H., 1998. Applications and limitations of interspecies scaling and in vitro extrapolation in pharmacokinetics. Drug Metabolism and Disposition 26, 1202–1212.

Lin, J. H., Lu, A. Y., 1998. Inhibition and induction of cytochrome p450 and the clinical implications. Clinical Pharmacokinetics 35, 361–390.

Lipinski, C., Lombardo, F., Dominy, B., Feeney, P., 1997. Experimental and computational approaches to estimate solubility and permeability in drug discovery and development settings. Advanced Drug Delivery Reviews 23, 3–25.

Lombardo, F., Obach, R. S., Shalaeva, M. Y., Gao, F., 2002. Prediction of volume of distribution values in humans for neutral and basic drugs using physicochemical measurements and plasma protein binding data. Journal of Medicinal Chemistry 45, 2867–2876.

Lu, Y., Cederbaum, A., 2008. Cyp2e1 and oxidative liver injury by alcohol. Free Radical Biology & Medicine 44, 723738.

Lüpfert, C., Reichel, A., 2005. Development and application of physiologically based pharmacokinetic-modeling tools to support drug discovery. Chemistry & Biodiversity 2, 1462–1486.

Macé, K., Bowman, E. D., Vautravers, P., Shields, P. G., Harris, C. C., Pfeifer, A. M., 1998. Characterisation of xenobiotic-metabolising enzyme expression in human bronchial mucosa and peripheral lung tissues. European Journal of Cancer 34, 914–920.

Mager, D. E., 2006. Quantitative structure-pharmacokinetic/pharmacodynamic relationships. Advanced Drug Delivery Review 58, 1326–1356.

Marechal, J.-D., Yu, J., Brown, S., Kapelioukh, I., Rankin, E. M., Wolf, C. R., Roberts, G. C. K., Paine, M. J. I., Sutcliffe, M. J., 2006. In silico and in vitro screening for inhibition of cytochrome p450 cyp3a4 by comedications commonly used by patients with cancer. Drug Metabolism and Disposition 34, 534–538.

Martin, E., Hine, R., 2004. Oxford Dictionary of Biology, 5th Edition. Oxford University Press.

Martínez, C., García-Martín, E., Blanco, G., Gamito, F. J. G., Ladero, J. M., Agúndez, J. A. G., 2005. The effect of the cytochrome p450 cyp2c8 polymorphism on the disposition of (r)-ibuprofen enantiomer in healthy subjects. British Journal of Clinical Pharmacology 59, 62–69.

Maurer, S., Kühnel, K., Kaysser, L., Eiben, S., Schmid, R., Urlacher, V., 2005. Catalytic hydroxylation in biphasic systems using cyp102a1 mutants. Advanced Synthesis & Catalysis 347 (7-8), 1090–1098.

McFadyen, M., McLeod, H., Jackson, F., Melvin, W., Doehmerd, J., Murray, G., 2001. Cytochrome p450 cyp1b1 protein expression: a novel mechanism of anticancer drug resistance. Biochemical Pharmacology 62, 207212.

McFadyen, M. C. E., Melvin, W. T., Murray, G. I., 2004. Cytochrome p450 enzymes: novel options for cancer therapeutics. Molecular Cancer Therapeutics 3, 363–371.

McLean, K. J., Sabri, M., Marshall, K. R., Lawson, R. J., Lewis, D. G., Clift, D., Balding, P. R., Dunford, A. J., Warman, A. J., McVey, J. P., Quinn, A.-M., Sutcliffe, M. J., Scrutton, N. S., Munro, A. W., 2005. Biodiversity of cytochrome p450 redox systems. Biochemical Society Transactions 33, 796–801.

Melicow, M., 1982. The three steps to cancer: A new concept of carcinogenesis. Journal of T 94, 471–511.

Meyer, U. A., 2000. Pharmacogenetics and adverse drug reactions. Lancet 356, 1667–1671.

Miksys, S., Lerman, C., Shields, P. G., Mash, D. C., Tyndale, R. F., 2003. Smoking, alcoholism and genetic polymorphisms alter cyp2b6 levels in human brain. Neuropharmacology 45, 122–132.

Miners, J., 2002. Evolution of drug metabolism: Hitchhiking the technology bandwagon. Clinical and Experimental Pharmacology and Physiology 29, 10401044.

Miyoshi, Y., Ando, A., Takamura, Y., Taguchi, T., Tamaki, Y., Noguchi, S., 2002. Prediction of response to docetaxel by cyp3a4 mrna expression in breast cancer tissues. International Journal of Cancer 97, 129–132.

Mollá, G., Padilla, G., 2002. Description of the MATLAB functions $SENS\_SYS$ and $SENS\_IND$.
URL `http://www.mathworks.com/matlabcentral/fileexchange/`

Morita, T., Tei, Y., Inoue, S., 2003. Correlation of the dose of midazolam for symptom control with administration periods: the possibility of tolerance. Journal of Pain and Symptom Management 25, 369–375.

Munro, A. W., Lindsay, J. G., 1996. Bacterial cytochromes p-450. Molecular Microbiology 20, 1115–1125.

Nebert, D. W., Russell, D. W., 2002. Clinical importance of the cytochromes p450. Lancet 360, 1155–1162.

Novak, B., Tyson, J., 2004. A model for restriction point control of the mammalian cell cycle. Journal of Theoretical Biology 230, 563–579.

Omura, T., 2010. Structural diversity of cytochrome p450 enzyme system. The Journal of Biochemistry 147, 297306.

Online., E. B., March 2011a. Liver: anterior and posterior views. Art.
URL `http://www.britannica.com/EBchecked/media/68633/`

Online., E. B., March 2011b. Liver: structure of human liver. Art.
URL `http://www.britannica.com/EBchecked/media/60419/`

Parikh, A., Gillam, E. M., Guengerich, F. P., 1997. Drug metabolism by escherichia coli expressing human cytochromes p450. Nature Biotechnology 15, 784–788.

Park, B., Kitteringham, N., Pirmohamed, M., Tucker, G., 1996. Relevance of induction of human drug-metabolizing enzymes: pharmacological and toxicological implications. British Journal of Clinical Pharmacology 41, 477–491.

Pass, G. J., Carrie, D., Boylan, M., Lorimore, S., Wright, E., Houston, B., Henderson, C. J., Wolf, C. R., 2005. Role of hepatic cytochrome p450s in the pharmacokinetics and toxicity of cyclophosphamide: studies with the hepatic cytochrome p450 reductase null mouse. Cancer Research 65, 4211–4217.

Phillips, K. A., Veenstra, D. L., Oren, E., Lee, J. K., Sadee, W., 2001. Potential role of pharmacogenomics in reducing adverse drug reactions: a systematic review. Journal of the American Medical Association 286, 2270–2279.

Pirmohamed, M., Park, B. K., 2003. Cytochrome p450 enzyme polymorphisms and adverse drug reactions. Toxicology 192, 23–32.

Plant, N., 2007. The human cytochrome p450 sub-family: Transcriptional regulation, inter-individual variation and interaction networks. Biochimica et Biophysica Acta 1770, 478488.

Poulin, P., Theil, F. P., 2000. A priori prediction of tissue:plasma partition coefficients of drugs to facilitate the use of physiologically-based pharmacokinetic models in drug discovery. Journal of Pharmaceutical Sciences 89, 16–35.

Raabe, D., 2004. Continuum Scale Simulation of Engineering Materials: Fundamentals, Microstructures, Process Applications. Wiley, Ch. 3, pp. 57–74.

Rabitz, H., Kramer, M., Dacol, D., 1983. Sensitivity analysis in chemical-kinetics. Annual Review of Physical Chemistry 34, 419–461.

Ramchandani, V. A., Bosron, W. F., Li, T. K., 2001. Research advances in ethanol metabolism. Pathologie Biologie 49, 676–682.

Rang, H., e. a., 2003. Pharmacology, 5th Edition. Churchill Livingstone.

Ribba, B., Alarcon, T., Marron, K., Maini, P., Agur, Z., 2004. The use of hybrid cellular automaton models for improving cancer therapy. Lecture Notes in Computer Science 3305, 444–453.

Ribba, B., Saut, O., Colin, T., Bresch, D., Grenier, E., Boissel, J., 2006. A multiscale model of avascular tumor growth to investigate the therapeutic benefit of anti-invasive agents. Journal of Theoretical Biology 243, 532–541.

Rieger, T. R., Morimoto, R. I., Hatzimanikatis, V., 2005. Mathematical modeling of the eukaryotic heat-shock response: dynamics of the hsp70 promoter. Biophysical Journal 88, 1646–1658.

Rodriguez-Antona, C., Gomez, A., Karlgren, M., Sim, S., Ingelman-Sundberg, M., 2010. Molecular genetics and epigenetics of the cytochrome p450 gene family and its relevance for cancer risk and treatment. Human Genetics 127, 117.

Rodriguez-Antona, C., Ingelman-Sundberg, M., 2006. Cytochrome p450 pharmacogenetics and cancer. Oncogene 25, 1679–1691.

Rogers, J. F., Nafziger, A. N., Bertino, J. S., 2002. Pharmacogenetics affects dosing, efficacy, and toxicity of cytochrome p450-metabolized drugs. American Journal of Medicine 113, 746–750.

Roy, P., Yu, L. J., Crespi, C. L., Waxman, D. J., 1999. Development of a substrate-activity based approach to identify the major human liver p-450 catalysts of cyclophosphamide and ifosfamide activation based on cdna-expressed activities and liver microsomal p-450 profiles. Drug Metabolism and Disposition 27, 655–666.

Saltelli, A., Ratto, M., Tarantola, S., Campolongo, F., 2005. Sensitivity analysis for chemical models. Chemical Reviews 105, 2811–2828.

Schenkman, J., Greim, H., 1993. Cytochrome P450. Handbook of Experimental Pharmacology Vol. 105. Springer-Verlag.

Scripture, C. D., Sparreboom, A., Figg, W. D., 2005. Modulation of cytochrome p450 activity: implications for cancer therapy. Lancet Oncology 6, 780–789.

Sigmund, K., 1993. Games of Life: Explorations in Ecology, Evolution, and Behaviour. Oxford University Press.

Sinek, J., Sanga, S., Zheng, X., Frieboes, H., Ferrari, M., Cristini, V., 2009. Predicting drug pharmacokinetics and effect in vascularized tumors using computer simulation. Journal of Mathematical Biology 58, 485–510.

Singh, M. N., Stringfellow, H. F., Paraskevaidis, E., Martin-Hirsch, P. L., Martin, F. L., 2007. Tamoxifen: important considerations of a multi-functional compound with organ-specific properties. Cancer Treatment Reviews 33, 91–100.

Smith, D., van de Waterbeemd, H., Walker, D., 2001. Pharmacokinetics and Metabolism in Drug Design. Wiley.

Smith, J., Martin, L., 1973. Do cells cycle? Proceedings of the National Academy of Sciences 70 (4), 1263–1267.

Sotaniemi, E., Arranto, A., Pelkonen, O., Pasanen, M., 1997. Age and cytochrome p450 -linked drug metabolism in humans: An analysis of 226 subjects with equal histopathologic conditions. Clinical Pharmacology and Therapeutics 61, 331–339.

Spratlin, J., Sawyer, M., 2007. Pharmacogenetics of paclitaxel metabolism. Critical Reviews in Oncology/Hematology 61, 222229.

Strasser, K., Ludwig, H., 2002. Thalidomide treatment in multiple myeloma. Blood Reviews 16, 207–215.

Takors, R., Froemel, C., Dikta, G., Degenring, D., 2004. Sensitivity analysis for the reduction of complex metabolism models. Journal of process control 4, 729 –745.

Tanaka, T., Tanimoto, K., Otani, K., Satoh, K., Ohtaki, M., Yoshida, K., Toge, T., Yahata, H., Tanaka, S., Chayama, K., Okazaki, Y., Hayashizaki, Y., Hiyama, K., Nishiyama, M., 2004. Concise prediction models of anticancer efficacy of 8 drugs using expression data from 12 selected genes. International Journal of Cancer 111, 617626.

Tang, W., Stearns, R. A., 2001. Heterotropic cooperativity of cytochrome p450 3a4 and potential drug-drug interactions. Current Drug Metabolism 2, 185–198.

Tredger, J., Stoll, S., 2002. Cytochromes p450 - their impact on drug treatment. Hospital Pharmacist 9 (6), 167–173.

Tsui, W. S., 2003. Drug-associated changes in the liver. Current Diagnostic Pathology 9, 96–104.

Turanyi, T., 1990. Sensitivity analysis of complex kinetic systems - tools and applications. Journal of Mathematical Chemistry 5, 203–248.

Turner, S., Sherratt, J., 2002. Intercellular adhesion and cancer invasion: A discrete simulation using the extended potts model. Journal of Theoretical Biology 216, 85–100.

Tyson, J., Novak, B., 2001. Regulation of the eukaryotic cell cycle: Molecular antagonism, hysteresis, and irreversible transitions. Journal of Theoretical Biology 210, 249–263.

Urlacher, V. B., Eiben, S., 2006. Cytochrome p450 monooxygenases: perspectives for synthetic application. Trends in Biotechnology 24, 324–330.

van Beilen, J. B., Holtackers, R., Lscher, D., Bauer, U., Witholt, B., Duetz, W. A., 2005. Biocatalytic production of perillyl alcohol from limonene by using a novel mycobacterium sp. cytochrome p450 alkane hydroxylase expressed in pseudomonas putida. Applied Environmental Microbiology 71, 1737–1744.

van de Waterbeemd, H., Gifford, E., 2003. Admet in silico modelling: towards prediction paradise? Nature Reviews Drug Discovery 2, 192–204.

van Schaik, R. H. N., 2008. Cyp450 pharmacogenetics for personalizing cancer therapy. Drug Resistance Updates 11, 77–98.

Varma, A., Morbidelli, M., Wu, H., 1999. Parametric Sensitivity in Chemical Systems. Cambridge University Press.

Venkatakrishnan, K., Moltke, L. L. V., Greenblatt, D. J., 2001. Human drug metabolism and the cytochromes p450: application and relevance of in vitro models. The Journal of Clinical Pharmacology 41, 1149–1179.

Wani, M. C., Taylor, H. L., Wall, M. E., Coggon, P., McPhail, A. T., 1971. Plant antitumor agents. vi. the isolation and structure of taxol, a novel antileukemic and antitumor agent from taxus brevifolia. Journal of the American Chemical Society 93, 2325–2327.

Ward, J., King, J., 2003. Mathematical modelling of drug transport in tumour multicell spheroids and monolayer cultures. Mathematical Biosciences 181, 177–207.

Winklerb, M., Gliederb, A., Fraaije, M., 2010. Monooxygenases as biocatalysts: Classification, mechanistic aspects and biotechnological applications. Journal of Biotechnology 146, 924.

Wishart, D. S., Knox, C., Guo, A. C., Shrivastava, S., Hassanali, M., Stothard, P., Chang, Z., Woolsey, J., 2006. Drugbank: a comprehensive resource for in silico drug discovery and exploration. Nucleic Acids Research 34, D668–D672.

Wolf, C. R., Smith, G., 1999. Pharmacogenetics. British Medical Bulletin 55, 366–386.

Wolf-Gladrow, D. A., 2000. Lattice-gas Cellular Automata and Lattice Boltzmann Models: An Introduction (Lecture Notes in Mathematics). Springer.

Wolfram, S., 1983. Statistical-mechanics of cellular automata. Reviews of Modern Physics 55 (3), 601–644.

Wolfram, S., 1984. Universality and complexity in cellular automata. Physica D 10 (1-2), 1–44.

Yamazaki, H., Johnson, W. W., Ueng, Y. F., Shimada, T., Guengerich, F. P., 1996. Lack of electron transfer from cytochrome b5 in stimulation of catalytic activities of cytochrome p450 3a4. characterization of a reconstituted cytochrome p450 3a4/nadph-cytochrome p450 reductase system and studies with apo-cytochrome b5. Journal of Biological Chemistry 271, 27438–27444.

Yang, X.-X., Hu, Z.-P., Chan, S. Y., Zhou, S.-F., 2006. Monitoring drug-protein interaction. Clinica Chimica Acta 365, 9–29.

Yang, Y.-J., Wilkinson, J., Russell, A., 1997. Fast, direct sensitivity analysis of multidimensional photochemical models. Environmental Science and Technology 31, 2859–2868.

Yengi, L. G., Xiang, Q., Pan, J., Scatina, J., Kao, J., Ball, S. E., Fruncillo, R., Ferron, G., Wolf, C. R., 2003. Quantitation of cytochrome p450 mrna levels in human skin. Analytical Biochemistry 316, 103–110.

Yu, L. J., Drewes, P., Gustafsson, K., Brain, E. G., Hecht, J. E., Waxman, D. J., 1999. In vivo modulation of alternative pathways of p-450-catalyzed cyclophosphamide metabolism: impact on pharmacokinetics and antitumor activity. Journal of Pharmacology and Experimental Therapeutics 288, 928–937.

Zahra, M., Taylory, A., Mouldy, G., Coles, C., Crawfordz, R., Tan, L., 2008. Concurrent weekly cisplatin chemotherapy and radiotherapy in a haemodialysis patient with locally advanced cervix cancer. Clinical Oncology 20, 6–11.

Zak, D., Stelling, J., Doyle III, F., 2005. Sensitivity analysis of oscillatory (bio)chemical systems. Computers & chemical engineering 29, 663–673.

Zhang, M.-Q., Wilkinson, B., 2007. Drug discovery beyond the 'rule-of-five'. Current Opinion in Biotechnology 18, 478–488.

Zhou, S., Chan, S., Goh, B., Chan, E., Duan, W., Huang, M., McLeod, H., 2005. Mechanism-based inhibition of cytochrome p450 3a4 by therapeutic drugs. Clinical Pharmacokinetics 44, 279–304.

Ziaee, V., Hamed, E. A., Hoshmand, A., Amini, H., Kebriaeizadeh, A., Saman, K., 2005. Side effects of dextromethorphan abuse, a case series. Addictive Behaviour 30, 1607–1613.